

NPS ARCHIVE
1969
GRAHAM, C.

THE LIMITING HEAT TRANSFER MECHANISMS
OF DROPWISE CONDENSATION

by

Clark Graham

LIBRARY
NAVAL POSTGRADUATE SCHOOL
MONTEREY, CALIF. 93940

THE LIMITING HEAT TRANSFER MECHANISMS OF DROPWISE CONDENSATION

by

Clark Graham

B. S. U. S. Naval Academy
(1964)

S. M. Massachusetts Institute of Technology
(1967)

Mech. E. Massachusetts Institute of Technology
(1967)

Submitted in Partial Fulfillment

of the Requirements for the

Degree of Doctor of

Philosophy

at the

Massachusetts Institute of

Technology

March 1969

NPS ARCHIVE

1969

GRAHAM, C.

76015
~~06522~~

THE LIMITING HEAT TRANSFER MECHANISMS OF DROPWISE CONDENSATION

BY

Clark Graham

Submitted to the Department of Mechanical Engineering on March 26, 1969, in partial fulfillment of the requirement for the degree of Doctor of Philosophy

ABSTRACT

An experimental and analytical study has been carried out to determine the limiting heat transfer mechanisms of dropwise condensation.

Extensive heat transfer measurements were made for drop condensation of saturated "gas free steam" on a vertically oriented copper surface. Dioctadecyl disulphide and Teflon were used as promoter agents. The parametric effects of ΔT , pressure, surface roughness, vapor velocity, and time were investigated.

Visual experiments were carried out to determine the drop size distribution and nucleation site density. Microphotographs taken of the condensing process resulted in a measured distribution of drop sizes from 10 to 3000 microns.

A model of the dropwise condensation process has been proposed which correctly predicts the observed parametric trends. The problem was divided into analyzing the heat transfer through a single drop and then utilizing the drop distribution to predict the average heat transfer through the surface.

The results of the experimentally determined heat transfer measurements have been compared to those predicted by the model. It was concluded that the drop conduction resistance represents the major limitation to drop condensation heat transfer. Interfacial effects account for 25 percent of the total resistance during low pressure ($T_{\text{sat}} = 88^\circ\text{F}$) and 10 percent during atmospheric pressure condensation. For dropwise condensation on a vertically oriented, chemically promoted copper surface the sum of all other resistances is less than 15 percent.

Thesis Supervisor: Peter Griffith
Title: Professor of Mechanical Engineering

ACKNOWLEDGMENTS

The author wishes to express his sincere thanks to Professor Peter Griffith, his thesis supervisor, for his guidance throughout this investigation. The helpful advice of the rest of the thesis committee, Professors J. W. Rose, E. Rabinowicz, and K. C. Russell, is gratefully appreciated. Discussions with Professors B. B. Mikic and L. R. Glicksman proved to be extremely valuable throughout the course of the thesis.

Two of my fellow students, Mr. J. S. Horowitz and Mr. S. J. Hynek, were extremely helpful in writing the numerous computer programs. Thanks are also due to Mr. F. Johnson who assisted in the construction of the apparatus and Miss S. Gold who typed the manuscript.

TABLE OF CONTENTS

	Page
TITLE PAGE	1
ABSTRACT	2
ACKNOWLEDGMENTS	3
TABLE OF CONTENTS	4
LIST OF TABLES	7
LIST OF FIGURES	8
NOMENCLATURE	11
 CHAPTER I: INTRODUCTION	 15
 CHAPTER II: DESCRIPTION OF THE DROPWISE CONDENSATION PROCESS	 17
2.1 The "Film Theory"	17
2.2 The "Nucleation Theory"	18
2.3 Description of Process	18
 CHAPTER III: VISUAL OBSERVATIONS OF THE DROPWISE CONDENSATION PROCESS	 24
3.1 Drop Population and Area Coverage	25
3.2 Nucleation	27
3.3 Drop Growth Rate	30
3.4 Maximum Drop Size	31
3.5 Conditions Required for Dropwise Condensation	33
3.6 Sweeping Drops	34
 CHAPTER IV: PARAMETRIC EFFECTS ON DROPWISE CONDENSATION HEAT TRANSFER	 36
4.1 Heat Flux	36
4.2 Pressure	38
4.3 Non-Condensable Gases	40
4.4 Vapor Velocity	41
4.5 Conductivity of Condensing Surface	42
4.6 Surface Finish	43
4.7 Surface Inclination	43
4.8 Location on Condensing Plate	44
4.9 Condensing Vapor	45
4.10 Promoter	46
4.11 Summary	47
 CHAPTER V: EXPERIMENTAL APPARATUS AND PROCEDURES	 48
5.1 Description of Apparatus	48
5.1.1 Design of Vapor System and Chamber	48
5.1.2 Design of Test Section	50
5.1.3 Microscopic and Photographic Equipment	51
5.2 Heat Measurement Procedures	52
5.2.1 Preparation of Surfaces	52
5.2.2 Heat Transfer Data Taking and Processing Procedures	54

5.3	Drop Distribution Measurement Procedures	55
5.3.1	Photographic Procedure	55
5.3.2	Drop Counting Procedure	57
5.3.3	Limitations of Microscopic Equipment	58
CHAPTER VI:	RESULTS OF HEAT TRANSFER MEASUREMENTS	60
6.1	General	60
6.2	Results for a Mirror Smooth, Chemically Promoted Surface	61
6.3	Results for a Rough, Chemically Promoted Surface	62
6.4	Results for a Teflon Coated Surface	63
6.5	Results of Pressure Tests	63
6.6	Results of Velocity Tests	64
6.7	Transient Effects	65
6.8	Results of Vibration of Surface	67
6.9	Conclusions	67
CHAPTER VII:	PHOTOGRAPHIC MEASUREMENTS	69
7.1	Drop Distribution	69
7.2	Nucleation	74
7.3	Discussion of Photographic Study	75
CHAPTER VIII:	MODEL OF THE HEAT TRANSFER PROCESS FOR DROPWISE CONDENSATION	77
8.1	Heat Transfer Through a Single Drop	77
8.1.1	Resistance Concept	77
8.1.2	Temperature Drop Due to Curvature Resistance	81
8.1.3	Temperature Drop Due to Interfacial Resistance	81
8.1.4	Temperature Drop Due to Conduction Resistance	82
8.1.5	Heat Transfer Through a Drop	83
8.1.6	Total Temperature Drop	83
8.1.7	Drop Growth Rate	83
8.2	Heat Transfer Through the Surface	85
CHAPTER IX:	PREDICTION OF HEAT TRANSFER FOR DROPWISE CONDENSATION	88
9.1	Determination of Drop Growth Rate	88
9.2	Selection of "Correct" Drop Distribution	90
9.3	Relative Importance of Resistances	91
9.4	The Effect of Pressure on Dropwise Condensation Heat Transfer	94
9.5	The Effect of ΔT on Dropwise Condensation Heat Transfer	95
9.6	"Active" Surface Area	96
9.7	Minimum Value of the Condensation Coefficient	96
9.8	Conclusions	97
CHAPTER X:	CONCLUSIONS	98
10.1	Heat Transfer Measurements	98
10.2	Visual Investigation	98
10.3	Prediction of Heat Transfer	99
10.4	The Limiting Heat Transfer Mechanisms	100
10.5	Recommendations for Further Study	101

REFERENCES	102
APPENDIX A HEAT MEASUREMENT TECHNIQUES	108
APPENDIX B DISCUSSION OF DROP DEPARTURE MECHANISMS	113
APPENDIX C DISCUSSION OF CURVATURE RESISTANCE	117
APPENDIX D DISCUSSION OF NUCLEATION CRITERION	125
APPENDIX E DISCUSSION OF INTERFACIAL RESISTANCE	133
APPENDIX F DISCUSSION OF DROP CONDUCTION RESISTANCE	136
APPENDIX G DISCUSSION OF CONSTRICTION RESISTANCE	138
APPENDIX H DISCUSSION OF TEFLON RESISTANCE	141
APPENDIX I LISTING OF COMPUTER PROGRAMS	144
APPENDIX J DROP COUNTING DATA AND PROCEDURES	156
TABLES	168
FIGURES	187
BIOGRAPHICAL NOTE	272

LIST OF TABLES

Table

1	Drop Distribution and Area Coverage Experiments
2	Nucleation Site Densities Observed During Drop Condensation
3	Variation of Heat Transfer Coefficient with Heat Flux
4	Variation of Heat Transfer Coefficient with Steam Pressure
5	Variation of Heat Transfer Coefficient with Vapor Velocity
6	Variation of Heat Transfer Coefficient with Surface Material and Finish
7	Variation of Heat Transfer Coefficient with Surface Inclination
8	Summary of Parametric Effects
9	Summary of Heat Transfer Data
11	Results of Preliminary Vibration Tests
12	Drop Distributions for Low Pressure Condensation
13	Drop Distributions for Atmospheric Pressure Condensation
14	"Correct" Drop Distributions for Low and Atmospheric Pressures
15	Summary of "Active" Area Information
16	Minimum Value of Condensation Coefficient
G-1	Evaluation of the Constriction Resistance

LIST OF FIGURES

Fig.

- 1 Drop Distribution. Reproduced from Fatica and Katz [5]
- 2 Area Covered. Reproduced from Hampson and Ozisik [30]
- 3 Drop Distribution. Reproduced from Sugawara and Katsuta [11]
- 4 Drop Distribution. Reproduced from McCormick and Westwater [15]
- 5 Comparison of Area Covered Data
- 6 Drop Growth Rate. Reproduced from McCormick and Baer [13]
- 7 Maximum Size Drop and Contact Angle Measurement. Reproduced from Sugawara and Michiyoshi [9]
- 8 Area Covered by Moving Drops. Reproduced from Rose [24]
- 9 Variation of Heat Transfer Coefficient with Heat Flux for "Gas Free" Systems
- 10 Variation of Heat Transfer Coefficient with Heat Flux
- 11 Variation of Heat Transfer Coefficient with Steam Pressure (Below 1 atmos.)
- 12 Variation of Heat Transfer Coefficient with Steam Pressure (Above 1 atmos.)
- 13 Variation of Heat Transfer Coefficient with Vapor Velocity
- 14 Variation of Heat Transfer Coefficient with Surface Material
- 15 Variation of Heat Transfer Coefficient with Surface Finish
- 16 Variation of Heat Transfer Coefficient with Surface Inclination
- 17 Schematic Layout of Vapor System
- 18 Condensing Chamber - Test Section-Cooling Chamber Assembly
- 19 Test Section with Detail of Thermocouple Installation in Hole
- 20 Test Section Construction Details
- 21 Schematic Layout of Cooling Water Loop
- 22 Photo of Condensing Chamber

- 23 Photo of Apparatus
- 24 Heat Flux- ΔT Curves for Mirror Smooth Surface
- 25 Heat Flux- ΔT Curves for Rough Surface
- 26 Heat Flux- ΔT Curves for Teflon Surface
- 27 H vs. ΔT for Mirror Smooth Surface
- 28 H vs. ΔT for Atmospheric Pressure Condensation ($T_{\text{sat}} = 212 \text{ }^{\circ}\text{F}$)
- 29 H vs. ΔT for Low Pressure Condensation ($T_{\text{sat}} = 88 \text{ }^{\circ}\text{F}$)
- 30 H vs. T_{sat} for Mirror Smooth Surface
- 31 H vs. Vapor Velocity for Mirror Smooth Surface
- 32 Transient Curves for Mirror Smooth Surface
- 33 Measured Drop Distribution for Mirror Smooth Surface
- 34 Proposed Drop Distributions for Low Pressure Condensation
- 35 Proposed Drop Distributions for Atmospheric Pressure Condensation
- 36 Comparison of "Correct" Distributions for Low and Atmospheric Pressures
- 37 Percent of Surface Area Covered by Drops During Low Pressure Condensation
- 38 Percent of Surface Area Covered by Drops During Atmospheric Pressure Condensation
- 39 Dropwise Condensation at High Heat Flux (5X Photo)
- 40 Dropwise Condensation at Low Heat Flux (5X Photo)
- 41 Effect of ΔT on Nucleation (200X Photo)
- 42 Effect of Pressure on Nucleation (200X Photo)
- 43 Effect of Pressure on Nucleation (120X photo)
- 44 Heat Transfer Model for Dropwise Condensation
- 45 Drop Growth Rate Distributions for Low and Atmospheric Pressure Condensation
- 46 Drop Growth Rate Distributions for Low Pressure Condensation (Varying Equations)

- 47 Drop Growth Rate Distributions for Atmospheric Pressure Condensation (varying Equations)
- 48 Drop Growth Rate Distributions for Low Pressure Condensation (varying ΔT)
- 49 Drop Growth Rate Distributions for Atmospheric Pressure Condensation (varying ΔT)
- 50 Effect of ΔT on Maximum Drop Growth Rate
- 51 Drop Growth Rate for Low Pressure Condensation (D vs. t)
- 52 Drop Growth Rate for Atmospheric Pressure Condensation (D vs. t)
- 53 Drop Growth Rate for Low and Atmospheric Pressure Condensation (D vs. t)
- 54 Drop Growth Rate for Low and Atmospheric Pressure Condensation (D^2 vs. t)
- 55 Integrated Heat Flux Distributions for Low Pressure Condensation (Varying Drop Distribution)
- 56 Integrated Heat Flux Distributions for Atmospheric Pressure Condensation (Varying Drop Distribution)
- 57 Integrated Heat Flux Distributions for Low Pressure Condensation (Varying Integrand)
- 58 Integrated Heat Flux Distributions for Atmospheric Pressure Condensation (Varying Integrand)
- 59 Relative Magnitude of Resistances for Water
- 60 Relative Magnitude of Resistances for Water and Mercury
- 61 H vs. T_{sat} for Mirror Smooth Surface. Predicted vs. Measured Results
- 62 H vs. ΔT for Low Pressure Condensation - Mirror Smooth Surface. Predicted vs. Measured Results
- 63 H vs. ΔT for Atmospheric Pressure Condensation - Mirror Smooth Surface. Predicted vs. Measured Results
- A-1 Thermocouple Set-Up
- A-2 Details of Thermocouple Installation
- A-3 Schematic Representation of Temperature Distribution in Holes and at Wall. Reproduced from Wilcox [76].

- A-4 Typical Temperature Distributions in Test Section
- B-1 Forces Acting on a Droplet
- B-2 Prediction of Maximum Drop Size. Reproduced from Fatica and Katz [5]
- C-1 Equilibrium of a Vapor with a Curved Liquid Surface
- C-2 Equilibrium between Liquid and Vapor at a Curved Surface. Reproduced from Keenan [73].
- C-3 Equilibrium of a Liquid Drop
- C-4 Equilibrium of a Vapor Bubble
- C-5 Effect of Temperature on Minimum Size of Drops and Bubbles
- D-1 The Free Energy of Formation as a Function of Nucleus Size
- D-2 Effect of Degree of Supersaturation on the Critical Nucleus Size and Free Energy of Formation
- D-3 Contact Angle Function
- D-4 Effect of Contact Angle on the Critical Free Energy of Formation
- D-5 Variation of ΔG^* and $\Delta G^*/\bar{RT}$ with Temperature
- D-6 Variation of Contact Angle with Temperature
- E-1 Variation of Interfacial Heat Transfer Coefficient with Temperature
- F-1 Comparison of Conduction through a Drop and a Right Circular Cylinder
- F-2 Drop Conduction Shape Factor, $f(\theta)$. Reproduced from Fatica and Katz [5]
- G-1 Local Surface Temperature due to Non-Uniform Heat Flux over Surface
- H-1 Model of Teflon Resistance
- H-2 Predicted Total Heat Transfer Coefficient for Teflon Surfaces

NOMENCLATURE

a	=	acceleration of drop due to vibratory motion
A	=	area
b	=	constant defined in Eq. (6.1)
C	=	constant defined in Eq. (8.12)
D	=	drop diameter
g	=	local acceleration of gravity
h	=	heat transfer coefficient defined in Eq. (8.2)
\bar{h}	=	average heat transfer coefficient defined in Eq. (8.1)
H	=	latent heat of vaporization
J	=	nucleation rate defined in Eq. (D.21)
k	=	thermal conductivity
ℓ	=	thickness of promoter layer
L	=	height
m	=	constant defined in Eq. (6.1)
M	=	molecular weight
n	=	constant
$\bar{N}dD$	=	number of drops of diameter D to $D + dD$ per square centimeter of condenser surface
p	=	pressure
Q	=	rate of heat transfer
r	=	radius of drop
R	=	resistance
\bar{R}	=	universal gas constant
S	=	surface tension force
t	=	time

T	=	temperature
V	=	volume of drop
w	=	net rate of evaporation ($w = W_+ - W_-$)
W	=	weight of drop
W_+	=	flux of molecules away from interface
W_-	=	flux of molecules toward interface
Y	=	constant defined in Eq. (D.10)
z	=	constant
α	=	mass transfer accommodation coefficient, condensation coefficient
α_1	=	modified condensation coefficient
β	=	angle of inclination
γ	=	surface area covered by inactive drops
ΔD	=	drop counting band width
ΔG	=	Gibbs free energy of formation
ΔG_v	=	Gibbs free energy of condensation per unit volume
ΔG^*	=	Gibbs free energy of formation of a nucleus of critical size
ΔG^*_1	=	critical Gibbs free energy for heterogeneous nucleation on a plane substrate
ΔG^*_L	=	critical Gibbs free energy for heterogeneous nucleation on a 90° ledge
ΔN	=	number of drops counted per square centimeter in the size range D to $D \pm \Delta D$
ΔT	=	temperature difference
θ	=	contact angle
$\phi(\theta)$	=	contact angle function defined in Eq. (D.8)
ρ	=	density

σ = surface tension

SUBSCRIPTS

a = advancing

avg = average

c = curvature

cm = constriction

cyl = cylinder

crit = critical

d = dead

dc = drop conduction

f = fluid

fc = fluid at curved interface

fg = refers to change by condensation

fs = fluid at saturation conditions (plane interface)

g = vapor

gc = vapor at curved interface

gs = vapor at saturation conditions (plane interface)

i = interfacial

m = mean

max = maximum

min = minimum

nc = non-condensable

nuc = nucleation

o = ambient conditions

p = promoter

r = receding

s, sat = saturation condition at flat liquid-vapor interface
sc = saturation condition at curved liquid-vapor interface
sys = system
t = total
T = Teflon
v = vapor
V = Volume
w = wall

I. INTRODUCTION

Compared to the boiler section of modern steam power plants, the condenser has received very little attention and consequently advanced ever so slightly in terms of performance and size reduction. Significant improvement in condenser design will come, however, when the drop-wise mode of condensation is utilized. It has been shown that heat transfer coefficients for dropwise condensation can be 30 to 40 times greater than for filmwise condensation. Converting this to hardware could mean a reduction in condenser size by a factor of one third.

There are three areas that need thorough investigation before dropwise condensation will appear attractive to condenser designers:

1. The Non-Condensable Gas Problem. The slightest amount of non-condensable gas in the vapor causes a drastic drop in the condensing rate for dropwise condensation. Drop condensation is not significantly better than film condensation for contaminated steam. The location and design of vents to reduce the build up of non-condensables to a tolerable limit is an area which has not received enough attention to date.
2. The Promoter Problem. In order to obtain dropwise condensation, a non-wetting surface must be produced by "promoting" the surface. At present, a long-lasting promoter which causes good quality drop condensation is lacking. The ideal promoter must be relatively inexpensive and must not introduce a significant thermal resistance to heat transfer. Without such a promoter, dropwise condensation will never be reliable or practical.
3. The Limit Problem. The heat transfer coefficient for dropwise

condensation decreases as the pressure and the vapor to surface temperature difference decrease. Designers must know the magnitude of this drop in heat transfer performance to determine whether drop condensation is beneficial under certain extreme operating conditions. Information on the mechanisms which limit heat transfer for dropwise condensation under all conditions would be very valuable.

The purpose of this work is to investigate the limit problem and determine the factors which affect dropwise condensation. In this thesis, the author will first present a description of the dropwise condensation process. The purpose of this section will be to specify how heat is transferred in dropwise condensation and what factors affect this process. Following this section will be a documentation of the visual observations and heat transfer measurements which have been performed by past researchers. At this time a brief description of the cause of parametric effects will be supplied.

The author carried out careful heat transfer measurements to supply further information on some of the more important parametric trends. The results of these measurements serve as a basis for comparison for the later analytical work.

One of the more important parts of this work involves the modeling of the heat transfer process of dropwise condensation. The proposed model correctly predicts all of the parametric trends observed to date.

The primary experimental work involved the measurement of the drop distribution. This distribution is used in conjunction with the model to predict the heat transfer performance for dropwise condensation.

From the experimental data and the heat transfer model, conclusions have been drawn concerning the limiting mechanisms of dropwise condensation.

II. DESCRIPTION OF THE DROPWISE CONDENSATION PROCESS

Nearly forty years have elapsed since Schmidt and his co-workers [1] first examined the heat transfer process for dropwise condensation. During this period, conflicting views have arisen concerning the mechanisms of dropwise condensation. The controversy focuses on two important aspects of the process. The first question involves the origin of the droplets observed on the surface. The second point needing clarification is whether the heat is being transferred through the drops or through the "bare" area between the drops.

2.1 The "Film Theory"

The early investigators in the field of drop condensation believed that a thin film of liquid existed between the visible drops. As a group, they contended that heat is transferred both through the drops and through this liquid film. Furthermore, they explained that this film was the source of the larger visible drops.

In 1936, Jakob [2] proposed that vapor molecules condense on the bare surface between drops forming a film of liquid. This film grows until it reaches a critical thickness when it "rolls itself together and fractures" to form droplets. Eucken [3] also assumed that condensation takes place on a continuous film between the drops. However, he stated that by means of a mechanism which he called "surface diffusion", the condensed liquid migrates into the base of drops. Emmons [4] proposed a slightly different mechanism for heat transfer. He contended that vapor molecules condense in the region between the drops, lose some thermal energy, re-evaporate, and then condense again on the surface of the drop.

These three viewpoints have two ideas in common: that vapor condenses in the region between the drops and that the resulting liquid film is the source of the drops. A number of investigators [5-11] have utilized this general model in developing equations to predict the heat transfer in dropwise condensation.

2.2 The "Nucleation Theory"

More recent investigations tend to disprove the "film theory". Adherents of the "nucleation theory" believe that drops originate from discrete nucleation sites randomly distributed on the surface. They contend that there is no liquid film between drops and that the only path for heat transfer is through the drops.

Tammann and Boehme [12] first suggested in 1935 that droplet formation is a result of a nucleation process. He observed that drops form at the same sites during successive condensation cycles. Several recent investigators [13 to 20] have substantiated his observations.

Umur and Griffith [21] supplied a piece of evidence which strongly proves that dropwise condensation is a nucleation phenomenon. Based on thermodynamic considerations and an optical study designed to determine film thickness, they showed that a film no greater than a monolayer thick can exist in the area between drops. This work proved that there is no liquid film between drops.

Several investigators, McCormick and Baer [22], Le Fevre and Rose [23], Rose [24], Gose et al. [25], Hurst [26], Mikic [27] and Glicksman [28] have utilized the nucleation theory in their modeling of the dropwise condensation process.

2.3 Description of Process

Dropwise condensation is one of the most complex heat transfer processes which exist. Strictly speaking, the process is neither steady nor uniform over the condensing surface. Furthermore, many different heat transfer mechanisms are involved in drop condensation.

When a vapor comes in contact with a cold non-wetting surface, dropwise condensation results. Because of the non-wetting or hydrophobic nature of the surface, the liquid condensate forms as droplets as opposed to a continuous film as in the case of film condensation.

When the vapor first encounters the condensing surface, the vapor makes the phase transformation at discrete nucleation sites. These tiny microscopic drops grow by direct condensation onto their surface. As the drops grow and occupy more surface area, they bump into each other and coalesce. At this stage, drops grow both by condensation and coalescence. As a drop increases in size, its rate of growth by condensation decreases due to conduction limitations. These drops now grow primarily due to smaller drops feeding them by means of the coalescence process. When a drop reaches a critical size, the surface tension is overcome by gravity and the drop departs. This is the end of one complete cycle.

As drops coalesce and depart, bare surface area is exposed to the vapor. Primary drops form at the uncovered nucleation sites thus supplying a fresh batch of growing drops. In the case of a vertically oriented surface, the departing drops slide down the condenser surface sweeping the area in its path of all drops. This exposure of surface area by coalescence and departure is essential to the continuation of the process.

On a condensing surface one encounters a range of drop sizes from a fraction of a micron up to a few millimeters in diameter. Drops can be said to be in one of four stages of development: 1) nucleation, 2) condensation and coalescence, 3) coalescence, and 4) departure. The rate of growth and the number of drops of a particular size depend on which stage of development it belongs to.

As a drop grows in size and passes from one stage to the next, its rate of growth decreases. Furthermore, due to the mechanism of coalescence, the number of drops of a particular size decreases with increasing diameter. It is through the numerous small drops that the majority of the heat is transferred.

Assuming the drops are hemispherical in shape, there are two factors which affect heat transfer:

- 1) the condensation rate on the "active" drops, and
- 2) the number and size distribution of the "active" drops.

The "active" drops are those which are growing by condensation. These drops are in the nucleation and condensation-coalescence stage of development and transfer the majority of heat to the surface. In contrast, the "dead" drops, belonging to the coalescence and departure stages, transfer little heat. They essentially act like insulators occupying a certain amount of the condenser surface area.

For a given fluid-surface combination, the condensing or growth rate of the "active" drops of a given size is governed by two factors:

- 1) the system pressure, and
- 2) the "true" surface to vapor temperature difference.

Altering the system pressure changes the thermodynamic properties of

the steam and liquid phases. These property changes affect the drop growth rate. The "true" temperature difference may be defined as the difference between the flat interface saturation temperature of the vapor and the actual surface temperature under an active drop. The measured temperature difference is often much greater than the true temperature driving potential.*

The number of "active drops" is determined by the nucleating ability of the surface and factors which affect the coalescence and departure mechanisms. Increasing the nucleation site density increases the number of primary drops which are the source of the active drops. Mechanisms which cause "good quality" coalescence and early departure of the large drops increase the amount of area available for active drops. Thus, nucleation, coalescence, and drop departure affect the number of active drops on the surface.

It is quite easy to explain all parametric trends for dropwise condensation heat transfer by considering just two factors: the size distribution and the growth rate of active drops. Theoretical equations have been derived by previous investigators and modified by this author to predict the drop growth rate. From these expressions one can predict what factors affect the condensation rate on the active drops. All these expressions for the growth rate include a temperature difference. It should be pointed out that the driving potential used in these equations should be the "true" temperature difference. The drop growth equations will be derived in Chapter 8. At that time, further discussion

*

The actual surface temperature under an active drop differs from the mean surface temperature because of the non-uniform heat flux through the condensing surface. This "constriction" effect will be described later in this thesis. Any temperature drop through the promoter layer will also lower the temperature driving force.

of the true temperature driving potential will be given.

The second factor which affects dropwise condensation heat transfer, the size distribution of active drops, is more difficult to predict. No theory exists to predict fully how parameters such as temperature difference and surface chemistry determine the nucleation site density. Trends can be predicted, and one must rely on these to explain heat transfer performance. The amount of area vacated by the dead drops (and thus made available to active drops) is governed by coalescence and drop departure mechanisms. Again, these effects can only be predicted qualitatively.

The present understanding we have of the subject of dropwise condensation is a result of three main lines of investigation by past researchers: 1) modeling of the drop condensation process, 2) visual observations, and 3) heat transfer measurements. Since so many of the previous models relied on the erroneous film theory of drop condensation, it is not worthwhile to make an extensive literature search in this area. The model proposed by this author in Chapter 8 will be presented with reference to the more recent model of Rose [23,24].

Visual observations of the dropwise condensation have been beneficial in describing many of the parametric trends. Areas of investigation have included determination of nucleation site density, drop population, and size and shape of coalescing and departing drops. These works will be reviewed in the next chapter.

A wealth of heat transfer data exists illustrating the parametric effects on dropwise condensation. This data is useful in testing the accuracy of our heat transfer models and knowledge of the drop condensation process.

Upon completion of the review of visual observations and parametric effects on heat transfer, the work carried out in this investigation will be fully described.

III. VISUAL OBSERVATIONS OF THE DROPWISE CONDENSATION PROCESS

Nearly every experimental paper to be found on the subject of dropwise condensation describes some visual observations of the process. Frequently, the visual portion of the work is merely a verification that good quality drop condensation is taking place. However, some researchers have taken great pains to measure parameters such as nucleation site density, area covered by drops, drop population, departure sizes, and sweeping cycles which are very basic to the full understanding of the dropwise condensation process.

It is unfortunate that a good deal of the visual data obtained by some of the earlier investigators cannot be directly applied to heat transfer measurements. The reason for this is that temperature and heat flux measurements carried out in conjunction with the visual observations are in error for most of these experiments. The effects of these heat measurement errors are discussed in detail in the next two chapters.

As will be shown in Chapters 8 and 9, the correct determination of the drop distribution is essential for the accurate prediction of the heat transfer. Several investigators have counted and measured the number of drops on the condenser surface and presented their results in many different ways. Unfortunately, because of omittance of important pieces of information on their methods of taking and processing their raw data, the results of these investigations are of little use for the purpose of predicting drop condensation heat transfer. For this reason, an experimental program was carried out by this author to supply the necessary measurement of the drop distribution.

The results of past visual investigations of the dropwise conden-

sation process will now be reviewed. The principal purpose in doing this is to supply information to help explain the basic mechanisms of the heat transfer process. In addition, the results of several of the works serve as a basis for comparison for the experimental work carried out by this investigator.

3.1 Drop Population and Area Coverage

Dropwise condensation heat transfer cannot be predicted unless the drop size distribution is known. To perform this calculation, an expression for the number of drops of diameter D to $D + \Delta D$ per unit area as a function of D is needed. Unfortunately, this expression is very difficult to predict analytically and equally difficult to determine experimentally.

Fatica and Katz [5] were the first to attempt such a measurement. Their results, reproduced in Fig. 1, give the number of droplets per unit area as a function of time after the beginning of a cycle. From the distribution data, Fatica and Katz computed that 45 percent of the area was covered by drops of diameter 100 microns or greater. Because of the inconvenient form, no further information can be drawn from their measurements.

Hampson and Ozisik [30] performed a similar experiment and their results are reproduced as Fig. 2. Their data is also not presented in a form useful for computing heat transfer. Figure 2 shows that at the end of a cycle about 54 percent of the surface was covered by drops greater than 125 microns in diameter.

The drop distribution measured by Sugawara and Katsuta [11] and Sugawara and Michiyoshi [29] is presented in Fig. 3. From this figure, the drop distribution $N = 2 \times 10^7 D^{-2}$ can be computed. However, the

authors do not mention the drop measurement band width, ΔD , so that the use of this data is somewhat restricted. The area covered by visible drops (greater than 300μ in diameter) was calculated by the authors to be 54 percent. In addition, the authors figure that another 19 percent of the surface is covered by drops greater than 10 microns but less than 300 microns. They thus concluded that 27 percent of the surface area was available for active drops. This figure agrees reasonably well with the results of this research.

The distributions measured by Sugawara and Katsuta were obtained using surfaces with six different roughnesses. It is interesting to note that within this range of roughness, there is little variation in the drop distribution. However, not enough information was presented in their paper concerning roughness measurements or surface preparation techniques to draw any further conclusions.

The most recent attempt at measuring the drop distribution was carried out by McCormick and Westwater [15]. Their results are reproduced as Fig. 4. The most interesting fact that can be drawn from this work is that the drop distribution for drops smaller than 160 microns is dependent on the temperature difference. There is too little data for diameters greater than 160 microns to make such a judgement. The fractional area covered by drops greater than 2 microns was calculated to be .64 for the lowest drop population (lowest ΔT) and .72 for the highest population.

The temperature differences measured by McCormick and Westwater are not the true temperature potential discussed in the previous chapter. Because they operated with a stagnant system one can rest assured that non-condensable gases affected their experiment. The very low measured

heat transfer coefficient of less than $500 \text{ Btu/hr ft}^2\text{°F}$ substantiates this view. This author feels that the true temperature difference was so low in these experiments that the surface was not saturated with nucleation sites. This accounts for the dependence of the drop distribution on temperature difference as reported in this work.

The results of these four investigations along with the data obtained in this work are compared in Fig. 5 by plotting the area covered by drops versus a nondimensionalized drop diameter. The experimental conditions for these works are summarized in Table 1.

3.2 Nucleation

The nucleation experiments carried out by past researchers were involved in three principal areas:

- 1) Proof that dropwise condensation is a nucleation phenomenon and identification of the nucleation sites;
- 2) Measurement of the number of nucleation sites on the surface as a function of temperature difference; and
- 3) Measurement of the critical temperature difference needed for nucleation and determination of the factors which affect the process.

All of the ten papers which will be mentioned in this section prove that dropwise condensation is a nucleation phenomenon. Tammann and Boehme [12] were the first investigators to determine this fact. The series of papers by McCormick and Westwater et al. [13 to 16] drive home the nucleation concept in a very dramatic fashion.

A great many facts about nucleation have been brought out in these papers. To describe each fact and observation in detail would take a great amount of space. In order to bring together in one paper the experimental observations in this area, the following list is supplied.

List of Experimental Observations Concerning the Nucleation Phenomenon
Associated with Dropwise Condensation

Statement	Reference	Observation
1	12,13,14, 15,16,17, 18,19	Primary drops form at the same sites during successive condensation cycles (whenever surface area is exposed to the vapor due to coalescence or drop departure).
2	12,13,14, 15,16,17, 18,19	Imperfection in the surface such as scratches and pits can be identified as nucleation sites.
3	14,16,19	Liquid debris left in scratches by large sweeping drops became nucleation sites for the next generation of drops.
4	13,14	Artificial sites can be produced by making cavities in the surface with a small needle and by spark erosion. Scratches made by a scalpel also served as nucleation sites.
5	13,14	Foreign particles placed on a condensing surface served as nucleation sites. The relative nucleating ability of particles can be determined by comparing their net heat of adsorption. Particles with the highest net heat of adsorption nucleate best.

Statement	Reference	Observation
6	14,15,19	The number of nucleation sites on a surface increases as the surface to vapor temperature difference increases.
7	13	The nucleation site density is greater for rough surfaces than for smooth surfaces.
8	13	Stainless steel surfaces exhibit greater nucleating ability than copper surfaces.
9	19	The wettability of the surface is an important parameter for nucleation. As the contact angle decreases, the critical temperature difference decreases.
10	15	The nucleation site density increases with pressure for the same surface at the same temperature difference.
11	13,14,15,19	Nucleation sites can be deactivated by drying the surface. The shape of the cavity is important in determining its stability.
12	17,18	The critical temperature difference needed for nucleation depends on the surface energy of the substrate.
13	19	The critical temperature difference for nucleation varies among sites. Pit-like sites are preferred to slip lines and scratches. The size and

Statement	Reference	Observation
		shape of pits and scratches are also important in determining the critical temperature difference.
14	13	Natural nucleation sites are randomly distributed on the surface.
15	19	The presence of nearby large drops tends to suppress formation of primary drops at known nucleation sites.
16	19	Oxide residue in surface blemishes enhances nucleation.

The number of nucleation sites for a particular surface and temperature difference have been measured by several investigators. Table 2 summarizes the experimental conditions and results for these experiments. The temperature differences reported with these densities are probably in error. None of the investigators making these microscopic studies of nucleation took the necessary care in removing non-condensable gases. The ΔT 's so reported are much higher than the true temperature difference. The high nucleation site densities found in this work at the low ΔT of .5 °F (non-condensable gas free system) tend to prove this point. The nucleation results obtained during this investigation will be discussed in Chapter 7.

3.3 Drop Growth Rate

McCormick and Baer [13], McCormick and Westwater [15], and Dolloff and Metzger [31] measured the drop growth rate for dropwise condensation. In all three experiments, the diameter squared was found to vary linearly

with time for all but the smallest drops (see Fig. 6). This relationship for the drop growth agrees with theoretical equations derived by McCormick and Baer [13], Umur and Griffith [21] and Scriven [33].

In Chapter 8, the theoretical prediction of the growth rate of drops will be discussed in detail. It will be shown that for large drops where conduction limits growth, the diameter squared is linear with time. For small drops other resistances dominate and this relationship breaks down.

McCormick and Westwater [15] measured the drop growth rate at two pressures. They estimated that increasing the pressure from 19 mm to 39 mm of mercury increased the drop growth rate by a factor of about 2. Dolloff and Metzger [31] found a similar increase when the pressure was increased from 44.7 psia to 89.7 psia. The pressure effect on growth rate will be discussed from a theoretical standpoint in Chapters 8 and 9.

The above authors also observed that the crowding together of drops on the surface slowed down their growth rate. From their movies they determined that a drop grows fastest when its neighbors were furthest away. McCormick explained this slow down in growth rate to be due to competition for vapor. This author believes that it is the "constriction" resistance caused by non-uniformities in surface temperature that is the real cause. This effect will be discussed later in this paper.

McCormick and Baer [13] noticed a sharp decrease in drop growth rate when non-condensable gases were introduced with the steam. The added diffusion resistance offered by the non-condensables accounts for this slower growth.

3.4 Maximum Drop Size

The maximum size drop which can exist in equilibrium on a surface has been observed in detail in works by Fatica and Katz [5] and Sugawara and Michiyoshi [29]. In these papers a relationship between departure drop size and contact angle has been derived and then confirmed by experimental evidence.

Sugawara and Michiyoshi measured the maximum drop size and the advancing and receding contact angles for a brass surface promoted by oleic acid at several different surface inclinations. Their results are reproduced as Fig. 7. They found that the maximum drop diameter was independent of inclination but that the volume of the drop increased as the inclination approached horizontal down. Their predictions of maximum drop diameters from contact angle measurements, indicated by the x points in Fig. 7, agree well with measured values.

It should be noted that these measurements were made while the condensation was stopped. Therefore no dynamic effects such as drop vibration caused by coalescence are included. Sugawara obtained this data at room temperature ($T = 20^{\circ}\text{C}$).

Fatica and Katz performed similar experiments in obtaining contact angle and maximum drop size information for six metal-promoter systems during atmospheric pressure condensation on a vertical surface. Advancing contact angles ranged from 90 to 110 degrees and receding contact angles from 50 to 85 degrees. The diameter of departing drops varied from 1.6 mm to 3.8 mm. Their measured and calculated results agreed in a similar fashion as did those of Sugawara and Michiyoshi.

A discussion of factors which affect departure drop size is provided in Appendix B. The importance of departure mechanisms will be emphasized in that appendix.

3.5 Conditions Required for Dropwise Condensation

In order to maintain dropwise condensation, nucleation sites must continually be exposed to the vapor. When two drops coalesce, surface area is exposed provided the liquid can recede over the surface.

McCormick and Baer [13,34] have determined that the receding contact angle must be greater than zero for drop condensation to continue.

According to MacDougall and Ockrent [35], the receding contact angle will be greater than zero provided that the normal contact angle measured on a horizontal surface is larger than 50 degrees.* In terms of surface tension, McCormick and Baer [13] demonstrated that for surface tensions less than 46 dyn/cm, no area was vacated after coalescence and mixed condensation resulted.

McCormick and Westwater [15] analyzed the coalescence problem and determined that the maximum area is vacated when coalescing drops are the same size. For equal size drops with 90 degree contact angles, a maximum of 21 percent of the previously wetted area will be vacated during coalescence.

One of the interesting pieces of information obtained from the high-speed movies of Peterson and Westwater [16] is that a drop experiences as many as 400,000 coalescences going from nucleation to departure size. The large number of coalescences emphasizes the tremendous "activity" of the drop condensation process. The authors estimated this coalescence number for their ethylene glycol system (contact angle 72 degrees and maximum drop diameter 1.6 mm).

*The author feels that the receding contact angle must be a good deal greater than zero and the normal contact angle greater than 50 degrees in order to have "good quality" drop condensation. Further research is needed to verify these numbers.

3.6 Sweeping Drops

For condensing surfaces in the vertical orientation, departing drops leave the surface by sweeping down the surface. Sugawara and Michiyoshi [29] determined that the sweeping cycle is reduced as the heat flux is increased and is shorter at the lower part of the condensing surface. Increasing the heat flux results in a higher condensation rate and more departing drops. The reason why the lower portion of a condenser surface gets swept more often than the upper area is that a drop increases in size as it proceeds down the surface sweeping a larger area before it. Fatica and Katz [5] noticed these same effects but added the fact that the track width of sweeping drops becomes constant within 3 to 4 inches of the top of the surface. The increased condensate in the drop from then on elongates rather than widens the drop.

Le Fevre and Rose [36] determined by heat measurements that the drop condensation heat transfer coefficient is independent of plate height in the range of 1 to 4 inches. This seems contradictory to the fact that the sweeping cycle decreases with height in this same range. The probable explanation is that area exposure due to coalescence is more important than area exposure by sweeping at the heat fluxes in the above experiment.

Rose [24] observed that the fractional area covered by moving drops increases as the heat flux is increased from 60,000 to 600,000 Btu/hr ft². His results are reproduced as Fig. 8. He concluded from this observation that the "blanketing" by falling drops should cause a reduction in condenser performance at very high heat fluxes.

The visual observations documented in this chapter help clarify

the mechanisms of dropwise condensation. These results will be used in the next chapter to help explain the parametric effects on drop condensation heat transfer.

IV. PARAMETRIC EFFECTS ON DROPWISE CONDENSATION HEAT TRANSFER

Experimenters have determined the effects of ten parameters on the heat transfer for drop condensation. In this chapter the author will carefully tabulate the results of experiments which best illustrate the parametric trends. In addition, the cause of these effects will be discussed in the light of the previous description of the dropwise condensation process.

It is important to point out that wide discrepancies exist between the results of early investigators. As will be explained in detail in the next chapter on experimental techniques, the principal cause of these discrepancies is the presence of non-condensable gases in the steam. The slightest trace of gas will drastically reduce the heat transfer rate in dropwise condensation. When low coefficients are reported, the probable reason for the error is non-condensable gas effects.

The reader should realize that the graphs presented in Figs. 9 through 16 are intended primarily to illustrate trends. Frequently the levels of the heat transfer coefficient reported for a certain parametric study by different experimenters are not in agreement. This is because other effects (such as non-condensables) are also influencing the particular experiment. However, the parametric trends are usually quite consistent.

4.1 Heat Flux

For pure steam void of non-condensable gases condensing on a vertical copper plate, the heat transfer coefficient increases with heat flux as shown in Fig. 9. At very low heat fluxes (low ΔT 's), the coefficient rises sharply. For higher heat fluxes the coefficient has

been shown to remain nearly constant (curves 1, 3, and 6 of Fig. 9) or increase gradually with heat flux (curves 2, 4, and 5). It will be shown that heat flux does affect the departure sizes of drops and that this could cause slightly increased steam side coefficients.

One of the causes for the increasing coefficient with heat flux is the drop distribution. As the ΔT is increased from zero, the number of nucleation sites increases rapidly. The larger number of sites mean more "active" drops and increased heat transfer. The number of nucleation sites soon reaches a limit which is then little affected by increasing the ΔT , and at this point nucleation ceases to be a controlling factor in the heat transfer process.

As the heat flux is increased, however, the number and size of the large departure size drops are affected. Higher heat fluxes cause early departure of drops resulting in more area available for the "active" drops. This in turn causes a higher heat transfer coefficient. This effect is expected to be small and barely measurable. Other parameters such as vapor velocity and surface roughness can also affect the departure size and the coefficient in a similar way.

It should also be pointed out that the drop growth rate of the very small drops decreases with ΔT to a power greater than one. Since the majority of the heat is transferred through these small drops, then lowering the ΔT should decrease the heat transfer coefficient. The analysis developed in Chapters 8 and 9 verifies this hypothesis.

Figure 10 shows the results of all the experiments attempting to measure the variation of heat transfer coefficient with heat flux for a vertical copper surface. Curves 7 through 14 of Fig. 10 are for experiments where non-condensables have been a strong factor. The re-

maining curves (duplicated in Fig. 9) are, in the opinion of this author, most representative of drop condensation with "gas free" steam. Curves 4a, 4b and 10 of Fig. 10 are much higher than the others due to vapor velocity effects. Table 3 lists the experimental conditions reported in the references [5,7,8,30 and 36 to 46].

The earlier heat transfer data [5,7,8 and 40 to 45] for dropwise condensation is strongly affected by non-condensables. The low coefficients (below 30,000 Btu/hr ft²°F for heat fluxes greater than 50,000 Btu/hr ft² for atmospheric condensation of steam) are primarily due to non-condensable gas effects. Furthermore, many of these investigations have shown that the heat transfer coefficient decreases with heat flux after a certain heat flux is exceeded. Since the non-condensable gas effect increases with heat flux, this also indicates that this data has been governed by non-condensables.

In conclusion, one can say that the heat transfer coefficient increases rapidly at low heat fluxes due to nucleation and drop growth limitations. After this initial rise, the coefficient remains constant or gradually increases with the heat flux depending on how the system affects the departure size of drops. For steam contaminated by non-condensables, low heat transfer coefficients can be expected.

4.2 Pressure

When describing the effects of pressure on the heat transfer coefficient, it is convenient to divide the data into below and above atmospheric pressure. As the sub-atmospheric pressure is increased, the heat transfer coefficient increases. This trend has been substantiated by the works of Gnam [41], Ma [47], Brown and Thomas [48], Tanner et al. [49] and the data obtained in this work (see Fig. 11). The in-

crease in coefficient with pressure is due partly to higher growth rates of the "active" drops caused by variation in thermodynamic properties and partly to the alteration in the size and numbers of "active" drops on the surface. The relative importance of these two factors will be discussed in Chapter 9.

There is rather poor agreement between the two experiments carried out to measure the heat transfer coefficient for pressures greater than atmospheric (Fig. 12). Wenzel [38] reported a gradually decreasing coefficient as the pressure increased from 1 to 4 atmospheres. Contrarily, in this region Dolloff and Metzger [31] found the coefficient to increase sharply. However, above a certain critical pressure, he observed that the coefficient decreases and then gradually increases again as the pressure is increased.

It is difficult to say which of these pieces of data should be trusted. As will be pointed out in Chapter 9, increasing the pressure beyond atmospheric causes property changes resulting in slower drop growth rates and a gradual decrease in coefficient. However, if the number of "active" drops continues to increase with pressure (the trend noticed for sub-atmospheric pressures), then this could cause an increase in coefficient. Depending on which effect is stronger, decrease in growth rate or increase in number of drops, the coefficient could increase or decrease with pressure above atmospheric.

The experimental conditions described in the seven investigations into pressure effects are tabulated in Table 4.

It can safely be said that experiments have shown that the heat transfer coefficient for dropwise condensation increases with pressure below atmospheric. This increase is due both to favorable drop growth

and drop distribution effects. Above atmospheric pressure there is discrepancy in the heat transfer data. Drop growth rates are expected to decrease with higher pressures but population of active drops to increase. The result could be a steady increase, steady decrease, or increase and then decrease in coefficient with increasing pressure above atmospheric.

4.3 Non-Condensable Gases

Undoubtedly, non-condensable gases can affect the performance of dropwise condensation more than all the other parametric changes combined. Even the smallest amounts of non-condensables allowed to accumulate near the condensing surface offer such a high thermal resistance that it dominates over the small thermal resistance of drop condensation. Wenzel [38], Furman and Hampson [50], Hampson [51], Tanner et al. [39, 49], Le Fevre and Rose [36] and others have shown that the steam side heat transfer drops rapidly as non-condensable gas content is increased.

The velocity of the steam-gas mixture is actually more important than the concentration of gas. For a stagnant system the gases in the steam are carried towards the condensing surface by the steam and remain in the vicinity of the surface causing a high mass transfer resistance. A large enough steam velocity past the surface, however, will sweep away the non-condensables reducing this resistance greatly.

When comparing heat transfer data in the drop condensation literature, one frequently finds low values for the heat transfer coefficient for experiments with supposedly "gas free steam". Le Fevre and Rose [36] have shown that no matter how long one deaerates the steam, sufficient non-condensables remain to affect drop condensation. The six investiga-

tions in which the correct heat transfer coefficient for gas free steam have been measured have demonstrated the need for close venting [36,46] or reasonably high vapor velocities past the condensing surface [30, 37 to 39] to minimize the resistance due to non-condensable gases.

Non-condensables can also affect drop condensation by causing early breakdown of the promoter. The result is a "sloppy" drop condensation and a lower condensing rate.

The conclusion that can be drawn about non-condensing gases is that they drastically reduce the dropwise condensation heat transfer coefficient. The reduction is due to the addition of a large diffusional resistance effectively lowering the temperature difference which drives the condensation. The effect of non-condensables increases with gas concentration but can be minimized by providing sufficient vapor velocity past the condensing surface.

4.4 Vapor Velocity

The most important role that vapor velocity plays in dropwise condensation is in the removal of non-condensable gases near the condensing surface. However, it has been shown by Tanner et al. [39], O'Bara et al. [52], and this author (see Fig. 13 and Table 5) that increasing the velocity in excess of the critical velocity needed to eliminate non-condensables also increases the heat transfer coefficient. This increase is due to early removal of departing drops.

O'Bara, et al. [52] have shown that too high a velocity can decrease the heat transfer. They explained that high velocities (greater than 5 ft/sec) cause a large shear stress which tends to flatten the drops. These flat drops will then occupy more surface area leaving less area available to the small "active" drops on the surface.

In conclusion, one can say that velocity increases the heat transfer coefficient for dropwise condensation. Starting from a stagnant system, the initial increase in velocity causes a rapid increase in condensation rate by removing non-condensing gases. Further increase in velocity above the value needed to remove non-condensables, increases the coefficient by early removal of departing drops. At very high vapor velocities, there could be an adverse effect caused by a flattening of the drops by the shearing action of the vapor.

4.5 Conductivity of Condensing Surface

Increasing the thermal conductivity of the condensing surface increases the heat transfer coefficient. Both Tanner et al. [53] and Griffith and Man Suk Lee [54] have shown that the steam side heat transfer coefficient is nearly 5 times greater for copper than for stainless steel. This trend is illustrated in Fig. 14 and Table 6*. Tanner and his colleagues demonstrated that this effect is most pronounced at larger heat fluxes. The paper of Hampson and Ozisik [30] showed that the coefficient decreased in the order: Copper > Brass > Cr Ni > Monel > Staybrite.

Mikic [28] has explained the effect of conductivity by describing a "constriction" resistance caused by the non-uniformity in surface temperature. He shows that lowering the conductivity of the surface increases this resistance and thus lowers the measured steam side coefficient. Lowering the thermal conductivity of the substrate decreases the "true" vapor to surface temperature difference. This in turn decreases the growth of the "active" drops and lowers the heat transfer

*The data of Griffith and Man Suk Lee is for a horizontal surface facing down. This is one reason why their data is considerably lower than that of Tanner. Also the author feels that there were errors in the measurement of the wall temperature in the former experiment. Neither of these effects alter the reported trend for conductivity and roughness.

coefficient. A further description of the constriction resistance will be presented in Chapter 8 and in Appendix G.

It is interesting to note that the increased nucleating ability of stainless steel as compared to copper (reference [13]) is offset by the constriction resistance. That is, the large "dead" drops affect heat transfer more than the increased number of "active" drops for low conductivity surfaces.

4.6 Surface Finish

Tanner et al. [53], Griffith and Man Suk Lee [54] and this author have found that heat transfer is higher for mirror smooth surfaces than for rough surfaces (Fig. 15 and Table 6). Surface finish can affect dropwise condensation by (1) altering the nucleation characteristics of the surface, and (2) changing the shape and size of the large drops.

Rough surfaces have more nucleation sites than smooth surfaces. Thus rough surfaces should have a greater number of "active" drops and exhibit higher heat transfer coefficients. Since it has been demonstrated that the coefficient decreases with roughness, it can be concluded that nucleation effects are again offset by other considerations.

Due to contact angle hysteresis caused by rough surfaces, the size and shape of drops are altered. It can be expected that more irregularly shaped drops will occur on rough surfaces decreasing the area exposed when two drops coalesce. In addition, the departing drops will be held back longer on rough surfaces. Both of these effects tend to decrease the amount of "active" area and consequently the heat transfer performance.

4.7 Surface Inclination

Surface inclination affects the dropwise condensation process by

varying the shape, volume, and sliding speed of falling drops. It will be shown in this paper that 90 percent of heat is transferred through the small drops (less than 150 microns). Therefore the inclinations that cause early departure of drops and rapid sliding speeds should give the best heat transfer.

The investigators [30,32, and 38] who measured the effect of surface inclination on heat transfer, all found that the coefficient is greatest when the plate is in the vertical position and decreases with departure from the vertical in either direction (see Fig. 16 and Table 7). Rose [32] performed the most exacting experiments varying the inclination in intervals of 10 degrees for five different heat fluxes. He observed that the coefficient has two maximums: one at 90° (vertical) and the other at 135° (45° facing down). These peaks in the coefficient versus inclination curves are most pronounced at the higher heat fluxes.

In Appendix C, the topic of drop departure mechanisms and their effect on heat transfer will be discussed. The experimental results, that the coefficient is greatest for a vertical surface, is consistent with the fact that departure sizes are smallest for this orientation.

4.8 Location on Condensing Plate

Le Fevre and Rose [36] measured local steam-side coefficients at three locations on a vertical copper surface. They found that the local coefficient does not significantly depend on plate height from 1 to 4 inches from the top. Shea and Krase [43] also measured coefficients at several height locations and found the coefficient to decrease with distance from the top surface. However, this decrease can be attributed to velocity and non-condensable effects.

It is surprising that distance from the top of a vertical plate

has so little effect on the heat transfer coefficient. The frequency at which a point on the surface is swept increases with distance down the plate. This means that the maximum drop size at points toward the bottom of the surface should be less than at the top of the surface. However, it is not certain whether the amount of area cleared by the sweeping action of falling drops is significant compared to that cleared by the coalescence mechanism at certain heat fluxes.

Since Rose has shown that the heat transfer coefficient is not height dependent, then one can conclude that the number of "active" drops does not vary significantly with the location on the surface.

4.9 Condensing Vapor

Dropwise condensation has been observed for many vapors besides steam. Topper and Baer [55], using a Teflon-coated surface, maintained drop condensation with aniline, ethylene glycol, benzene, and nitrobenzene. Bobco and Gosman [56] observed dropwise condensation of isooctane, decalin, ethanol, carbon disulphide, cyclohexane, isooheptene, and methyl alcohol on a surface promoted by fluorinated acids. Without any promoter, mercury has been observed to condense in the dropwise mode by Misra and Bonilla [57] and Ivanovski [58].

Due to the wide variation in apparatus used by the experimenters, it is fruitless to compare the heat transfer from vapor to vapor. Since the largest resistance for "gas free" drop condensation is the conduction resistance through the drop, one can surmise that liquids with the largest thermal conductivity will exhibit the highest heat transfer. Of course, this statement is made assuming that the drop distribution and the quality of the drop condensation for the materials are comparable. Because of the large range of wetting ability of various fluids, this

assumption is probably not valid.

4.10 Promoter

In order to obtain dropwise condensation, steam must come in contact with a cold hydrophobic (non-wetting) surface. The non-wetting characteristic of the surface is brought about by "promoting" the surface. The best promoter is one which adds an insignificant thermal resistance due to its thickness, has a long life, and causes "good quality" dropwise condensation. Promoters can be categorized as: (1) chemically adhering, (2) physically adhering, (3) non-adhering, and (4) noble metals. A wealth of literature [59 to 68] exists describing studies of promotion techniques. These deal with the structure of the promoters, the length of their lives, and their applicability for industrial condensers.

It is not advisable to measure the performance of promoters by comparing data of one experimenter with another. Other considerations such as non-condensable gases, velocity, orientation, etc. outweigh the promoter effect. However, Tanner et al. [53] and Le Fevre and Rose [36] each took heat transfer data with several promoters and thus the relative merit of these promoters can be compared. Tanner reported that the heat transfer coefficient increased in the promoter series: Dibenzyl disulphide < Dioctadecyl disulphide < Montan wax and Montanic acid. Rose reports higher coefficients in the series: Dioctadecyl disulphide < "No. 1 Amine" (octadecylamine) < Di-S-octadecyl, 10 decanedixanthate < Dodecanetris (ethanethio) silane. In each investigation there was an increase in coefficient by about 50 percent in going from the first to the last promoter in the series.

The promoter can affect the condensation by altering the contact angle of the drops and introducing a significant thermal resistance due

to its thickness. Lowering the contact angle decreases the amount of area exposed by coalescence and adversely affects the size and shape of drops. These in turn decrease the number of "active" drops on the surface. Introduction of an added promoter resistance lowers the "true" temperature difference and thus slows down the condensation rate. The results of both effects would be a lowering of the measured heat transfer coefficient.

4.11 Summary

The parametric effects on dropwise condensation heat transfer are summarized in Table 8. The primary cause for the performance of the heat transfer (whether due to growth rate or number of "active" drops) is indicated for each case.

V. EXPERIMENTAL APPARATUS AND PROCEDURES

The previous chapter has demonstrated that extreme care is needed in order to obtain accurate heat transfer measurements for dropwise condensation. The series of papers by Rose [36 and 46] and Tanner [39,49, 53] and their colleagues have carefully documented the important factors which affect accuracy in drop condensation experiments. The papers emphasize that non-condensable gases and errors in measuring the surface temperature account for the large discrepancies in heat transfer data encountered in the literature.

Several months were wasted in this research because some of the recommended procedures were not closely observed. In order that future researchers do not encounter the same problems which this author did, a detailed description of the steps the author took in obtaining accurate heat transfer and photographic measurements will be provided.

5.1 Description of Apparatus

5.1.1 Design of Vapor System and Chamber

There were two principal considerations governing the design of the vapor system: elimination of the non-condensable gas problem and convenience for microscopic investigation. Luckily, the best designs for each consideration were compatible with each other.

The non-condensable gas problem was overcome by building a small, reasonably vacuum tight, "straight through" system. Vapor was generated in the boiler section in two 4 liter glass Erlenmeyer flasks at a maximum rate of one cubic foot per minute. The vapor was led to the condensing chamber by a short section of 3/4 inch ID rubber vacuum tubing and passed "straight through" into the exit end of the system. At the highest condensation rates only one quarter to one third of the steam

was condensed. In all tests the vapor flow was great enough to sweep away any non-condensables from the condensing surface.

The system could be operated at pressures from atmospheric down to 30 mm of mercury. For atmospheric pressure operation, heat was supplied to the boilers by two 1.5 KW hot plates and the vapor was allowed to pass through the exit valve into the atmosphere. Lower pressures were maintained by lowering the power of the hot plates and utilizing an aspirator pump. The pressure desired could be regulated by controlling the bleed valve in conjunction with the power input to the boiler. The pressure in the chamber was measured to .1 mm Hg with an absolute mercury manometer.

A vapor flow rate of .25 cubic feet per minute (corresponding to an entrance vapor velocity into the chamber of 3 feet per second) was found to be sufficient to minimize non-condensable gas effects for both atmospheric and low pressure operations. The vapor flow rates were determined by passing the vapor produced in the boiler into a large condenser and measuring the condensate flow with time. A flow meter was also used to check these results. Agreement to within ± 10 percent was obtained. Figure 17 represents a schematic of the vapor system.

The design of the condensing chamber is particularly important in insuring "gas free" results. The chamber should be small and free of potential dead air spaces. The chamber used, illustrated in Figs. 18 and 22, was the second one designed, built, and tested. The original chamber was much larger (6 inches ID and 4 inches deep) than the second (2.65 inches ID and .5 inch deep). In the first chamber, because of its size, non-condensables were allowed to collect in stagnant pockets. At the time the large chamber was used, the boiler output was also

lower resulting in a significantly slower vapor velocity past the condensing surface. Table 9 dramatically shows the increase in measured coefficient when the small "gas free" system was used as opposed to the larger system. This again emphasizes the importance of taking great care in eliminating non-condensable gases in dropwise condensation experiments.

While testing out the condensing chambers, the author noticed that when non-condensables were present, low frequency temperature fluctuations of up to 1 °F existed at the surface. Le Fevre and Rose [36] have explained that these fluctuations are due to a mixing of the gas-vapor mixture by the action of the falling drops. When the small chamber was used with high vapor flow rates, these temperature fluctuations at the surface ceased to exist.

5.1.2 Design of Test Section

Because of the high heat transfer coefficients (up to 50,000 Btu/hr ft²°F) encountered in dropwise condensation, precise temperature measurement techniques are required. The papers by Le Fevre and Rose [36] and Citalogu and Rose [46] carefully outline some of the more important considerations.

Great care was carried out in this experiment to insure accurate temperature readings. Only high precision thermocouple wire, lead wire, thermocouple switches, and potentiometer were used. Seven thermocouples were placed along the axis of the .8 inch diameter, 2 inch long copper test section. In order to minimize errors due to conduction along the thermocouple wire, .005 inch diameter wire (copper-constantan) folded over twice was inserted in the .030 inch diameter holes (see Figs. 19

and 20 for details). In this way, the immersion depth was increased from .4 inch to over 1.5 inches. Appendix A describes the thermocouple mounting techniques and immersion tests in greater detail. In Table 9, the magnitude of the error due to incorrect temperature measurement is estimated.

The copper test section was soldered to the stainless steel adaptor sleeve which provided a tight O-ring seal in the back of the condensing chamber. Cork and fiber glass insulation wrapped around the copper section insured uniform axial conduction along its length. The condensing surface protruded about .1 inch beyond the inside chamber wall into the vapor (see Fig. 18).

The rear of the test section butted up against the cooling water chamber. Figure 21 represents a schematic of the cooling water loop. Ice water from a 60 gallon drum, warm water from a 30 gallon drum, or city water could be pumped through the cooling chamber at rates from 1 to 10 gallons per minute. The heat flux was controlled by varying the flow rate and temperature of the water flow. In addition, minor changes in heat flux could be controlled by varying the pressure of the cooling chamber against the rear of the test section (thus varying the contact resistance between the two surfaces).

5.1.3 Microscopic and Photographic Equipment

One of the primary goals in the experimental program was to obtain detailed microphotographs of the dropwise condensation process. The purpose was to take pictures at several magnifications in order to measure the drop size distribution.

A specially constructed microscope mount was designed to enable

movement of the scope in the vertical and horizontal directions. This permitted exact location of the microscope's field of view on the surface. Long working distance objective lenses (made by Vickers) permitted high magnification (up to 400X) observation of the condensation process through the glass window. A Polaroid film pack adapted to a Leitz shutter mechanism was used to take the microphotographs.

Two types of lighting were utilized in order to get the large range of pictures needed for complete photographic coverage of the drop size spectrum. Most of the pictures were taken using a standard vertical illuminator mounted behind the objective lens. When the 1/125 second shutter speed of the camera was sufficient to stop the action, an incandescent bulb was used as the light source for the illuminator. For high magnification (200X and 400X) pictures, it was necessary to use a strobe lamp of duration 10 microseconds placed inside the vertical illuminator to stop the action of the small "active" drops. When this technique was used, two vertical illuminators were mounted in series on the microscope. The illuminator with an incandescent bulb was first used to focus the microscope on the surface and then shut off. The strobe illuminator could then be blinked while the shutter of the camera was opened to take the picture. Figure 23 shows the complete test setup.

5.2 Heat Measurement Procedures

5.2.1 Preparation of the Surfaces

Most of the heat transfer and photographic data were taken using a mirror smooth, chemically promoted, copper surface. The steps in preparing the surface for a typical run were as follows:

1. The surface was polished to a mirror finish by rubbing it on

a metalurgical polishing cloth soaked with first .3 micron and then .05 micron aluminum oxide polishing compound. All traces of oxide and promoter debris were removed by this process.

2. The polished surface was carefully washed with a cotton swab and distilled water.

3. The specimen was further washed by rubbing the surface with a cotton swab soaked with carbon tetrachloride. At this time the surface was examined to insure that it was free of lint or other impurities. Following this washing, the surface was immersed face down in a basin of carbon tetrachloride for 10 minutes.

4. The surface was then immersed face down in a basin of promoter solutions consisting of 1 percent by weight of dioctadecyl disulphide dissolved in carbon tetrachloride and allowed to stand 15 minutes.

5. From the promoter bath, the test section was quickly placed in position in the condensing chamber, the cooling water turned on, vapor introduced, and condensation begun.

The rough surface used in the tests was prepared by rubbing the mirror smooth surface in random directions on 500 grit aluminum oxide emery paper. The same cleaning and promoter sequence used for the mirror surface followed after this roughening.

It should be noted that on several occasions when a new test section was promoted for the first time, poor quality drop condensation resulted. After several polishing, cleaning, and promotion cycles were carried out, good quality drop condensation was obtained. The same event occurred when first attempting to promote the newly roughened surface. The explanation must be that the chemical bond between the promoter and copper is not strong for first-time promoted surfaces.

The procedure used to produce the Teflon surface was recommended by engineers from the E. I. Du Pont De Nemours Company. Teflon 30 TFE fluorocarbon resin was diluted to a 5 to 10 percent solid dispersion. A .1 mil brushed chrome surface was first electrodeposited on the mirror smooth, copper surface.* The surface was then dipped in the TFE resin, withdrawn, and the excess liquid drained. A hot air gun was used to fully dry the surface. After drying, the test section was then sintered in a 700 °F oven for 30 minutes. This completed the coating procedure.

Before each condensing run, the Teflon surface was merely wiped clean with a cotton swab soaked with carbon tetrachloride. The same teflon surface was used for three condensing runs spread over a period of one month. During this period the quality of the condensation was as good as the chemically promoted surface.

5.2.2 Heat Transfer Data Taking and Processing Procedures

Citakoglu and Rose [46] have shown that promoting a copper surface with dioctadecyl disulphide in the above manner leaves an overabundance of promoter on the surface. This extra promoter thickness constitutes a measurable thermal resistance. As the washing action of the condensation process removes the excess promoter from the surface, the measured heat transfer coefficient increases. It is not until all but a monolayer of promoter is left that the coefficient levels out at its steady value.

The procedure used in this experiment was to permit rapid condensation to take place for at least 3 hours before reportable heat transfer data was taken. In the next chapter, this transient effect is further described. Later in the project, it was found that the transient time

*The chrome prevented oxidation of the copper during the high temperature sintering step.

(time before excess promoter was washed off and the coefficient remained steady), could be shortened by spraying the surface with carbon tetrachloride just after removing it from the promoter bath and before placing it into the chamber.

A typical "data point" was taken by measuring the vapor temperature with two thermocouples located inside the condenser chamber and the temperature at seven locations along the axis of the test section. The average of the two vapor thermocouple readings were taken as the vapor temperature.* Excellent linear gradients (see Fig. A-4) were found to exist along the test section and these were converted to heat flux by the Fourier rate equation. The surface temperature was found by extrapolating the temperature gradient to the surface. Knowing the heat flux and the vapor and surface temperatures, the heat transfer coefficient can be computed.

The selection of the "best" straight line temperature gradient through the temperature data was done using least square techniques with a computer. This procedure removes any bias the experimenter might be inclined to add to the data. Appendix I lists the computer program written to process the data, and several examples of the linear temperature gradient measured through the test section.

5.3 Drop Distribution Measurement Procedures

5.3.1 Photographic Procedure

The mirror smooth chemically promoted surface was used for the runs in which microphotographs were taken of the dropwise condensation process. The surface was prepared in the same way as for a heat transfer

*The two vapor thermocouples consistently agreed with each other to within .05 °F.

run. Photographs were not taken until after three to four hours of condensation had taken place to insure that data was taken while on the flat portion of the transient curve. While photographs were taken, heat flux- ΔT measurements were made to determine the operating conditions.

Once steady condensation was achieved, the photographic work was begun. In order to obtain data over the complete range of measurable drop sizes (diameters from 10 to 3000 microns), photographs were taken at six magnifications from 5X to 400X. Photographs were taken randomly with respect to time so that there would be no agreement between the frequency of the pictures and the frequency of the coalescence and sweeping cycles.

The ideal way to measure the drop distribution is to take a picture of a large section of condenser surface. By measuring and counting every drop from nucleation to departure size on the surface and dividing by the surface area, an accurate spatial average could be obtained. Unfortunately, due to limitations of optics, this is not possible.* Instead, pictures must be taken at several different magnifications. Because the field of view at the high magnifications is so small, a large number of pictures must be taken to insure that a representative sample is obtained.

By counting the number of drops of a particular diameter on each picture and then taking the average over the number of pictures, a representative count can be obtained for that drop size. This was the procedure used in this experiment. The microscope was focused at a particular point on the condenser surface** and a sequence of pictures taken in a

*To get sufficient optical resolution to see the smallest drops (order of .1 micron) would require magnifications of over 400X. The field of view at this magnification is so small that the large drops could not be seen.

**The point of focus was chosen arbitrarily near the center of the surface.

random fashion with respect to time. In this way a time average of the number of drops of a particular size appearing within the field of view of the microscope was obtained.

The time average can be shown to be equal to the space average by relying on the ergotic hypothesis. The ergotic hypothesis states that for random processes, the two averages are equal. It has been shown by McCormick and Baer [13] that nucleation sites are randomly distributed on the surface. Thus, it can be assumed that any size drop in the drop spectrum can exist on any point of the surface at any time.

A question arises concerning how many pictures should be taken at each magnification. In order to obtain approximately the same confidence level for the drop counting data at each magnification, it is necessary to increase the sample size with magnification. This is because at high magnifications the field of view is small with respect to the large size drops. For this reason, 150 pictures were taken at 400X, 100 at 200X, 55 at 120X, 40 at 60X, 24 at 10X and 16 at 5X. Appendix J discusses the picture taking procedures in greater detail.

5.3.2 Drop Counting Procedure

After the sample of photographs were taken, the next job was to count and measure the drops. At first an attempt was made to count and measure every drop which could be resolved in the pictures. It soon became evident, after counting several hundred drops on each photograph, that this procedure was far too time consuming. A drop was measured by comparing its size with the spacing between two parallel lines scribed on a clear plastic sheet.

The procedure decided upon was to choose ten to twenty drop sizes ranging from 10 microns to departure size. Next, by examining the photo-

graphs, it was decided at which magnifications a particular size drop could be most accurately counted and measured. All drops within a certain band width on either side of the mean diameter were counted and considered to be of that size. Thus, on any one photograph all drops of size $(D-\Delta D)$ to $(D+\Delta D)$ were counted and recorded to be of size D . Frequently the same size drop was measured and counted at two different magnifications to insure agreement from one set of photos to another.

The entire sample of photographs were first processed using a drop measurement band width of ± 10 percent. Because of the lack of clarity of the periphery of the drops at higher magnifications, it was decided that this band width was too small. It was just too difficult to decide for sure whether or not a drop should be considered to be in that small band width. For this reason the pictures were again analyzed using a band width of ± 20 percent. The author feels that the results obtained from this counting are more accurate.

5.3.3 Limitations of Microscopic Equipment

The smallest drops which could be accurately measured and counted on the surface were 10 microns. Smaller drops down to about 1 micron in diameter could be seen on the microphotographs but not measured and counted with sufficient accuracy. Greater microscopic resolution will be required in order to obtain data for drops less than 10 microns.

It is difficult to get improved resolution because of two experimental problems. First, higher power objective lenses needed to give greater resolution have working distances so small that the large drops bump into the lense. Second, it is extremely difficult to stop the motion of the small "active" drops at high magnifications. These short-

comings must be overcome to obtain drop distribution data down to nucleation size drops.

VI. RESULTS OF HEAT TRANSFER MEASUREMENTS

6.1 General

The parametric effects of heat flux, pressure, surface roughness, vapor velocity, Teflon promotion, and time have been investigated in this work. These parameters were chosen because they are applicable in answering the basic question of what are the limiting mechanisms for dropwise condensation. The data presented here is for steady state, "non-condensable free"* , good quality dropwise condensation of steam on a vertical copper surface promoted by dioctadecyl disulphide and Teflon.

In the paper of Le Fevre and Rose [36], the authors discuss the advantages and disadvantages of certain ways of presenting drop condensation heat transfer data. They pointed out that the traditional plot of heat transfer coefficient versus heat flux can be misleading when errors in temperature difference are appreciable. For this reason graphs of surface to vapor temperature difference versus heat flux are used to present the basic heat transfer data. Where appropriate, the heat transfer coefficient is plotted against the parameter being varied (such as pressure or velocity). In addition, plots of heat transfer coefficient versus temperature difference are provided to illustrate trends used for comparison purposes in later chapters.

For all cases in which heat flux- ΔT data was taken, the results were well represented by a linear relation:

$$\Delta T = m Q/A + b \quad . \quad (6.1)$$

*The term "non-condensable free" is used to signify the absence of errors due to non-condensing gases. As discussed in the previous chapter, extensive precautions were taken to insure that non-condensing gases were not allowed to accumulate near the surface.

The best straight line was chosen through the data by least squares technique with a computer (see Appendix I for listing of program). The heat transfer coefficient- ΔT relationship can be determined from equation (6.1):

$$h = \frac{1}{m} \left(1 - \frac{b}{\Delta T} \right) \quad . \quad (6.2)$$

This equation predicts that the coefficient is zero for $\Delta T < b$. Thus, the critical temperature difference, ΔT_{crit} , needed to drive the drop condensation process is b . The coefficient increases with ΔT until, for large ΔT 's, the heat transfer coefficient is nearly constant and equal to $1/m$.

The author feels that the principal contribution made by the heat transfer data obtained during this experiment is the accurate coefficients measured at very low surface to vapor temperature differences. Up to now there has been little reliable data taken of ΔT 's below 1 °F. It is hoped that these experiments will clarify the temperature difference effect on the heat transfer coefficient for dropwise condensation.

6.2 Results for a Mirror Smooth, Chemically Promoted Surface

Figures 24 and 27 present "gas free", dropwise condensation heat transfer data for a vertically oriented, mirror smooth, chemically promoted surface at atmospheric and low pressure (34 mm Hg). The data presented in these figures was taken over a period of several months.

Greater scatter existed in the data taken from day to day as compared to the data taken during one run. Over 90 percent of all the data was well within the ± 10 percent scatter band on ΔT - q/A plots. The straight line plotted through the data is the one chosen by least squares technique by computer.

Figure 27 illustrates the performance of heat transfer coefficient

as a function of temperature difference.* The constant value of the coefficient for atmospheric pressure (38,200 Btu/hr ft²°F) is nearly three times greater than that for low pressure (13,500 Btu/hr ft²°F). In both cases, the coefficient starts to drop sharply at about .5 °F. At a ΔT of .15 °F, the coefficients are 50 percent of their constant values. The decrease in coefficient at the low ΔT 's is due partly to a slowing down of the growth rates and partly to a decrease in the number of "active" drops. The model derived in Chapter 8 and discussed in Chapter 9 predicts this trend.

6.3 Results for a Rough, Chemically Promoted Surface

The rough surface (prepared by rubbing on 500 grit emery paper) showed a similar trend with ΔT as the mirror smooth surface (see Figs. 25, 28 and 29). The constant value coefficient (for $\Delta T > 1^\circ\text{F}$) for the rough surface was 30 percent below that for the mirror surface at atmospheric pressure and 20 percent lower for low pressure condensation. This drop in heat transfer performance with roughness is attributed to the adverse effects on the shape and size of large drops.

An important observation can be made about the rough surface operating at low ΔT 's. For a ΔT below .2°°F, the rough surface exhibits higher heat transfer rates than the mirror smooth surface. The relatively high coefficient at low ΔT for the rough surface is due to its greater nucleation characteristics. At very low ΔT 's, nucleation theory predicts that a rough surface will have a greater number of nucleation sites.

From these results it can be concluded that a mirror smooth surface gives better performance than a rough surface at normal operating conditions.

* The curve plotted through the h versus ΔT data was chosen by computer from Eqs. (6.1) and (6.2).

However, when operating at extremely low ΔT 's, a rough surface may be desirable due to its greater nucleating ability.

6.4 Results for a Teflon Coated Surface

Figures 26, 28, and 29 show the rather large decrease in heat transfer performance for the Teflon surface compared to the chemically promoted surfaces. The reason for this is that the Teflon coating introduces a significant thermal resistance due to the conduction loss across its thickness. The resistance of the Teflon layer can be calculated knowing its thickness and thermal conductivity and added in series with the condensation resistance.

The conduction heat transfer coefficient for Teflon 30 TFE-Fluorocarbon resin of thickness 1.5 microns (5×10^{-5} inches) is 20,000 Btu/hr ft²°F.* The overall coefficient (promoter in series with condensation resistance) of the Teflon surface is about one third that of the mirror smooth, chemically promoted surface at atmospheric pressure and a little over half at low pressure. In Appendix H, the overall heat transfer coefficient is predicted as a function of the thickness of the Teflon layer.

6.5 Results of Pressure Tests

Heat transfer data was taken with the vertically oriented, mirror smooth, chemically promoted surface at 30 different pressures ranging from 24 mm Hg up to 760 mm Hg. A constant ΔT of about 3 °F was maintained while the pressure was varied. As demonstrated in Fig. 30, the heat transfer coefficient decreases linearly with saturation temperature over this range. Figure 11 shows the same data plotted against saturation pressure and compared to the data of previous investigators.

* Du Pont, the manufacturer of Teflon 30, predicts a layer thickness of 1.5 microns when following their suggested application techniques.

The following linear relation was found to exist between the heat transfer coefficient and the saturation temperature in the range of T_{sat} between 77 °F to 212 °F for a ΔT of 3 °F:

$$h = 220 (T_{sat} - 32) \quad . \quad (6.3)$$

In this relation, h is measured in units of Btu/hr ft²°F and T_{sat} in °F.

Equation (6.3) probably specifies the relation between heat transfer coefficient and saturation temperature over a sizeable range of ΔT 's. However, at low ΔT 's where nucleation becomes important, this relation would change. Also, at very high heat fluxes other mechanisms would dominate and the equation would not be valid.

Chapter 9 will explain that the decrease in heat transfer coefficient with pressure is due to two factors: the decrease in drop growth rate due to property changes, and the alteration in the drop distribution resulting in fewer active drops.

6.6 Results of Velocity Tests

During early tests, a low capacity boiler was used resulting in an insufficient vapor velocity past the condensing surface. The heat transfer coefficient (see Table 9) was found to be low for these low velocity tests due to non-condensable gas effects.

With the higher capacity boiler, a vapor flow rate of 1 cubic foot per minute could be achieved resulting in a maximum vapor velocity at the entrance of the chamber of about 12 feet per second. It was found that a velocity of 3 feet per second at the chamber entrance was sufficient to eliminate all non-condensable effects.* With this velocity

* In all tests the vapor blew across the condensing surface.

the downward track of the falling drops was nearly vertical.

Heat measurements were made at four velocities to determine the effect of excess velocity on drop condensation on a vertical surface. The sweeping angle which the falling drops made with the vertical was also measured. The variation of heat transfer coefficient and sweeping angle with vapor velocity is shown in Fig. 31. For velocities less than 3 feet per second, surface temperature fluctuations indicative of non-condensable gas effects became noticeable. Because of these temperature fluctuations, heat transfer-velocity measurements were not made in this region. The dotted line represents only the author's guess at the shape of the curve for low vapor velocities.

The initial rapid increase in coefficient with velocity (illustrated by the dotted line of Fig. 31) is due to the removal of non-condensing gases from the vicinity of the condensing surface. The gradual rise in heat transfer for velocities greater than 3 feet per second is a result of early departure of the large drops due to the shearing action of the vapor.

6.7 Transient Effects

Surfaces promoted with dioctadecyl-disulphide (and probably other chemical promoters of the same type) are strongly time dependent in the early stages of their use. During the first hour or two of condensation, the coefficient first rises and then drops sharply (see Fig. 32).

The rise in coefficient is due to the removal of excess promoter by the washing action of the drop condensation process. As the thickness of the promoter layer is decreased, the conduction loss through the promoter is lowered and the overall steam side coefficient (promoter plus condensation resistance) increases. It is thought that all but a monolayer of promoter remains chemically bonded to the surface.

The sharp drop-off in coefficient is surmised to be due to an alteration in the wetting characteristics of the surface. This could affect both the quality of the condensation and the nucleating ability of the surface.

After about three to four hours of rapid condensation, the coefficient levels off and remains nearly constant with time. The results of runs made on five different days are illustrated in Fig. 32. One notices that there is a slight difference in the steady state value of coefficient from day to day. The scatter of ± 10 percent about the average of 38,200 Btu/hr ft²°F is the maximum encountered throughout the experiments. The data indicated by dots is for the rough surface.

Thirteen hours was the longest duration of any run made during this project. One should note, however, that the coefficient will begin to decrease gradually after an extended period of condensation. This is due to a breakdown in promoter effectiveness in maintaining a non-wetting surface. As the quality of the condensation becomes poorer, the coefficient will decrease.

Citakoglu and Rose [46] also reported a transient effect during their experiments with a surface promoted with dioctadecyl-disulphide. They noticed that the coefficient increased sharply during the initial stages of condensation similar to this experiment. However, they noticed no peak and subsequent decrease in coefficient. Their coefficient merely leveled out after the initial increase. The disagreement between Rose's and this author's transient curves is probably due to different surface-promoter characteristics.

6.8 Results of Vibration of Surface^{*}

Some preliminary heat transfer measurements were made while vibrating the test section in and out of the condensing chamber. The vibration was done by coupling the test section and cooling water chamber assembly to a "shaker" manufactured by Goodman Industries. The purpose of the test was to show that vibrating the surface would shake off the departure size drops prematurely and result in an increase in heat transfer.

Unfortunately, only a limited amount of data was taken during these vibration tests. The shaker burned out after part of the data was taken for the first heat flux to be investigated. The results are summarized in Table 11.

The slight increase in coefficient with vibration is due to early removal of departing drops. This effect is discussed in Appendix B. The data indicates that high vibrational frequencies are more effective to this end.

It should be pointed out that vibration should show a greater effect for horizontally oriented and low conductivity surfaces. For these surfaces, the large departing drops play a significant role in lowering the coefficient. Verification of this trend would be beneficial in understanding the importance of the departure region of the drop distribution spectrum on heat transfer.

6.9 Conclusions

The author feels confident that the heat transfer measurements reported

* The design and construction of the "shaker" used in the vibration tests were done by Mr. Howard Charney as a term project for a Heat Transfer Course at M.I.T. This author acted as one of the supervisors for the project.

in this chapter correctly demonstrate the parametric trends of heat flux, pressure, surface roughness, vapor velocity, and Teflon promotion. The two experimental errors, non-condensables and surface temperature measurement, which have plagued past researchers, have been minimized in this work. The results are summarized in Table 10.

VII. PHOTOGRAPHIC MEASUREMENTS

7.1 Drop Distribution

The principal goal of the visual experiments was to measure the drop distribution for dropwise condensation on a vertical copper surface. A secondary goal was to determine the nucleation site density.

The shortcomings of the previous attempts to obtain these measurements have been mentioned in previous chapters. Accurate heat transfer data was not taken in conjunction with visual data. In addition, insufficient background information limited the usefulness of previous drop distribution data.

The resulting drop distributions obtained in this experiment for system pressures of 34 mm Hg and 760 mm Hg and a ΔT of .5 °F are plotted in Fig. 33 and listed in Tables 12 and 13. These two distributions were measured using a band width, ΔD , of ± 20 percent.

Due to the resolution limitations of the optics, the smallest drop which could be accurately measured and counted was 10 microns for low pressure and 20 microns for atmospheric pressure condensation.* Drops down to size of one to two microns in diameter could be seen on the microphotographs but could not be measured and counted with sufficient accuracy to include in the distribution data. Thus, the drop distribution below 10 microns could not be obtained.

Since the distribution at the low end of the drop spectrum could not be measured, "educated" guesses were required to continue the distri-

* The more rapid growth rate at atmospheric as opposed to low pressure condensation at the same ΔT results in less clarity in the microphotographs. In addition, the much larger number of small drops at high pressure made counting more difficult.

bution down to the smallest drop size. Six distributions, illustrated in Figs. 34 and 35, were chosen spanning the possible choices between two extreme cases. The lowest distributions (L-0 for low pressure and A-0 for atmospheric pressure condensation) approximate the case where no coalescence takes place between nucleation size drops and drops of 10 microns. These distributions also assume that the drop growth rate is constant in this size range. The highest distributions (L-6 and A-6) assume that the coalescence and growth rates for drops within this range are the same as for a drop of 10 microns. The real drop distribution must lie between these two extreme distributions.

From the measured and predicted distributions, the area covered by drops could be computed. The results for three distributions at each pressure are plotted in Figs. 37 and 38.

Because drop distribution data can be interpreted in many ways, the raw counting data is supplied in Appendix J. In addition, a step by step description of the data taking processing procedures are listed. The taking of the photographs and counting of the drops involved over six months of painstaking labor. The purpose for presenting all the raw data is to make it available for other possible interpretations and processing schemes.

In Chapter 2, it was stated that there are four possible stages of development for a drop: the nucleation stage, the condensation-coalescence stage, the coalescence stage, and the departure stage. The growth rate and coalescence rate varies for a drop as it progresses from one stage to the next. This would imply that there should be four separate distributions over the complete range of drops from nucleation to departure size.

When a "primary" drop nucleates from a site, its growth is purely due

to condensation. Because of the very small size of the nucleating drop (order of .1 to 1 micron in diameter), neighboring drops appear to be distant from each other. Thus there is little probability that these primary drops will bump into each other and coalesce. Since there is virtually no coalescence among the primary drops, their number remains constant. The result of this reasoning will be a drop distribution which remains constant in this nucleation region as shown in Figs. 34 and 35.*

As the drops continue to grow in size, the probability that coalescence will occur increases. Thus, the number of drops of a particular size will decrease. The point at which coalescence becomes important is unknown at this time. The author arbitrarily chose one micron as the separation point of the nucleation region with the condensation-coalescence region. Figures 34 and 35 illustrate the change in distribution from a constant value in the nucleation region to a decreasing value in the condensation-coalescence region.

The distributions within the nucleation and condensation-coalescence regions are dependent on the nucleation site density and the growth rate of drops. In addition, the amount of surface area which the drops in the coalescence and departure regions occupy has a strong effect on the number of "active" drops which can exist on the surface. Thus it can be concluded that the distribution at the low end of the drop spectrum will vary with experimental conditions.

When a drop reaches a size somewhere between 10 and 150 microns in diameter (depending on the pressure), the conduction resistance becomes so large that very little condensation takes place on its surface. At

* The drop distribution will be constant in this region only if the growth rate is reasonably independent of size. Also, it is assumed that the sweeping actions of the large drops do not affect these primary drops. For first approximations, these assumptions are valid.

this stage the growth of the drop is governed primarily by coalescence. Glicksman and Rose [27] have analyzed the coalescence and packing process in an attempt to predict what the distribution should be in this region. In their analysis they show that the distribution would be independent of all variables which affect the condensation rate. They conclude that the distribution for good quality drop condensation within this region is universal for all condensing surfaces operating at normal operating conditions (where nucleation is not a limitation).

Glicksman's predicted results in the form of area coverage as a function of nondimensionalized drop size are compared to measured values in Fig. 5. The agreement with this author's measured distributions for large drop sizes is quite close.

Departure mechanisms affect the distribution of the very large drops on the surface. The number and size of the departing drops will vary with the orientation of the surface. Any of the parameters which affect contact angle such as surface roughness and the surface tension of the liquid also alter the size of departing drops.

The author observed that the condensation rate affects the drop distribution in the departure region. The effect of heat flux is illustrated in the photographs of Figs. 39 and 40. For the same surface at the same operating pressure, it is evident that departing drops are larger for low heat fluxes. As the heat flux increases, the rate at which the "active" drops bump into the large drops increases. This coalescing action causes the large drops to vibrate. Due to the greater vibration rate at higher fluxes, departure-size drops are more unstable and leave prematurely. A further discussion of the departure mechanism, including the heat flux effect, is included in Appendix B.

The photographs also show heat flux has an effect on the velocity of falling drops. At high heat fluxes, the departing drops accelerate rapidly and never hesitate during their fall. (Note that the shutter speed of 1/125 sec could not stop the action of the falling drops.) But at low heat fluxes, the falling drops are sluggish and frequently stop momentarily during their downward journey. Again the explanation is that the rapid coalescence rate lowers the restraining force on the large drops.

Figure 36 compares the drop distribution for atmospheric and low pressure condensation at the same ΔT and for the same surface. It is evident that there are fewer large drops on the surface during atmospheric as compared to low pressure condensation. The author believes that the reason for this is a combination of the higher heat flux and lower surface tension for the condensation at the higher pressure. Appendix B outlines some of the parameters which can affect the distribution in the departure region. The analysis is by no means complete and serves only to introduce an area of study of dropwise condensation which has been chiefly neglected up to now.

The point separating the coalescence and departure regions seems to be somewhere between 500 and 1000 microns. This conclusion is reached by observing where the low pressure and atmospheric pressure distributions cross in Fig. 36.

The principal purpose in measuring the drop distribution was to enable one to predict the heat transfer for dropwise condensation. Unfortunately, the complete distribution could not be obtained due to experimental difficulties in obtaining data for drops smaller than 10 microns in diameter. Figures 34 and 35 illustrate seven distributions for each operating pressure which span the possible limits. The problem

now was to choose one of these distributions for each pressure which approximates the true distribution.

The procedure used to choose the "correct" distribution was to determine which one made the predicted heat flux equal the measured heat flux. In the next two chapters this procedure will be described in detail. The distributions so chosen for each of the operating pressures are compared in Fig. 36 and Table 14. These are the distributions which the author feels correctly approximate the true distributions for the experimental conditions used in this investigation.

7.2 Nucleation

Originally, the primary goal of this thesis was the determination of the nucleation site density for dropwise condensation as a function of surface chemistry and surface to vapor temperature difference. Although the emphasis was shifted to the measurement of the drop distribution, some observations can be made concerning nucleation.

Figure 41 compares the density of small drops condensing at the same pressure ($T_{\text{sat}} = 88^\circ\text{F}$) at a ΔT of $.12^\circ\text{F}$ and $.37^\circ\text{F}$. The photographs certainly demonstrate that the nucleation site density has increased in this ΔT range. The effect of pressure on nucleation is illustrated by the photographs of Figs. 42 and 43. The nucleation site density is considerably greater at the same ΔT for the atmospheric pressure compared to the low pressure conditions.

The theory of nucleation related to dropwise condensation is outlined in Appendix D. The effects of ΔT and pressure are discussed in some detail in this appendix. Briefly, it can be said that the surface to vapor temperature difference is the potential which drives the phase transformation over the nucleation energy barrier. More nucleation sites

are activated at higher ΔT 's. The primary effect of pressure is the lowering of this energy barrier due to property changes. The lower contact angles at the higher saturation temperatures also add to this decrease in the energy barrier.

The main body of photographs taken for the drop distribution study were for a temperature difference of .5 °F. This ΔT was chosen because the relatively low resulting condensation rates enabled easier examination of the process. The large sample of high magnification photos obtained at this ΔT for low and atmospheric pressures enabled the author to estimate the nucleation site density. At a pressure of 34 mm Hg and a ΔT of .5 °F, a site density of 200 million (2×10^8) per square centimeter was estimated. For atmospheric pressure at the same ΔT of .5 °F, the density was approximately two to three times greater than at the low pressure.

The nucleation site density was estimated by counting the smallest drops (about 1 to 2 microns) which could be resolved on the microphotographs. When the location of primary drops coincided on several photos then that location was considered a nucleation site.

The reason why only approximate values are stated is that it was extremely difficult to identify the great number of primary drops on the surface at this ΔT . The primary drops are so small and so close together at the magnifications used (200X and 400X), that resolution limitations prevented any greater accuracy. As the ΔT is lowered, nucleation studies become easier because the density decreases (see Fig. 41). However, detailed counting of the nucleation site density was not carried out for temperature differences lower than .5 °F.

7.3 Discussion of Photographic Study

The photographic data obtained in this work extends our knowledge of the drop distribution and nucleation site density. Accurate heat measurements made in conjunction with the photographic work enable one to use the data in predicting heat transfer performance for dropwise condensation.

VIII. MODEL OF THE HEAT TRANSFER PROCESS FOR DROPWISE CONDENSATION

The model of the heat transfer process for dropwise condensation proposed in this section is similar to that developed by Rose [23,24]. The problem is analyzed by first determining the heat transfer through a single drop and then calculating the heat flux through the surface from knowledge of the drop distribution. Rose's analysis successfully predicts heat transfer performance when compared to experimental results. However, four constants had to be "fit" into his equations to achieve this agreement.

The basic concept of Rose's model has been continued in this analysis. However, because of more precise knowledge of the drop distribution, a bit "cleaner" presentation can be afforded. Also, two additional resistances to drop condensation heat transfer are considered in the present model to take into account the promoter and surface conductivity effects.

8.1 Heat Transfer Through a Single Drop

8.1.1 Resistance Concept

The basic assumption for this model for the heat transfer through a single drop is that the resistances due to the various heat transfer mechanisms are independent and additive. Although this is not completely true, the origins of the resistances are sufficiently remote from one another that the assumption is valid for first approximations.

Throughout this analysis drops will be assumed to be hemispherical in shape. Contact angle measurements very close to 90° for most of the promoted surfaces substantiate this assumption. Internal circulation within a drop due to thermocapillarity will be neglected. Lorenz and

Mikic [69] have shown that circulation increases the heat transfer through large drops by less than 5 percent. In addition, it will be assumed that the vibratory motion of the drop due to coalescence (discussed in Appendix B) does not alter the heat transfer through a drop.

Heat transfer will be assumed to take place only through drops. The present school of thought, that no liquid film exists between the drops and that no heat is transferred through the "bare" surface area, will be accepted. Overwhelming experimental evidence supports this view.

The resistances to heat transfer for dropwise condensation are:

1. Diffusion Resistance, R_{nc} , through non-condensable gases concentrated near the surface. The temperature drop, ΔT_{nc} , due to this resistance can be estimated by considering the relationship among the partial pressures of the gas and vapor and the saturation pressure. However, little detailed analysis has been carried out to predict this diffusion resistance. The importance of non-condensables has been dramatically demonstrated in the discussion of past heat transfer measurements (see Fig. 10).
2. Curvature Resistance, R_c . Because of the curved interface, the saturation temperature of the vapor in equilibrium with a drop is less than the saturation temperature of vapor in equilibrium with a liquid at a flat interface at the same pressure. Thus for a drop, there will be a temperature difference (T_{sat} for a curved interface - T_{sat} for a flat interface) which must be exceeded in order for it to exist on a condensing surface. This ΔT_c can be thought of in terms of an equivalent resistance in order to compare it with other effects. However, the "curvature" resistance is not a resistance ($\Delta T/Q/A$) in the true sense of the word since the temperature difference is independent of heat flux.
3. Interfacial Mass Transfer Resistance, R_i . A pressure difference is

required to drive the mass transfer across the vapor-liquid interface. This pressure difference can be converted to a temperature difference and a resistance calculated.

4. Drop Conduction Resistance, R_{dc} . The resistance to conduction heat transfer through a drop is the governing resistance for the large drops. This resistance is computed considering no internal circulation or drop motion.

5. Promoter Resistance, R_p . There is a temperature drop through the promoter layer due to conduction losses. Since the thickness of most chemical promoters are extremely thin, this resistance can often be neglected. However, for Teflon it has been shown that the promoter resistance must be considered.

6. Constriction Resistance, R_{cm} . Because the majority of heat is transferred through the small "active" drops, the heat flux is not uniform over the condenser surface. The crowding of the heat flow lines results in a temperature drop in the substrate which is greater than that due to straight conduction. This "constriction" resistance, analyzed by Mikic [28], has been shown to be significant for low conductivity condensing surfaces.

The six resistances and the resulting temperature drops are illustrated in Fig. 44. These resistances are discussed in greater length in Appendices C and E through H.

For most drop condensation heat transfer experiments, the average heat transfer coefficient is measured. The usual technique is to obtain the temperature gradient through the bulk material on which the condensation is occurring and convert this to heat flux using the known thermal conductivity. The average surface temperature is determined by extrapo-

lation of the straight line temperature gradient to the surface. The average heat transfer coefficient is then defined as

$$\bar{h} = \frac{\bar{Q}/A}{(T_s - T_w)} \quad (8.1)$$

where T_s is the saturation temperature at a flat interface. The local heat transfer coefficient on the surface is the coefficient for a single drop

$$h = \frac{Q/A}{T_s - T_w} \quad (8.2)$$

In this equation Q is the heat transferred through a single drop and A is the base area of a drop. Defined in this way, the local coefficient is

$$\frac{1}{h} = R_{nc} + R_c + R_i + R_{dc} + R_p + R_{cm} \quad (8.3)$$

The next step in the analysis entails evaluation of the six resistances. For this work, the diffusion resistance due to non-condensable gases will be neglected. In addition, the vapor will be assumed to be saturated. The justification for this is that the experiments were carried out with "gas free", saturated steam.

For the computation of the heat transfer through a single drop, the "true" temperature driving potential is $(T_s - T_p)$ where T_s is the saturation temperature at a flat interface and T_p is the average temperature at the base of the drop. The temperature drop due to constriction resistance $(T_w - T_{cm})$ and due to the promoter layer $(T_{cm} - T_p)$ can be neglected when discussing the heat transfer through a single drop.* Then their effects can be added in series with the average resistance of all the

* Mikic [28] has shown that the constriction effect due to the crowding of heat flow through the periphery of a drop where the conduction path is shortest is of little importance compared to the crowding due to the distribution of "dead" drops on the surface.

drops when computing the overall heat transfer coefficient (see Appendix G and H). Thus for this analysis, the total temperature difference to be considered is

$$\Delta T_t = \Delta T_{nc} + \Delta T_c + \Delta T_i + \Delta T_{dc} + \Delta T_p + \Delta T_{cm} . \quad (8.4)$$

That is

$$\Delta T_t = \Delta T_c + \Delta T_i + \Delta T_{dc} . \quad (8.5)$$

8.1.2 Temperature Drop Due to Curvature Resistance

In order for a drop to be in mechanical and thermodynamic equilibrium on a surface, the temperature of the drop must be colder than the plane interface saturation temperature corresponding to the system pressure. The derivation for the temperature drop through the interface due to curvature is outlined in detail in Appendix C. The resulting equation is

$$\Delta T_c = \frac{2 T_s \sigma}{H_{fg} \rho_f} \frac{1}{r} . \quad (8.6)$$

When the ΔT due to curvature is equal to the total ΔT_t available (that is $T_s - T_p$), then the minimum size drop which can exist on the surface is

$$r_{min} = \frac{2 T_s \sigma}{H_{fg} \rho_f} \frac{1}{\Delta T_t} . \quad (8.7)$$

Substituting (8.7) in (8.6), a simple expression for the temperature difference to curvature can be found to be

$$\Delta T_c = \frac{r_{min}}{r} \Delta T_t . \quad (8.8)$$

8.1.3 Temperature Drop Due to Interfacial Resistance

The temperature drop due to the interfacial resistance is

$$\Delta T_i = \frac{Q}{h_i 2\pi r^2} \quad (8.9)$$

where Q is the heat transferred through a single drop of radius r , and h_i is the interfacial heat transfer coefficient. The coefficient, h_i , can be evaluated from the equation derived by Nabavian and Bromley [70]

$$h_i = \left(\frac{2\alpha}{2 - \alpha}\right) \left(\frac{M}{2\pi RT_s}\right)^{1/2} \frac{H_{fg}^2}{T_s v_g} \quad (8.10)$$

The term, α , is called the condensation coefficient and can be thought of as the fraction of vapor molecules striking the liquid interface which enter the liquid phase.

Appendix E outlines the derivation of equation (8.10). Also included in this section is a discussion of the condensation coefficient. Throughout this paper it will be assumed that $\alpha = 1$. The justifications for making this assumption are discussed in the appendix.

8.1.4 Temperature Drop Due to Conduction Resistance

The conduction resistance for a hemispherical drop of radius, r , can be approximated by comparing it to the resistance for a right-circular cylinder of radius, r , and height, r . The resistance for the cylinder is

$$R_{cyl} = \frac{r}{k\pi r^2} \quad (8.11)$$

and for the drop

$$R_{dc} = C \frac{r}{k\pi r^2} \quad (8.12)$$

where C is a shape factor which must be less than one. Mikic [28] has shown that if $C = 1/4$, this approximation for R_{dc} agrees well with an exact solution of the problem derived by Umur and Griffith [21]. Other investigators [13,24] agree that the shape factor is near $1/4$.

The derivation of the drop conduction resistance is given in greater detail in Appendix F. The resulting temperature drop due to

conduction through a drop assuming a shape factor of 1/4 is

$$\Delta T_{dc} = \frac{Qr}{4k\pi r^2} \quad (8.13)$$

8.1.5 Heat Transfer Through a Drop

The transfer of sensible heat from the vapor to the drop is negligible compared to the latent heat released as a result of condensation. For this case

$$Q = \rho H_{fg} \frac{dV}{dt} \quad (8.14)$$

where the volume, V , for a hemispherical drop is equal to $2/3 \pi r^3$. Thus

$$Q = \rho H_{fg} 2\pi r^2 \frac{dr}{dt} \quad (8.15)$$

8.1.6 Total Temperature Drop

The total temperature drop due to curvature, interfacial, and drop conduction resistances can be found by substituting equations (8.8), (8.9) and (8.13) into (8.5):

$$\Delta T_t = \frac{r_{min}}{r} \Delta T_t + \frac{Q}{h_i 2\pi r^2} + \frac{Qr}{4k\pi r^2} \quad (8.16)$$

Now if the expression for the heat transferred through a drop (8.15) is substituted in (8.16), then

$$\Delta T_t = \frac{r_{min}}{r} \Delta T_t + \frac{\rho H_{fg}}{h_i} \frac{dr}{dt} + \frac{\rho H_{fg}}{2k} r \frac{dr}{dt} \quad (8.17)$$

8.1.7 Drop Growth Rate

Solving for $\frac{dr}{dt}$ and substituting $D = 2r$, one gets an expression for the drop growth rate

$$\frac{dD}{dt} = \frac{4}{\rho H_{fg}} \Delta T_t \left[\frac{1 - D_{min}/D}{D/2k + 2/h_i} \right] \quad (8.18)$$

Equation (8.18) can be integrated to find the relationship between diameter, D , and time, t . Assuming that at $t = 0$, $D = D_{\min}$, then

$$\begin{aligned} & \frac{1}{2k} [1.5 (D - D_{\min})^2 + 2 D_{\min} (D - D_{\min}) + D_{\min}^2 \ln(D - D_{\min})] \\ & + \frac{2}{h_i} [(D - D_{\min}) + D_{\min} \ln(D - D_{\min})] \\ & - \frac{1}{2k} D_{\min}^2 - \frac{2}{h_i} D_{\min} = \frac{4}{\rho H_{fg}} \Delta T_t t \quad . \end{aligned} \quad (8.19)$$

If the curvature term is neglected, then (8.19) simplifies to

$$\frac{1}{4k} (D^2 - D_{\min}^2) + \frac{2}{h_i} (D - D_{\min}) = \frac{4}{\rho H_{fg}} \Delta T_t t \quad . \quad (8.20)$$

When the interfacial term is neglected, the relationship becomes

$$\begin{aligned} & \frac{1}{2k} [1.5(D - D_{\min})^2 + 2D_{\min} (D - D_{\min}) + D_{\min}^2 \ln(D - D_{\min})] \\ & - \frac{1}{2k} D_{\min}^2 = \frac{4}{\rho H_{fg}} \Delta T_t t \quad . \end{aligned} \quad (8.21)$$

When only the conduction term is kept

$$\frac{1}{4k} (D^2 - D_{\min}^2) = \frac{4}{\rho H_{fg}} \Delta T_t t \quad . \quad (8.22)$$

Throughout this derivation, the drop growth rate has been derived for an "isolated" drop. In reality, drops are growing in the presence of their neighboring drops. The constriction resistance takes into account the nonuniform surface temperature due to the crowding of the heat flow through the active drops. This resistance has the effect of lowering the "true" ΔT as compared to the measured ΔT (see Appendix H). Instead of substituting the measured ΔT into (8.16), the "true" ΔT driving the

condensation rate should be used. However, this will not be the procedure carried out in this derivation. Instead, the computed value of the constriction resistance will be added in series with the resistance of all the drops averaged over the surface area. In this way the total temperature difference ($\Delta T = T_s - T_w$) can be used in the above expressions.

8.2 Heat Transfer Through the Surface

If there is one drop of diameter, D , on a unit area of condenser surface, then the heat transfer per unit area, A , would be

$$(Q/A)_1 = \rho H_{fg} \frac{dV}{dt} = \rho H_{fg} \frac{1}{4} \pi D^2 \frac{dD}{dt} \quad (8.23)$$

Substituting (8.18) into (8.23)

$$(Q/A)_1 = \pi D^2 \Delta T_t \left[\frac{1 - D_{\min}/D}{D/2k + 2/h_i} \right] \quad (8.24)$$

Now if there are $\bar{N} dD$ drops of diameter D to $D + dD$ per square centimeter of condenser surface*, then the heat transfer through that area would be

$$d(Q/A)_t = \bar{N} dD (Q/A)_1$$

or

$$d(Q/A)_t = \bar{N} dD \pi D^2 \Delta T_t \left[\frac{1 - D_{\min}/D}{D/2k + 2/h_i} \right] \quad (8.25)$$

On a condenser surface there are drops ranging in size from D_{\min} (the minimum drop size) to D_{\max} (the maximum drop size). If the drop distribution, $\bar{N} dD$, is continuous over this range, then the average heat transfer per square centimeter of condenser surface is

* The total number of drops of size D_1 to D_2 is $N_T = \int_{D_1}^{D_2} \bar{N} dD$. According to this definition $\bar{N} = \Delta N / \Delta D$ where ΔN is the number of drops counted per square centimeter in the size range D to $D \pm \Delta D$.

$$(Q/A)_t = \int_{D_{\min}}^{D_{\max}} d(Q/A)_t$$

or

$$(Q/A)_t = \pi \Delta T_t \int_{D_{\min}}^{D_{\max}} \bar{N} D^2 \left[\frac{1 - D_{\min}/D}{D/2k + 2/h_i} \right] dD \quad (8.26)$$

The heat flux for dropwise condensation can be predicted using (8.26) provided that the minimum and maximum drop sizes and the drop distribution are known. The maximum drop size was determined experimentally from the low magnification photographs. For low pressure condensation, D_{\max} was found to be 3 mm whereas for atmospheric pressure it was 2.5 mm. These numbers were used as the upper limits in (8.26).

Due to microscopic limitations, the drop distribution could not be determined experimentally over the complete range of drop sizes. Therefore it was necessary to use a trial and error approach to determine the most "correct" distribution at the low end of the spectrum. The details of this procedure will be discussed in the next chapter.

The minimum size drop which exists on a condenser surface is the smallest drop which has just nucleated. For heterogeneous nucleation from a uniform temperature vapor on a plane substrate, the size of a nucleating drop is the same as the minimum drop size specified by (8.7). No smaller drop than this can exist on the surface.

Because there is a temperature gradient in the vapor near the wall, one can argue that the nucleating drop will be as much as twice as large as the minimum drop size. Therefore, the actual size of a nucleating drop is somewhere between D_{\min} and $2 D_{\min}$. As will be shown in the next chapter, a negligible amount of heat is transferred through drops smaller than one micron. Thus it is important whether one uses D_{\min} or $2D_{\min}$ as

the lower limit for the integration of (8.7). For the sake of simplicity the smallest drop which can exist on the surface will be considered to be D_{\min} .

To summarize the results of the analysis, the following equations are restated:

$$(Q/A)_t = \pi \Delta T_t \int_{D_{\min}}^{D_{\max}} \bar{N} D^2 \left[\frac{1 - D_{\min}/D}{D/2k + 2/h_i} \right] dD$$

$$D_{\min} = \frac{4 T_s \sigma}{H_{fg} \rho_f} \frac{1}{\Delta T_t}$$

(8.27)

$$h_i = \left(\frac{2\alpha}{2 - \alpha} \right) \left(\frac{M}{2\pi R T_s} \right)^{1/2} \frac{H_{fg}^2}{T_s V_g}$$

D_{\max} = measured maximum drop size

\bar{N} = measured and proposed drop distribution

IX. PREDICTION OF HEAT TRANSFER FOR DROPWISE CONDENSATION

9.1 Determination of Drop Growth Rate

In the previous chapter, the growth rate due to condensation for an isolated hemispherical droplet was derived by considering the curvature, interfacial mass transfer, and drop conduction resistances. Equation (8.18) states the relationship between growth rate, $\frac{dD}{dt}$ and diameter, D .

Figure 45 compares the growth rate distributions ($\frac{dD}{dt}$ vs. D) for low and atmospheric pressure conditions. From this plot, one sees that the drop growth rate increases with pressure for all size drops. The maximum growth rate, occurring at .2 microns for atmospheric pressure, is nearly eight times greater than the maximum rate, occurring at .4 microns, for low pressure condensation. It is the interfacial resistance which primarily accounts for this decrease in the growth rate with pressure.

The individual effects of the three resistances on drop growth rate can be seen by dropping off terms in Eq. (8.18). The curvature effect can be neglected by setting $D_{\min} = 0$. In reality, this is saying that all size drops are large compared to D_{\min} . Letting the interfacial heat transfer coefficient, h_i , go to infinity results in the neglecting of interfacial effects. When both of these simplifications are made simultaneously, then only the drop conduction term is left.

This procedure of dropping off terms was carried out and the results plotted in Figs. 46 and 47. At both low and atmospheric pressures, neglecting the curvature term doubles the growth rate for the smallest size drops. However, by the time the drops have grown to a diameter of 5 microns, curvature effects have disappeared completely.

In the case of low pressure condensation, the maximum drop growth rate increases from 280 μ /sec to 4000 μ /sec when the interfacial resistance is neglected. Whereas for atmospheric conditions, the maximum growth rate increases from 2000 μ /sec to 4400 μ /sec. This indicates that if it were not for the mass transfer effects, the growth rate for small size drops would be nearly independent of pressure. Only drops smaller than 40 microns in diameter are affected by the interfacial resistance.

For drops much larger than the minimum size, the rate of growth is very nearly linear with ΔT . However, since the D_{\min} of Eq. (8.18) varies inversely with ΔT (see Eq. (8.7)), the growth rate does not exhibit this linear relation for small drops. Figures 48 and 49 illustrate the effect of varying ΔT on the drop growth rate distribution. Since the expression for the average heat flux through the surface (Eq. (8.26)) involves the integral of the growth rate distribution, these figures show that the heat transfer rate will decrease sharply at low ΔT 's.

The effect of ΔT on the maximum drop growth rate is described in Fig. 50. This plot shows that the growth rate decreases rapidly for ΔT 's less than 1 °F. This trend forecasts a decreasing heat transfer coefficient in this low ΔT region. This observation will be discussed again in Section 9.5 of this chapter.

The relationships between diameter and time, as derived in equations (8.19) through (8.22), are presented in Figs. 51 to 54. The first graph demonstrates how the interfacial resistance dominates at low pressures for small drop sizes. The difference between curves 1 and 3 of this figure illustrates this point. Figure 52 shows that the interface resistance loses its dominating role as the pressure is increased. (The

difference between curves 1 and 3 of Fig. 52 is slight as compared to Fig. 51.)

Figure 51 indicates that when the interfacial mass transfer resistance plays a dominant role, the diameter varies linearly with time. It appears that this will be the case only for small size drops growing in a low pressure system.

Figure 53 continues the display of diameter versus time for larger diameters. In this range, the mass transfer effects are beginning to become unimportant.

The drop continues to grow rapidly until conduction limitations take over. Figure 54 shows that D^2 is linear with time for drops greater than about 40 microns. This growth rate law has been experimentally verified by McCormick and Baer [13] (see Chapter 3).

The growth rate process is but half the picture in dropwise condensation. The number and distribution of drops on the surface are equally important. The growth rate effects are "weighted" because there are more small drops on the surface. This concept will be explained in the next section.

9.2 Selection of "Correct" Drop Distribution

Since the drop distribution was not measured down to the minimum drop size, the heat transfer cannot fully be predicted utilizing the model outlined in the previous chapter. Figures 34 and 35 graphically illustrate seven distributions which span the range of possible distributions for the low end of the drop spectrum. Each of these distributions was substituted in Eq. (8.27) and the resulting heat flux obtained by integrating over the complete range of drop sizes. Numerical integration

was required for this job due to the complexity of the integrand. A list of the thermodynamic properties and the computer program written to perform this calculation are listed in Appendix I.

The "correct" distribution is the one which results in a predicted heat flux closest to the measured heat flux for that pressure. Figures 55 and 56 illustrate the results of these calculations. From these calculations, distribution A-3 was chosen to be the "correct" one for atmospheric distribution and L-3 for low pressure distribution.

Chapter 7 included a discussion of the expected shape of the drop distribution curve. It was noted at that time that the distribution is constant in the nucleation region and begins to decrease in the condensation-coalescence region because of the mechanics of the drop growth and coalescence process. The nucleation drop size, the level of the constant distribution, and the demarcation point between the two regions have all been guessed at and then determined by "forcing" the predicted heat flux to equal the measured value. Other shaped distributions could have been chosen between the minimum drop size and the smallest measurable drop which would have predicted the heat flux. The author feels that the shape of the distribution chosen in this work is in agreement with the basic mechanisms governing the process in this region. The two correct distributions, L-3 for low pressure and A-3 for atmospheric pressure conditions, were used for all subsequent calculations.

9.3 Relative Importance of Resistances

The relative importance of the three resistances included in this analysis can be determined by neglecting terms in Eq. (8.27) before performing the integration. This procedure of dropping off terms was carried out and the results illustrated in Figs. 57 and 58. Curve 1 in

each graph represents the heat transferred through drops greater than diameter, D , taking into account the three resistances: curvature, interfacial, and drop conduction. Curve 2 predicts the heat transfer neglecting the curvature resistance, and curve 3 the heat transfer neglecting the interfacial resistance. Curve 4 represents the heat transfer for the most simplified case of considering only the drop conduction resistance.

The magnitude of each of the three resistances can be computed from data of Figs. 57 and 58 by the equation

$$R = \frac{\Delta T}{Q/A} \quad . \quad (9.1)$$

Using the heat flux predicted by curve 1, the total resistance (drop conduction, interface, and curvature) can be calculated. When the heat flux from curve 2 is used, the resistance found from Eq. (9.1) is for drop conduction plus interface. Similarly, curve 3 gives the drop conduction plus curvature resistance, and curve 4 gives the drop conduction resistance alone. By subtracting the resistance found from curve 4 from that of curves 2 and 3, the interface and curvature resistances can be computed respectively.

The magnitudes of the resistances so calculated are displayed as bar graphs A and D of Fig. 59. The total resistance for low pressure condensation is about 3 times greater than for atmospheric conditions. The relative magnitudes of the individual resistances (i.e., comparing the drop conduction resistance for low and atmospheric pressures) are deceptive. Because the drop distribution is different for the two pressures, the values of the resistances for a single drop are "weighted". The drop conduction resistance averaged over the surface is over twice as large for low pressure as compared to atmospheric pressure conditions mainly because there are more large "dead" drops at the lower pressure.

The true effect of property variation (as opposed to drop distribution plus property variation) can be realized by comparing bar graphs A with B and C with D. The low pressure distribution, L-3, was kept constant and the pressure varied between the two extremes (T_{sat} of 88 °F and 212 °F) and the results plotted as graphs A and B. The drop conduction term decreases by about 10 percent in going from low to high pressure because of the drop in the thermal conductivity of water. The interfacial resistance is nearly 7 times greater for the low pressure conditions. This is purely due to property changes and not due to alteration of the value of the condensation coefficient (kept at 1 for both cases). The magnitude of the constriction resistance is about the same for the two pressures and results in less than 3 percent of the total resistance in either case.

A similar calculation was performed holding the atmospheric distribution, A-3, constant and varying the properties. Graphs C and D of Fig. 59 show similar trends as mentioned for the low pressure distribution.

The effect of the drop distribution on the relative magnitudes of the resistances can be obtained by comparing the bar graphs A with C and B with D. For graphs A and C, the thermal properties at $T_{\text{sat}} = 88$ °F were held constant and the distribution varied. The drop conduction resistance drops by a factor of one half in going from the low to the atmospheric distribution. As stated before, this is because there is more "dead" surface area due to large drops for the lower pressure. The other resistances are little affected by distribution changes.

The conclusion which can be drawn from Fig. 59 is that pressure affects dropwise condensation by varying both the drop distribution and drop growth rates. In general, when considering the magnitude of

the resistances averaged over the surface, both drop distribution and growth rate must be taken into account.

From Fig. 59, it is evident that the conduction resistance represents the major portion of the total resistance for dropwise condensation. Therefore, for the same drop distribution fluids with higher thermal conductivities should exhibit greater heat transfer.

The heat transfer for dropwise condensation of mercury was calculated using the drop distribution data measured for water. The results are presented in Fig. 60. As expected, the total resistance for mercury is less than that for water. The conduction resistance is approximately 10 times less for mercury compared to water. However, the interfacial resistance is much larger for mercury. These trends are purely due to the property differences between the two materials.

It should be noted that due to the large variation in wetting properties for mercury and water, the drop distributions for the two materials will be greatly different. There will be far fewer nucleation sites for mercury and thus a smaller number of active drops. For this reason, it is doubtful whether drop condensation for mercury will even be an equal to that for water. The purpose of the above analysis was merely to show the effect of large differences of fluid properties.

9.4 The Effect of Pressure on Dropwise Condensation Heat Transfer

The preceding section indicates that both the drop growth and the drop distribution vary with pressure. How well one can predict the variation of drop condensation heat transfer with pressure by considering only the drop growth rate effects is illustrated in Fig. 61. The dashed line represents the experimental heat transfer data. The lower solid line is the predicted curve varying the properties but keeping the drop

distribution (measured at a saturation temperature of 88 °F) constant over the complete pressure range. The upper curve varies the thermodynamic properties in Eq. (8.27) while holding the atmospheric pressure distribution constant.

Equation (8.27) predicts the heat transfer correctly only at a T_{sat} of 88 °F and 212 °F where the distributions were measured. In between these values, the measured and predicted trends agree but the absolute values do not. This again confirms the statement that it is necessary to know the effect of pressure on both drop growth rate and distribution in order to correctly predict the variation of drop condensation heat transfer with pressure.

9.5 The Effect of ΔT on Dropwise Condensation Heat Transfer

The effect of ΔT on drop growth rate has been discussed in section 9.1 of this chapter. The observation was made that the rapid decrease in growth rate for low ΔT 's will result in a decreasing heat transfer coefficient. The dashed curves of Figs. 62 and 63 represent the predicted H versus ΔT according to Eq. (8.27).^{*} For these calculations, the drop distributions measured at a ΔT of .5 °F for each pressure were assumed to be constant over the range of ΔT 's from 0 to 4 °F.

Referring to Fig. 62, one can conclude that since the measured and predicted curves deviate, the drop distribution varies with ΔT . The predicted curve shows a decreasing coefficient for ΔT 's below .5 °F. However, the drop in the predicted coefficient is not as rapid as the measured curve. This indicates that nucleation is probably becoming important in this low ΔT range. Thus one can conclude that ΔT changes,

^{*}The solid curve represents the curve chosen by least squares technique through the experimental heat transfer data (see Section 6.1 for details).

especially for very low ΔT 's, alter both the drop growth rate and drop distribution.

The ΔT effect on drop distribution is not as evident for atmospheric pressure condensation (see Fig. 63) since the predicted and measured curves are nearly the same shape. This indicates that nucleation is not as much of a limitation for atmospheric as compared to low pressure condensation.

9.6 "Active" Surface Area

Information concerning the amount of "active" surface area is useful when discussing dropwise condensation. Table 15 summarizes the results obtained by examining Figs. 37, 38, 55 and 56. For low pressure condensation, drops smaller than 150 microns occupying about 35 percent of the surface area transfer 90 percent of the total heat. At atmospheric pressure, drops of diameter less than 40 microns covering 23 percent of the surface transfer 90 percent of the heat. In each case about 10 percent of the surface is bare.

Fifty percent of the heat is transferred through drops smaller than 10 microns for low pressure and 4 microns for atmospheric pressure condensation. In both cases half the heat is transferred through 5 percent of the surface area.

The data on "active" area is useful when estimating the magnitude of the constriction resistance developed by Mikic [28]. Sample calculations and a discussion of constriction effects are supplied in Appendix G.

9.7 Minimum Value of the Condensation Coefficient

For all calculations performed up to this point, it has been assumed that the condensation coefficient is equal to one. In order to check the validity of this assumption, the coefficient was varied from the

lowest value reported (.006) up to one. The results of these calculations are summarized in Table 16.

For low pressure condensation, the analysis shows that the coefficient must be greater than .35. Using the maximum drop distribution, L-6, and $\alpha = .35$, the predicted heat flux is only 98 percent of the measured value. Since the true drop distribution must be lower than distribution L-6, one can conclude that the condensation coefficient must be greater than .35.

A further discussion on the correct value of condensation coefficient is supplied in Appendix E.

9.8 Conclusions

Since some guess-work was necessary to obtain the drop distribution over the complete range of drop sizes, it cannot be concluded at this time that the proposed model successfully predicts dropwise condensation heat transfer. An analytical prediction or further experimental measurement of the drop distribution of the small drops is necessary before the model can be verified quantitatively. However, the scheme of dividing the problem into drop distribution and drop growth effects results in a model which explains all the parametric trends observed to date.

The validity of the information drawn from the heat transfer analysis concerning the relative magnitude of the resistances, pressure and ΔT effects, and the minimum value of the condensation coefficient also depends on the "correctness" of the chosen drop distribution. The author feels reasonably confident that the chosen drop distribution approximates the true distribution close enough to insure that the discussions in the above areas are valid.

X. CONCLUSIONS

10.1 Heat Transfer Measurements

1. For the three condensing surfaces tested (Teflon, mirror smooth, and rough), the heat transfer coefficient rose sharply with ΔT in the range from .1 °F to 1 °F and then remained relatively constant for ΔT 's to 3 °F.

2. A critical ΔT is necessary to initiate the dropwise condensation process. This ΔT_{crit} is .075 °F for mirror smooth surfaces and .03 °F for 500 grit roughened surfaces.

3. For a ΔT of 3 °F, the heat transfer coefficient decreases linearly with the saturation temperature of the vapor according to the relation: $h = 220 (T_{sat} - 32)$. For a mirror smooth chemically promoted vertical surface, the coefficient decreases from 37,000 Btu/hr ft²°F for T_{sat} of 212 °F to 13,000 Btu/hr ft²°F for T_{sat} of 88 °F.

10.2 Visual Investigation

1. The drop distribution spectrum can be divided into four regions according to the governing drop growth mechanism. They have been defined as the nucleation, condensation-coalescence, coalescence, and departure regions. Within each of these regions, the number of drops of a particular diameter varies with diameter according to the form: $\bar{N} = n D^{-2}$.

2. The drop distribution varies with the system pressure and the surface to vapor temperature difference. Excess vapor velocity, surface roughness and inclination can also alter the distribution.

3. For a ΔT of .5 °F during low pressure condensation ($T_{sat} = 88$ °F), the nucleation site density was measured to be about 200 million per

square centimeter. At the same ΔT for atmospheric pressure conditions, the density is increased by a factor of about three. Below a ΔT of .5 °F, the nucleation site density drops sharply with ΔT .

10.3 Prediction of Heat Transfer

1. Heat transfer for dropwise condensation can be modeled by considering the growth rate of individual drops and the drop distribution to be the two important factors affecting the process. The heat transfer through a single drop can be calculated from the drop growth rate. The average heat flux through the surface can be found by integrating the heat transfer through a single drop over the complete range of drop sizes. The drop distribution is needed to perform this calculation.

2. The growth rate for a single drop can be predicted by assuming that the resistances affecting the heat transfer act in series. The curvature, interfacial mass transfer, and drop conduction resistances have been included in this analysis. The resistances due to constriction and promoter effects can be added in series with the average resistance due to all the drops on the surface. The non-condensable resistance has been ignored throughout this analysis.

3. For low pressure condensation ($T_{\text{sat}} = 88 \text{ °F}$), drops smaller than 150 microns in diameter occupying 35 percent of the surface area transfer 90 percent of the total heat. At atmospheric pressure, drops of diameter less than 40 microns covering 23 percent of the surface transfer 90 percent of the heat. In each case, about 10 percent of the surface is bare. Fifty percent of the heat is transferred through 5 percent of the surface area for both low and atmospheric pressure condensation.

4. The resistance due to conduction through the drops accounts for

70 percent of the total resistance for a vertically oriented, mirror smooth, chemically promoted, copper surface during low pressure ($T_{\text{sat}} = 88^\circ\text{F}$) condensation. For atmospheric pressure, the drop conduction resistance is nearly 85 percent of the total.

5. The interfacial mass transfer resistance is nearly 8 times greater at low pressure ($T_{\text{sat}} = 88^\circ\text{F}$) as compared to atmospheric pressure. This increase is due solely to property changes.

6. The condensation coefficient must be greater than .35. A value of one was used for all heat transfer calculations throughout this thesis.

10.4 The limiting Heat Transfer Mechanisms

1. When determining why a parametric change alters the heat transfer for dropwise condensation, one must consider how it affects the drop growth rate of individual drops and also how it affects the drop distribution. Frequently a change in operating conditions has an effect on both growth rate and drop distribution.

2. The decrease in heat transfer with decreasing pressure is due to a slowing down of the drop growth rate and an alteration of the drop distribution. The changes in thermodynamic properties with decreasing pressure result in the lower growth rate. The less desirable drop distribution at lower pressures is caused by poorer drop nucleation and drop departure.

3. The rapid decrease in heat transfer coefficient for ΔT 's below $.5^\circ\text{F}$ is due to a slowing down of the drop and also to nucleation limitations.

4. The promoter limits drop condensation by offering an added conduction resistance in series with the condensation resistance. For

Teflon surfaces this is a serious limitation.

5. Low thermal conductivity of the substrate causes a non-uniform heat flux over the condenser surface and limits the heat transfer by introducing a constriction resistance.

10.5 Recommendations for Further Study

The determination of the drop distribution over the complete range of drop sizes is the most important piece of information needed to prove the validity of the heat transfer model proposed in this thesis. At very low ΔT 's where the number and size of the active drops are greatly decreased, the entire drop distribution could be measured using standard microscopic techniques. However, for ΔT 's in the normal operating range (above .5 °F), special experimental techniques will be required to obtain this data. The analytical prediction of the drop distribution in the small size range is equally difficult. Computer simulation of the drop condensation process should prove to be a useful approach.

REFERENCES

1. Schmidt, E., W. Schurig, W. Sellschopp, "Versuche iiber die Kondensation von Wasserdampf in Film-und Tropfenform", Tech. Mech. Thermo-Dynam., 1, p 53 (1930).
2. Jacob, M., "Heat Transfer in Evaporation and Condensation II," Mechanical Engineers, 58, p 729 (1936).
3. Eucken, A., Naturwiss., 25, p 209 (1937).
4. Emmons, H., "The Mechanism of Drop Condensation", Transactions A.I.Ch.E., 35, p 109 (1939).
5. Fatica, N., D. L. Katz, "Dropwise Condensation", Chem. Eng. Progress, 45, p 661 (1949).
6. Baer, E., J. M. McKelvey, "Heat Transfer in Dropwise Condensation", Delaware Science Symposium (1958).
7. Welch, J. F., J. W. Westwater, "Microscopic Study of Dropwise Condensation", Int. Dev. in Heat Trans., p 302 (1961).
8. Kast, W., "Heat Transfer with Drop Condensation", Chemie-Ingenieur-Technik, 31, p 163 (1963), (Translated from German - NSTIC Translation No. 1564).
9. Sugawara, S., I. Michiyoshi, "Dropwise Condensation", Memoirs of Faculty of Engineering, Kyoto Univ., 18, p 84 (1956).
10. Silver, R. S., "An Approach to a General Theory of Surface Condensers", Proc. Inst. Mech. Engrs., 178, p 339 (1963).
11. Sugawara, S., K. Katsuta, "Fundamental Study on Dropwise Condensation", Third Int. Heat Trans. Conf., 2, p 354 (1966).
12. Tammann, Von. G., W. Boehme, "Die Zuhl der Wassertröpfchen he der Kondensation auf verschiedenen festen Stoffen", Annalen der Physik, 5, p 22 (1935).
13. McCormick, J. L., E. Baer, "Dropwise Condensation on Horizontal Surfaces", Devel. in Mech. (Proc. of 8th Midwestern Mech. Conf. 1963) (1965).
14. McCormick, J. L., J. W. Westwater, "Nucleation Sites for Dropwise Condensation", Chem. Eng. Science, 20, p 1021 (1965).
15. McCormick, J. L., J. W. Westwater, "Drop Dynamics and Heat Transfer During Dropwise Condensation of Water Vapor on a Horizontal Surface", Chem. Eng. Prog. Sym. Series, 62, p 120 (1966).
16. Peterson, A. C., J. W. Westwater, "Dropwise Condensation of Ethylene Glycol", Chem. Eng. Prog. Sym. Series, 62, p 135 (1966).

17. Baer, E., J. A. Koutsy, A. G. Walton, "The Nucleation of Water Vapor on Surface Films Formed by Adsorption on Metal Surfaces", Surface Science, 3, p 280 (1965).
18. Koutsy, J. A., A. G. Walton, E. Baer, "Heterogeneous Nucleation of Water Vapor on High and Low Energy Surfaces", Surface Science, 3, p 165 (1965).
19. Erb, R. A., "Heterogeneous Nucleation on Single-Crystal Silver and Gold Substrates in Cyclic Condensation of Water Vapor", Ph.D. Thesis, Temple Univ. (1965).
20. Erb, R. A., "Wettability of Metals under Continuous Condensing Conditions", J. of Physical Chemistry, 69, p 1306 (1965).
21. Umur, A., P. Griffith, "Mechanism of Dropwise Condensation", ASME, Paper No. 64-WA/HT-3 (1964).
22. McCormick, J. L., E. Baer, "On the Mechanism of Heat Transfer in Dropwise Condensation", Journ. of Colloid Science, 18, p 208 (1963).
23. Le Fevre, E. J., J. W. Rose, "A Theory of Heat Transfer by Dropwise Condensation", Proc. Third Int. Heat Trans. Conference, 2, p 362 (1966).
24. Rose, J. W., "On the Mechanism of Dropwise Condensation", Int. J. Heat Mass Transfer, 10, p 755 (1967).
25. Gose, E. E., A. N. Mucciardi, E. Baer, "Model for Dropwise Condensation on Randomly Distributed Sites", Int. J. Heat Mass Transfer, 10, p 15 (1967).
26. Hurst, C. J., "Transient Droplet Growth During Dropwise Condensation", Ph.D. Thesis, Penn. State University (1966).
27. Glicksman, L. R., "An Analytical Study of Dropwise Condensation", To be published in Int. J. Heat Mass Transfer.
28. Mikic, B. B., "On Mechanism of Dropwise Condensation", To be published in Int. J. Heat Mass Transfer.
29. Sugawara, S., I. Michiyoshi, "Dropwise Condensation", Memoirs of Faculty of Engineering, Kyoto Univ., 18, p 84 (1956).
30. Hampson, H., N. Ozisik, "An Investigation into the Condensation of Steam", Institution of Mech. Engrs., 13, p 282 (1952).
31. Dolloff, J. B., N. H. Metzger, "Dropwise Condensation of Steam at Elevated Pressures", ONR Tech Rpt #2, Contract Nonr 3357(02) (May 15, 1968).
32. Rose, J. W., "Dropwise Condensation - The Effect of Surface Inclination", To be published in Int. J. Heat Mass Transfer.

33. Scriven, L. E., Chem. Eng. Science, 10, p 1 (1959) and 17, p 55 (1962).
34. McCormick, J. L., E. Baer, "On the Mechanism of Heat Transfer in Dropwise Condensation", Journ. of Colloid Science, 18, p 208 (1963).
35. MacDougall, G., C. Ockrent, Proc. Royal Society, 180A, p 151 (1942).
36. Le Fevre, E. J., J. W. Rose, "An Experimental Study of Heat Transfer by Dropwise Condensation", Int. J. Heat Mass Transfer, 8, p 1117 (1965).
37. Krause, J., "Dropwise Condensation - Quantitative Research", Heat Div. Paper No. 28, National Eng. Lab., East Kilbride (1950).
38. Wenzel, H., "Versuch über Tropfenkondensation", Allg. Wärmetech, 8, p 53 (1957).
39. Tanner, D. W., C. J. Potter, D. Pope, D. West, "Heat Transfer in Dropwise Condensation. Part I The Effects of Heat Flux, Steam Velocity, and Non-Condensable Gas Concentration", Int. J. Heat Mass Transfer, 8, p 419 (1965).
40. Nagle, W. M., G. S. Bays, L. M. Blenderman, and T. B. Drew, "Heat-Transfer Coefficients during Dropwise Condensation of Steam", Trans. Amer. Inst. Chem. Engrs., 31, p 593 (1935).
41. Gnam, E., "Tropfenkondensation von Wasserdampf", Forschungsh. Ver. dtsh. Ing., 382, p 17 (1937).
42. Fitzpatrick, J. P., S. Baum, W. H. McAdams, "Dropwise Condensation of Steam on Vertical Tubes", Trans, Amer. Inst. Chem. Engrs., 35, p 97 (1939).
43. Shea, F. L., N. W. Krase, "Dropwise and Filmwise Condensation of Steam", Trans. Amer. Inst. Chem. Engrs., 36, p 463 (1940).
44. Kirschbaum, E., G. Winckelsesser, A. K. Wetjen, "Neues über den Wärmeanstausch", Chem.-Ing.-Tech., 23, p 361 (1951).
45. Costas, L. P., "Heat Transfer by Dropwise Condensation of Steam", Ph.D. Thesis, Univ. of Maryland (1959);
46. Citakoglu, E., J. W. Rose, "Dropwise Condensation - Some Factors Influencing the Validity of Heat Transfer Measurements", Int. J. Heat Mass Transfer, 10, p ? (1967).
47. Ma, J. T. S., Ph.D. Thesis, Iowa State College (1959).
48. Brown, A. R., M. A. Thomas, "Filmwise and Dropwise Condensation at Low Pressures", Third Int. Heat Trans. Conf., 2, p 300 (1966).

49. Tanner, D. W., D. Pope, C. J. Potter, D. West, "Heat Transfer in Dropwise Condensation at Low Steam Pressures in the Absence and Presence of Non-Condensable Gas", Int. J. Heat Mass Transfer, 11, p 181 (1968).
50. Furman, T., H. Hampson, "Experimental Investigation into the Effect of Cross Flow with Condensation of Steam and Steam-Gas Mixtures on a Vertical Tube", Prpc. Instn. Mech. Engrs., 173, p 147 (1959).
51. Hampson, H., "The Condensation of Steam on a Tube with Filmwise or Dropwise Condensation in the Presence of a Non-Condensable Gas", Int. Devel. in Heat Transfer, 2, p 310 (1961).
52. O'Bara, J. T., E. S. Killian, L. H. S. Roblee, "Dropwise Condensation of Steam at Atmospheric and Above Atmospheric Pressures", Chem. Eng. Science, 22, p 1305 (1967).
53. Tanner, D. W., C. J. Potter, D. Pope, D. West, "Heat Transfer in Dropwise Condensation. Part II Surface Chemistry", Int. J. Heat Mass Transfer, 8, p (1965).
54. Griffith, P., Man Suk Lee, "The Effect of Surface Finish and Material Thermal Properties on Dropwise Condensation", Int. J. Heat Mass Transfer, 10, p 697 (1967).
55. Topper, L., E. Baer, J. Colloid Science, 10, p 225 (1955).
56. Babco, R. P., A. L. Gosman, "Promotion of Dropwise Condensation of Several Pure Organic Vapors", Am. Soc. Mech. Eng., Paper No. 57-3-2 (1957).
57. Misra, B., C. F. Bonilla, "Heat Transfer in the Condensation of Metal Vapors: Mercury and Sodium up to Atmospheric Pressure", Chem. Eng. Progress Sym. Series, 52, p 7 (1956).
58. Ivanovskii, M. N., V. I. Subbotin, Yu. V. Milovanov, "Heat Transfer with Dropwise Condensation of Mercury Vapor", Teploenergetika, 14, p 81 (1967).
59. Drew, T. B., W. M. Nagle, W. G. Smith, "The Conditions for Dropwise Condensation of Steam", Trans. Amer. Inst. Chem. Engrs., 31, p 605 (1935).
60. Blackman, L. C. F., M. J. S. Dewar, H. Hampson, "An Investigation of Compounds Promoting the Dropwise Condensation of Steam", J. Appl. Chem., 7, p 160 (1957).
61. Osment, B. D. J., D. W. Tanner, "Promotion for the Dropwise Condensation of Steam", First European Symposium - Fresh Water from the Sea, Athens, 1962.

62. Osment, B. D. J., D. Tudor, R. M. M. Speirs, W. Rugman, "Promoters of the Dropwise Condensation of Steam", Trans. Instn. Chem. Engrs., 40, p 152 (1962).
63. Watson, R. G. H., D. C. P. Birt, C. W. Honour, B. W. Ash, "The Promotion of Dropwise Condensation by Montan Wax", J. Appl. Chem., 12, p 539 (1962).
64. Tanner, D. W., A. Poll, J. Potter, D. Pope, D. West, "The Promotion of Dropwise Condensation by Montan Wax. II. The Composition of Montan Wax and the Mechanism of Promotion", J. Appl. Chem., 12, p 547 (1962).
65. Watson, R. G. H., J. J. Brunt, D. C. P. Birt, "Dropwise Condensation of Steam", Proc. 1961-62 Int. Heat Trans. Conference, p 296 (1963).
66. Fox, R. M., "A Review of Literature on the Promotion of Dropwise Condensation", US Navy Marine Engineering Lab Report 71 106 (1964).
67. Erb, R. A., E. Thelen, "Dropwise Condensation on Hydrophobic Metal and Metal Sulfide Surfaces", Amer. Chem. Soc., p 100 (1965).
68. Bromley, L. A., J. W. Porter, S. M. Read, "Promotion of Drop-By-Drop Condensation of Steam from Seawater on a Vertical Copper Tube", A.I.Ch.E. Journal, 40, p 245 (1968).
69. Lorenz, J. J., B. B. Mikic, "The Effect of Thermocapillary Flow on Heat Transfer in Dropwise Condensation", To be published in the Trans. ASME Journ. Heat Transfer.
70. Nabavian, K., L. A. Bromley, "Condensation Coefficient of Water", Chem. Eng. Sci., 18, p 651 (1963).
71. Lord Kelvin, Proc. Roy. Soc. Edin., 7, p 63 (1870), and Phil. Mag., 42, p 448 (1871).
72. von Helmholtz, R., Wied. Ann., 27, p 508 (1886).
73. Hatsopoulos, G. N., J. H. Keenan, Principles of General Thermodynamics, John Wiley and Sons, Inc., New York (1965).
74. Shrager, R. W., A Theoretical Study of Interphase Mass Transfer, Columbia University Press, New York (1953).
75. Adt, R., "Bubble Formation and Growth, A Study of the Boundary Conditions at a Liquid-Vapor Interface through Ineversible Thermodynamics", Sc.D. Thesis, M.I.T. (1966).
76. Wilcox, S., "Film Condensation of Liquid Metals - Precision of Measurement", Ph.D. Thesis, M.I.T. (1969).

77. Volmer, M., A. Weber, Z. Physik. Chem., 119, p 277 (1925).
78. Becker, R., W. Döring, Ann. Physik, 24, p 719 (1935).
79. Hirth, J. P., G. M. Pound, Condensation and Evaporation, Nucleation and Growth Kinetics, Pergamon Press, Oxford (1963).
80. Adamson, A. W., Physical Chemistry of Surfaces, Interscience Publishers, Inc., New York (1960).
81. Sigsbee, R. A., G. M. Pound, "Heterogeneous Nucleation from the Vapor", Advan. Colloid Interface Sci., 1, p 335 (1967).
82. Gibbs, J. W., Collected Works, Vol. I, Thermodynamics, Yale University Press, New Haven (1948).
83. Volmer, M., Kinetik der Phasenbildung, Edwards Brothers, Inc., Ann Arbor, Mich. (1945).
84. Chakraverty, B. K., G. M. Pound, Acta Met., 12, p 851 (1964).

APPENDIX A HEAT MEASUREMENT TECHNIQUES

The precautions the author took to insure accurate heat transfer measurements will be discussed in this appendix. Chapters 4 and 5 have emphasized how the presence of non-condensable gases and errors in temperature measurement can drastically affect dropwise condensation heat transfer experiments. Table 9 outlines the major steps taken before the required accuracy was obtained.

A.1 Errors Due to Non-Condensable Gases

The original condensing chamber and boiler section of the apparatus was poorly designed. As described in Section 5.1, the original system was large and contained numerous potential dead air spaces. In addition, the vapor output from the boiler was small resulting in a low vapor velocity past the condensing surface.

The preliminary experiments run with the original system resulted in very low measured heat transfer coefficients. At a heat flux of $30,000 \text{ Btu/hr ft}^2$ the heat transfer coefficient was approximately $1,500 \text{ Btu/hr ft}^2\text{°F}$. Temperature fluctuations as great as 1 °F were observed at the surface. The low coefficients and the temperature fluctuations are indicative of non-condensable gas effects.

An attempt was made to reduce non-condensable gas effects in the original system by blocking off part of the chamber and increasing the output of the boiler. These modifications resulted in a doubling of the measured heat transfer coefficient. For a heat flux of $30,000 \text{ Btu/hr ft}^2$, the ΔT decreased from 20 °F to 10 °F . This error in the measured ΔT of 10 °F can be solely attributed to non-condensable gases.

Rather than continue to modify the original system, a completely new condensing chamber and boiler were designed and constructed. This new system, much smaller than the original one, is fully described in Section 6.1. Tests made with this system resulted in a measured coefficient comparable to those by Rose [36,46] and Tanner [39] and their colleagues (see Figs. 9 and 10). With this system, the author feels confident that the heat transfer measurements were free of non-condensable gas effects.

A.2 Temperature Measurement Techniques

Due to the high heat transfer coefficients (up to 50,000 Btu/hr ft²°F) encountered in dropwise condensation, extreme accuracy in temperature measurement is required. This section will mention the precautions taken in this experiment to obtain this accuracy.

A.2.1 Thermocouple Arrangement

The vapor temperature* and the temperature at seven locations within the test section were measured with .005 inch diameter copper-constantan thermocouples. The nine thermocouples were made from the same spool of highest precision thermocouple wire and installed in the system with identical thermocouple circuits (see Fig. A-1). All nine cold junctions were placed in individual glass tubes immersed in crushed ice.

Before and after each run, the output of the thermocouples were compared at room temperature. All agreed to within .05 °F. A newly calibrated Leeds and Northrup K-2 potentiometer was used to measure the thermocouple output.

* Two thermocouples were used to measure the vapor temperature.

A.2.2 Installation of Thermocouples

Significant errors in temperature measurement can result from improper thermocouple installation. One of the most important errors is due to heat conduction along the thermocouple lead. Even if the thermocouple leads are positioned in an isotherm, there can be an error due to insufficient immersion depth.

Figure A-2 illustrates the magnitude of the error that can result from insufficient immersion depth of thermocouples. The key to proper thermocouple installation is to maximize the heat transfer from the inside of the hole to the thermocouple junction as compared to the conduction heat transfer from the junction to the leads outside the hole. The ideal situation is to have long, low conductivity thermocouple wire and a tight fit between the junction and the hole.

A temperature drop of 10 °F was experienced when a copper constantan thermocouple wire of diameter .01 inch was traversed through the .034 inch thermocouple holes. The temperature versus distance plot is indicated in Fig. A-2(a). When a .005 inch diameter wire was used doubled over once, the temperature drop was decreased to 5 °F. It was not until the effective immersion depth was increased to 1.6 inches with the .005 inch wire that a flat temperature gradient was measured (see Fig. A-2(c)).

The installation technique used in the experiment is illustrated in Figs. A-2(d) and 19. The thermocouple wire was doubled over twice to give an effective immersion depth of 1.6 inches. The hole was filled with an anti-seizing compound called "silver goop" to enhance heat transfer from the inside of the hole to the thermocouple junction. The ends of the thermocouple holes were plugged with heavy copper wire. The resulting error due to conduction along the lead was thought to be less

than .05 °F.

To insure that there would be no error due to conduction along the thermocouple wires used to measure the vapor temperature, three inch long leads were used inside the condensing chamber. The wires inside the glass tubes used for the cold junctions were immersed 12 inches in the ice bath.

A.2.3. Error Due to Location of Thermocouple Junction

Wilcox [76] has carried out a detailed analysis to determine the temperature measurement error due to uncertainty of the precise location of the thermocouple measuring junctions within the hole. Figure A-3 shows how uncertainty in temperature measurement within each hole can result in a sizeable uncertainty in the determination of the wall temperature.

Wilcox has shown that the error in wall measurement can be decreased by using a large number of widely spaced, small thermocouple holes and a high conductivity bulk material. Since seven thermocouples (with spacing between the two most distant thermocouples of 1.8 inches) were embedded in the copper test section used in this experiment, high accuracy in the measurement of the wall temperature was obtained.

The details of the analysis of Wilcox will not be repeated here. Figure A-3 shows that a Gaussian distribution of possible temperature measurements about the correct one at the center of the hole, \bar{T} , was chosen. The resulting temperature distribution at the wall will be Gaussian with the magnitude of the standard deviation depending on the number, spacing, and size of the thermocouple holes and the conductivity of the bulk material.

The error in wall measurement for the test section used in this experiment was calculated from the analysis of Wilcox. The resulting error in wall measurement divided by the heat flux $((T_w - \bar{T}_w)/Q/A)$ was $2.8 \times 10^{-6} \text{ } ^\circ\text{F/Btu/hr ft}^2$. This analysis showed that the error in wall measurement was always less than 10% of the measured temperature difference $(T_s - T_w)$.

A.2.4 Conclusions

It is not possible to estimate exactly how efficient the final design of the apparatus was in ridding itself of non-condensable gas effects. The author feels certain that the high velocities past the condensing surface were sufficient to remove a build-up of gases. Thus it is thought that the results reported in this thesis are for "gas free" steam.

A typical plot of the measured linear temperature gradients are plotted in Fig. A-4. It is believed that the total error in temperature measurements was always less than 10 percent of the measured vapor to surface temperature difference.

APPENDIX B DISCUSSION OF DROP DEPARTURE MECHANISMS

B.1 Departure Criterion for a Static Droplet

The subject of drop departure has been discussed in papers by Fatica and Katz [5] and Sugawara and Michiyoshi [9]. In these two papers, models have been proposed which predict the maximum size drop which can exist in static equilibrium on an inclined surface. In both of these models, no vibrational motion of the drop due to coalescence is considered.

Figure B-1 illustrates the forces acting on a droplet. It is evident from this figure that the values of the contact angles (advancing and receding), the surface tension, and the weight of the drop determine its departure size.

Just before a drop begins to depart, components of the forces in the plane of the surface can be equated to give a departure criterion. The resulting force balance is

$$S \cos \theta_r = W \sin \beta + S \cos \theta_a \quad (B.1)$$

where

$$W = \rho g V$$

The volume of a drop depends on its shape (contact angles) as well as its diameter. Fatica and Katz and Sugawara and Michiyoshi have shown that the volume of a drop can be computed from the relation

$$V = D^2 f(\theta_a, \theta_r) \quad (B.2)$$

Substituting (B.2) in (B.1), the maximum drop size can be found to be

$$D_{\max}^2 = \frac{S}{\rho g \sin \beta} f(\theta) \quad (B.3)$$

Here $f(\theta)$ is a functional relationship including both the advancing and receding contact angles. According to Fatica and Katz,

$$f(\theta)^2 = \frac{1 + \tan \frac{\theta_a}{2}}{\tan \frac{\theta_r}{2}} \left\{ \frac{\cos \theta_r - \cos \theta_a}{\tan^2 \frac{\theta_a}{2} \cdot f(\theta_r) + f(\theta)} \right\} \quad (B.4)$$

and to Sugawara and Michiyoshi,

$$f(\theta) = \frac{16 \sin^3 \theta_m}{\pi \theta_m / 90 - \sin 2\theta_m} \sin \frac{\theta_a - \theta_r}{2} \quad (B.5)$$

where

$$\theta_m = \frac{\theta_a + \theta_r}{2}$$

Fatica and Katz summarized their results for the case of a water droplet on a vertical surface in graphical form (reproduced here as Fig. B-2). From this figure one sees that the maximum drop size decreases as the advancing and receding contact angles are increased. This figure may be used for other fluids and different temperatures by scaling the ratio of the two property terms, $\frac{S}{\rho}$.

B.2 Departure Criterion for a Dynamic Droplet

When two drops coalesce, they form a single drop located at the center of gravity of the two original drops. Thus, coalescence causes the drops to move toward each other. When a large "dead" drop is sitting on a surface, it is constantly being bumped into by the small "active" drops about its periphery. Each time a coalescence occurs, the large drop moves slightly. The random nature of the small drops coalescing into the big drop will set the big drop into some sort of a random vibratory motion.

As the condensing rate is increased, the rate at which active drops grow and bump into the large drops increases. Thus, it can be assumed that the large drops will vibrate faster at higher heat fluxes.

The motion imparted to the big drops by the coalescing action makes them less stable than static drops. Thus, the dynamic drops will depart from the surface prematurely. The lowering of the departure size due to the dynamic effects has been observed by Brown and Thomas [48] and this author.

B.3 Vapor Velocity Effect on Departure Size

This author and several other experimenters [39,52] have noticed that high vapor velocities past the condensing surface increase the heat transfer coefficient. The explanation for this increase in performance is the early removal of departing drops.

A high vapor velocity across the condenser surface introduces a shear force on the large drops which tends to sweep them from the surface. The appropriate component of this shear force can be added to the force balance of Eq. (B.1) and the departure size predicted. Most experimenters have blown the vapor across the condensing surface perpendicular to the downward track of departing drops. The velocity effect would be more dramatic if the vapor flow was directed in the downward direction.

B.4 Effect of Vibration of the Surface on Departure Size

The preliminary results of the surface vibration study mentioned in Section 6.7 demonstrated an increase in heat transfer performance with increased frequency. Mechanically vibrating the surface introduces an acceleration force on the drops which tends to shake them from the surface. The resulting early departure is similar to that caused by

the dynamic effect of the coalescing action.

The direction of the surface vibration with respect to the departure direction as well as its amplitude and frequency will determine the effectiveness of this heat transfer enhancing technique. The magnitude of the decrease in departure size can be predicted by introducing the acceleration force into Eq. (B.1).

B.5 Conclusions

This analysis of departure mechanisms is by no means complete. It would be very beneficial to be able to predict the drop distribution for the large departure size drops on the surface. How changes in the distribution of large drops affect dropwise condensation heat transfer is another area which needs further investigation.

APPENDIX C DISCUSSION OF CURVATURE RESISTANCE

C.1 Kelvin - Helmholtz Equation

The equilibrium between two phases of a pure substance across a curved interface is different than that for a flat interface. Lord Kelvin [71] and von Helmholtz [72] have shown that the curvature of the surface separating the two phases as well as the temperatures determine the equilibrium pressure. Thus,

$$p_{gc} = f(T, r) \quad . \quad (C.1)$$

The relationship stated in Eq. (C.1) can be derived by referring to Fig. C-1.

Assume that the system illustrated in Fig. C-1 is at a uniform temperature despite the variation in pressure caused by hydrostatic forces. For a liquid which does not wet the capillary tube, the liquid vapor interface will be a curved surface at a level of height L below the flat surface. This system simulates drop-like curvature.

The pressure of the liquid below the curved interface is

$$p_{fg} = p_s + \rho_f gL \quad . \quad (C.2)$$

For dynamic equilibrium across the curved interface

$$\pi r^2 p_{gc} + 2\pi r\sigma = \pi r^2 p_{fc} \quad . \quad (C.3)$$

For pressures well below the critical pressure,

$$p_{gc} \approx p_s$$

since the hydrostatic pressure $\rho_g gL$ is small. Thus,

$$p_{fc} - p_s \approx p_{fc} - p_{gc} \quad . \quad (C.4)$$

Substituting (C.4) in (C.3) and rearranging terms,

$$p_{fc} - p_s = \frac{2\sigma}{r} \quad . \quad (C.5)$$

Combining (C.2) with (C.5),

$$\rho_f gL = \frac{2\sigma}{r}$$

or

$$L = \frac{2\sigma}{\rho_f g r} \quad . \quad (C.6)$$

For an element of vapor, dy , in the capillary tube,

$$dp = \rho_g g dy \quad . \quad (C.7)$$

Assuming the perfect gas law is valid and since the temperature of the system is uniform, then

$$\frac{p}{\rho_g} = \frac{p_s}{\rho_{gs}} \quad . \quad (C.8)$$

Substituting (C.8) in (C.7),

$$p_s \frac{dp}{p} = \rho_{gs} g dy \quad . \quad (C.9)$$

Integrating Eq. (C.9) from $y = 0$ to $y = L$ gives

$$p_s \ln \frac{p_{gc}}{p_s} = \rho_{gs} g L \quad . \quad (C.10)$$

Again assuming that the perfect gas law holds,

$$\frac{p_s}{\rho_{gs}} = \overline{RT}_s \quad . \quad (C.11)$$

By combining Eqs. (C.10) and (C.11), the following relationship is found:

$$\ln \frac{p_{gc}}{p_s} = \frac{2\sigma}{r \rho_f \overline{RT}_s} \quad (C.12)$$

Equation (C.12) is known as the Kelvin-Helmholtz Equation. Since $r > 0$ for a drop, then this equation states that the pressure of the vapor above a curved interface is greater than the pressure above a flat interface. The analysis is equally valid for the case of a liquid which wets the capillary tube and rises to a concave liquid surface. This situation simulates bubble-like curvature.

The Kelvin-Helmholtz equation is displayed graphically in Fig. C-2. The dash lines give the pressure of the vapor in equilibrium with drops of radius, r . The dot and dash lines give the pressure of the liquid in equilibrium with bubbles of radius, r .

C.2 Temperature Difference for Drop-Like Curvature

The equilibrium condition for the curved interface is compared to the flat interface in Fig. C-3. The two systems are at the same temperature, T_o , but not the same pressure. For system 1, the system pressure, p_{sys_1} , as read from the pressure gauges, is equal to the saturation pressure, p_s , corresponding to the uniform temperature, T_o . However, for system 2, the system pressure, p_{sys_2} , is equal to the vapor pressure, p_{gc} , in equilibrium with the liquid drop at the temperature, T_o .

The Kelvin-Helmholtz equation states that

$$\ln \frac{p_{gc}}{p_s} = \frac{2\sigma}{r \rho_f \overline{RT}_o} \quad (C.13)$$

Since $\frac{p_{gc} - p_s}{p_s} < 1$, then

$$\ln \frac{p_{gc}}{p_s} \approx \frac{p_{gc} - p_s}{p_s} \quad (C.14)$$

Substituting (C.14) in (C.13),

$$p_{gc} - p_s = \frac{2\sigma p_s}{r \rho_f RT_o} \quad (C.15)$$

The saturation temperature corresponding to the pressure of system 2, p_{gc} , can be found from the Clausius-Clapyron equation

$$\frac{dT}{dp} = \frac{v_{fg} T_o}{H_{fg}} \quad (C.16)$$

If it is assumed that $\frac{v_{fg} T_o}{H_{fg}}$ is constant from p_s to p_{gc} then,

$$\frac{T_o - T_{gc}}{p_s - p_{gc}} = \frac{v_{fg} T_o}{H_{fg}} \quad (C.17)$$

Combining (C.15) and (C.17),

$$T_{gc} - T_o = \frac{2\sigma p_s}{r \rho_f RT_o} \frac{v_{fg} T_o}{H_{fg}} \quad (C.18)$$

For a perfect gas, $\frac{p_s v_{fg}}{R T_o} = 1$. Thus Eq. (C.18) simplifies to

$$T_{gc} - T_o = \frac{2\sigma T_o}{r H_{fg} \rho_f} \quad (C.19)$$

T_{gc} is the saturation temperature corresponding to the pressure measured for system 2. T_o is the saturation temperature of system 1. Thus,

$$T_{sat_2} - T_{sat_1} = \frac{2\sigma T_{sat_1}}{r H_{fg} \rho_f} \quad (C.20)$$

Here T_{sat_2} is the saturation temperature above a curved interface and T_{sat_1} is the saturation temperature above a flat interface. Equation (C.20) states that the vapor above a drop must be supersaturated compared to the vapor above a plane interface at the same temperature in order for the drop to be in thermodynamic and mechanical equilibrium.

The two systems illustrated in Fig. C-3 are at the same temperature, T_o . The systems can be modified so that the pressure instead of the temperature is kept constant. If the pressure is the same at both the curved and the flat interface, then the saturation temperature corresponding to the curved interface will be less than the saturation temperature at the flat interface. The resulting temperature difference is given by Eq. (C.20).

Setting $\Delta T_t = T_{sat_2} - T_{sat_1}$, then the minimum size drop which can exist on a surface is

$$r_{min} = \frac{2\sigma T_s}{H_{fg} \rho_f \Delta T_t} \quad . \quad (C.21)$$

A simple expression for the temperature drop due to curvature can be found by combining Eqs. (C.20) and (C.21):

$$\Delta T = \frac{r}{r_{min}} \Delta T_t \quad . \quad (C.22)$$

This temperature difference is illustrated in Fig. 44.

C.3 Temperature Difference for Bubble-Like Curvatures

For the sake of comparison, the temperature drop due to bubble-like curvature will be derived. Referring to Fig. C-4, one sees that the pressure of system 2 is now the pressure of the liquid. (For the case of drop-like curvature, the system pressure was the pressure of the vapor phase.)

The pressure of the vapor inside the bubble can be found from the Kelvin-Helmholtz equation,

$$p_{gc} - p_s = \frac{2\sigma p_s}{r \rho_f R T_o} \quad . \quad (C.23)$$

The pressure of the liquid near the interface is

$$p_{fc} = p_{gc} + \frac{2\sigma}{r} \quad . \quad (C.24)$$

Combining (C.23) and (C.24), the liquid pressure (and thus the system pressure) is

$$p_{fc} = p_s + \frac{2\sigma p_s}{r \rho_f \bar{RT}_o} - \frac{2\sigma}{r} \quad . \quad (C.25)$$

Since $p_s / \rho_f \bar{RT}_o \ll 1$, then Eq. (C.23) simplifies to

$$p_s - p_{fc} = \frac{2\sigma}{r} \quad . \quad (C.26)$$

The Clausius-Clapyron relation can be applied to (C.26) in a similar way as in Eq. (C.18). The resulting temperature difference is

$$T_o - T_{fc} = \frac{2\sigma}{r} \frac{v_{fg} T_o}{H_{fg}} \quad . \quad (C.27)$$

For pressures not near the critical point $v_{fg} \approx v_g = 1/\rho_g$ and thus Eq. (C.27) becomes

$$T_o - T_{fc} = \frac{2\sigma T_o}{r H_{fg} \rho_g} \quad . \quad (C.28)$$

T_{fc} is the saturation temperature corresponding to the pressure measured for system 2. The saturation temperature for system 1 is T_o .

Thus, Eq. (C.28) may be rewritten as

$$T_{sat_1} - T_{sat_2} = \frac{2\sigma T_{sat_1}}{r H_{fg} \rho_g} \quad . \quad (C.29)$$

T_{sat_2} is the saturation temperature above a curved interface and T_{sat_1} , the saturation temperature above a flat interface. T_{gc} is the temperature of the vapor within the bubble.

Equation (C.29) states that the vapor inside a bubble must be superheated as compared to the saturation temperature of the liquid.

Since the bubble ΔT involves the reciprocal of the vapor density (as compared to the reciprocal of the liquid density for the droplet ΔT), the temperature drop predicted by Eq. (C.29) is large compared to that predicted in Eq. (C.20).

The minimum bubble size will be

$$r_{\min} = \frac{2\sigma T_s}{H_{fg} \rho_g \Delta T_t} \quad \text{where} \quad (C.30)$$

$$\Delta T_t = T_{\text{sat}_1} - T_{\text{sat}_2} .$$

C.4 Effect of System Pressure on Minimum Size Drop and Bubble

The minimum size drop which can exist in equilibrium is

$$D_{\min_D} = \frac{4\sigma T_s}{H_{fg} \rho_f \Delta T_t} . \quad (C.31)$$

For a bubble, the minimum size is

$$D_{\min_B} = \frac{4\sigma T_s}{H_{fg} \rho_g \Delta T_t} . \quad (C.32)$$

At the same operating conditions,

$$\frac{D_{\min_D}}{D_{\min_B}} = \frac{\rho_g}{\rho_f} = \frac{v_f}{v_g} . \quad (C.33)$$

This relation shows why the minimum drop size is smaller by more than three orders of magnitude than the minimum bubble size.

The effect of varying the pressure of the minimum drop and bubble size is displayed in Fig. C-5. It is evident from this figure that pressure has little effect on the minimum size of drops but a large effect on minimum bubble sizes. The reason for this is that the liquid

density is nearly independent of pressure while the vapor density is strongly pressure dependent.

APPENDIX D DISCUSSION OF NUCLEATION

Heat transfer engineers encounter the nucleation phenomenon in nucleate boiling and dropwise condensation. For the case of boiling, the nucleation criterion has been well developed and the predicted trends have been experimentally verified. However, droplet nucleation has not been as well covered. Because of the great difference in the size and number of nucleation sites, droplet and bubble nucleation are not entirely analogous.

For both nucleate boiling and dropwise condensation, the nucleus has been observed to form at imperfections such as cavities or scratches on the surface. For boiling, the size and shape of the cavity which will produce a stable vapor nucleus for a given system pressure and surface to liquid temperature difference has been predicted and verified by experimental observations. If the same analysis is used for drop condensation, the critical size cavity can be predicted. At atmospheric pressure, the cavity size for droplet formations is nearly 2000 times smaller than for bubble formation at the same ΔT . As the pressure is lowered to 34 mm Hg, the ratio of critical bubble size to droplet size increases to 40,000.

The purpose of this discussion is to show that one can expect surface chemistry to play a vastly different role in the nucleation process for dropwise condensation as compared to nucleate boiling. The arguments concerning the size, shape, and number of surface imperfections which serve as nucleation sites for nucleate boiling are not likely to be appropriate for dropwise condensation.

Because of the disparity between the nucleus size for boiling and

condensation, the standard approach used to predict bubble nucleation will not be used in this discussion of droplet nucleation. Instead, the author will revert back to the more classical approach of comparing heterogeneous nucleation of a droplet on a substrate to homogeneous nucleation of a droplet from a uniform temperature vapor.

D.1 Homogeneous Nucleation

Coverage of homogeneous vapor-liquid nucleation can be found in the works of Volmer and Weber [77], Becker and Döring [78], Hirth and Pound [79], and many others. Much of the material presented in this appendix was taken from the reviews of nucleation by Adamson [80] and Sigsbee and Pound [81].

Gibbs [82] determined that there is a certain free energy of formation involved in the transformation of vapor to a liquid droplet. The reversible work required to form a droplet from the vapor phase involves a volume and surface contribution and can be expressed as

$$\Delta G = \frac{4}{3}\pi r^3 \Delta G_v + 4\pi r^2 \sigma \quad (D.1)$$

where

$$\Delta G_v = - \frac{\overline{RT}}{v_f} \ln \frac{p}{p_s} \quad (D.2)$$

A plot of ΔG versus radius is given in Fig. D-1. By maximizing Eq. (D.1) with respect to r , the critical size nucleus, r^* , and the Gibbs free energy of formation of a nucleus of critical size, ΔG^* , can be found to be

$$r^* = - \frac{2\sigma}{\Delta G_v} \quad (D.3)$$

and

$$\Delta G^* = \frac{16}{3} \pi \frac{\sigma^3}{\Delta G_v} \quad (D.4)$$

By substituting (D.2) into (D.3) and rearranging terms, the following equation is obtained:

$$\ln \frac{p}{p_s} = \frac{2\sigma v_f}{r^* RT} \quad (D.5)$$

Equation (D.5) is simply the Kelvin-Helmholz equation for the effect of curvature on vapor pressure (see Appendix C). ΔG^* can be considered an "energy barrier" which must be overcome in order for nucleation to take place. As ΔG^* is lowered, nucleation becomes easier. Figure D-2 shows that increasing the supersaturation ratio, $S = p/p_s$, lowers the critical free energy of formation and thus causes more nucleation to take place.

D.2 Heterogeneous Nucleation on a Plane Substrate

The free energy of formation involved in the transformation of vapor to liquid in the presence of a solid surface is lower than for the case of no third phase present. The equation for homogeneous nucleation can be modified by taking into account the contact angle the liquid nucleus makes with the plane substrate. The resulting critical radius and Gibbs free energy of formation as derived by Volmer [83] are,

$$r^* = - \frac{2\sigma}{\Delta G_v} \quad (D.6)$$

and

$$\Delta G_1^* = \frac{16}{3} \pi \frac{\sigma^3}{\Delta G_v} \phi(\theta) \quad (D.7)$$

where

$$\phi(\theta) = \frac{(2 - 3 \cos\theta + \cos^3\theta)}{4} \quad (D.8)$$

The result of this analysis is that the radius of curvature of the

critical nucleus is not affected by the presence of the solid interface. It is a function only of the surface tension and the Gibbs free energy difference, ΔG_v . However, the "energy barrier" is lowered. The contact angle function, $\phi(\theta)$, plotted in Fig. D-3, varies from 1 for $\theta = 180^\circ$ to 0 for $\theta = 0^\circ$. When the liquid completely wets the surface ($\theta = 0^\circ$), there is no energy barrier to nucleation, whereas for the other extreme ($\theta = 180^\circ$) the energy barrier is the same as for homogeneous nucleation.

The effect of contact angle on nucleation is illustrated in Fig. D-4. At the same supersaturation ratio, lowering the contact angle decreases the energy barrier to nucleation.

D.3 Heterogeneous Nucleation on a Substrate at a Ledge

The Gibbs free energy for the formation of a nucleus at a ledge is lower as compared to that on a plane surface. Chakraverty and Pound [84] determined that the critical Gibbs free energy at a 90° ledge is

$$\Delta G_L^* = \frac{16}{3} \pi \frac{\sigma^3}{\Delta G_v^2} \phi_L(\theta) \quad (D.9)$$

where

$$\begin{aligned} \phi_L(\theta) = 1/4 \left[(\sin \theta - \cos \theta) + (2/\pi) \cos^2 \theta (\sin^2 \theta - \cos^2 \theta)^{1/2} \right. \\ + (2/\pi) (\cos \theta \sin^2 \theta \sin^{-1} \cot \theta) - \cos \theta \sin^2 \theta \\ \left. - (2/\pi r^*) \int_{r^* \cos \theta}^{r^* \sin \theta} \sin^{-1} [r^* \cos \theta / (r^{*2} - y^2)^{1/2}] dy \right] \quad (D.10) \end{aligned}$$

y is a variable of integration.

When $\theta < 45^\circ$ and $50^\circ < \theta < 105^\circ$, ΔG_L^* will be less than ΔG_1^* . Thus, providing the contact angle is within these ranges, nuclei will form

first at ledges and other surface faults.

The effect of a substrate on nucleation depends on its surface energy. One can consider the substrate as contributing its surface energy to help overcome the energy barrier to the formation of a stable nucleus. The higher the surface energy, the less "push" is needed in the form of a ΔT to initiate nucleation. Surface flaws such as scratches and pits have a higher "energy" than the average for the entire surface. This is why the nucleation rate is greatest at imperfections on the surface.

D.4 Nucleation Equation in Terms of ΔT

Heat transfer engineers prefer to work with a temperature difference as opposed to a supersaturation ratio p/p_s . By using the Clausius-Clapyron equation, the term $\ln p/p_s$ can be written in terms of ΔT . The Clausius-Clapyron equation can be written as

$$\frac{dT}{dp} = \frac{v_{fg} T_s}{H_{fg}} \quad . \quad (D.11)$$

If it is assumed that $\frac{v_{fg} T_s}{H_{fg}}$ is constant from p_s to p , then

$$\frac{T - T_s}{p - p_s} = \frac{v_{fg} T_s}{H_{fg}} \quad . \quad (D.12)$$

If $\frac{p - p_s}{p_s} < 1$, then

$$\ln \frac{p}{p_s} \approx \frac{p - p_s}{p_s} \quad . \quad (D.13)$$

Combining (D.12) and (D.13),

$$\ln \frac{p}{p_s} = \frac{(T - T_s) H_{fg}}{p_s T_s v_{fg}} \quad . \quad (D.14)$$

If the vapor is considered a perfect gas, then

$$p_s v_{fg} \approx \bar{RT}_s \quad . \quad (D.15)$$

Equation (D.15) can be rewritten as

$$\ln \frac{p}{p_s} = \frac{\Delta T H_{fg}}{\bar{RT}_s^2} \quad (D.16)$$

where $\Delta T = T - T_s$.

The nucleation equations outlined in the previous sections can be rewritten in terms of a temperature difference by using Eq. (D.16). Performing this substitution results in the following equations for homogeneous nucleation:

$$\Delta G_v = \frac{-H_{fg}}{v_f} \frac{\Delta T}{T_s} \quad (D.17)$$

$$r^* = \frac{2\sigma v_f T_s}{H_{fg} \Delta T} \quad (D.18)$$

and

$$\Delta G^* = \frac{16}{3} \pi \sigma^3 \left(\frac{T_s}{\rho_f H_{fg} \Delta T} \right)^2 \quad . \quad (D.19)$$

For heterogeneous nucleation on a flat substrate the critical Gibbs free energy of formation is

$$\Delta G_1^* = \Delta G^* \phi(\theta) \quad (D.20)$$

where

$$\phi(\theta) = \frac{(2 - 3 \cos \theta + \cos^3 \theta)}{4} \quad .$$

In the case of heterogeneous nucleation on a ledge then the contact angle terms $\phi_L(\theta)$, as specified in Eq. (D.10), should be substituted in Eq. (D.20).

D.5 Nucleation Rate

Volmer, Becker, and Döring [78 and 83] have determined what the

nucleation rate should be for a given nucleus of critical size. Details of this rather extensive analysis can be found in the above references. The nucleation rate for heterogeneous nucleation is

$$J = A e^{-\Delta G^*\phi/\overline{RT}} \quad (D.21)$$

In this expression, J is the number of nuclei per cubic centimeter forming per second. For first approximations, A can be considered a constant independent of pressure and temperature.

The term $\Delta G^*\phi/\overline{RT}$ is the quantity which must be evaluated to determine the rate of nucleation of a liquid droplet from a supersaturated vapor. The appropriate contact angle function (Eq. D.8 or Eq. D.10) should be used depending on how one models the surface.

No attempt will be made in this survey to quantitatively predict nucleation rates as parameters are varied. The author does, however, want to specify the trends which can be expected when the system pressure (at a constant ΔT) and the ΔT (at a constant pressure) are varied.

D.6 Effects of Pressure and ΔT on the Nucleation Rate

In order to determine the parametric effects on nucleation, the term $\Delta G^*\phi/\overline{RT}$ must be examined. From Eq. (D.19) this term may be written as

$$\frac{\Delta G^*\phi}{\overline{RT}} = \frac{16}{3} \pi \frac{\sigma^3 T_s}{\overline{R} \rho_f^2 H_{fg}^2 \Delta T^2} \phi \quad (D.22)$$

where ϕ is given by Eq. (D.8) or (D.10).

Decreasing $\Delta G^*\phi/\overline{RT}$ has the effect of increasing the nucleation rate. Equation (D.22) shows that as the ΔT is increased, $\Delta G^*\phi/\overline{RT}$ decreases and the nucleation rate increases. This is certainly the

expected trend, as ΔT can be considered the driving force which overcomes the energy barrier to nucleation.

The pressure effect on nucleation can be realized by examining Fig. D.5. Keeping the ΔT constant, the term $\Delta G^*/RT$ decreases with increasing pressure. This predicts superior nucleation at higher pressures.

The contact angle function, ϕ , also decreases with increasing pressure. Figure D.6 shows that for a given liquid-substrate combination, the contact angle decreases with temperature. Since it has been shown in Fig. D-3 that the contact angle function, $\phi(\theta)$, decreases with contact angle, then it can be concluded that the contact angle function decreases with pressure at a given ΔT .

Since the data of contact angle versus temperature is limited and since the precise contact angle function for an irregular surface is unknown, the relation between $\Delta G^*\phi/\overline{RT}$ and T will not be drawn in Fig. D-5. However, it can be concluded that a curve of $\Delta G^*\phi/\overline{RT}$ versus T would have a sharper decreasing slope than the one drawn for $\Delta G^*/\overline{RT}$. Thus, for heterogeneous nucleation at a constant ΔT , the nucleation rate can be expected to increase with pressure.

D.7 Conclusions

A typical condensing surface has nucleation sites of varying degrees of "potency". At a constant pressure, when the surface to vapor temperature difference is increased, more and more of these nucleation sites become active. In a similar way, at constant ΔT , increasing the pressure activates an increased number of sites. How rapid the number of active nucleation sites changes with ΔT and pressure depends on the characteristics (i.e. surface energy) of the surface.

APPENDIX E DISCUSSION OF INTERFACIAL MASS TRANSFER RESISTANCE

Past experiments have observed that there is a finite temperature difference at the liquid-vapor interface during the condensation and evaporation processes. The magnitude of this temperature difference can be computed by examining the mass transfer phenomenon at the interface. The most complete coverage of this subject can be found in the book by Schrage [74]. Recent works by Nabavian and Bromley [70], Silver [10], Umur and Griffith [21], Le Fevre and Rose [23], and others* have interpreted Schrage's equations.

The above references derive the expression for the interfacial heat transfer coefficient, h_i , by considering the mass flow equations at the interface. The mass flux toward and away from a condensing surface are respectively:

$$W_- = -p_v (M/2\pi\overline{RT}_v)^{1/2} \quad (E.1)$$

and

$$W_+ = p_s (M/2\pi\overline{RT}_s)^{1/2} \quad (E.2)$$

A net mass flux, w , may exist toward or away from the surface,

$$w = \alpha (W_+ - W_-) \quad (E.3)$$

Here α is the "condensation coefficient" or "evaporation coefficient." The condensation coefficient is defined as the fraction of vapor molecules which enter the liquid phase after striking the liquid surface.

Substituting (E.1) and (E.2) in (E.3), one gets

* No attempt will be made at this time to present a complete literature survey of this topic. Doctoral theses at M.I.T. by Adt [75] and Wilcox [76] cover the interface problem in great detail.

$$w \approx \alpha(p_s - p_v) \left(\frac{M}{2\pi RT_s} \right)^{1/2} \quad (E.4)$$

Equation (E.4) can be written in the form of temperature differences instead of pressure differences by utilizing the integrated form of the Clausius-Clapeyron equation:

$$p_v - p_s = \frac{H_{fg}}{T_s v_{fg}} (T_v - T_s) \quad (E.5)$$

The interfacial heat transfer coefficient is defined as

$$h_i = \frac{w H_{fg}}{T_s - T_v} \quad (E.6)$$

Combining (E.4), (E.5) and (E.6) gives

$$h_i = \alpha \left(\frac{M}{2\pi RT_s} \right)^{1/2} \frac{H_{fg}}{T_s v_g} \quad (E.7)$$

For net condensation, the vapor has a finite flow toward the surface. This would cause more vapor molecules to stick to the surface than would occur for an equilibrium system.

To account for this effect, Schrage determined that the condensation coefficient used in Eq. (E.7) should be

$$\alpha_1 = \frac{2\alpha}{2 - \alpha} \quad (E.8)$$

Thus,

$$h_i = \frac{2\alpha}{2 - \alpha} \left(\frac{M}{2\pi RT_s} \right)^{1/2} \frac{H_{fg}}{T_s v_g} \quad (E.9)$$

The value to use for α has been a topic of controversy for several decades. The condensation (or evaporation) coefficient as measured in over a dozen experiments has ranged from .006 to 1.0, depending on the pressure. It has been shown conclusively in the recent research by Wilcox [76] that the low values for α at high pressures can be attributed



to experimental errors. The accepted value used today for the condensation coefficient is 1, and is believed to be independent of pressure.

Assuming α to be 1, the interfacial heat transfer coefficient can be evaluated from equation (E.9). Values for h_i as a function of the interface temperatures have been calculated and plotted in Fig. E-1.

Figure E-1 shows that the interfacial heat transfer coefficient increases sharply with temperature. It should be emphasized that this increase in h_i is due solely to property changes. The value for the condensation coefficient has been kept constant at 1 throughout this temperature range.

APPENDIX F DISCUSSION OF DROP CONDUCTION RESISTANCE

The conduction resistance for a hemispherical drop of radius, r , can be approximated by comparing it to the resistance for a right-circular cylinder of radius, r , and height, r (see Fig. F-1). Assuming that the top and bottom surface temperatures, T_1 and T_2 , are uniform for the cylinder, then its conduction resistance can be defined as

$$R_{cyl} = \frac{T_1 - T_2}{Q} = \frac{r}{k\pi r^2} \quad (F.1)$$

Since the average conduction path is shorter for the case of the drop, then its resistance assuming uniform surface temperatures is

$$R_{dc} = \frac{T_1 - T_2}{Q} = C \frac{r}{k\pi r^2} \quad (F.2)$$

where $C < 1$.

Fatica and Katz [5] analyzed the drop conduction problem for an isolated spherical segment assuming the vapor-liquid interface temperature, T_1 , and the liquid-solid interface temperature, T_2 , are constant. For any spherical segment they found the heat transfer coefficient through the drop to be

$$h_{dc} = f(\theta) \frac{k}{D} \quad (F.3)$$

where $f(\theta)$ is a drop shape factor. They presented the value of the shape factor as a function of contact angle, θ , in graphical form (reproduced here as Fig. F-2).

The constant, C , of equation (F.2) is related to the shape factor of Fatica and Katz by the relation

$$C = \frac{2}{f(\pi/2)} \quad (F.4)$$

From Fig. F-2 and equation (F.4), C can be found to be .241.

Mikic [28] analyzed the exact solution of the conduction problem performed by Umur and Griffith [21] and found that if $C = .25$, the simple equation (F.2) closely approximated the exact solution.

McCormick and Baer [13,34] and Rose [24] accepted the value of .241 for C in their analyses of the drop conduction problem. This author used the value of .25. Since the two approximate solutions are so close, the convenience of using .25 instead of .241 was the basis of its selection.

APPENDIX G DISCUSSION OF CONSTRICTION RESISTANCE

Until the work of Mikic [28], none of the proposed theories for dropwise condensation considered the effect of the thermal properties of the condenser surface. Three investigators, Hampson and Ozisik [30], Tanner et al. [53], and Griffith and Lee [54] have shown that lowering the thermal conductivity of the substrate lowers the measured heat transfer coefficient for dropwise condensation. In the latter two references, the decrease in coefficient going from copper to stainless steel was over five fold. Certainly the effect of thermal conductivity of the condenser surface must be considered when talking about dropwise condensation.

The model proposed by Mikic states that the cause of the decrease of the measured coefficient for lower conductivity substrates is the non-uniformity in surface temperature. Because of the variations in size and spacing of drops on the surface, the local surface to vapor resistance varies over the condenser surface. Consequently, the surface temperature and thus the heat flux is also non-uniform over the surface.

The effect of non-uniform heat flux is illustrated in Fig. G-1. At any point on the surface, the temperature driving force is not the measured $(T_s - T_w)$ but the local temperature difference $(T_s - T_{cm})$. Mikic calls the resistance due to non-uniformities in heat flux a "constriction" resistance. If the drop condensation rate is to be considered as that due to the temperature difference $(T_s - T_w)$, then one must introduce an additional resistance. If R_{total} is the total resistance of the system, R_t the resistance due to the drop condensation process, and R_{cm} the average "constriction" resistance over the surface, then

$$R_{\text{total}} = R_t + R_{\text{cm}} \quad (\text{G.1})$$

or

$$\frac{T_s - T_w}{Q/A} = \frac{T_s - T_{\text{cm}}}{Q/A} + \frac{T_{\text{cm}} - T_w}{Q/A} \quad (\text{G.2})$$

where T_{cm} is now the "true" mean surface temperature.*

The paper of Mikic proceeds to derive an expression for the "constriction" resistance. Without going into further details concerning the derivation, the most usable expression for this resistance will be stated to be

$$R_{\text{cm}} \approx \frac{1}{3} \frac{\gamma}{(1 - \gamma)^{.5}} \frac{r_d}{k} \quad (\text{G.3})$$

where r_d is the radius of a typical inactive drop, γ is the surface area covered by inactive drops, and k is the liquid conductivity.

To evaluate the constriction resistance from equation (G.3), one must use some judgment. If one considers inactive drops to be those transferring less than 10 percent of the average heat, and chooses the typical inactive drop to be approximately one half the maximum drop size, then using the results of Figs. 37, 38, 55, and 56, the constriction resistance can be computed.

For low pressure condensation, drops with diameter greater than 150 microns transfer less than 10 percent of the total heat. According to Fig. 37, 56 percent of the surface is inactive. One half of the maximum drop size for low pressure condensation is a drop having a radius of 750 microns. For atmospheric pressure condensation, Figs. 38 and 56 show that drops greater than 40 microns in diameter are inactive,

* T_{cm} is actually not the temperature at the base of drops. There is an additional ΔT through the promoter layer (see Appendix H). In this analysis the promoter resistance has been neglected.

the inactive area is 68 percent, and the typical inactive drop is one of 625 microns.

The results of substituting the above values into equation (G.3) are summarized in Table G-1.

Table G-1 indicates that even for copper with a very high thermal conductivity, the "constriction" resistance is significant for atmospheric pressure condensation. Mikic showed that for stainless steel the constriction resistance would be as much as 80 percent of the total resistance. These results show that the effect of thermal conductivity of the surface, as exemplified in the "constriction" resistance, cannot be neglected.

APPENDIX H DISCUSSION OF TEFLON RESISTANCE

For chemically promoted surfaces the thermal resistance due to the promoter layer is usually so small that it can be neglected. However, for Teflon this is not the case. Because the thickness of the physically adhering Teflon is at least an order of magnitude greater than for the chemical promoters, there is a temperature drop through the Teflon which is appreciable.

If the rate of condensation is to be considered as that due to the temperature difference $(T_s - T_w)$, then one must introduce an additional resistance. The resistance due to the conduction loss across the Teflon can be assumed to be in series with the resistance due to the dropwise condensation process (see Fig. H-1).^{*} Accordingly,

$$R_{\text{total}} = R_t + R_p$$

or

(H.1)

$$\frac{T_s - T_w}{Q/A} = \frac{T_s - T_p}{Q/A} + \frac{T_p - T_w}{Q/A}$$

where R_{total} is the total resistance, R_t is the resistance due to dropwise condensation, and R_p is the Teflon resistance. The teflon resistance is given by

$$R_p = \frac{\ell}{k_T} \quad (\text{H.2})$$

where ℓ is the thickness and k_T is the thermal conductivity of the Teflon. Substituting (H.2) in (H.1),

$$R_{\text{total}} = R_t + \frac{\ell}{k_T} \quad (\text{H.3})$$

^{*}The constriction resistance, discussed in Appendix G, has been neglected in this analysis.

Talking in terms of heat transfer coefficients as opposed to resistances, equation (H.3) becomes

$$\frac{1}{h_{\text{total}}} = \frac{1}{h_t} + \frac{k_T}{\ell} \quad . \quad (\text{H.4})$$

Now assuming that the heat transfer coefficient for the drop condensation process, h_t , is the same for Teflon as for chemical promoters, then the overall coefficient of the Teflon systems is dependent on the thickness and conductivity of the Teflon layer.*

The procedure for applying the Teflon on copper described in Chapter 5 was recommended by consultants from Du Pont. The thickness of the resulting layer, after following these procedures, was predicted to be 6×10^{-5} inches from past experience of Du Pont engineers. Using this thickness and a conductivity of .1 Btu/hr ft °F, the heat transfer coefficient of the Teflon layer can be computed to be about 20,000 Btu/hr ft² °F. Assuming that 37,000 Btu/hr ft² °F is the coefficient for atmospheric pressure drop condensation, the overall coefficient will be 13,000 Btu/hr ft² °F. This is very close to the measured heat transfer coefficient for the Teflon surface of 12,500 Btu/hr ft² °F.

Figure H-2 represents the predicted values for the heat transfer coefficient for atmospheric pressure dropwise condensation on varying thicknesses of Teflon. In all cases the coefficient for the drop condensation itself is 37,000 Btu/hr ft² °F.

Figure H-2 shows that manufacturers must produce commercially

* This will be true provided that the nucleation site density and contact angle are comparable in both cases. Experimental observation by this author showed that the condensation process for Teflon and chemically promoted surfaces were very similar.

available Teflon coatings of thicknesses significantly less than a thousandth of an inch in order to make the total resistance (Teflon plus drop condensation) less than the resistance for film condensation.

APPENDIX I LISTING OF COMPUTER PROGRAMS

The following 7 programs were used extensively during this thesis.

The programs were written in Fortran IV for use on the IBM 1130 digital computer.

AGE 2 GRAHAM HEAT TRANSFER DATA REDUCTION PROGRAM-PART I

THIS PROGRAM WRITTEN TO PERFORM THE FOLLOWING JOBS
 CONVERT MILLIVOLT TC OUTPUT TO DEGREE F
 MAKE LEAST SQUARES FIT STRAIGHT LINE OF TEMP GRADIENT
 COMPUTE HEAT FLUX, SURFACE TEMP, HEAT TRANS COEFF.

DATA INPUT

```

REAL MVLT(10,30)
DIMENSION DIST(10),TMP(10,30),Y(30),PT(30),SLOP(30)
DIMENSION HTFX(50),HTC(50),VTMP(50),STMP(50),DTMP(50)
DIMENSION DEV(10,30)
1 IR=2
2 IW=3
4 READ(2,91) NORUN
91 FORMAT(I2)
READ(2,92) NOPT
92 FORMAT(I2)
5 COND=215
NO=NOPT-1
READ(IR,9) (DIST(I),I=1,NO)
NN=NOPT
NM=NORUN
7 READ(IR,9) ((MVLT(I,J),I=1,NN),J=1,NM)
9 FORMAT (7F5.3)
  
```

CONVERSION OF MILLIVOLT TC OUTPUT TO DEGREE F USING FOURTH
 ORDER CURVE FIT OF CU-CONST TC TABLES

```

12 DO 15 J=1,NORUN
13 DO 15 I=1,NOPT
14 CALL CCMVT (MVLT(I,J),TMP(I,J),DUMMY)
15 CONTINUE
  
```

LEAST SQUARES FIT OF STRAIGHT LINE TEMP GRADIENT

```

16 DO 20 J=1,NORUN
17 DO 18 I=1,NOPT
18 Y(I)=TMP(I,J)
19 CALL SJHLS(NOPT-1,DIST,Y,POIN,SLEP)
PT(J)=POIN
SLOP(J)=SLEP
DO 20 I=1,NOPT
DEV(I,J) =TMP(I,J) - (PT(J)+SLOP(J)*DIST(I))
20 CONTINUE
  
```

COMPUTATION OF HEAT FLUX, SURFACE TEMP, HEAT TRANS COEFF

```

21 DO 27 J=1,NORUN
22 HTFX(J)=-12*COND*SLOP(J)
23 VTMP(J)=TMP(NOPT,J)
24 STMP(J)=PT(J)
25 DTMP(J)= VTMP(J)-STMP(J)
26 HTC(J)=HTFX(J)/DTMP(J)
  
```


PAGE 3 GRAHAM HEAT TRANSFER DATA REDUCTION PROGRAM-PART I

7 CONTINUE

C DATA OUTPUT

2 DO 32 J=1,NM

9 WRITE(IW,33)J, HTFX(J),DTMP(J),HTC(J)

0 DO 31 I=1,NN

1 WRITE(IW,34) I,DIST(I),MVL(T(I,J),TMP(I,J),DEV(I,J)

2 WRITE(IW,35) SLOP(J),PT(J)

3 FORMAT (1H1,40X'RUN NO',I3 // 10X'HEAT FLUX=',F9.1,10X'TEMP DIF=',
1F4.2,10X'HEAT TRANS COEFF=',F9.1 // 9X'POSITION NO',12X'DISTANCE',
2 11X'MILLIVOLT',13X'TEMP(F)',11X'DEVIATION')

4 FORMAT(I20,2F20.3,F20.2,E20.3)

5 FORMAT (//10X'TEMP = ',F8.2,' X DIST + ',F8.2)

CALL EXIT

END

PAGE 2 GRAHAM HEAT TRANSFER DATA REDUCTION PROGRAM-PART 2

THIS PROGRAM WRITTEN TO PERFORM THE FOLLOWING JOBS
FIT STRAIGHT LINE THROUGH DELTA T - HEAT FLUX DATA
DETERMINE RELATION BETWEEN HEAT TRANSFER COEFF. VS DELTA T

DATA INPUT

DIMENSION T(200), Q(200), TT(40), H(40)
READ (2,1) M
FORMAT(I3)
DO 100 J=1,M
READ(2,1)N
READ(2,2)(T(I),I=1,N)
READ(2,2)(Q(I),I=1,N)
FORMAT(8F10.3)

LEAST SQUARES FIT STRAIGHT LINE THRU DELTA T - HEAT FLUX DATA.

CALL SJHLS(N,Q,T,A,B)
WRITE (3,3)A,B
FORMAT(1H1' INTERCEPT' ,F10.5,10X,'SLOPE',E15.5////)

DETERMINATION OF H VS DELTA T RELATION

TT(2)=.01
TT(3)=.05
TT(4)=.07
TT(5)=.1
DO 11 K=2,5
H(K)=(1.-A/TT(K))/B
CONTINUE
DO 10 K=6,39
TT(K)=TT(K-1)+0.1
H(K)=(1.-A/TT(K))/B
CONTINUE
WRITE(3,4)
FORMAT(' DELTA T',10X,'HEAT TRANSFER COEF.')

WRITE(3,5)(TT(I),H(I),I=2,31)
FORMAT(5X,F10.2,20X,F10.2)
CONTINUE
CALL EXIT
END


```

PAGE 2 GRAHAM COMPUTATION OF DROP GROWTH RATE DISTRIBUTIONS

C THIS PROGRAM WRITTEN TO PERFORM THE FOLLOWING JOBS
C COMPUTES RELATIONSHIP BETWEEN DROP GROWTH RATE AND DROP DIAMETER
C COMPUTES RELATIONSHIP BETWEEN DIAMETER AND TIME

C DATA INPUT

DIMENSION Y(1001)
TSAT=672.0
HFG=970.3
DENL=59.8086
CON=.388
STEN=.004032
VV=26.78
QONAM=35000.
SIG=2.0
DT=1.
M=18.
R=1544.
Q=4.17E8
O=((Q*M)/(6.283*R*TSAT))**.5
B=(HFG**2)/(TSAT*VV)
HE=778.*SIG*O*B
H= 1.8E6/HE
G= 1.52/CON
E=2.9E-2
F=.5*392.*8.*TSAT*STEN/(DENL*HFG*DT)
DMIN=2.*F
F=0.0
H=0.0
WRITE(3,26) DT,DMIN
6 FORMAT(1H1 // 15X,2E15.5)
WRITE(3,10) TSAT,HFG,VV,DENL,CON,STEN
0 FORMAT(//10X,2F10.1,2F10.4,F10.3,E11.4)
WRITE(3,25) SIG,HE,QONAM
5 FORMAT(/// 15X,3E15.5)
WRITE(3,19)
9 FORMAT( /// 6X'DIAM',10X'RATE1',10X'RATE2',10X'RATE3',
2 10X'RATE4')
READ(2,3) D
FORMAT(F10.2)

COMPUTATION OF DROP GROWTH RATE VS. DIAMETER

RATE1 = E*DT/(DENL*HFG)*((1-F/D)/(G*D+H))
RATE2 = E*DT/(DENL*HFG)/(G*D+H)
RATE3 = E*DT/(DENL*HFG)*((1-F/D)/(G*D))
RATE4 = E*DT/(DENL*HFG)/(G*D)
WRITE(3,33) D,RATE1,RATE2,RATE3,RATE4,DD
33 FORMAT(F10.2,4E15.5,F15.3)
IF(.1-D)2,13,13

```


PAGE 3 GRAHAM COMPUTATION OF DROP GROWTH RATE DISTRIBUTIONS

```

3  CONTINUE
   WRITE(3,18)
8  FORMAT(1H1/// 6X'DIAM',10X'RATE1',10X'RATE2',10X'RATE3',
2   10X'RATE4',3X'DIAM SQUARED')

```

COMPUTATION OF DIAMETER VS. TIME

```

DO 14 ID=1,10
D=ID*.1
DD=D**2
GG= G*(.5*(D-F)**2+2*F*(D-F)+F**2*ALOG(D-F))
HH = H*(D-F+F*ALOG(D-F))
GI=G*F**2*(2.5+ALOG(F))
HI=H*F*(1+ALOG(F))
TIME1= DENL*HFG/(E*DT)*(GG+HH-GI-HI)
TIME3=DENL*HFG/(E*DT)*(GG-GI)
TIME2 = DENL*HFG/(E*DT)*(G/2*(D**2-4*F**2)+H*(D-2*F))
TIME4 = DENL*HFG/(E*DT)*G/2*(D**2-4*F**2)
WRITE(3,33) D,TIME1,TIME2,TIME3,TIME4,DD

```

```

4  CONTINUE
DO 11 IDD=1,21,2
D=IDD
DD=D**2
GG= G*(.5*(D-F)**2+2*F*(D-F)+F**2*ALOG(D-F))
HH = H*(D-F+F*ALOG(D-F))
GI=G*F**2*(2.5+ALOG(F))
HI=H*F*(1+ALOG(F))
TIME1= DENL*HFG/(E*DT)*(GG+HH-GI-HI)
TIME3=DENL*HFG/(E*DT)*(GG-GI)
TIME2 = DENL*HFG/(E*DT)*(G/2*(D**2-4*F**2)+H*(D-2*F))
TIME4 = DENL*HFG/(E*DT)*G/2*(D**2-4*F**2)
WRITE(3,33) D,TIME1,TIME2,TIME3,TIME4,DD

```

```

1  CONTINUE
DO 12 IA=20,200,10
D=IA
DD=D**2
GG= G*(.5*(D-F)**2+2*F*(D-F)+F**2*ALOG(D-F))
HH = H*(D-F+F*ALOG(D-F))
GI=G*F**2*(2.5+ALOG(F))
HI=H*F*(1+ALOG(F))
TIME1= DENL*HFG/(E*DT)*(GG+HH-GI-HI)
TIME3=DENL*HFG/(E*DT)*(GG-GI)
TIME2 = DENL*HFG/(E*DT)*(G/2*(D**2-4*F**2)+H*(D-2*F))
TIME4 = DENL*HFG/(E*DT)*G/2*(D**2-4*F**2)
WRITE(3,33) D,TIME1,TIME2,TIME3,TIME4,DD
2  CONTINUE
   CALL EXIT
   END

```


GE 2 GRAHAM INTEGRATION OF HEAT FLUX DISTRIBUTION

THIS PROGRAM WRITTEN TO PERFORM THE FOLLOWING JOBS
INTEGRATE THE PREDICTED HEAT FLUX DISTRIBUTION
COMPARE PREDICTED WITH MEASURED HEAT FLUX

DATA INPUT

```
DIMENSION Y(1001)
TSAT=672.0
HFG=970.3
DENL=59.8086
CON=.388
STEN=.004032
VV=26.78
QONAM=35000.
SIG=2.0
DT=1.
M=18.
R=1544.
Q=4.17E8
O=((Q*M)/(6.283*R*TSAT))**.5
B=(HFG**2)/(TSAT*VV)
HE=778.*SIG*O*B
H= 1.8E6/HE
G= 1.52/CON
E=2.9E-2
F=.5*392.*8.*TSAT*STEN/(DENL*HFG*DT)
DMIN=2.*F
F=0.0
H=0.0
WRITE(3,26) DT,DMIN
6 FORMAT(1H1 // 15X,2E15.5)
WRITE(3,10) TSAT,HFG,VV,DENL,CON,STEN
0 FORMAT(//10X,2F10.1,2F10.4,F10.3,E11.4)
WRITE(3,25) SIG,HE,QONAM
5 FORMAT(/// 15X,3E15.5)
WRITE(3,19)
9 FORMAT(/// 11X'DIAM',7X'HEATFLUX',10X'RATIO',
2 9X'FACTOR',12X'EXP')
```

INTEGRATION BY SIMPSON'S RULE

```
SUM=0.
ANT=0
XU=2500.
ANT=0.0
READ(2,3) D,J
3 FORMAT(F10.1,I2)
IF(J-1)8,8,4
4 READ(2,22)Z,A
22 FORMAT(F10.4,E15.4)
```


PAGE 3 GRAHAM INTEGRATION OF HEAT FLUX DISTRIBUTION

```

      XH=(XU-D)/10.
      DO 102 I=1,11
      X= D+XH*(I-1)
      Y(I)=E*A*X**(2.-Z)*DT*(1.-F/X)/(G*X+H)
002  ANT=ANT+Y(I)
      DO 103 I=2,10
003  ANT=ANT+Y(I)
      DO 104 I=2,10,2
004  ANT=ANT+Y(I)+Y(I)
      ANT=ANT*XH/3.
      SUM=SUM+ANT
      RATIO=SUM/QONAM
      XU=D
      IF(J-1)88,88,44
```

C DATA OUTPUT

```

003  FORMAT(F15.2,E15.5,F15.4,E15.4,F15.3)
004  WRITE(3,333) D,SUM,RATIO,A,Z
      IF(.01-D)2,9,13
008  WRITE(3,333) D,SUM,RATIO
      IF(.01-D)2,9,13
010  CONTINUE
      CALL EXIT
      END
```


PAGE 2 GRAHAM DETERMINATION OF DROP SIZE DISTRIBUTION

C THIS PROGRAM WRITTEN TO PERFORM THE FOLLOWING JOBS
C COMPUTES COMMON LOG OF NO OF DROPS AND SIZE OF DROPS
C FITS STRAIGHT LINE THRU LOG NO. VS LOG DIAM

C DATA INPUT

DIMENSION D(100),DD(100),AN(100),ANN(100)
READ(2,1) N
FORMAT(I3)
READ(2,2)(D(I),I=1,N)
FORMAT(10F8.0)
READ(2,3)(AN(I),I=1,N)
FORMAT(8E10.3)

C COMPUTE LOG NO. AND LOG DIAM.

DO 4 I=1,N
DD(I)=ALOGT(D(I))
ANN(I)=ALOGT(AN(I))
CONTINUE
C FITS LEAST SQUARES STRAIGHT LINE THRU LOG NO. VS LOG DIAM.
C FORM OF EQUATION IS $N=A \cdot D^{**Z}$

CALL SJHLS(N,DD,ANN,POINT,SLOPE)
PINT=10.**POINT
WRITE(3,7)
FORMAT(1H1,'INTERCEPT',10X,'SLOPE')
WRITE(3,5)PINT,SLOPE
FORMAT(E15.5,10X,E15.5)
CALL EXIT
END

PAGE 2 GRAHAM CONVERSION OF THERMOCOUPLE OUTPUT TO DEGREES F

SUBROUTINE CCMVT (TMV,TF,TR)

THIS PROGRAM WRITTEN TO PERFORM THE FOLLOWING JOB
THIS SUBROUTINE CONVERTS THE OUTPUT OF A COPPER CONSTANTIN
THERMOCOUPLE, IN MILLIVOLTS, TO TEMPERATURE IN DEGREES
FAHRENHEIT, OR DEGREES RANKINE.

IF(TMV+5.379) 1,2,3

1 TF=-310.+(TMV+5.379)/0.009

GO TO 50

2 TF=-310.

GO TO 50

3 IF(TMV+5.284) 4,5,6

4 TF=-300.+(5.284+TMV)/0.0095

GO TO 50

5 TF=-300.

GO TO 50

6 IF(TMV+4.111) 7,8,9

7 TF=-.1336559E4-.1171498E4*TMV-.4090264E3*TMV**2-

1 .6076486E2*TMV**3-.3461118E1*TMV**4

GO TO 50

8 TF=-200.

GO TO 50

9 IF(TMV+2.559) 10,11,12

10 TF=.5024062E2+.6708685E2*TMV+.654206E1*TMV**2

1 +.1366154E1*TMV**3+.3468611E-1*TMV**4

GO TO 50

11 TF=-100.

GO TO 50

12 IF(TMV+0.67) 13,14,15

13 TF=.3235749E2+.4761401E2*TMV-.81807*TMV**2

1 +.2912321*TMV**3-.6431592E-2*TMV**4

GO TO 50

14 TF=0.0

GO TO 50

15 IF(TMV-1.517) 16,17,18

16 TF=.3200279E2+.4679051E2*TMV-.1382542E1*TMV**2

1 +.9235143E-1*TMV**3-.2356772E-1*TMV**4

GO TO 50

17 TF=100.

GO TO 50

18 IF(TMV-3.967) 19,20,21

19 TF=.3562773E2+.4092755E2*TMV+.1955488E1

1 *TMV**2-.7420778*TMV**3+.7092966E-1*TMV**4

GO TO 50

20 TF=200.

GO TO 50

21 IF(TMV-6.647) 22,23,24

22 TF=.4580235E2+.3610307E2*TMV+1.644181*TMV**2

1 -.2974033*TMV**3+.148139E-1*TMV**4

GO TO 50

23 TF=300.

PGE 3 GRAHAM CONVERSION OF THERMOCOUPLE OUTPUT TO DEGREES F

GO TO 50

24 IF(TMV-9.525) 25,26,27

25 TF=- .1375061E3+ .1323431E3*TMV- .1745894E2*TMV**2+
1 .1408984E1*TMV**3 -.4333291E-1*TMV**4

GO TO 50

26 TF=400.

GO TO 50

27 IF(TMV-12.575) 28,29,30

28 TF= .6999211E2+ .3403852E2*TMV+ .2749543*TMV**2
1 - .2620201E-1*TMV**3+ .4238036E-3*TMV**4

GO TO 50

29 TF=500.

GO TO 50

30 IF(TMV-15.773) 31,32,33

31 TF= .3107037E3- .3299964E2*TMV+ .7306085E1*TMV**2
1 - .3568681*TMV**3+ .6341877E-2*TMV**4

GO TO 50

32 TF=600.

GO TO 50

33 IF(TMV-19.1) 34,35,36

34 TF= .2632777E3- .929301E1*TMV+ .3896596E1*TMV**2
1 - .1619059*TMV**3+ .2410772E-2*TMV**4

GO TO 50

35 TF=700.

GO TO 50

36 TF=- .427098E4+ .9391044E3*TMV- .704867E2*TMV**2
1 + .2430854E1*TMV**3- .3147985E-1*TMV**4

50 TR=TF+459.69

RETURN

END

PAGE 2 SAKHUJA' THIS SUBROUTINE FITS A FIRST ORDER CURVE

```
SUBROUTINE SJHLS (N,X,Y,A,B)
DIMENSION X(1), Y(1),AA(2), BB(2,2)
SET SUMS TO ZERO
YY=0.0
XX=0.0
XY=0.0
X2=0.0
FORM SUMS
DO 1 I=1,N
XX=XX +X(I)
YY=YY+ Y(I)
XY=XY+X(I)*Y(I)
X2=X2+ X(I)**2
1 CONTINUE
SETUP THE INPUT FOR SIMQ
AA(1)=YY
AA(2)=XY
BB(1,1)=N
BB(1,2)=XX
BB(2,1)=XX
BB(2,2)=X2
SOLVE MATRIX
SIMQ IS A IBM SCIEN.SUB. PACKAGE WHICH SOLVES SIM. LIN. EQS.
CALL SIMQ(BB,AA,2,K)
A=AA(1)
B=AA(2)
RETURN
END
```


APPENDIX J DROP COUNTING DATA AND PROCEDURE

In each photograph, the number of drops of a certain size was counted. The average number of drops per photo of this size was obtained by summing the number counted on each photo and dividing by the number of photos.

The average number of drops per photo was then converted to the average number per square centimeter by multiplying by a "magnification factor". The magnification factor equals the reciprocal of the actual surface area in the field of view of the photograph in square centimeters. The number so obtained represents one data point on the plots of ΔN versus diameter (Fig. 33). If the same size drop was counted at two different magnifications, the average of the two results was obtained before plotting.

The best straight line was fitted by least squares technique through the data of $\log \Delta N$ versus $\log D$ in each drop distribution region. The resulting form of the drop distribution equation in each region was of the form $\Delta N = n_1 D^{-z} l$. The equation for \bar{N} versus D was obtained by dividing ΔN by the band width ΔD . The data presented is for a band width $\Delta D = .4D$. Thus, $\bar{N} = \frac{\Delta N}{.4D} = n D^{-z}$.

J.1 Drop Counting Data for Low Pressure ($T_{\text{sat}} = 88^{\circ}\text{F}$) Condensation

J.1.1 Magnification = 400X. 150 photos taken. 25 photos counted

Photo No.	Number of Drops in Photo of Diameter		
	50 μ	25 μ	10 μ
1	0	6	10
2	0	3	30
3	1	3	8
4	0	6	11
5	0	16	5
6	1	2	13
7	2	2	12
8	0	0	0
9	0	2	5
10	1	2	9
11	2	3	20
12	0	1	4
13	1	0	12
14	0	2	20
15	0	0	0
16	1	5	11
17	2	4	21
18	0	6	38
19	2	0	15
20	0	0	0
21	0	0	0
22	1	3	10
23	0	3	22
24	0	0	0
25	0	1	1
<hr/>			
Total	14	70	278
Average	.56	2.7	11.1

J.1.2 Magnification = 200X. 100 photos taken. 25 photos counted

Photo No.	Number of Drops in Photo of Diameter		
	50μ	30μ	20μ
1	7	15	11
2	2	4	17
3	11	8	14
4	1	4	13
5	1	5	11
6	1	7	10
7	6	9	30
8	2	11	19
9	15	17	12
10	8	15	10
11	6	12	16
12	3	6	10
13	6	6	8
14	1	0	0
15	4	13	15
16	3	16	37
17	4	7	8
18	0	13	18
19	5	11	15
20	4	5	7
21	6	12	13
22	2	19	28
23	22	12	12
24	5	10	12
25	1	4	33
<hr/>			
Total	125	241	379
Average	5	9.6	15.2

J.1.3 Magnification = 120X . 55 photos taken. 25 photos counted

Photo No.	Number of Drops in Photo of Diameter		
	200μ	100μ	50μ
1	1	3	8
2	0	1	14
3	0	3	16
4	3	6	10
5	2	0	11
6	1	2	11
7	0	0	0
8	0	0	15
9	0	2	14
10	0	0	0
11	2	3	15
12	2	3	15
13	3	5	13
14	0	7	9
15	1	1	10
16	0	2	12
17	1	5	11
18	0	3	14
19	2	6	8
20	1	3	13
21	2	4	10
22	1	2	12
23	2	1	11
24	0	2	18
25	1	3	6
Total	23	67	269
Average	.92	2.68	10.8

J.1.4 Magnification = 60X . 40 photos taken. 25 photos counted

Photo No.	Number of Drops in Photo of Diameter			
	500μ	300μ	200μ	100μ
1	3	2	0	12
2	0	0	1	6
3	2	0	4	9
4	0	1	3	10
5	1	3	2	11
6	1	1	3	14
7	0	0	1	6
8	0	1	1	5
9	0	0	0	0
10	0	6	3	15
11	0	1	3	13
12	0	0	4	11
13	0	2	5	6
14	0	1	2	33
15	2	0	2	15
16	0	1	7	20
17	1	1	2	3
18	0	5	10	7
19	2	2	2	8
20	0	0	2	34
21	2	0	0	11
22	0	4	11	9
23	2	0	1	21
24	0	3	10	6
25	0	6	3	8
<hr/>				
Total	16	40	81	293
Average	.64	1.6	2.3	16.7

J.1.5 Magnification = 10X. 24 Photos taken. 24 photos counted

Photo No.	Number of Drops in Photo of Diameter	
	2000μ	1000μ
1	1	17
2	3	15
3	2	0
4	1	17
5	0	9
6	0	14
7	0	12
8	1	14
9	0	5
10	2	16
11	0	13
12	0	6
13	2	7
14	0	6
15	1	12
16	1	11
17	3	6
18	0	0
19	0	8
20	3	7
21	0	7
22	1	16
23	2	19
24	0	5
Total	23	242
Average	.96	10.1

J.1.6 Magnification = 5X . 15 photos taken . 15 photos counted

Photo No.	Number of Drops in Photo of Diameter	
	2500 μ	
1	4	
2	4	
3	3	
4	3	
5	3	
6	5	
7	4	
8	8	
9	5	
10	3	
11	7	
12	8	
13	9	
14	7	
15	4	
	<hr/>	
Total	77	
Average	5.1	

J.2 Drop Counting Data for Atmospheric Pressure Condensation

J.2.1 Magnification = 200X. 100 photos taken. 50 photos counted

Photo No.	Number of Drops of Diam.			Photo No.	Number of Drops of Diam.		
	50μ	30μ	20μ		50μ	30μ	20μ
1	3	5	7	26	1	3	17
2	4	24	48	27	4	6	31
3	7	7	22	28	6	5	10
4	4	9	19	29	2	2	13
5	2	8	13	30	9	1	13
6	0	11	130	31	0	0	0
7	14	9	9	32	4	13	15
8	4	5	12	33	4	8	31
9	1	4	21	34	4	7	8
10	1	10	24	35	7	8	21
11	3	9	25	36	2	11	7
12	5	9	15	37	1	2	12
13	4	4	20	38	4	13	7
14	2	12	21	39	4	13	22
15	1	5	28	40	6	4	15
16	2	12	23	41	1	3	9
17	3	4	14	42	10	6	12
18	2	19	4	43	1	9	7
19	7	11	13	44	3	2	18
20	2	10	30	45	3	12	20
21	2	60	57	46	9	18	12
22	3	6	14	47	4	2	11
23	2	7	31	48	5	4	10
24	3	5	8	49	7	6	19
25	3	8	15	50	5	2	10
<hr/>							
Total	84	275	640	Total	106	160	550
Average	3.4	11.0	25.6	Average	4.23	6.4	14.3

J.2.2 Magnification = 120X. 50 photos taken. 50 photos counted

Photo No.	Number of Drops of Diam.			Photo No.	Number of Drops of Diam.		
	200μ	100μ	50μ		200μ	100μ	50μ
1	3	3	5	26	0	0	52
2	0	3	9	27	0	0	16
3	1	4	15	28	0	1	18
4	1	3	9	29	1	2	5
5	0	1	6	30	0	3	25
6	1	3	18	31	1	2	8
7	0	4	14	32	1	6	11
8	0	5	24	33	4	3	14
9	0	6	2	34	1	5	8
10	0	9	9	35	0	5	11
11	1	6	9	36	1	13	9
12	1	0	11	37	0	12	3
13	3	3	9	38	0	2	26
14	0	9	5	39	0	4	3
15	2	2	7	40	0	0	11
16	1	5	8	41	3	3	11
17	0	1	2	42	4	1	7
18	2	2	16	43	1	4	4
19	2	3	5	44	0	17	5
20	4	3	14	45	0	1	20
21	2	1	8	46	0	1	18
22	1	4	9	47	2	7	10
23	4	0	12	48	0	2	7
24	2	8	4	49	0	1	11
25	0	0	6	50	3	5	9
Total	31	88	236	Total	22	98	304
Average	1.2	3.5	9.4	Average	.9	3.9	12.1

J.2.3 Magnification = 60X. 40 photos taken. 40 photos counted

Photo No.	Number of Drops of Diam.				Photo No.	Number of Drops of Diam.			
	500μ	300μ	200μ	100μ		500μ	300μ	200μ	100μ
1	1	7	0	11	21	0	0	3	22
2	0	3	15	11	22	0	0	0	0
3	0	0	0	3	23	2	0	3	13
4	0	0	0	45	24	1	4	2	13
5	0	0	3	50	25	0	0	1	50
6	1	4	0	8	26	1	1	0	10
7	1	5	1	16	27	4	3	1	15
8	0	0	0	0	28	0	2	0	42
9	0	2	7	6	29	0	2	3	1
10	2	0	3	13	30	3	2	0	17
11	0	1	16	15	31	0	0	0	0
12	2	1	3	7	32	0	0	1	45
13	4	1	1	13	33	0	1	0	10
14	2	2	0	21	34	1	1	11	9
15	0	7	9	8	35	0	0	3	4
16	2	0	1	29	36	0	0	4	10
17	2	2	1	11	37	4	1	1	7
18	4	1	1	7	38	0	0	0	0
19	1	6	2	13	39	0	0	0	0
20	0	6	9	8	40	2	2	3	9
Total	22	48	72	295		18	19	42	277
Average	1.1	2.4	3.6	14.7		.9	1.0	2.1	13.8

J.2.4 Magnification = 10X. 24 photos taken. 24 photos counted

Photo No.	Number of Drops of Diameter	
	2000 μ	1000 μ
1	1	3
2	0	7
3	0	5
4	1	9
5	0	0
6	1	0
7	1	4
8	1	3
9	0	12
10	0	16
11	0	1
12	0	8
13	0	2
14	1	12
15	0	9
16	1	7
17	0	3
18	0	8
19	0	6
20	0	14
21	2	7
22	1	9
23	0	4
24	0	0
		<hr/>
Total	10	149
Average	.42	6.2

J.2.5 Magnification = 5X. 16 photos taken. 15 photos counted

Photo No.	Number of Drops of Diameter
	2500 μ
1	3
2	1
3	0
4	3
5	2
6	2
7	1
8	3
9	1
10	2
11	1
12	2
13	1
14	1
15	4
	—
Total	27
Average	1.8

TABLE 1 DROP DISTRIBUTION AND AREA COVERAGE EXPERIMENTS

REFERENCE	PRESSURE	ORIENTATION	MATERIAL & FINISH	PROMOTER	HEAT FLUX Btu/Hr Ft ²	MIN. DROP COUNTED	TOTAL AREA COVERAGE	DROP DISTRIBUTION
Fatica & Katz [5]	760 mm Hg	Vertical	Cu, Ni, Cr Mirror	Stearic Acid	Unknown	100μ	.45	Unknown
Hampson & Ozisik [30]	760 mm Hg	Vertical	Brass Mirror	Oleic Acid	60,000 to 330,000	125μ	.54	Unknown
Sugawara & Katsuta [11]	Unknown	Unknown	Copper Varying Roughness	Silicon Oil KF-96	Unknown	300μ	.54	$\Delta N = 2 \times 10^7 D^{-2}$
McCormick & West- water [15]	19 mm Hg	Horizontal Facing Up	Copper Mirror	Benzyl Mercap- tan	200 to 600	2μ	.64 to .72	$\Delta N / \Delta D =$ $9.24 \times 10^4 D^{-2.02}$ $5.9 \times 10^5 D^{-2.3}$ $6.1 \times 10^6 D^{-2.74}$
Graham Present Work	760 mm Hg & 34 mm Hg	Vertical	Copper Mirror	Dioceta- decyl Disul- phide	19,000 & 6,000	10μ	.90	Depending on ΔT See Tables 12, 13 & 14

TABLE 2 NUCLEATION SITE DENSITIES OBSERVED DURING DROP CONDENSATION

Reference	Pressure	Orientation	Material	Surface Finish	Promoter	ΔT	Nucleation Density (No./cm ²)
Tammann & Boehme [12]	Unknown	Unknown	Copper	Unknown	Unknown	Unknown	2.25×10^6
McCormick & Baer [13]	19 mm Hg	Horizontal Up	Stainless Copper	Smooth Very Smooth Smooth Rough	Benzyl Mercaptan	Unknown	8.3×10^5 1.7×10^4 8.6×10^4 2.2×10^5
McCormick & Westwater [14, 15]	19 m Hg	Horizontal Up	Copper	Smooth	Benzyl Mercaptan	.5°C 3.5°C	3×10^4 1.4×10^5
Peterson & Westwater [16]	Unknown	Vertical	Copper	Smooth	Oleic Acid	Unknown	3.4×10^5 to 1.05×10^6 *
Erb [19]	30 mm Hg	Horizontal Up	Silver & Gold	Smooth	Non-needed	2.3 to 23°F	.496 to 7.4×10^6 ** 23.4×10^6
Present Work	34 mm Hg 760 mm Hg	Vertical	Copper	Mirror Smooth	Dioctadecyl Disulphide	.5°F	2×10^8 $\sim 5 \times 10^8$

* Vapor used was Ethylene Glycol

** Higher density is for low wettability surface

TABLE 3 VARIATION OF HEAT TRANSFER COEFFICIENT WITH HEAT FLUX

AUTHOR(S)	ORIENTATION	SURFACE MATERIAL	SURFACE FINISH	PROMOTER	VENTING ARRANGEMENT	GAS CONCENTRATION
Hampson & Ozisik [30]	Vertical	Copper	Mirror Smooth	Benzyl Mercaptan & Oleic Acid Mixed	Continuous Bleed	Unknown
Wenzel [38]	Vertical	Chromium Plated on Brass	Highly Polished	Oleic Acid	Unknown	Unknown
Krause [37]	Unknown	Unknown	Unknown	Unknown	Unknown	Unknown
Tanner et. al. [31]	Vertical	Copper	Mirror Smooth	Dioctadecyl Disulphide	Blow Past Surface	2 p.p.m.
Rose et. al. [40]	Vertical	Copper	Mirror Smooth	Dioctadecyl Disulphide	Close Vent	"Very Small"
Graham, Present Work	Vertical	Copper	Mirror Smooth	Dioctadecyl Disulphide	Blow Past Surface	"Very Small"

TABLE 3 - CONTINUED

AUTHOR(S)	ORIENTATION	SURFACE MATERIAL	SURFACE FINISH	PROMOTER	VENTING ARRANGEMENT	GAS CONCENTRATION
Nagle et. al. [40]	Vertical Tubes	Chromium Plated on Copper	Unknown	Oleic Acid	Continuous Bleed	Unknown
Cnam [41]	Vertical	Copper	Unknown	Oleic Acid	Blow Past Surface	Unknown
Fitzpatrick et. al. [42]	Vertical Tubes	Copper	Unknown	Benzyl Mercaptan	Continuous Bleed	Unknown
Shea & Krase [43]	Vertical	Copper	Highly Polished	Benzyl Mercaptan	Blow Past Surface	Unknown
Kirschbaum et. al. [44]	Unknown	Unknown	Unknown	Unknown	Unknown	Unknown
Costas [45]	Unknown	Unknown	Unknown	Unknown	Unknown	Unknown
Welch & Westwater [7]	Vertical	Copper	Polished	Cupric Oleate	Unknown	Unknown
Kast [8]	Vertical	Copper	Unknown	Benzyl Mercaptan	Blow Past Surface	Unknown
Fatica & Katz [5]	Vertical	Copper	Mirror Smooth	Stearic Acid	Unknown	Unknown

TABLE 4 VARIATION OF HEAT TRANSFER COEFFICIENT WITH STEAM PRESSURE

AUTHOR(S)	ORIENTATION	SURFACE MATERIAL	PROMOTER	GAS	VENTING ARRANGEMENT	HEAT FLUX		REMARKS
						RANGE	ft ² x 10 ³	
Gnam [41]	Vertical	Copper	Oleic Acid	Unknown	Blow Past Surface	30 to 120		
Ma [47]	Unknown	Unknown	Unknown	Unknown	Unknown	8		
Brown & Thomas [48]	Horizontal Tube	Admiralty Brass	Teflon .0001" Thick	Less Than 100 p.p.m.	"Continuous Steam Removal"	9 to 19		Coefficient Includes Resistance of Teflon Layer
Tanner et.al. [49]	Vertical	Copper	Montan wax Dioctadecyl Disulphide	Less Than 1 p.p.m.	Blow Past Surface	2 to 30		
Wenzel [38]	Vertical	Chromium Plated on Brass	Oleic Acid	Unknown	Unknown	110 to 150		
Dolloff & Metzger [31]	Vertical	Copper	Rupric Oleate (72 p.p.m.)	Unknown	Blow Past Surface	100 to 350		
Graham Present Work	Vertical	Copper	Dioctadecyl Disulphide	"Very Small"	Blow Past Surface	1 to 40		Data in figure is for constant ΔT of 3.0°F

TABLE 5 VARIATION OF HEAT TRANSFER COEFFICIENT WITH VAPOR VELOCITY

AUTHOR(S)	ORIENTATION	SURFACE MATERIAL	PROMOTER	VENTING ARRANGEMENT	GAS CONCENTRATION	HEAT FLUX RANGE Btu/Hr Ft ² x 10 ³
Tanner et. al. [39]	Vertical	Copper	Diiodadecyl Disulphide	Blow Past Surface	2 p.p.m.	5 to 200
O'Bara et. al. [52]	Vertical	Copper	Cupric Oleate	Blow Past Surface	.0036 weight percent	30 to 167
Graham Present Work	Vertical	Copper	Diiodadecyl Disulphide	Blow Past Surface	"Very Small"	30 to 40

TABLE 6 VARIATION OF HEAT TRANSFER COEFFICIENT WITH SURFACE MATERIAL & FINISH

AUTHOR(S)	ORIENTATION	SURFACE MATERIAL	SURFACE FINISH	PROMOTER	VENTING ARRANGEMENT	GAS CONCENTRATION	HEAT FLUX RANGE Btu/Hr ft ² x 10 ³
Tanner et. al. [53]	Vertical	Copper	Mirror: .1 and 6.μ diamond paste	Montanic Acid	Blow Past Plate	2 p.p.m.	10 - 200
			Rough: 00 emery & etched				
		Stainless Steel	Mirror: As Above				
Griffith & ManSuk Lee [54]	Horizontal Facing Down	Gold Plated on Copper	Mirror: No. 8 diamond paste	Oleic Acid	Blow Past Plate	Unknown	10 - 140
			Rougher: 500 grit lapping compound				
		Gold Plated on Zinc	Mirror: As Above				4 - 120
Graham, Present Work	Vertical	Copper	Mirror: As Above				2 - 60
			Mirror: .05μ Aluminum Oxide Compound	Dioctadecyl Disulphide	Blow Past Plate	"Very Small"	1 - 120
			Rough: 500 grit emery paper				

TABLE 7 VARIATION OF HEAT TRANSFER COEFFICIENT WITH SURFACE INCINATION

AUTHOR(S)	MATERIAL	PROMOTER	GAS CONCENTRATION	VENTING ARRANGEMENT	HEAT FLUX RANGE Btu/Hr Ft ² x 10 ³
Wenzel [38]	Chromium Plated on Brass	Oleic Acid	Unknown	Unknown	64
Hampson & Ozsisik [30]	Copper	Benzyl Mer- captan & Oleic Acid Mixed	Unknown	Continuous Bleed	50 - 350
Rose [55]	Copper	Dioctadecyl Disulphide	"Very Small"	Close Vent	57 - 580

TABLE 8 SUMMARY OF PARAMETRIC EFFECTS

PARAMETER	TREND	CAUSE
Heat Flux	As $Q/A \uparrow, h \uparrow$.	Nucleation is greater at higher ΔT 's resulting in more active drops. Growth rate of small drops increases rapidly with heat flux.
Pressure	Below 1 atm: As $p \uparrow, h \uparrow$. Above 1 atm: Trend not established.	Below 1 atm.: Increasing pressure enhances nucleation resulting in more active drops. Drop growth rate increases with pressure.
Non-Condensable Gases	As concentration $\uparrow, h \uparrow$. As vapor velocity $\uparrow, h \uparrow$.	Diffusional resistance increases with concentration. Vapor velocity past surface removes gases from condensing surface.
Vapor Velocity	As vapor velocity $\uparrow, h \uparrow$.	Vapor velocity removes non-condensables. Excess velocity causes premature departure of large drops resulting in more active drops.
Surface Conductivity	As $k \uparrow, h \uparrow$.	Constriction resistance decreases as k is increased. This has the effect of increasing ΔT driving potential and thus the growth rate.
Surface Finish	As roughness $\uparrow, h \uparrow$.	Roughness lowers contact angle resulting in poor quality coalescence and large departing drops. This decreases area available for active drops.

TABLE 8 - CONTINUED

Surface Inclination	As inclination ↑ away from vertical, h_v .	Inclination from the vertical results in larger departing drops and less area cleared by sweeping drops. This decreases number of active drops.
Location on Surface	h does not vary significantly with plate height	Number of active drops does not vary with location on condensing surface.
Condensing Vapor	Trend not established.	Variation in h would depend on differences in properties and wetting characteristics.
Promoter	Trend not established.	Variation in h would depend on promoter's ability to maintain non-wetting surface, and on its own thermal resistance.

TABLE 9 SUMMARY OF EXPERIMENTAL ERRORS

SYSTEM	MODIFICATIONS	DATA	ERRORS	COMMENTS
Chamber No. 1 Test Section No. 1		$h=1,500 \frac{\text{Btu}}{\text{HrFt}^2\text{°F}}$ $Q/A=30,000$ $\Delta T=20\text{°F}$	1. Q/A low due to heat losses 2. T_w high due to T.C. errors 3. Non-condensables	Large Temperature fluctuations at surface
Chamber No. 1 Test Section No. 1	Increased vapor velocity past surface	$h=3,000 \frac{\text{Btu}}{\text{HrFt}^2\text{°F}}$ $Q/A=30,000$ $\Delta T=10\text{°F}$	1. Q/A low due to heat losses 2. T_w high due to T.C. errors	Small temperature fluctuations at surface
Chamber No. 2 Test Section No. 2	Smaller chamber High vapor velocity T.C. emersion depth increased	$h=38,500 \frac{\text{Btu}}{\text{HrFt}^2\text{°F}}$ $Q/A=30,000$ $\Delta T=.8\text{°F}$	Errors minimized	No temperature fluctuations at surface. Good quality drop condensation

TABLE 10 SUMMARY OF HEAT TRANSFER DATA

FINISH	PROMOTER	PRESSURE	$\frac{h_r F t^{2^{\circ}F}}{m}$	$b^{\circ}F$	$h \frac{Btu}{Hr Ft^{2^{\circ}F}}$	RATIOS
Mirror	Dioc. Dis.	$T_s = 212^{\circ}F$	$.2622 \times 10^{-4}$.074	$h_{ma} = 38,200$	
Mirror	Dioc. Dis.	$T_s = 88^{\circ}F$	$.7409 \times 10^{-4}$.078	$h_{ml} = 13,500$	$\frac{h_{ml}}{h_{ma}} = .354$
Rough	Dioc. Dis.	$T_s = 212^{\circ}F$	$.3353 \times 10^{-4}$.044	$h_{ra} = 29,800$	$\frac{h_{ra}}{h_{ma}} = .780$
Rough	Dioc. Dis.	$T_s = 88^{\circ}F$	1.0841×10^{-4}	.015	$h_{rl} = 9,230$	$\frac{h_{rl}}{h_{ra}} = .310$ $\frac{h_{rl}}{h_{ml}} = .685$
Teflon	Teflon	$T_s = 212^{\circ}F$	$.7645 \times 10^{-4}$.030	$h_{ta} = 13,100$	$\frac{h_{ta}}{h_{ma}} = .343$
Teflon	Teflon	$T_s = 88^{\circ}F$	1.3025×10^{-4}	.050	$h_{tl} = 7,670$	$\frac{h_{tl}}{h_{ta}} = .585$ $\frac{h_{tl}}{h_{ml}} = .567$

Note the following notation:

ma = mirror smooth, atmos. pressure

ra = rough, atmos. pressure

ta = teflon, atmos. pressure

ml = mirror smooth, low pressure

rl = rough, low pressure

tl = teflon, low pressure

TABLE 11 RESULTS OF PRELIMINARY VIBRATION TESTS

FREQUENCY	H Btu/Hr Ft ² °F	RATIO OF $\frac{H, \text{ with vibration}}{H, \text{ no vibration}}$
No Vibration	33,400	
50 cps	31,300	.94
60 cps	35,700	1.07
70 cps	36,600	1.10
80 cps	37,700	1.13

NOTE: Heat Flux = 60,000 Btu/Hr Ft²

Vertical Orientation

Mirror Smooth Finish

Dioctadecyl Disulphide Promoter

TABLE 12 DROP DISTRIBUTIONS FOR LOW PRESSURE CONDENSATION

DIST. NUMBER	DIAMETER RANGE	ΔN	$N = \Delta N / \Delta D$
	500 < D < 3000	$5.73 \times 10^6 D^{-1.91}$	$1.43 \times 10^7 D^{-2.91}$
	30 < D < 500	$3.17 \times 10^6 D^{-1.83}$	$7.92 \times 10^6 D^{-2.83}$
	10 < D < 30	$8.72 \times 10^5 D^{-1.47}$	$2.18 \times 10^6 D^{-2.74}$
L-6	1 < D < 10	$8.72 \times 10^5 D^{-1.47}$	$2.18 \times 10^6 D^{-2.47}$
	D < 1	$8.72 \times 10^5 D^{-1.47}$	$2.18 \times 10^6 D^{-2.47}$
L-5	1 < D < 10	$8.72 \times 10^5 D^{-1.47}$	$2.18 \times 10^6 D^{-2.47}$
	D < 1	$8.72 \times 10^5 D^{-1.47}$	$2.18 \times 10^6 D^{-1.0}$
L-4	1 < D < 10	$2.00 \times 10^5 D^{-0.83}$	$5.00 \times 10^5 D^{-1.83}$
	D < 1	$2.00 \times 10^5 D^{-0.83}$	$5.00 \times 10^5 D^{-1.0}$
L-3	1 < D < 10	$1.50 \times 10^5 D^{-0.70}$	$3.75 \times 10^5 D^{-1.70}$
	D < 1	$1.50 \times 10^5 D^{-0.70}$	$3.75 \times 10^5 D^{-1.0}$
L-2	1 < D < 10	$9.00 \times 10^4 D^{-0.48}$	$2.20 \times 10^5 D^{-1.48}$
	D < 1	$9.00 \times 10^4 D^{-0.48}$	$2.20 \times 10^5 D^{-1.0}$
L-1	1 < D < 10	$6.00 \times 10^4 D^{-0.30}$	$1.50 \times 10^5 D^{-1.30}$
	D < 1	$6.00 \times 10^4 D^{-0.30}$	$1.50 \times 10^5 D^{-1.0}$
L-0	1 < D < 10	$2.98 \times 10^4 D^{-0.30}$	$7.36 \times 10^5 D^{-1.0}$
	D < 1	$2.98 \times 10^4 D^{-0.30}$	$7.36 \times 10^5 D^{-1.0}$

TABLE 13 DROP DISTRIBUTIONS FOR ATMOSPHERIC PRESSURE CONDENSATION

DIST. NUMBER	DIAMETER RANGE	ΔN	$N = \Delta N / \Delta D$
	500 < D < 2500	$2.07 \times 10^9 D^{-2.80}$	$5.17 \times 10^9 D^{-3.80}$
	10 < D < 500	$2.11 \times 10^6 D^{-1.73}$	$5.30 \times 10^6 D^{-2.73}$
A-6	1 < D < 10	$2.11 \times 10^6 D^{-1.73}$	$5.30 \times 10^6 D^{-2.73}$
	D < 1	$2.11 \times 10^6 D^{-1.73}$	$5.30 \times 10^6 D^{-2.73}$
A-5	1 < D < 10	$2.11 \times 10^6 D^{-1.73}$	$5.30 \times 10^6 D^{-2.73}$
	D < 1	$2.11 \times 10^6 D^{-1.0}$	$5.30 \times 10^6 D^{-1.0}$
A-4	1 < D < 10	$1.00 \times 10^6 D^{-1.39}$	$2.50 \times 10^6 D^{-2.39}$
	D < 1	$1.00 \times 10^6 D^{-1.0}$	$2.50 \times 10^6 D^{-1.0}$
A-3	1 < D < 10	$7.00 \times 10^5 D^{-1.23}$	$1.75 \times 10^6 D^{-2.23}$
	D < 1	$7.00 \times 10^5 D^{-1.0}$	$1.75 \times 10^6 D^{-1.0}$
A-2	1 < D < 10	$2.00 \times 10^5 D^{-0.69}$	$5.00 \times 10^5 D^{-1.69}$
	D < 1	$2.00 \times 10^5 D^{-1.0}$	$5.00 \times 10^5 D^{-1.0}$
A-1	1 < D < 10	$1.00 \times 10^5 D^{-0.39}$	$2.50 \times 10^5 D^{-1.39}$
	D < 1	$1.00 \times 10^5 D^{-1.0}$	$2.50 \times 10^5 D^{-1.0}$
A-0	1 < D < 10	$4.09 \times 10^4 D^{-1.0}$	$1.02 \times 10^5 D^{-1.0}$
	D < 1	$4.09 \times 10^4 D^{-1.0}$	$1.02 \times 10^5 D^{-1.0}$

TABLE 15 SUMMARY OF "ACTIVE" AREA INFORMATION

LOW PRESSURE, T _{sat} = 88°F			ATMOSPHERIC PRESSURE, T _{sat} = 212°F		
DROP RANGE	HEAT TRANSFERRED	AREA COVERED	DROP RANGE	HEAT TRANSFERRED	AREA COVERED
Bare Surface	0	.09	Bare Surface	0	.09
.13 < D < 150	.9	.35	.15 < D < 40	.9	.23
150 < D < 3000	.1	.56	40 < D < 2500	.1	.68
TOTAL	1.0	1.0	TOTAL	1.0	1.0
Bare Surface	0	.09	Bare Surface	0	.09
.13 < D < 10	.5	.05	.15 < D < 4	.5	.05
10 < D < 3000	.5	.86	4 < D < 2500	.5	.86
TOTAL	1.0	1.0	TOTAL	1.0	1.0

TABLE 16 MINIMUM VALUE OF CONDENSATION COEFFICIENT

RATIO OF PREDICTED TO MEASURED HEAT FLUX

CONDENSATION COEFFICIENT, α	LOW PRESSURE		ATMOSPHERIC PRESSURE	
	Dist. L-3	Dist. L-6	Dist. A-3	Dist. A-6
.006	.06	.07	.14	.19
.02	.09	.10	.20	.26
.04	.22	.26	.40	.65
.35	.67	.98	.85	2.26
1.0	1.00	1.96	1.06	3.86

$$T_{\text{sat}} = 88^{\circ}\text{F}$$

$$\Delta T = 1^{\circ}\text{F}$$

$$Q/A)_m = 13,000 \text{ Btu/Hr Ft}^2$$

$$T_{\text{sat}} = 212^{\circ}\text{F}$$

$$\Delta T = 1^{\circ}\text{F}$$

$$Q/A)_m = 37,000 \text{ Btu/Hr Ft}^2$$

TABLE G-1 EVALUATION OF THE CONSTRICTION RESISTANCE

PRESSURE	INACTIVE DROPS	TYPICAL INACTIVE DROP	INACTIVE AREA,	CONSTRICTION RESISTANCE, R _{cm}	% of DROP CONDENSATION RESISTANCE, h _t ·R _{cm}
Low T _{sat} = 88°F	D > 150μ	c = 750μ	56%	2.7x10 ⁻⁶ Hr/Ft ² °F/Btu	3.5%
Atmospheric T _{sat} = 212°F	D > 40μ	c = 625μ	68%	3.8x10 ⁻⁶ Hr Ft ² °F/Btu	13%

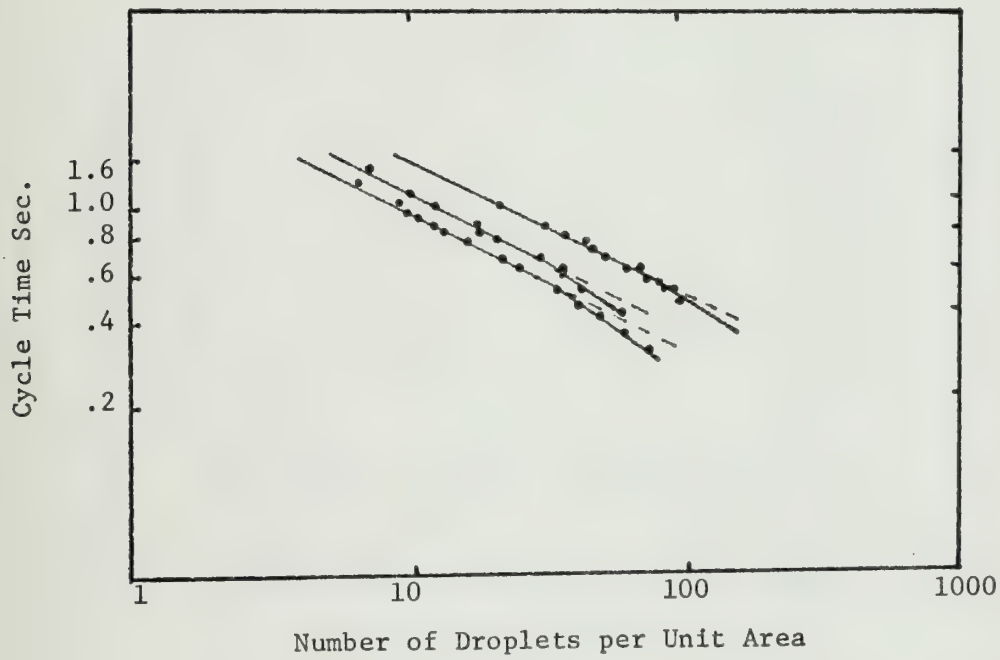


Fig. 1 Drop Distribution. Reproduced from Fatica and Katz [5]
(Unit Area = $5.15 \times 10^{-5} \text{ ft}^2$)

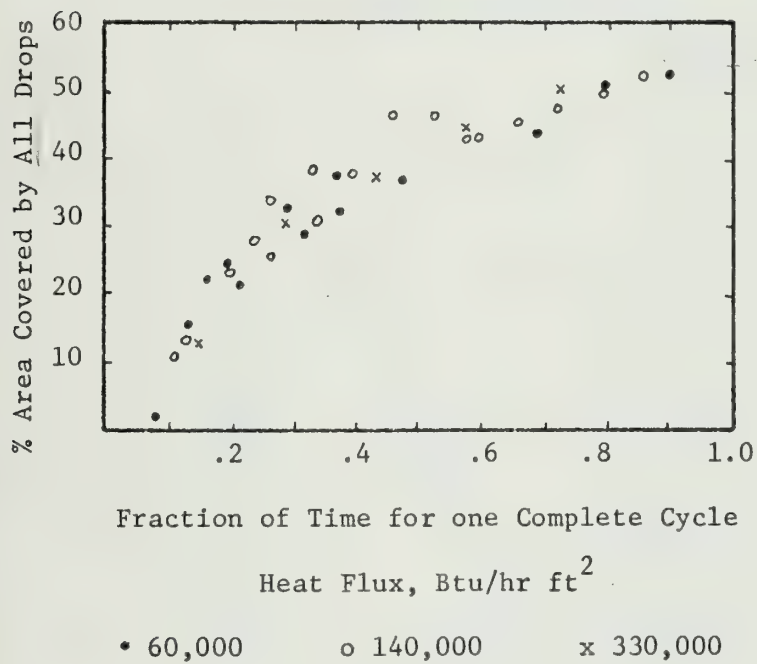


Fig. 2 Area Covered. Reproduced from
Hampson and Ozisik [30]

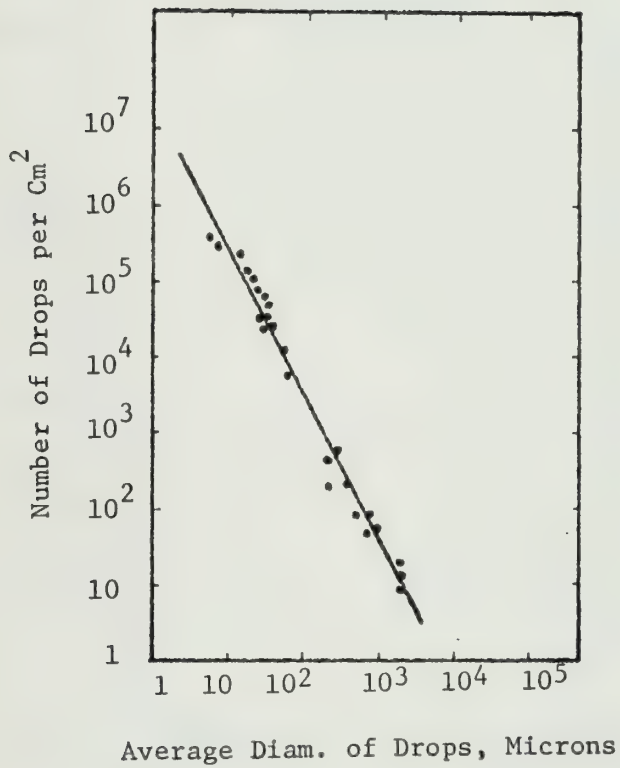


Fig. 3 Drop Distribution.
Reproduced from Sugawara and Katsuta [11]

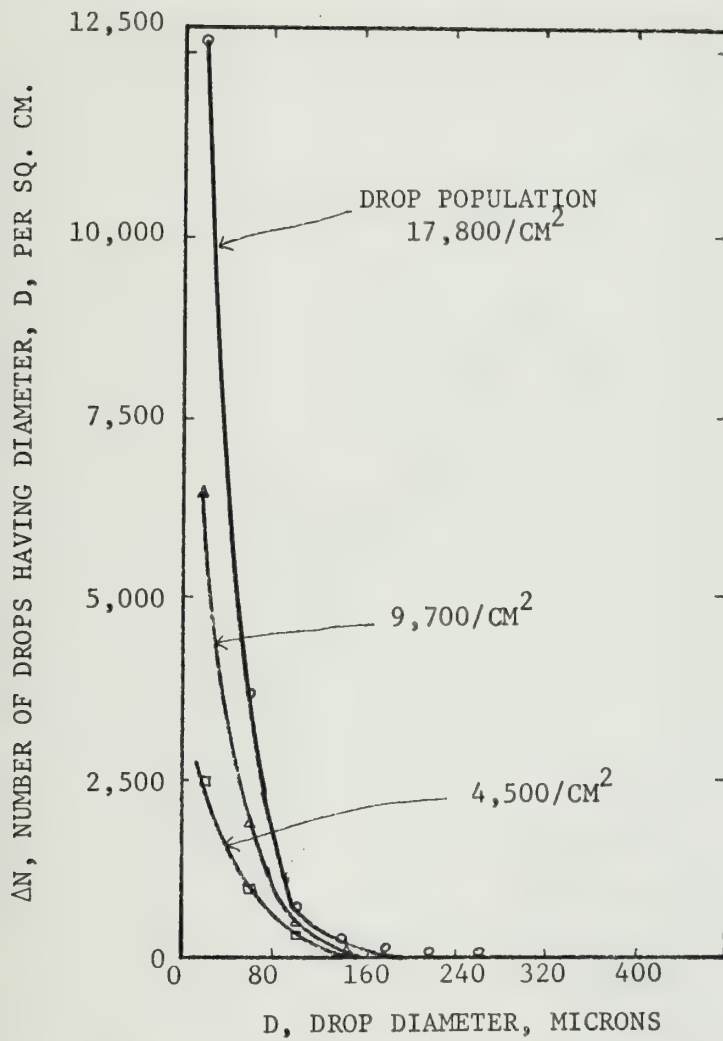


Fig. 4 Drop Distribution. Reproduced from McCormick and Westwater [15]

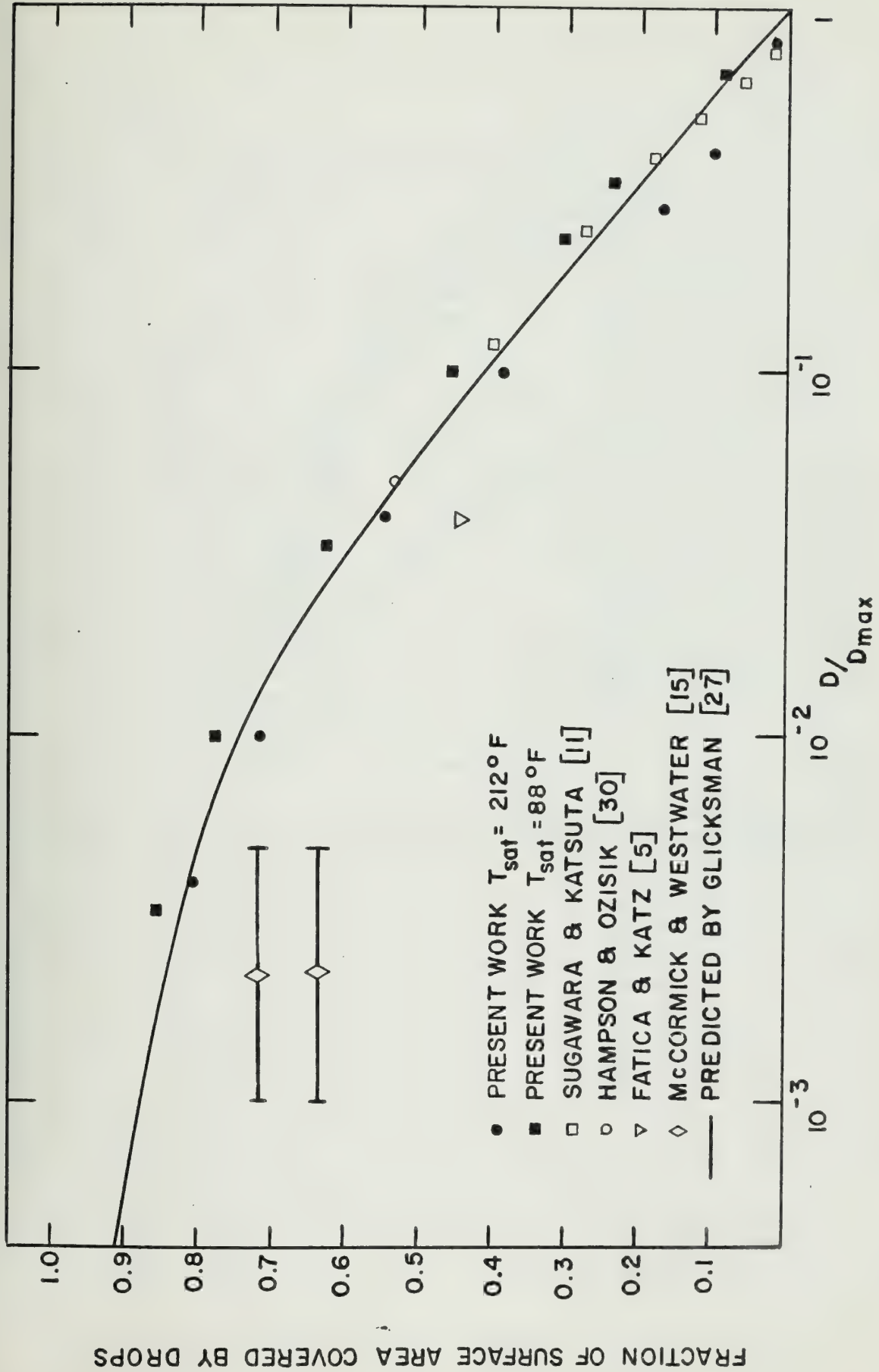


FIG 5 COMPARISON OF AREA COVERED DATA

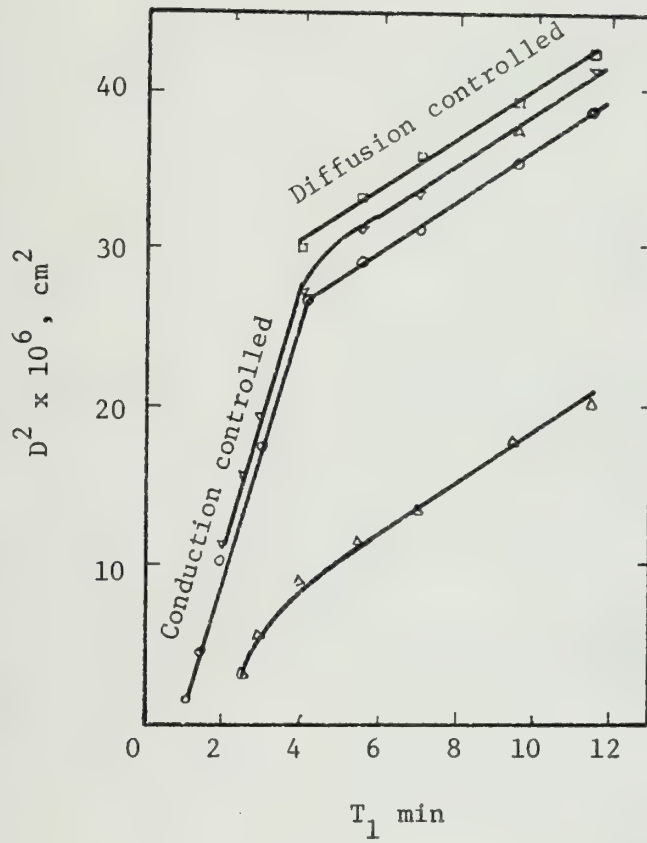


Fig. 6 Drop Growth Rate. Reproduced from McCormick and Baer [13]

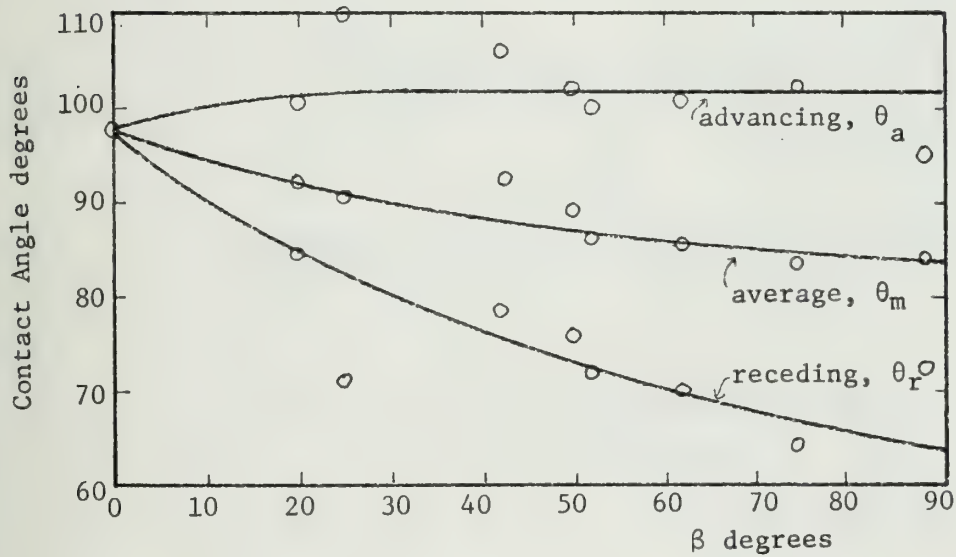
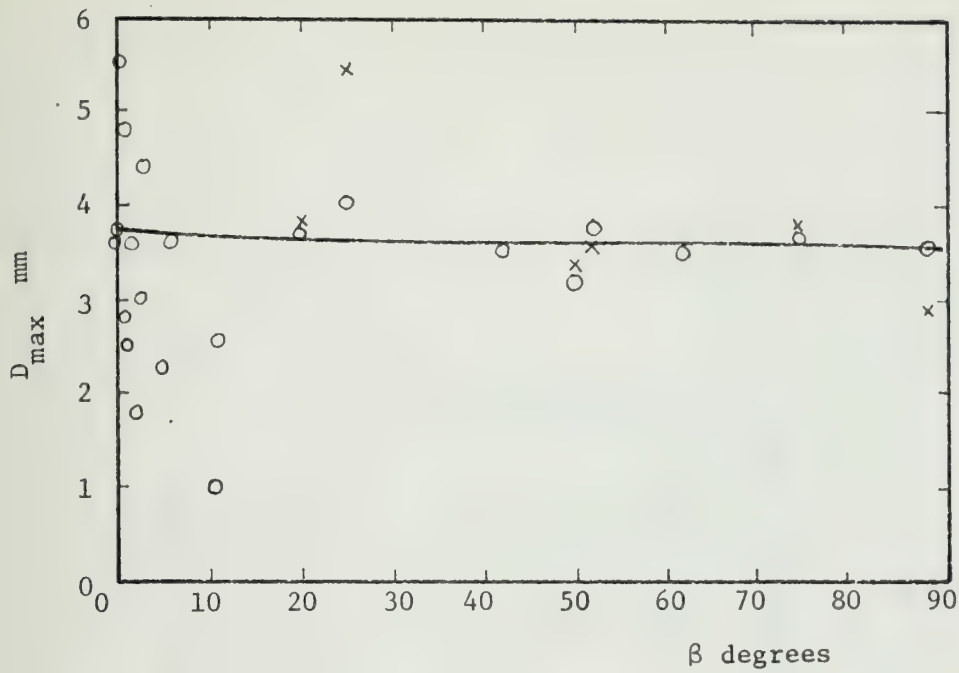
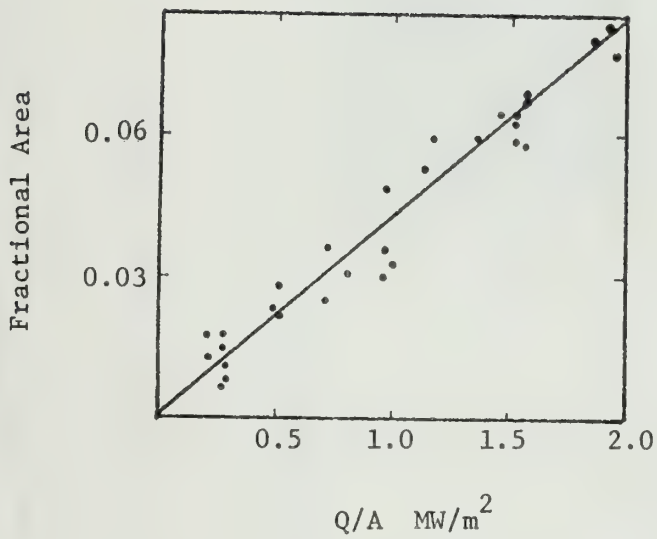


Fig. 7 Maximum Drop Size and Contact Angle Measurement.
Reproduced from Sugawara and Michiyoshi [29]



Variation of fractional area covered
by moving drops with heat flux.

Fig. 8 Area Covered by Sweeping Drops.
Reproduced from Rose [32].

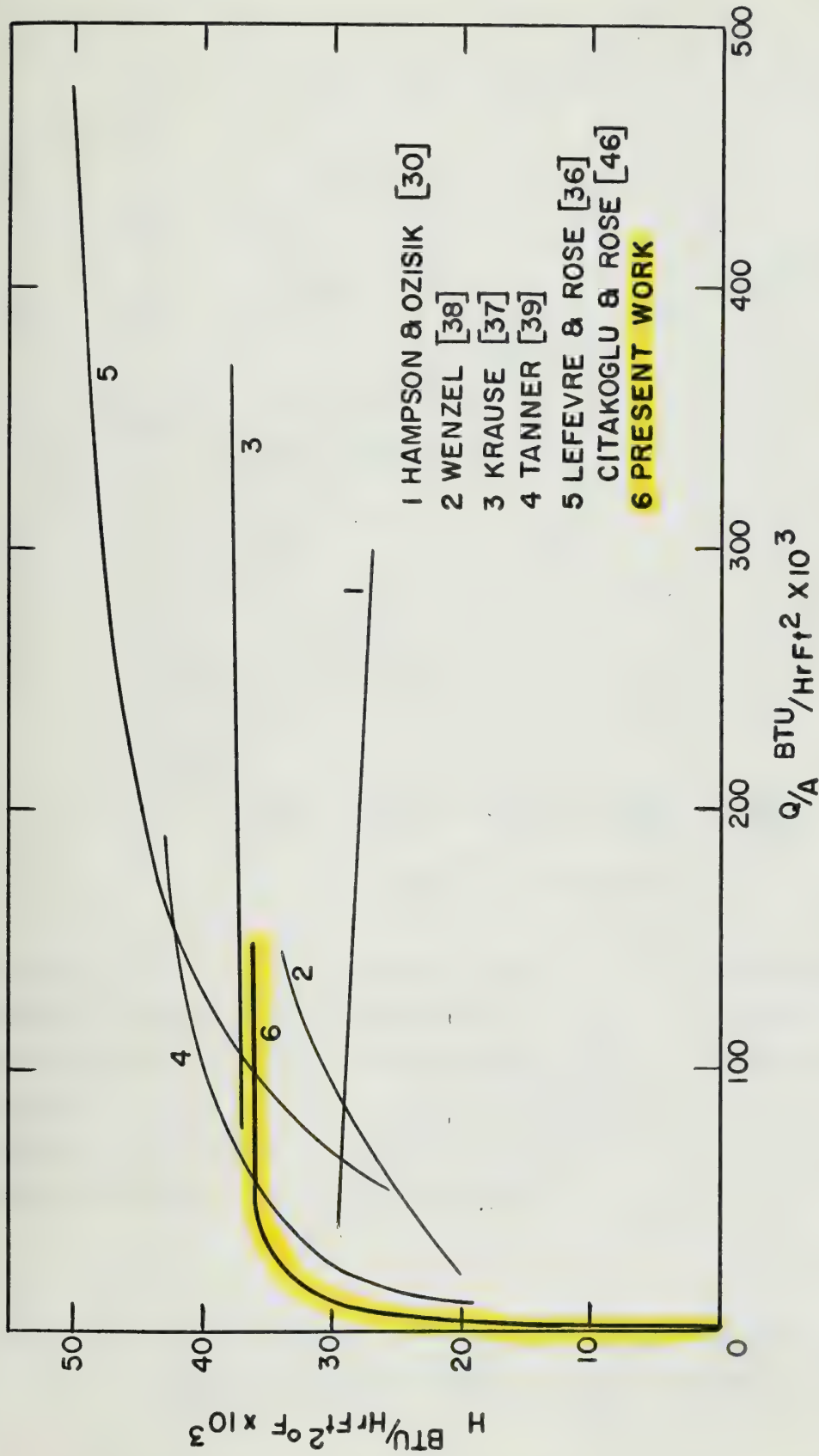
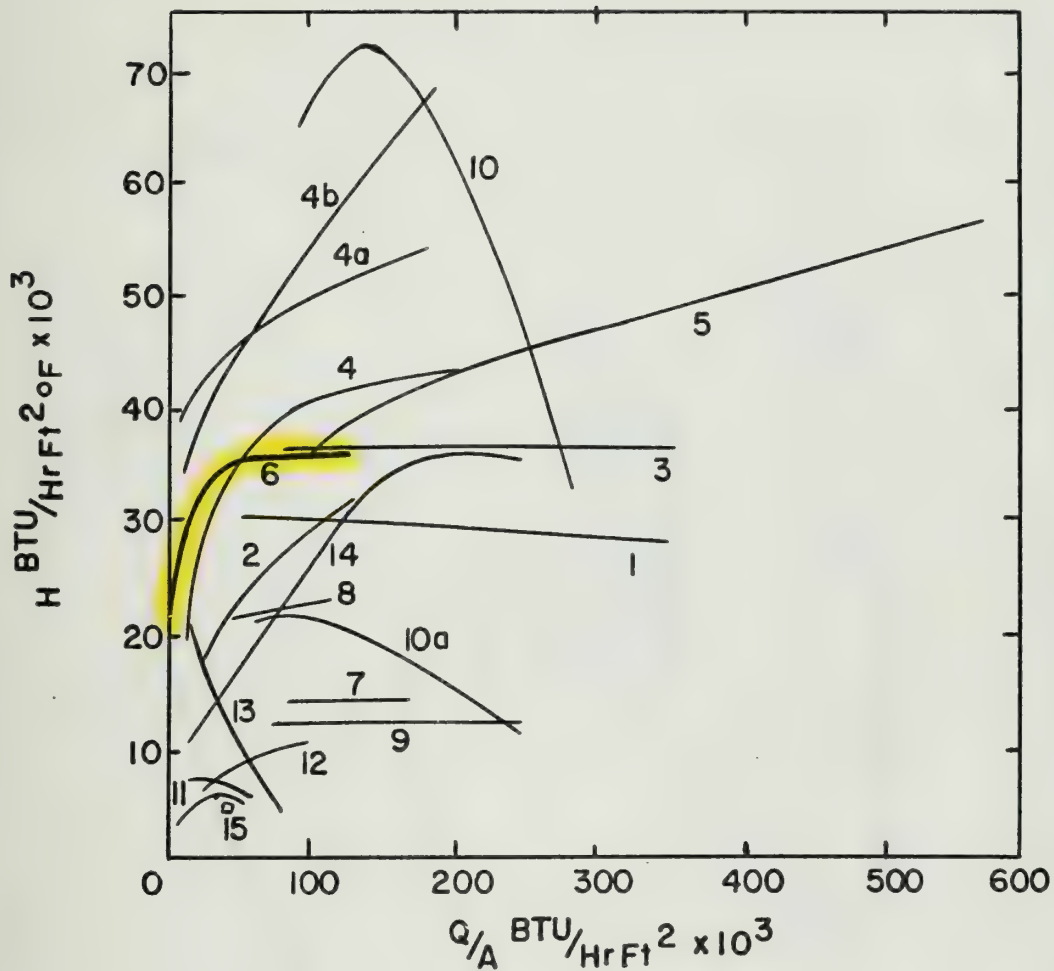


FIG 9 VARIATION OF HEAT TRANSFER COEFFICIENT WITH HEAT FLUX
FOR "GAS FREE" SYSTEMS



- | | | |
|-------------------------|----------------------|--------------------------|
| 1 KRAUSE [37] | 7 NAGLE [40] | 13 WELCH & WESTWATER [7] |
| 2 HAMPSON & OZISIK [30] | 8 GNAM [41] | 14 KAST [8] |
| 3 WENZEL [38] | 9 FITZPATRICK [42] | 15 FATICA & KATZ [5] |
| 4 TANNER et al. [39] | 10 SHEA & KRASE [43] | |
| 5 LeFEVRE & ROSE [36] | 11 KIRSCHBAUM [44] | |
| 6 PRESENT WORK | 12 COSTAS [45] | |

FIG 10 VARIATION OF HEAT TRANSFER COEFFICIENT WITH HEAT FLUX

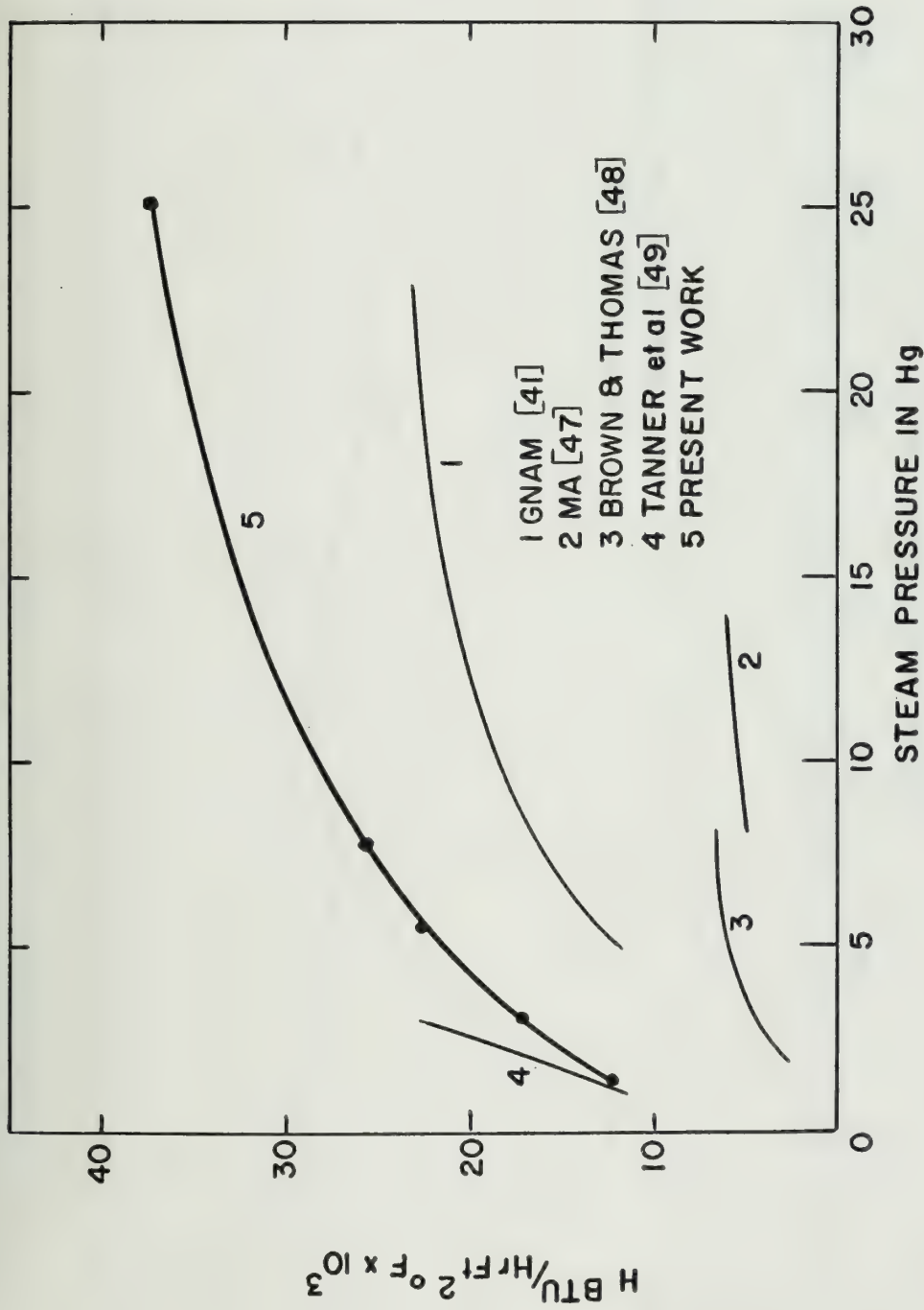


FIG 11 VARIATION OF HEAT TRANSFER COEFFICIENT WITH STEAM PRESSURE (BELOW 1 ATMOS.)

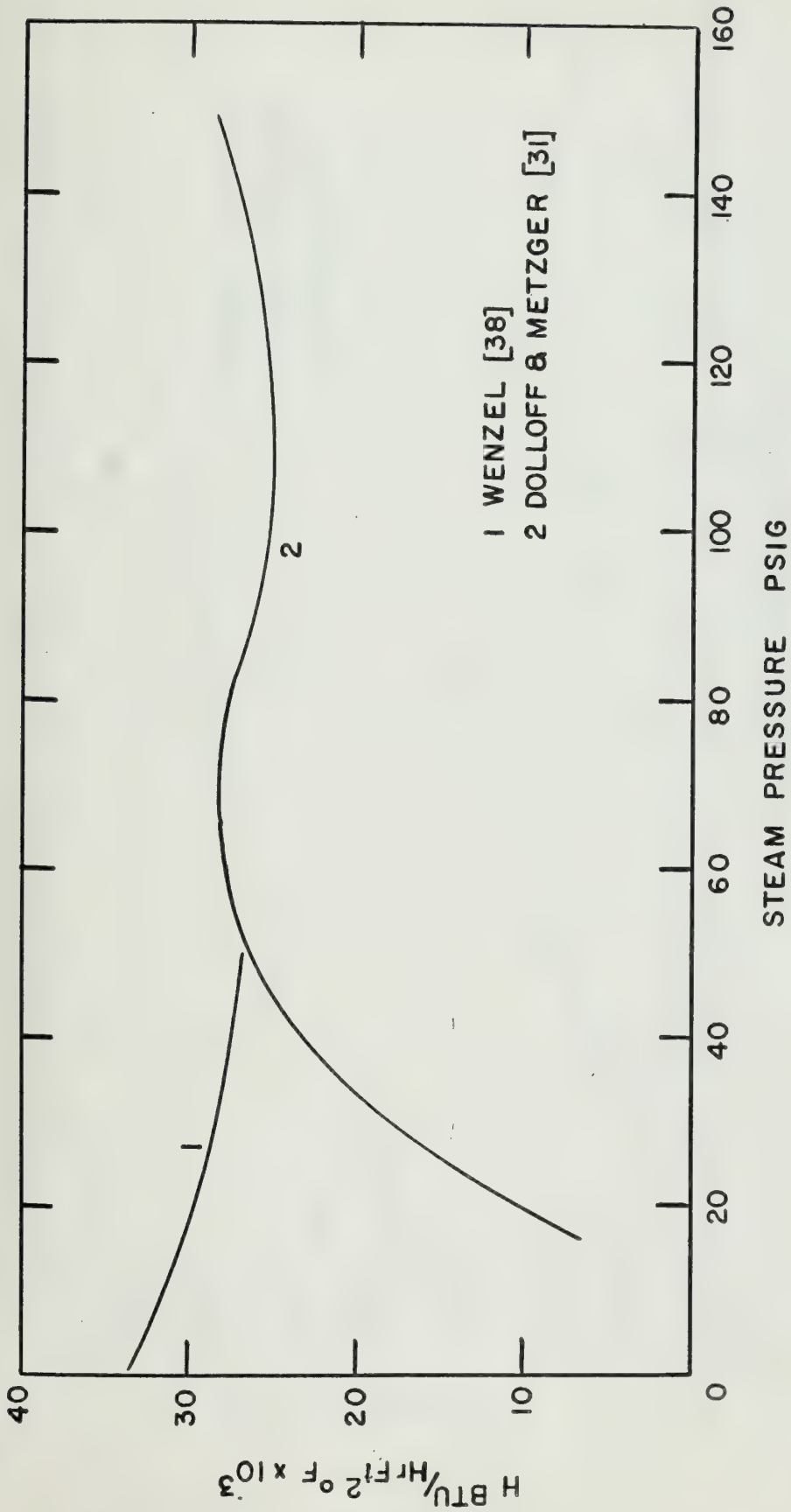


FIG I2 VARIATION OF HEAT TRANSFER COEFFICIENT WITH STEAM PRESSURE (ABOVE 1 ATMOS.)

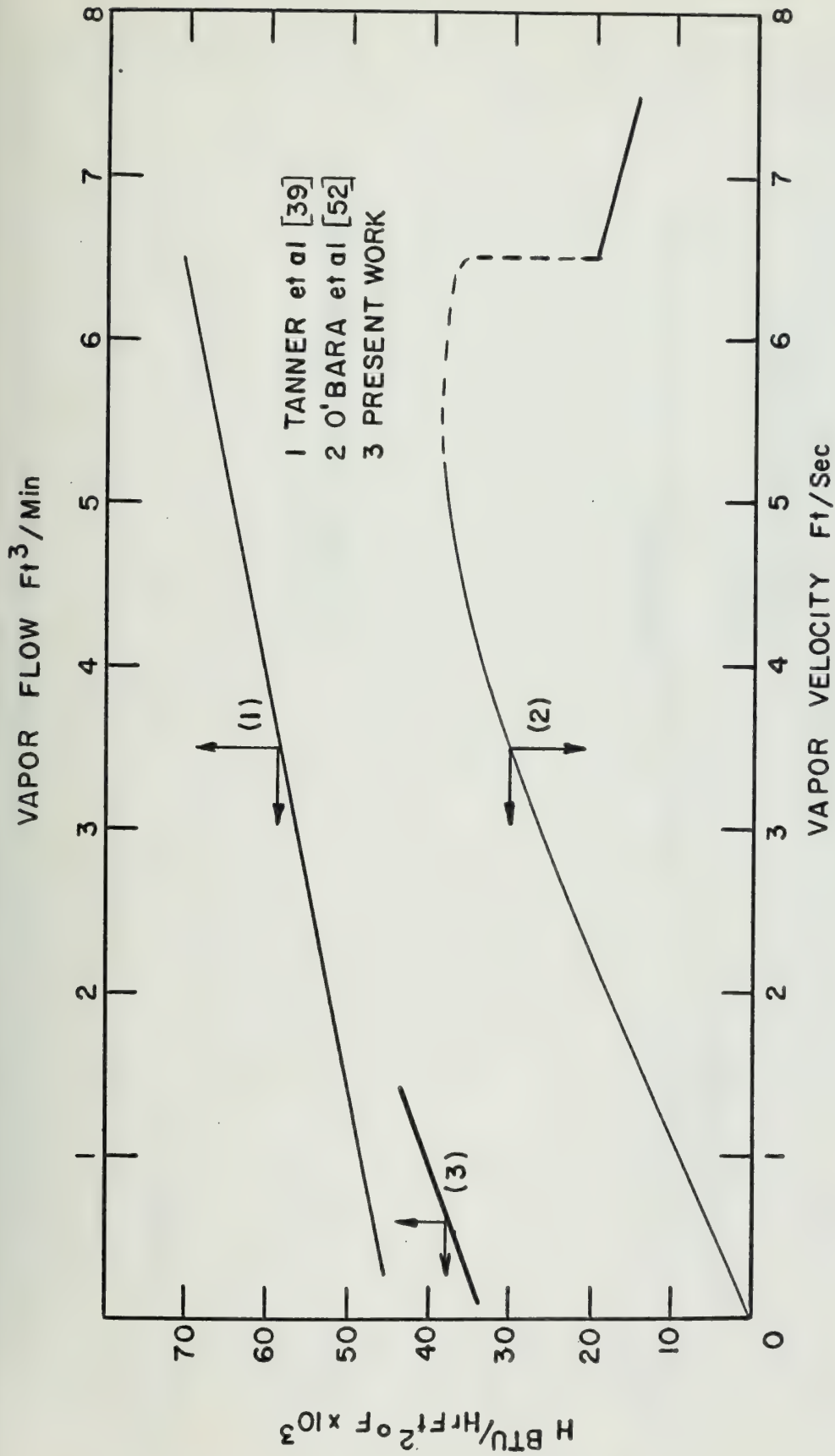


FIG 13 VARIATION OF HEAT TRANSFER COEFFICIENT WITH VAPOR VELOCITY

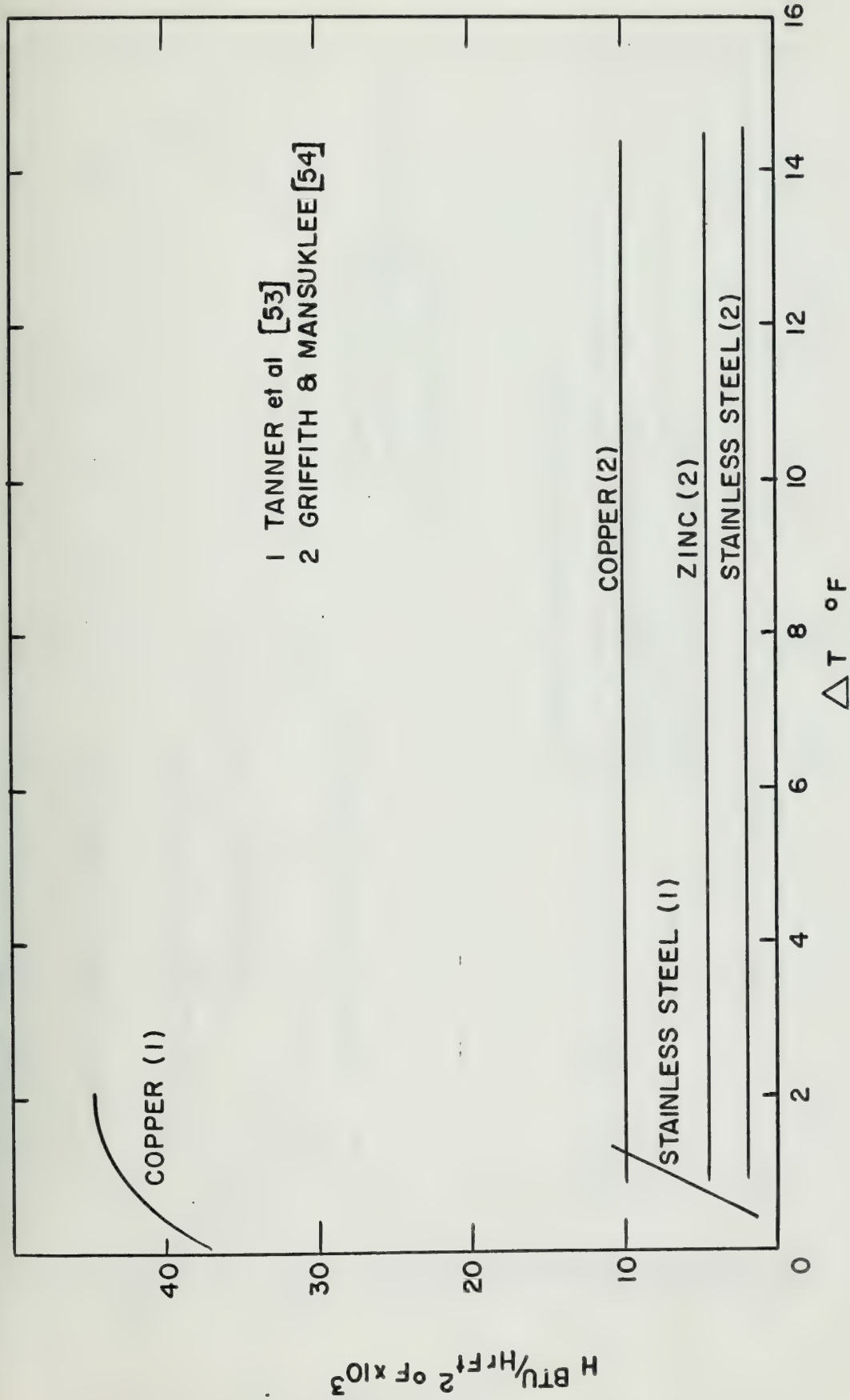


FIG 14 VARIATION OF HEAT TRANSFER COEFFICIENT WITH SURFACE MATERIAL

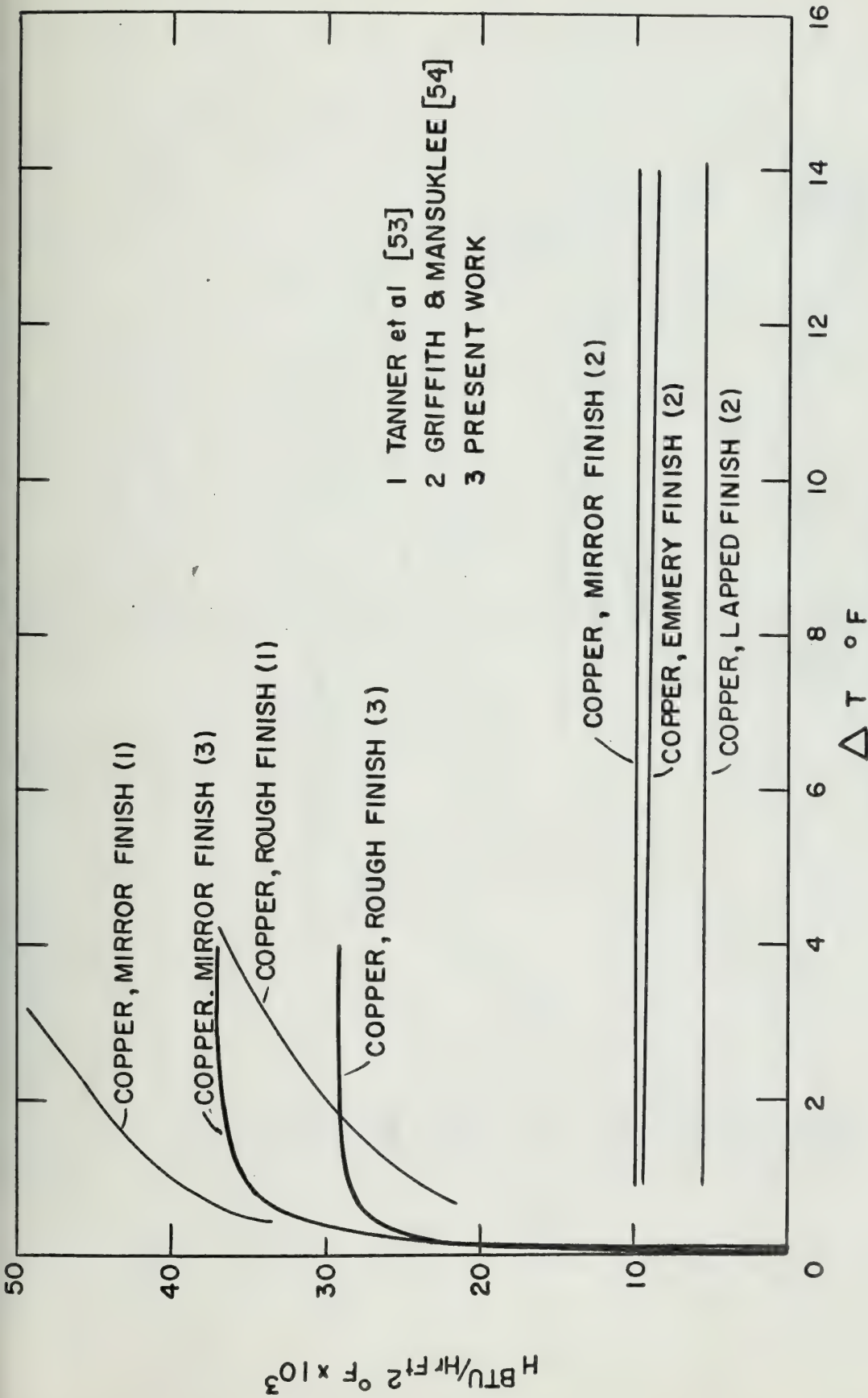


FIG 15 VARIATION OF HEAT TRANSFER COEFFICIENT WITH SURFACE FINISH

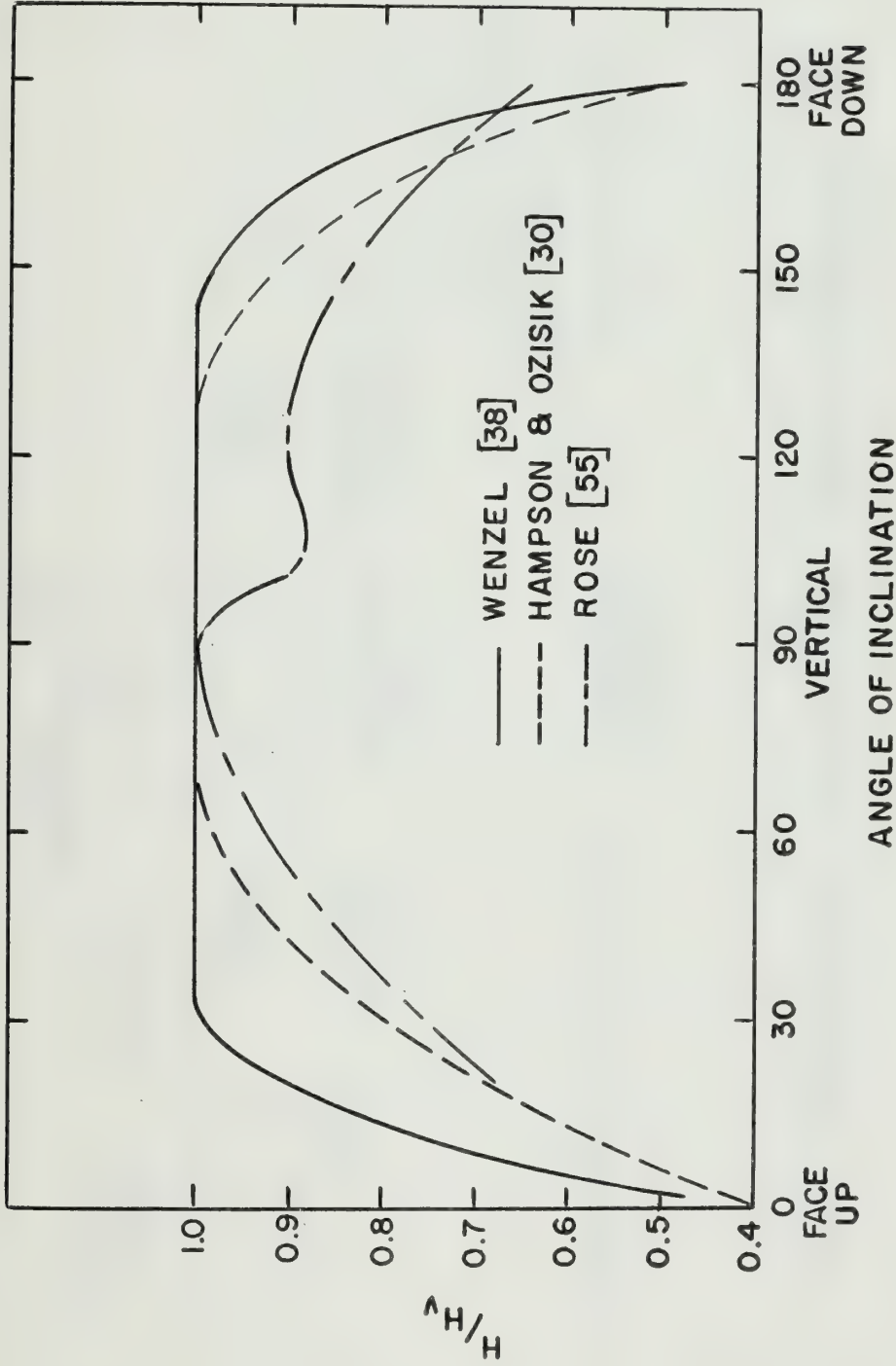


FIG 16 VARIATION OF HEAT TRANSFER COEFFICIENT WITH SURFACE INCLINATION

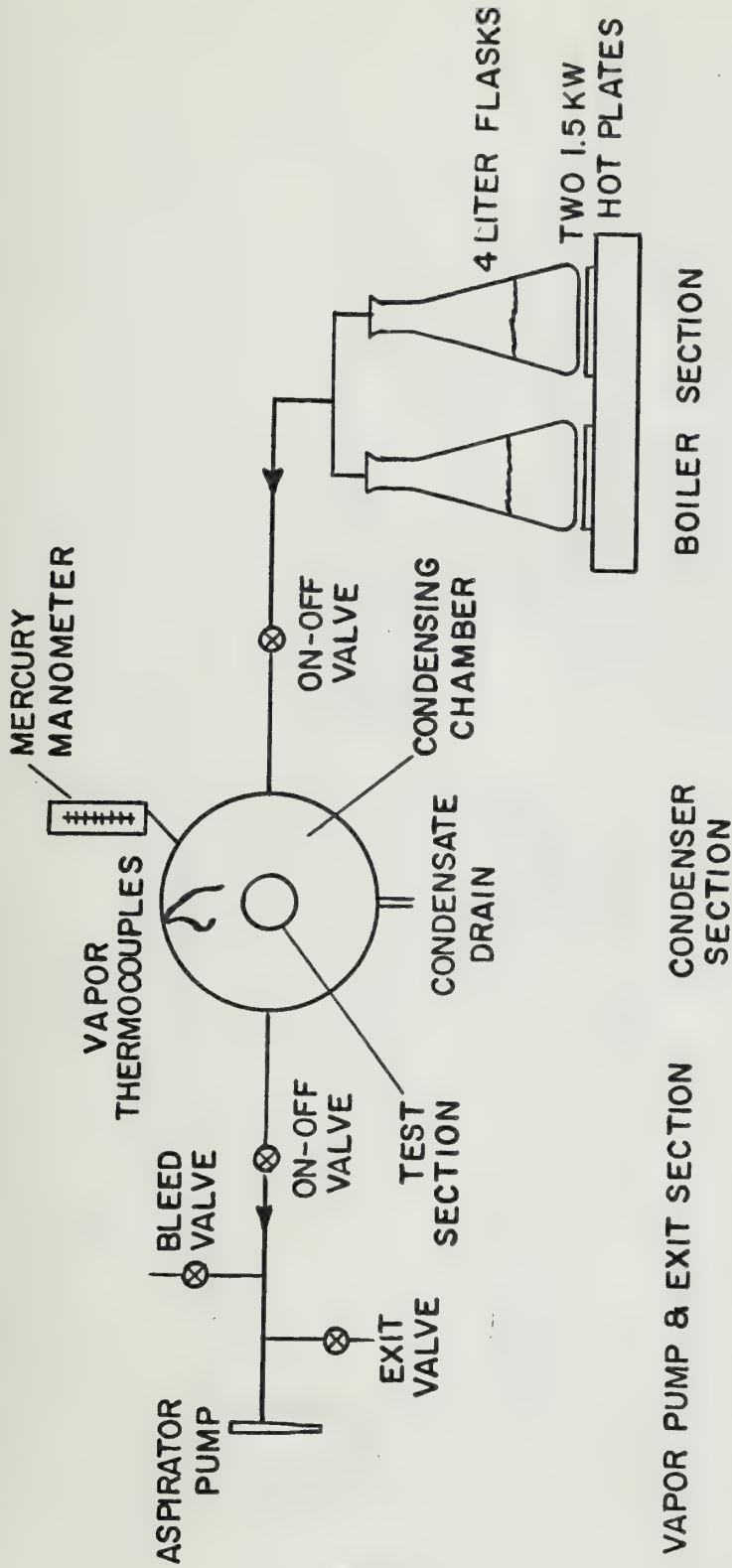


FIG 17 SCHEMATIC LAYOUT OF VAPOR SYSTEM

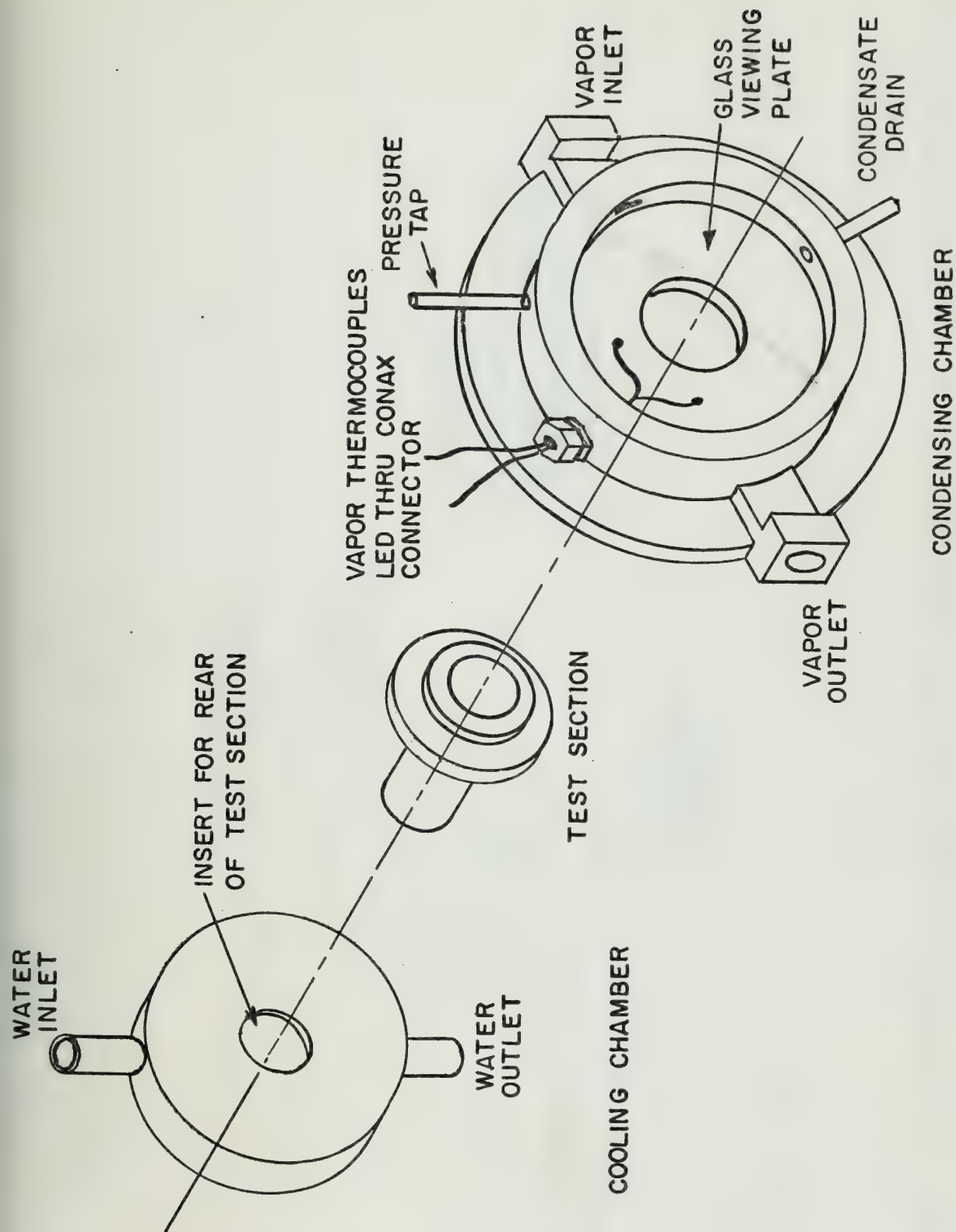


FIG 18 CONDENSING CHAMBER-TEST SECTION-COOLING CHAMBER ASSEMBLY

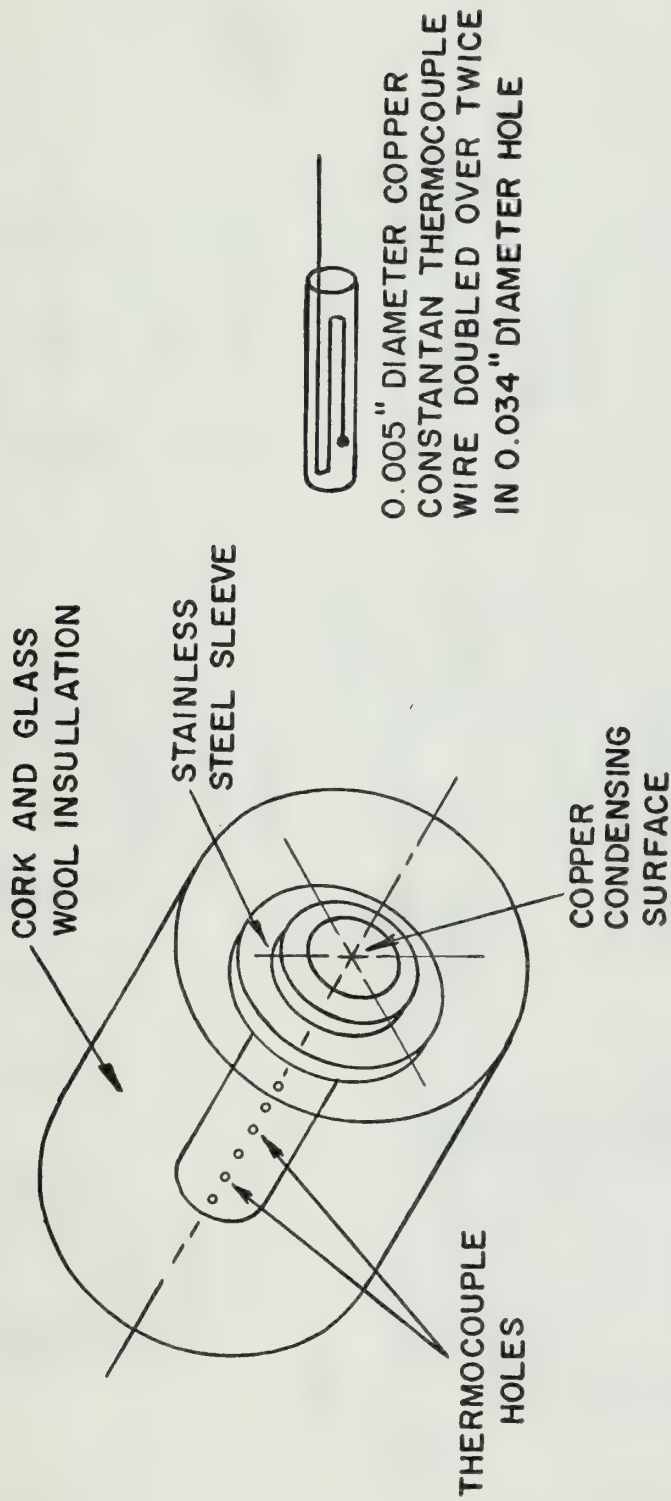


FIG 19 TEST SECTION WITH DETAIL OF THERMOCOUPLE INSTALLATION IN HOLE

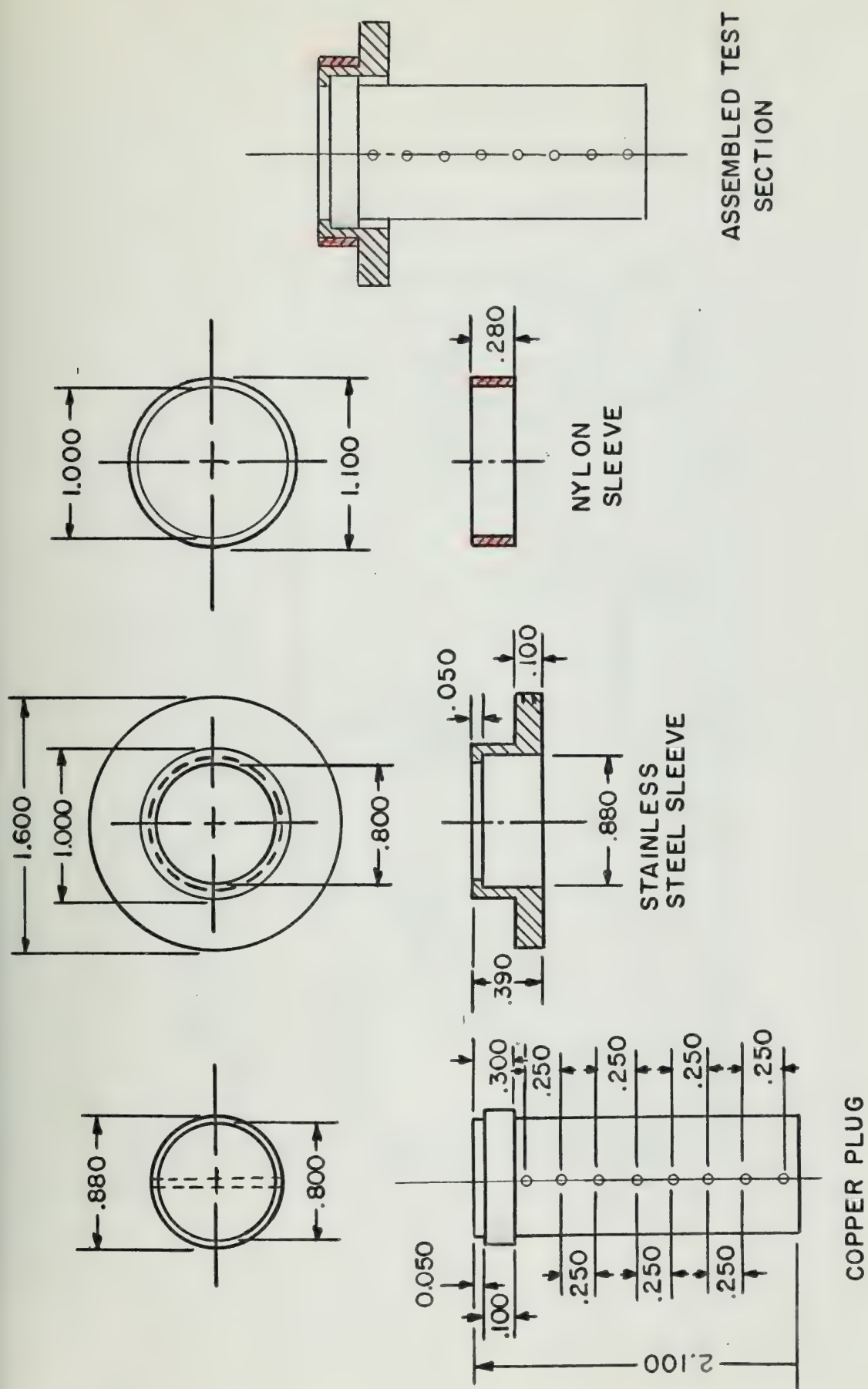


FIG 20 TEST SECTION CONSTRUCTION DETAILS

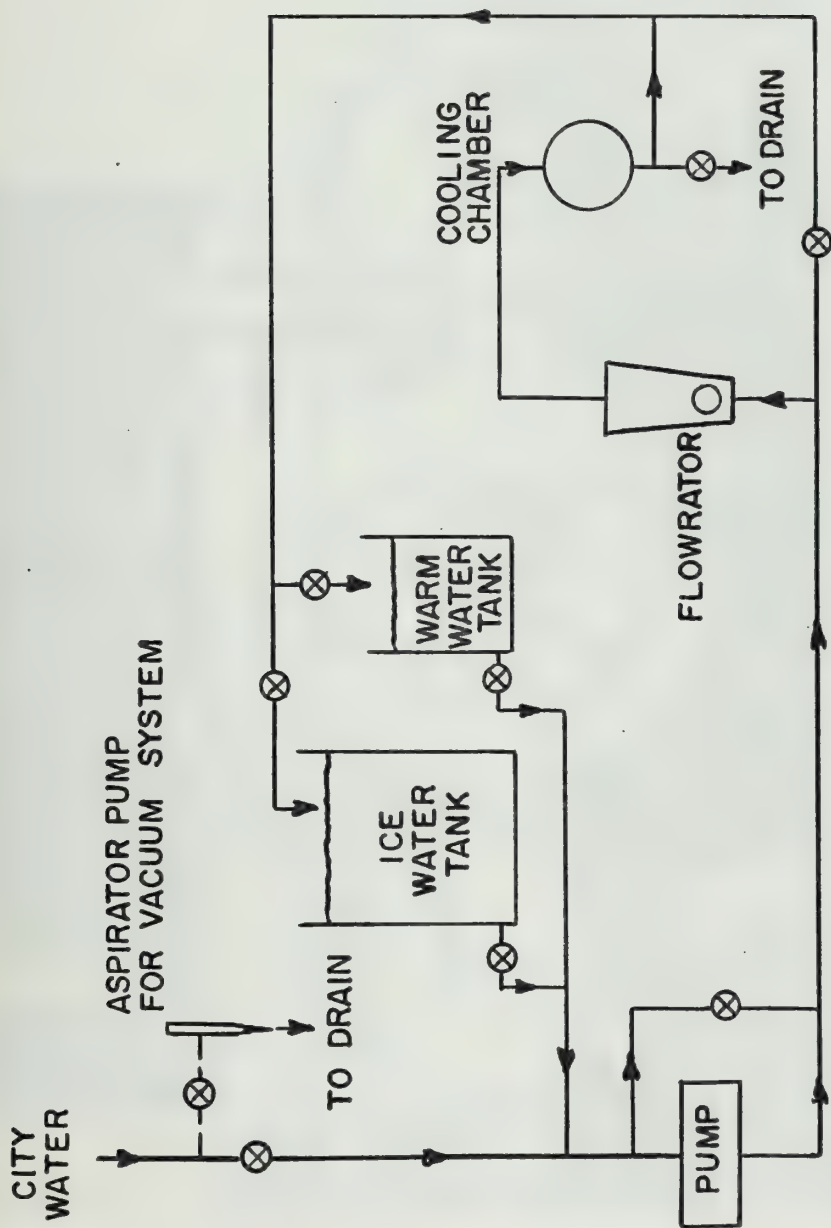


FIG 21 SCHEMATIC LAYOUT OF COOLING WATER LOOP

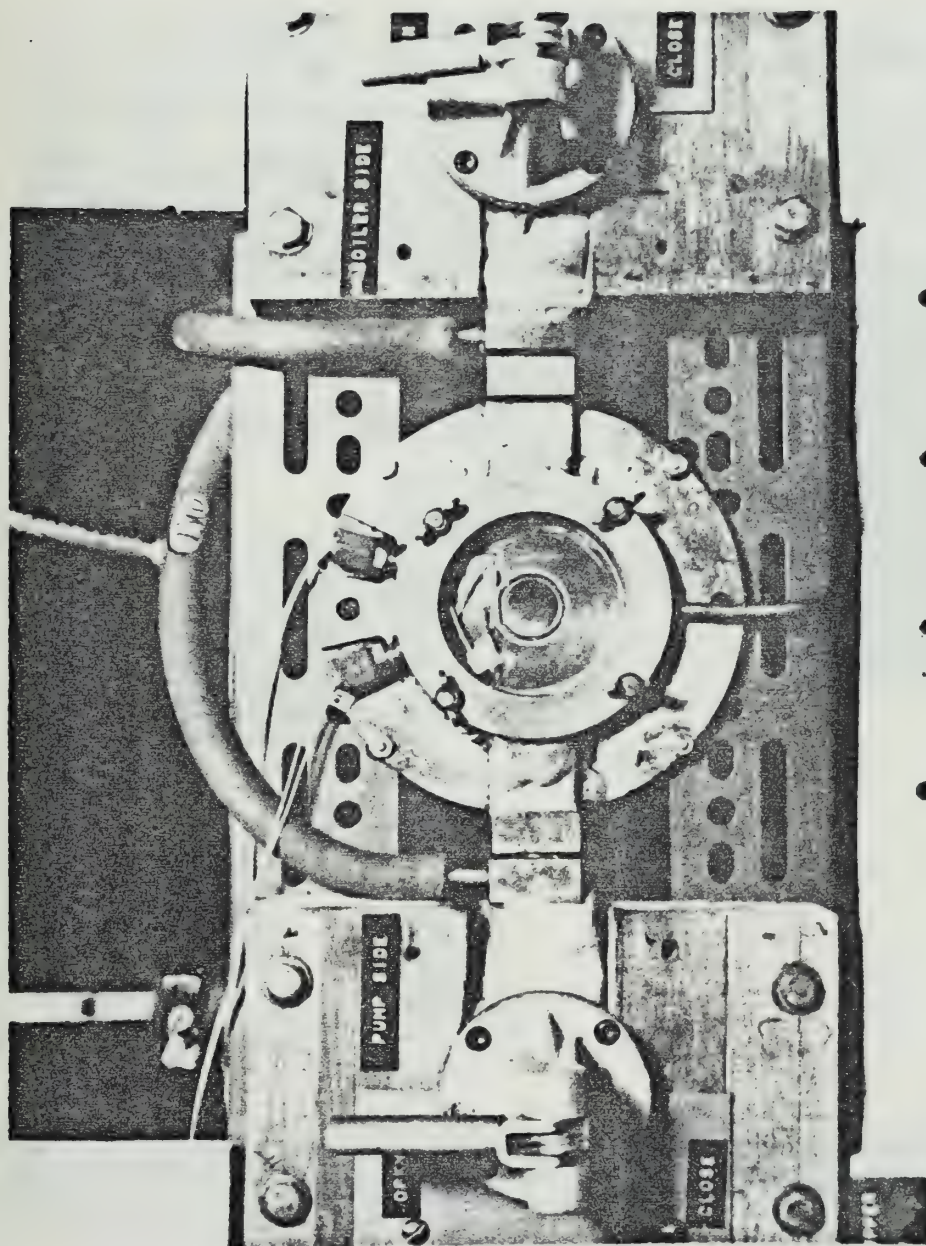


FIG. 22 PHOTOGRAPH OF CONDENSING CHAMBER

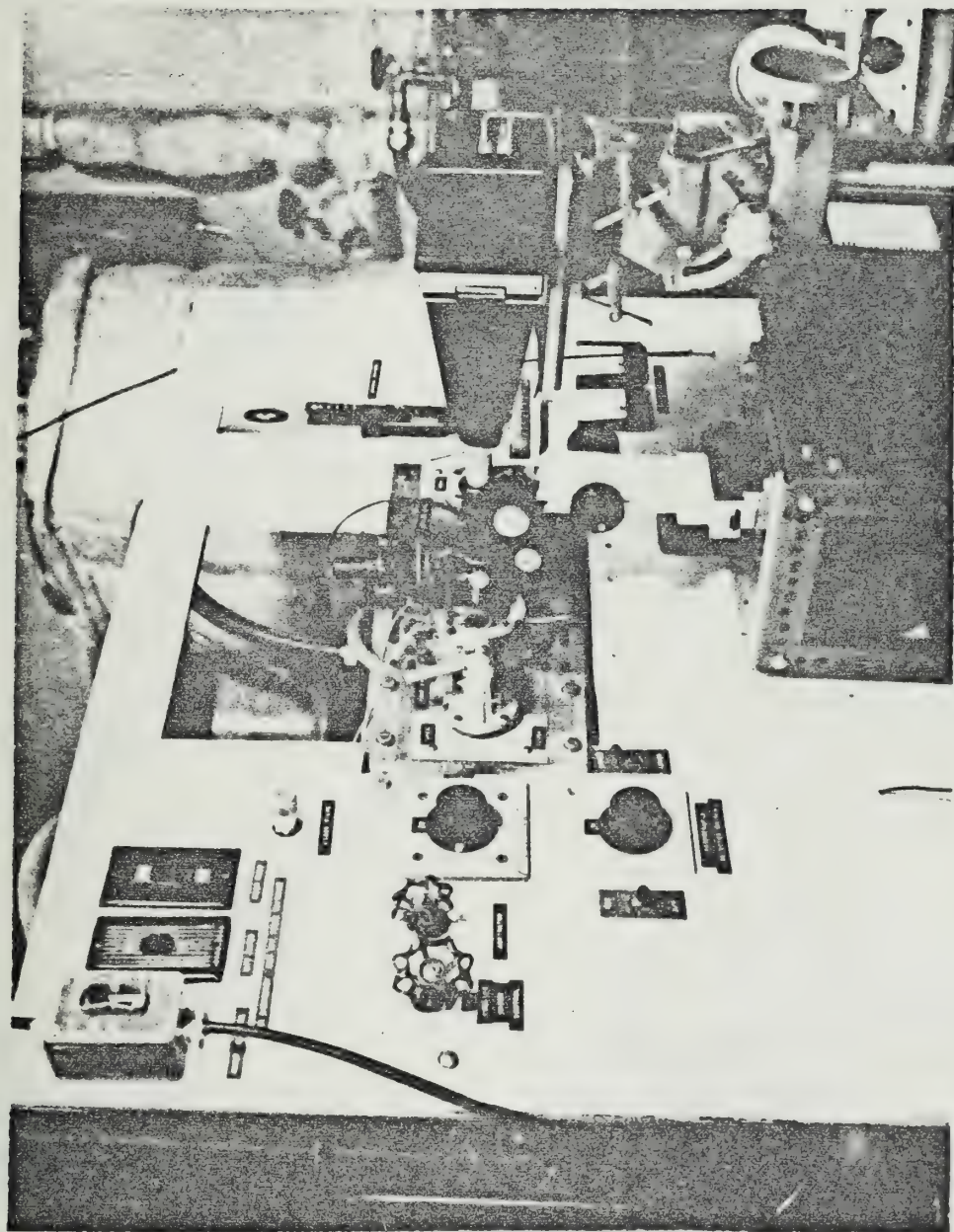


FIG. 23 PHOTOGRAPH OF APPARATUS

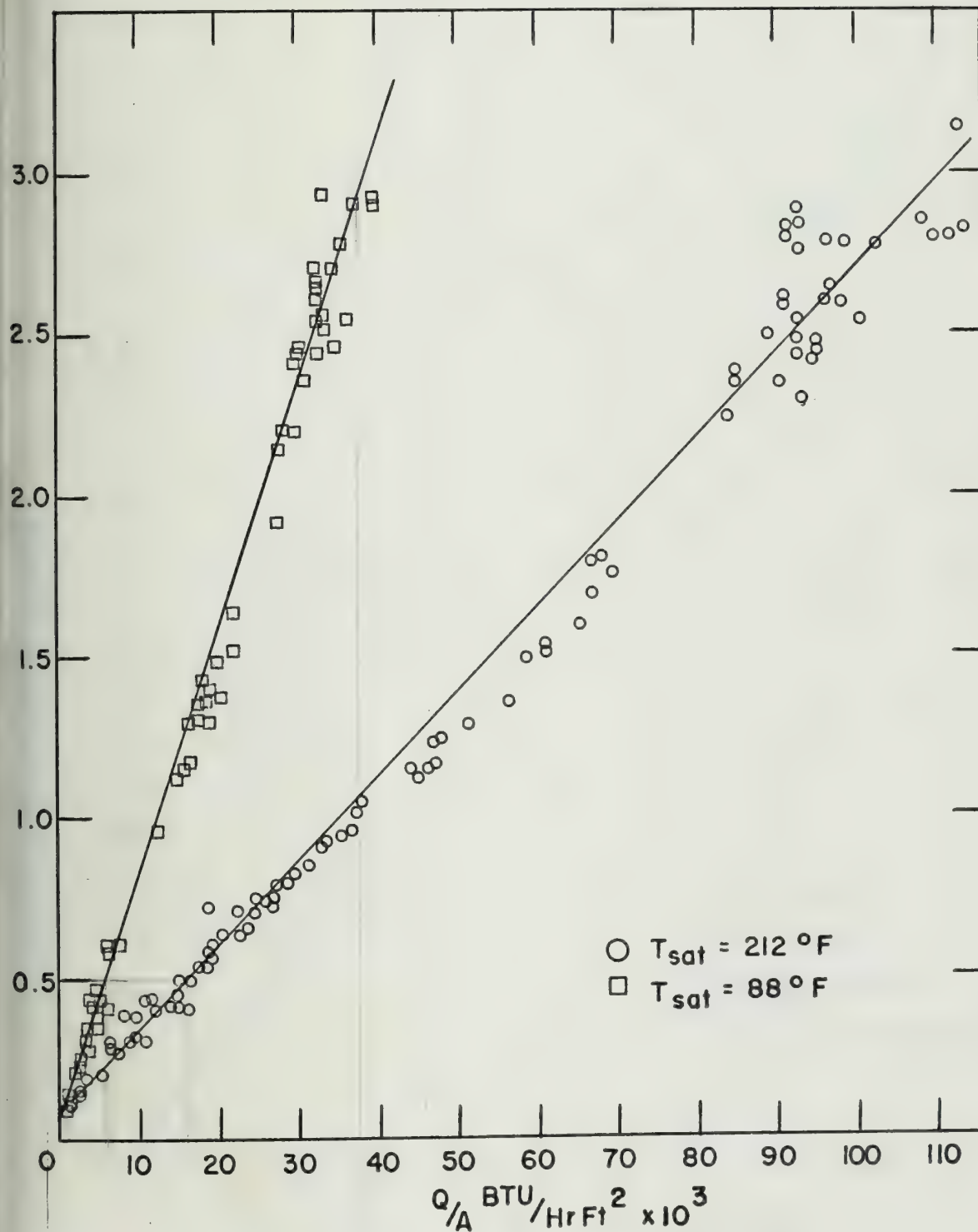


FIG 24 HEAT FLUX— ΔT CURVES FOR MIRROR SMOOTH SURFACE

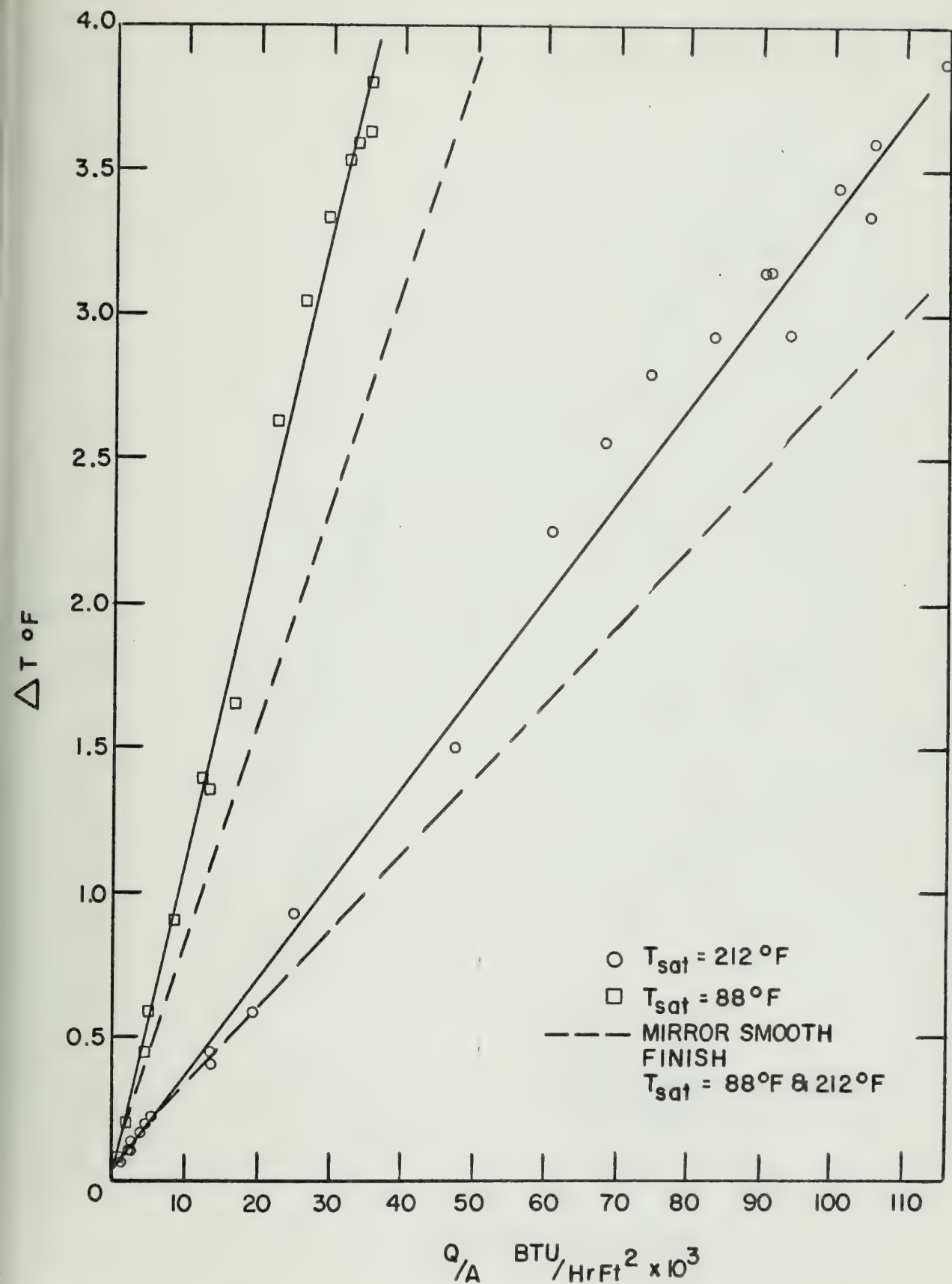


FIG 25 HEAT FLUX— ΔT CURVES FOR ROUGH SURFACE

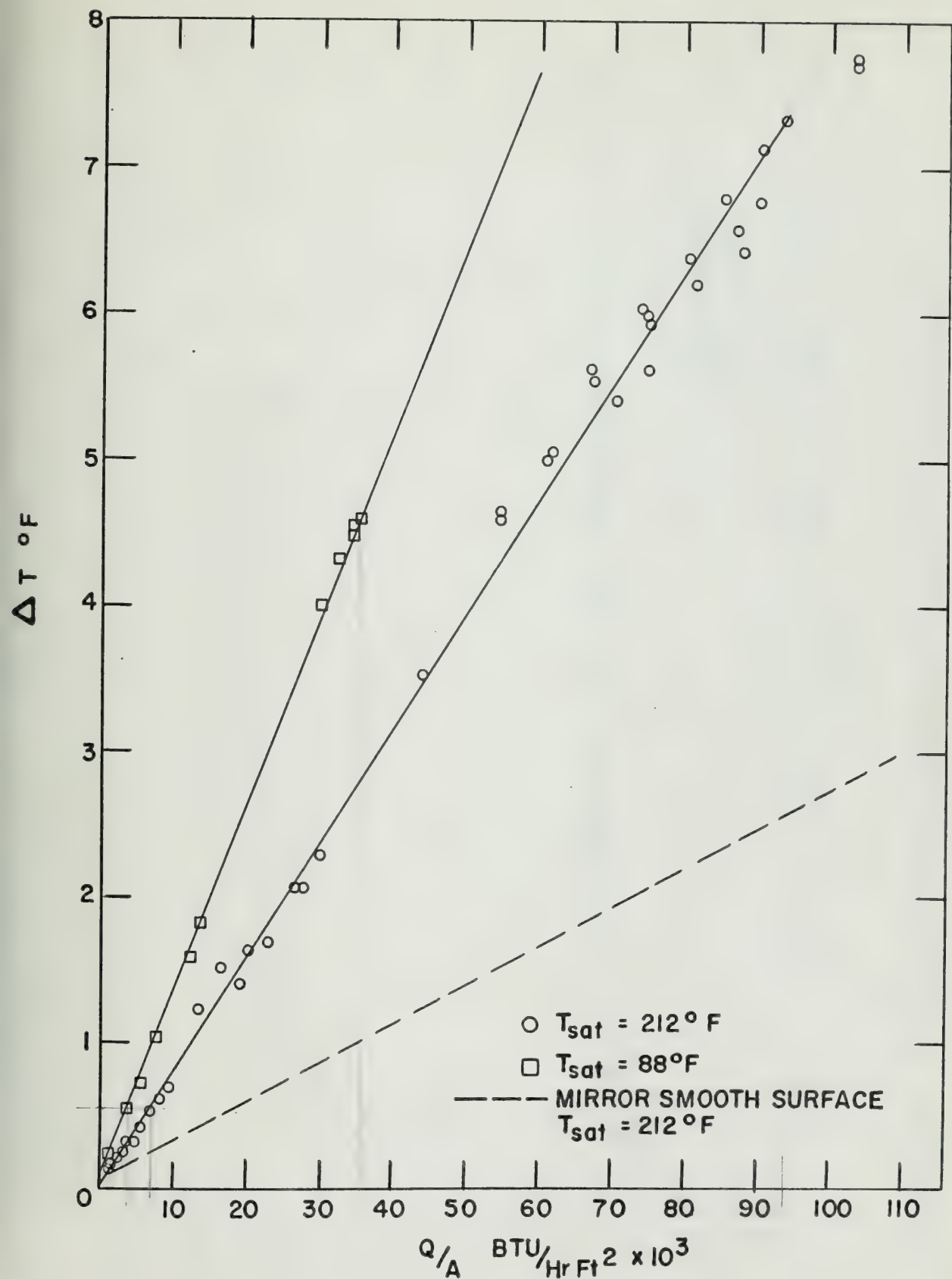


FIG 26 HEAT FLUX- ΔT CURVES FOR TEFLON SURFACE

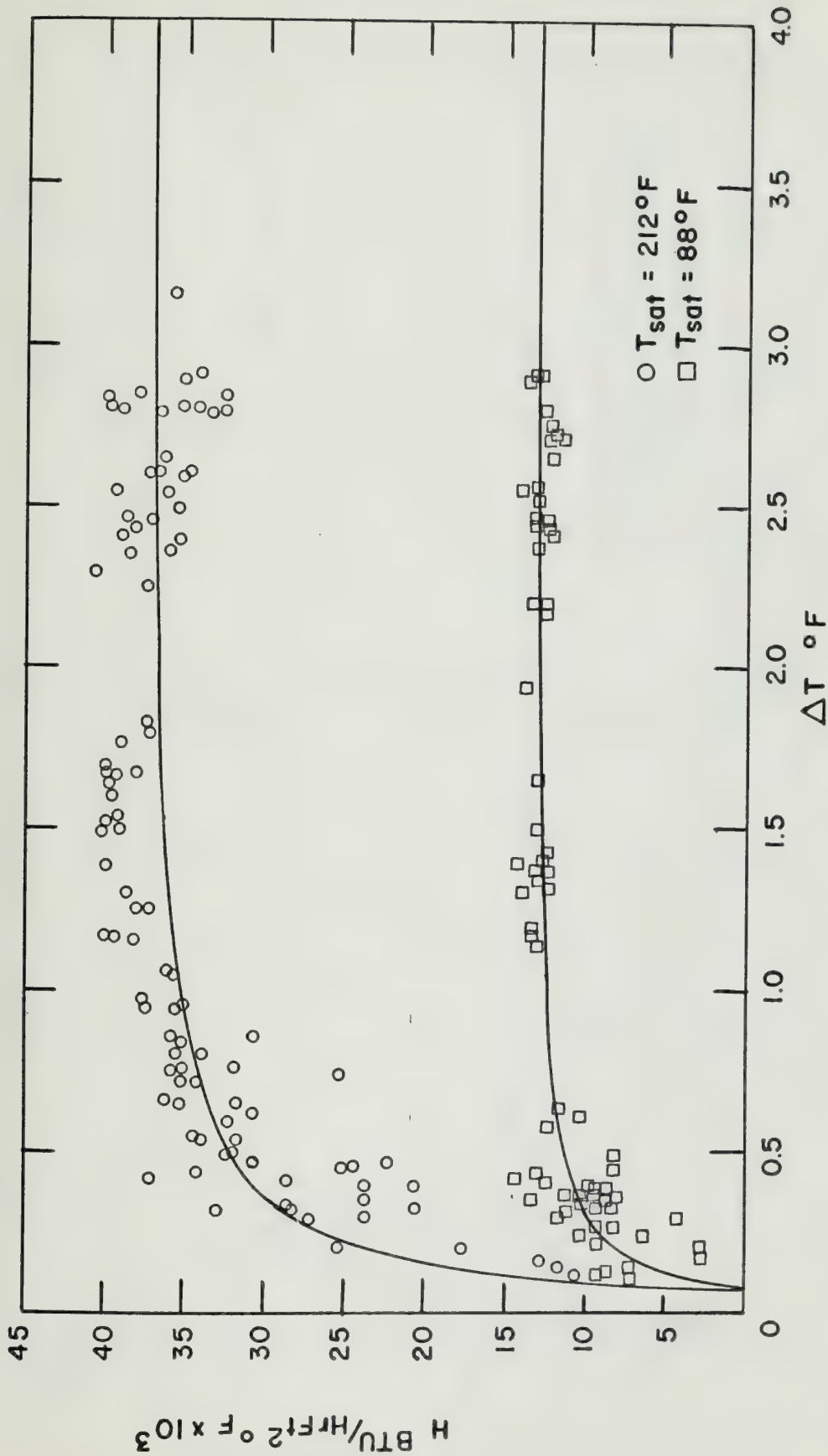


FIG 27 H vs ΔT FOR MIRROR SMOOTH SURFACE

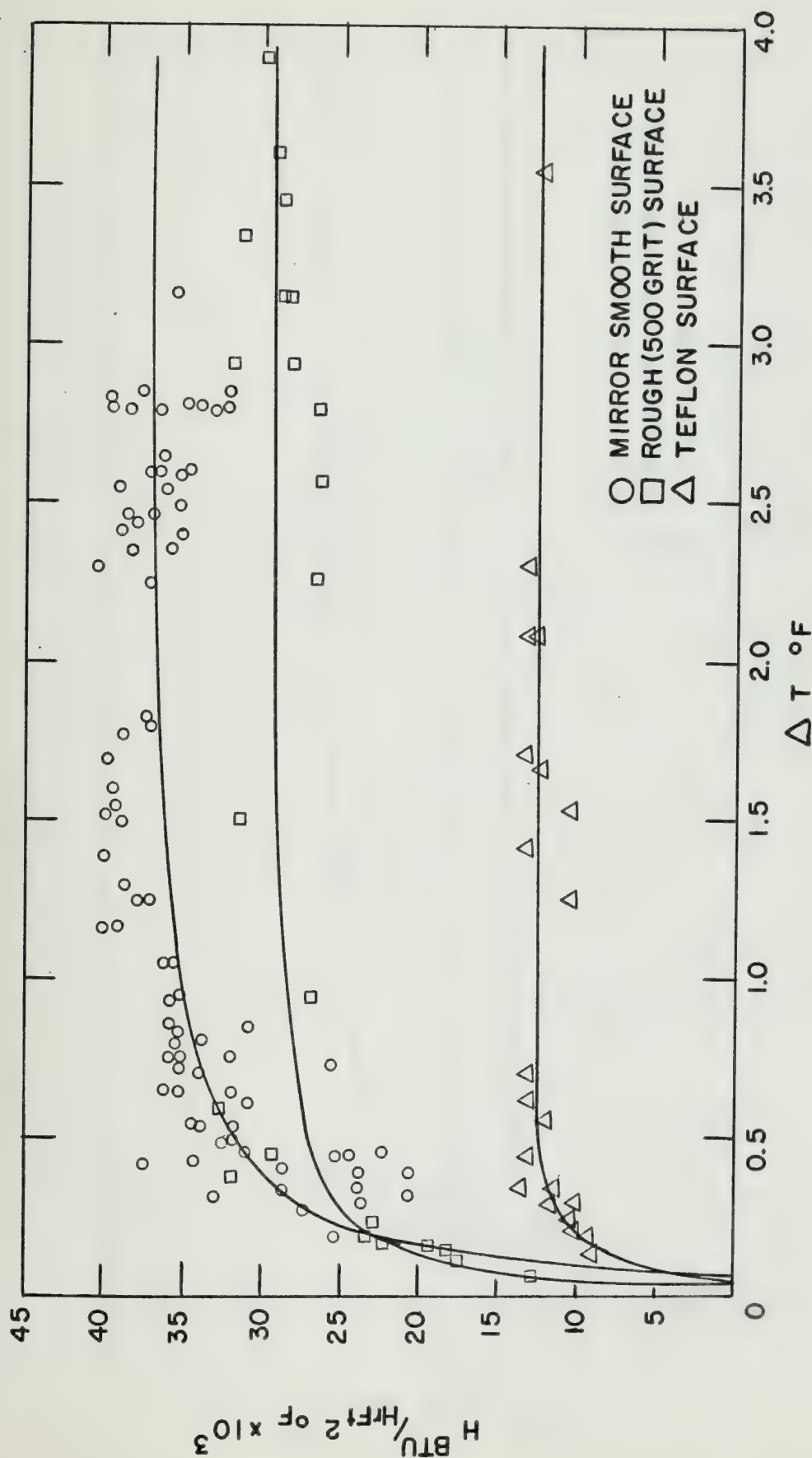


FIG 28 h vs ΔT FOR ATMOSPHERIC PRESSURE CONDENSATION
($T_{\text{sat}} = 212^\circ\text{F}$)

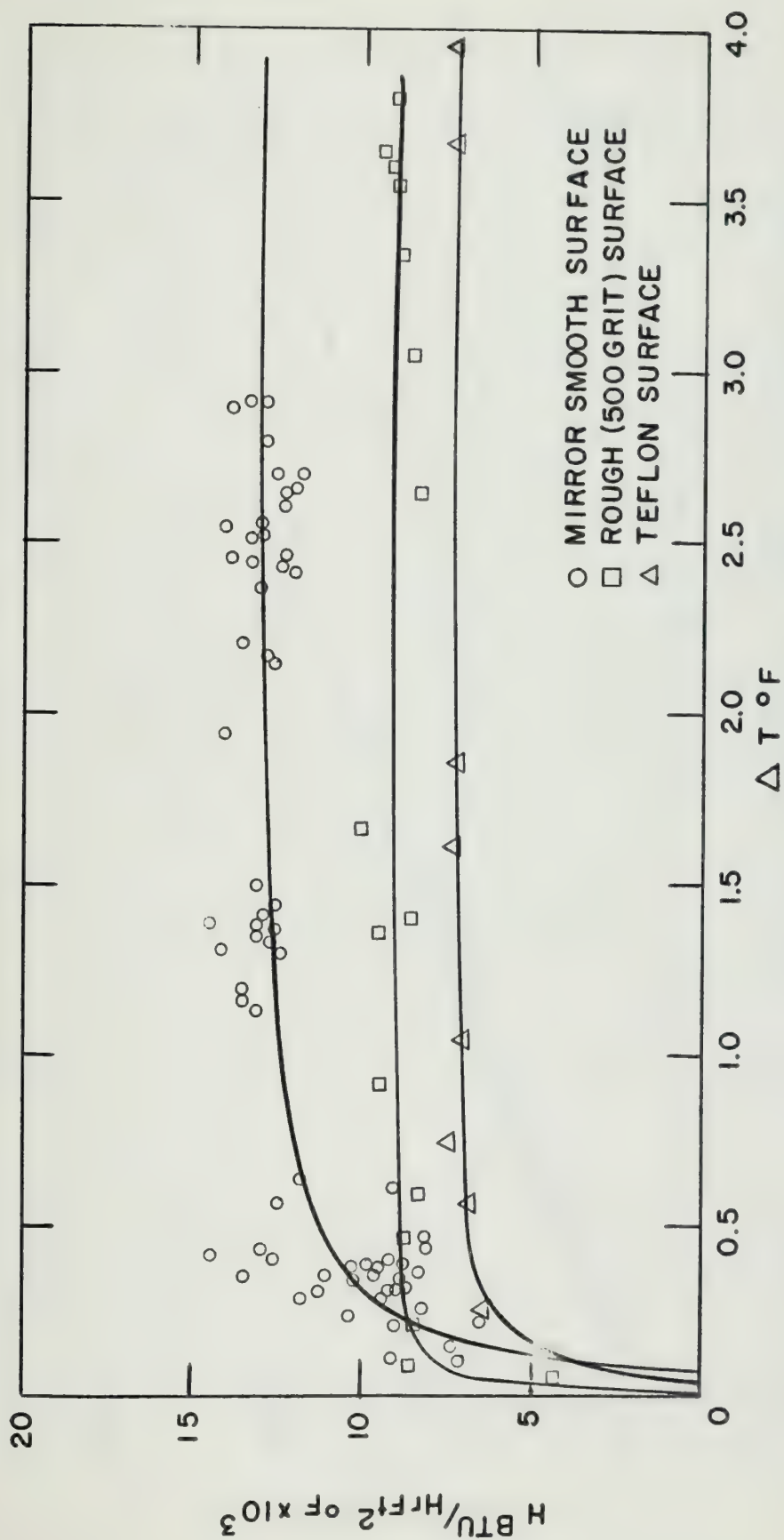


FIG 29 H vs ΔT FOR LOW PRESSURE CONDENSATION ($T_{\text{sat}} = 88^\circ\text{F}$)

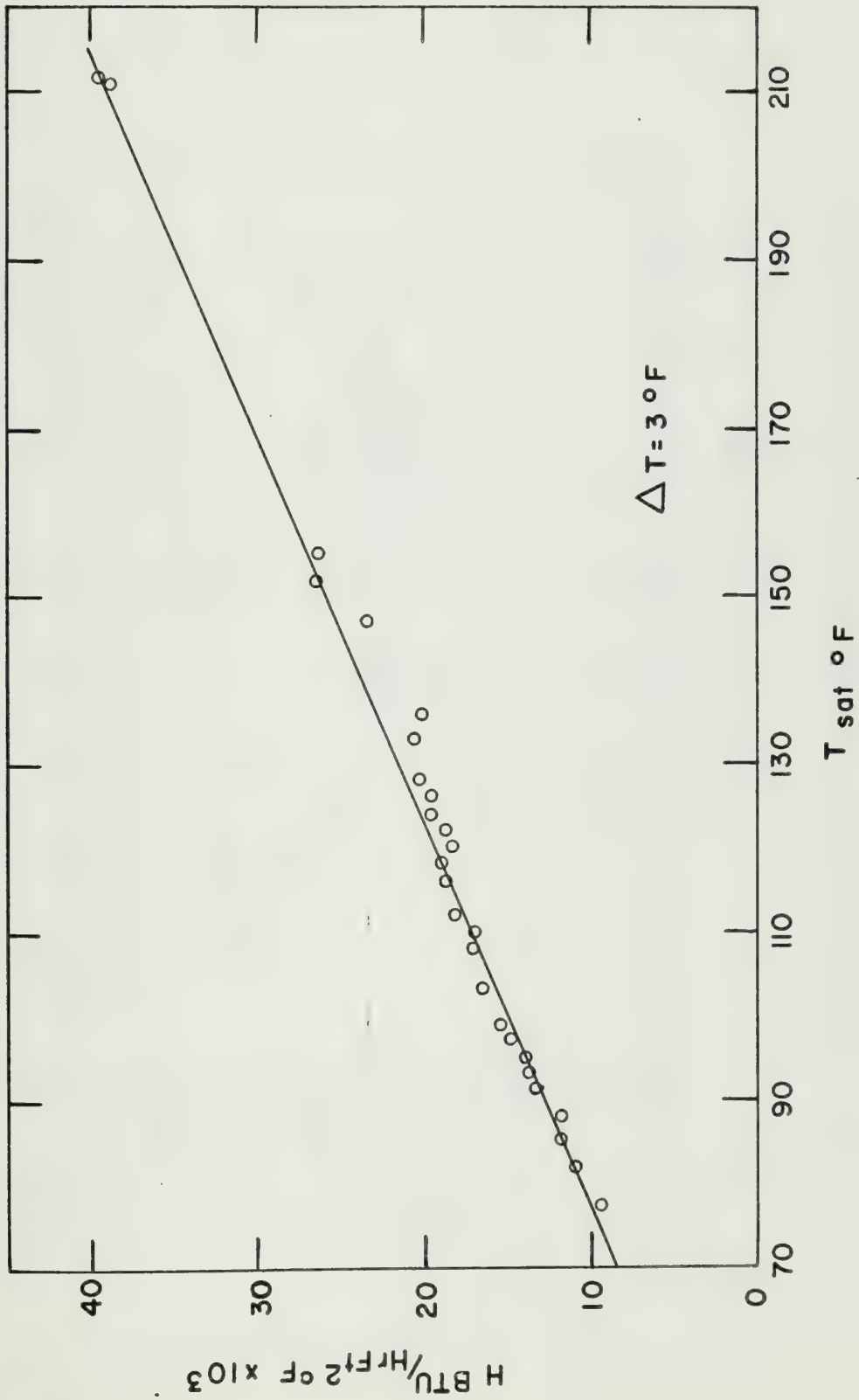


FIG 30 H vs T_{sat} FOR MIRROR SMOOTH SURFACE

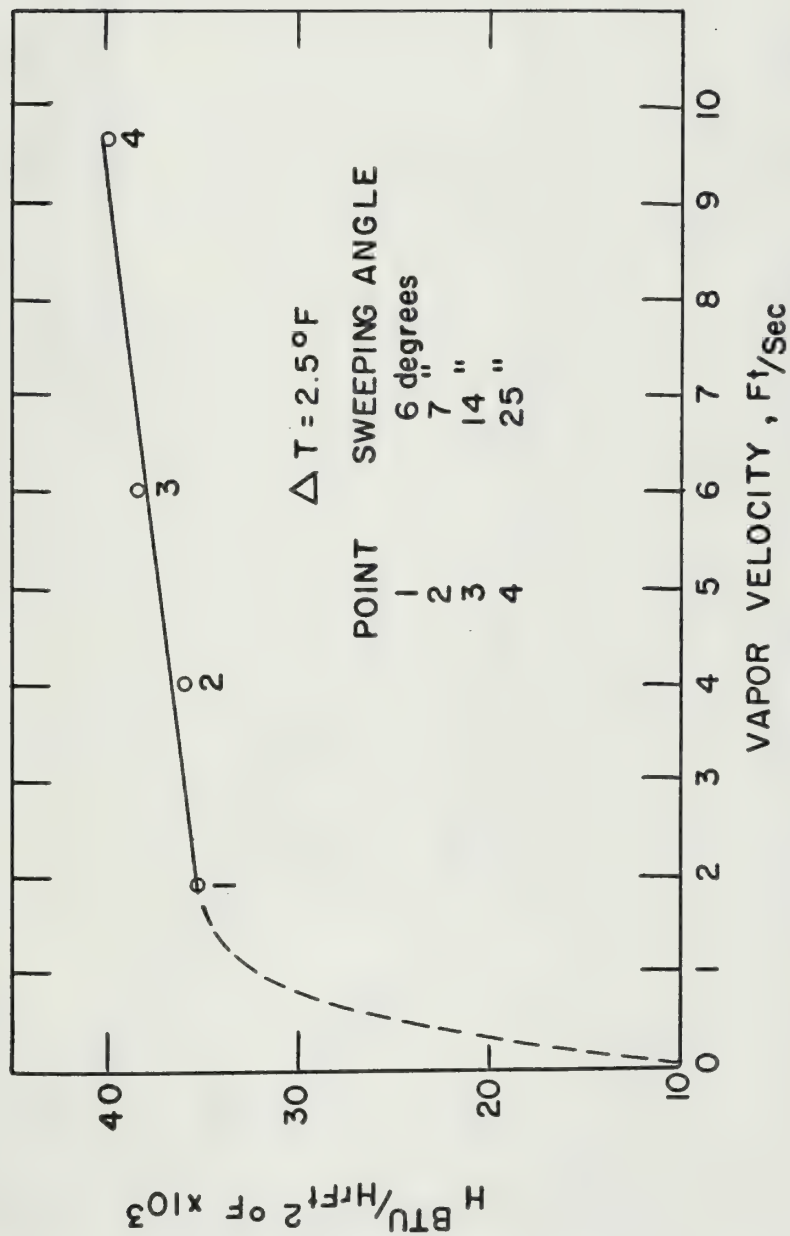


FIG 3I H vs VAPOR VELOCITY FOR MIRROR
SMOOTH SURFACE

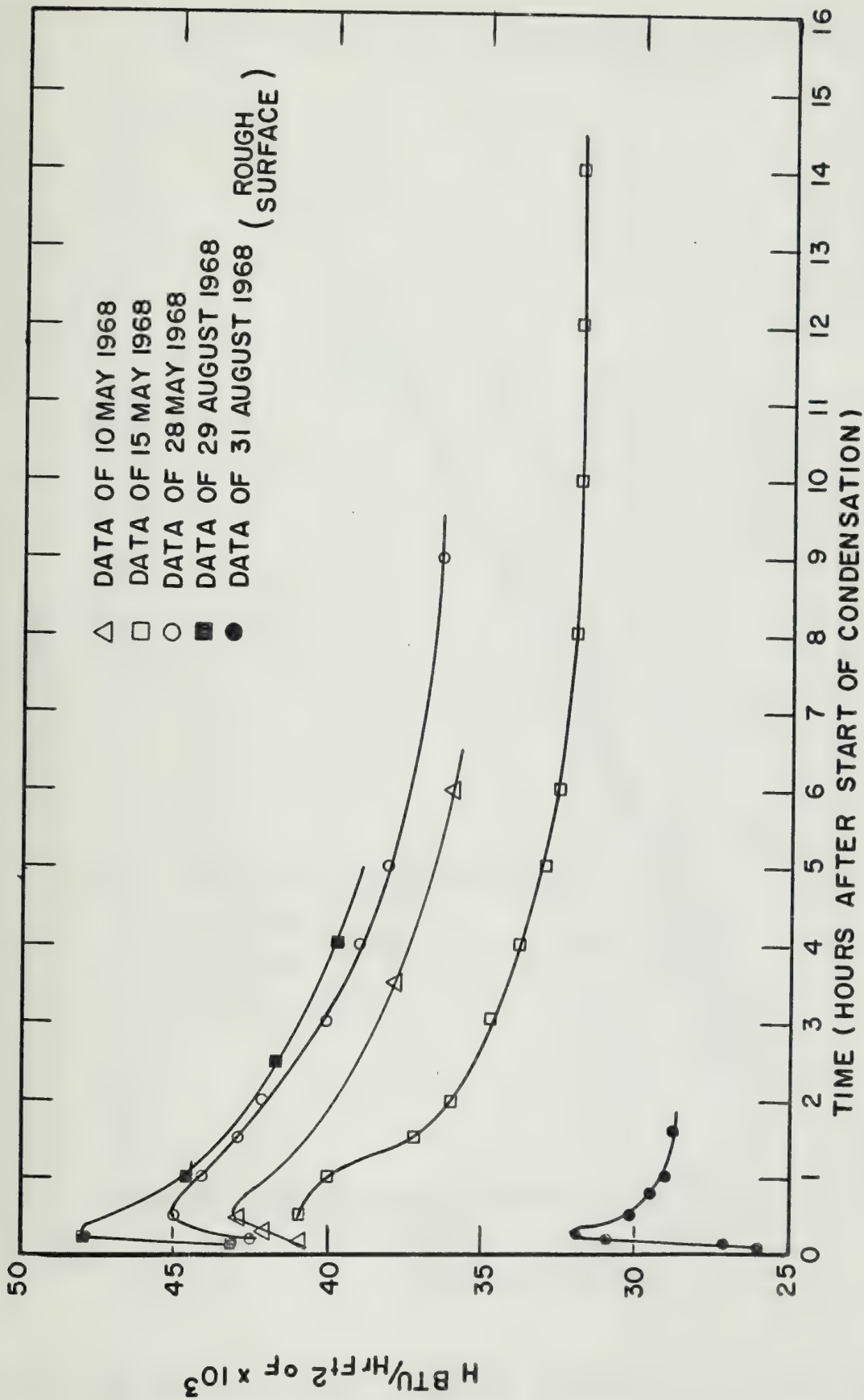


FIG 32 TRANSIENT CURVES FOR MIRROR SMOOTH SURFACE

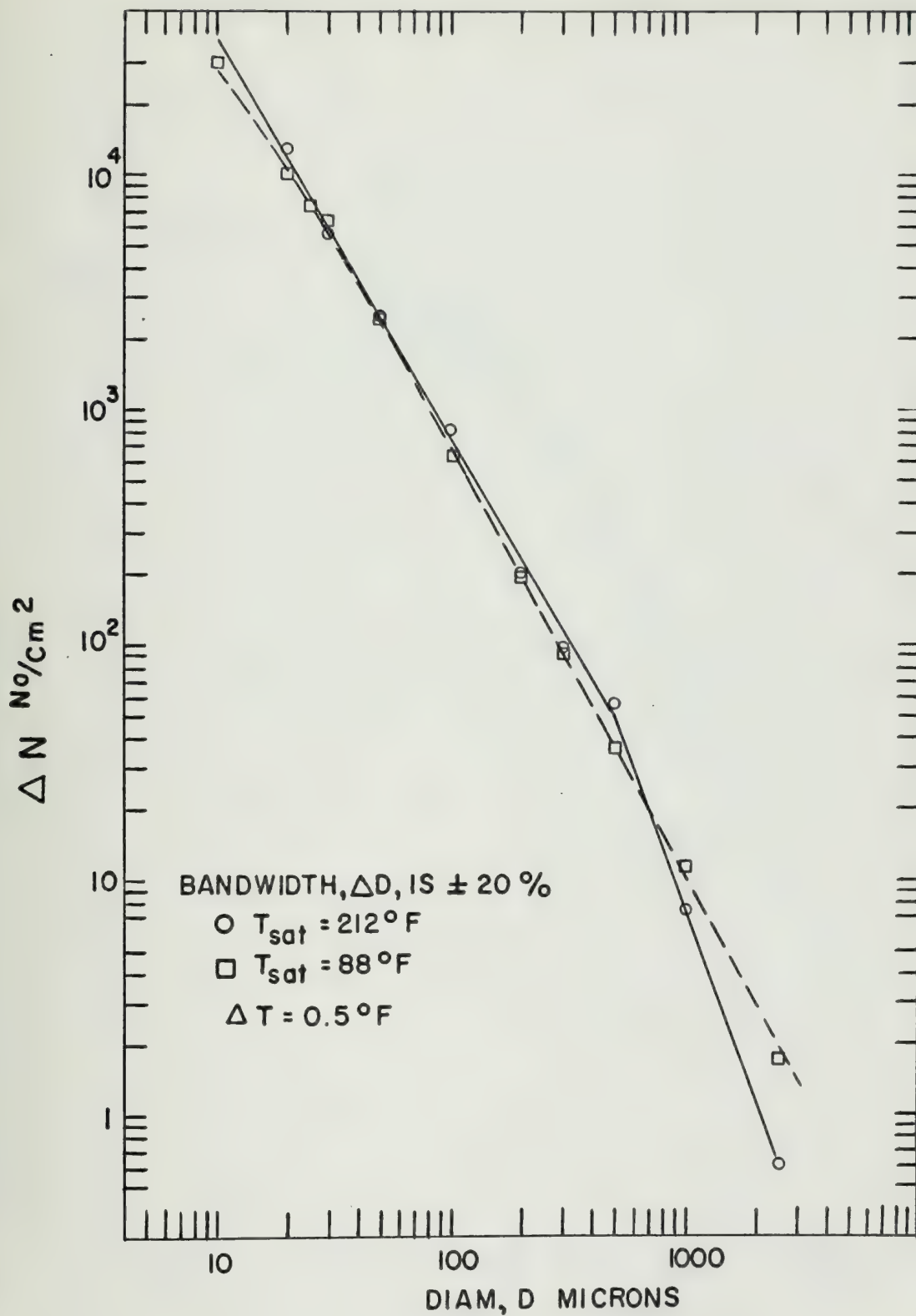


FIG 33 MEASURED DROP DISTRIBUTION FOR MIRROR SMOOTH SURFACE

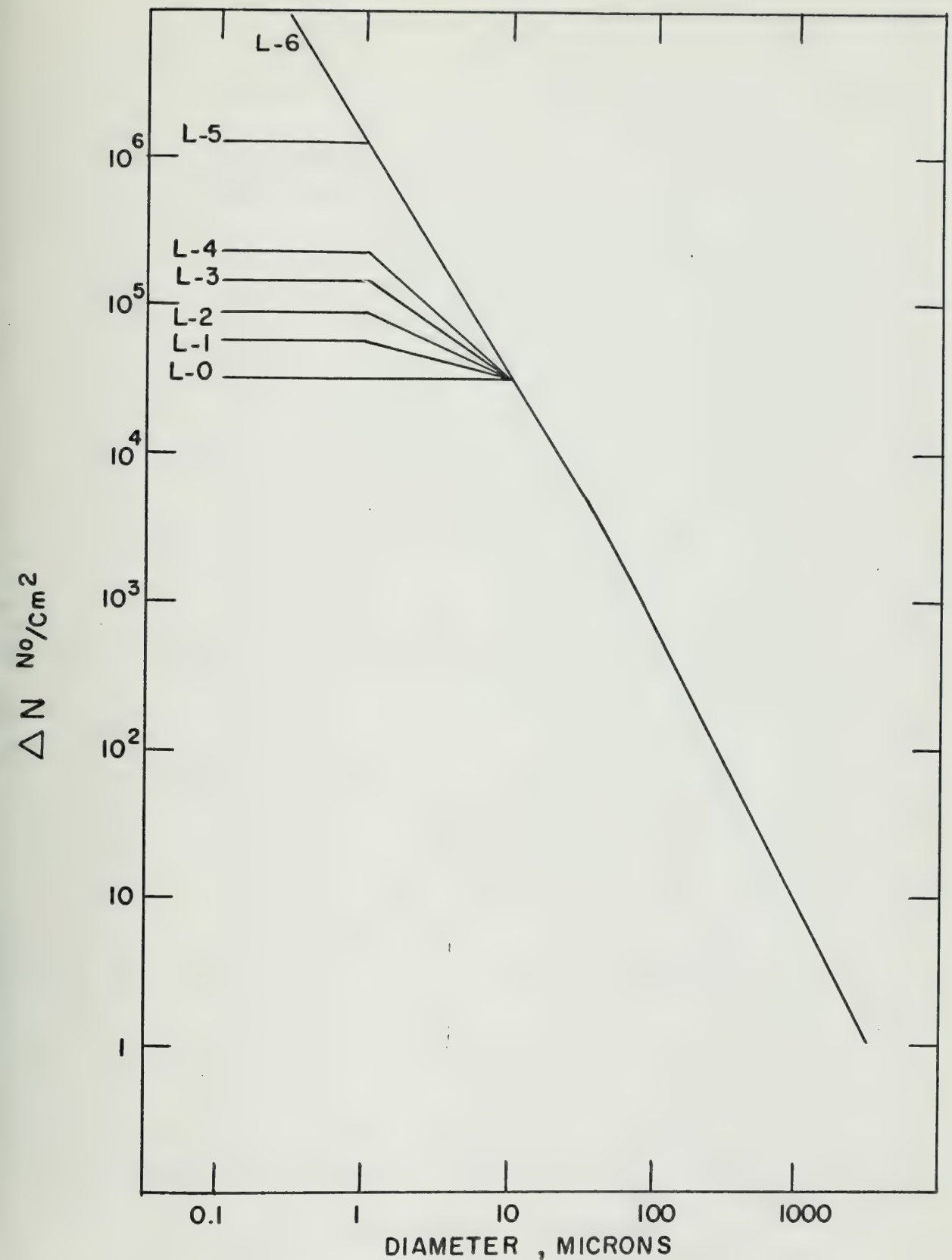


FIG 34 PROPOSED DROP DISTRIBUTIONS FOR LOW PRESSURE CONDENSATION

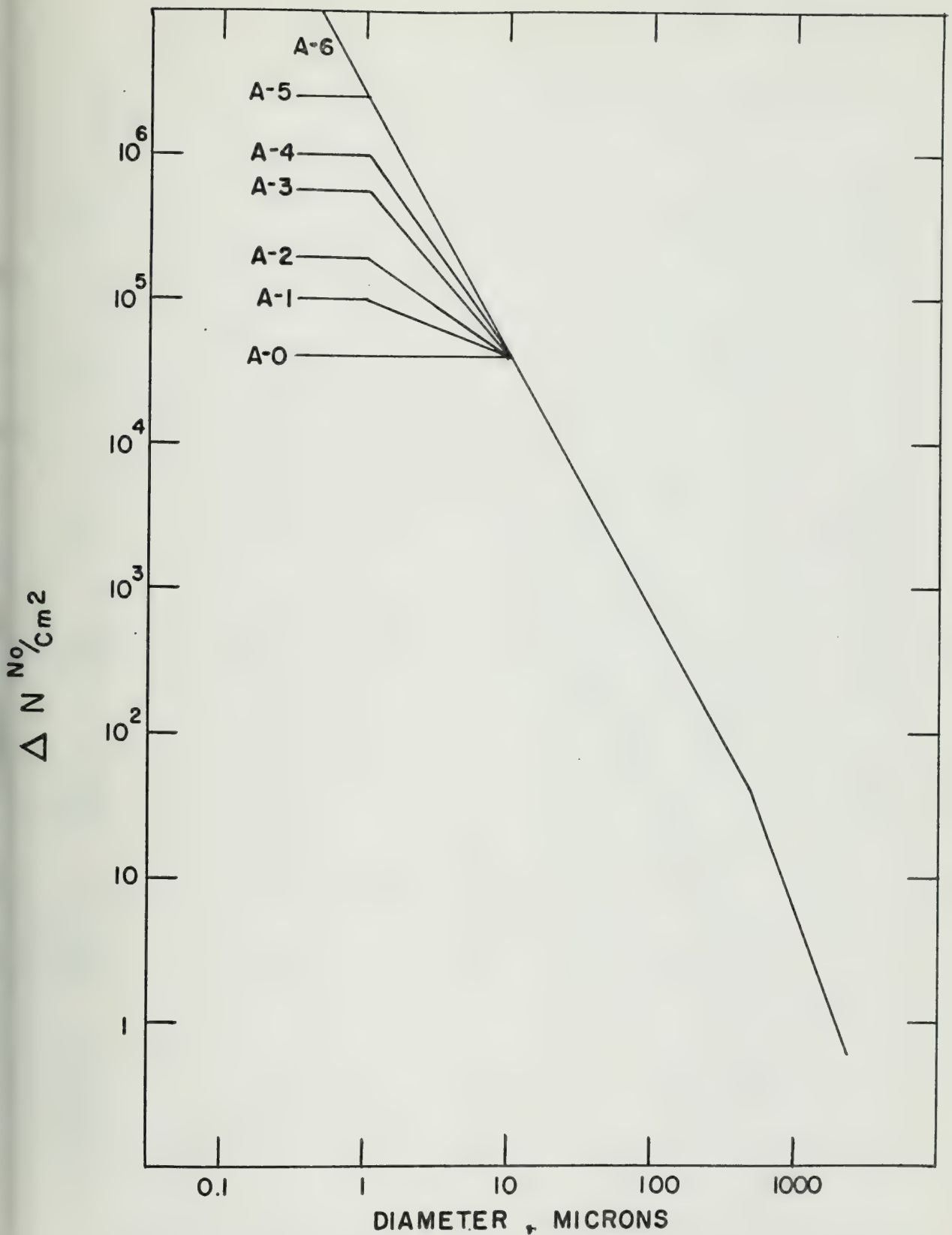


FIG 35 PROPOSED DROP DISTRIBUTIONS FOR ATMOSPHERIC PRESSURE CONDENSATION

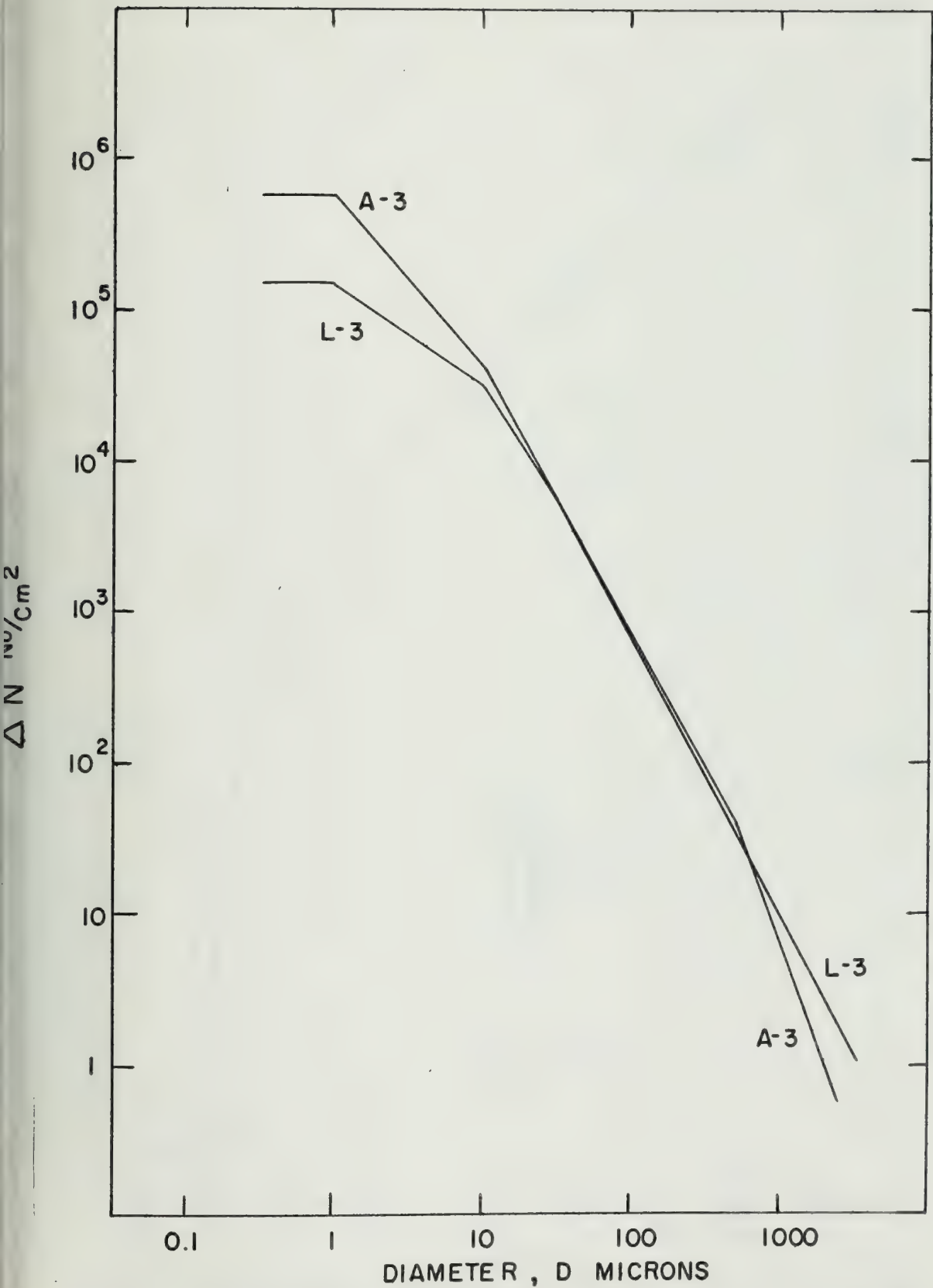


FIG 36 COMPARISON OF "CORRECT" DISTRIBUTIONS FOR LOW AND ATMOSPHERIC PRESSURES

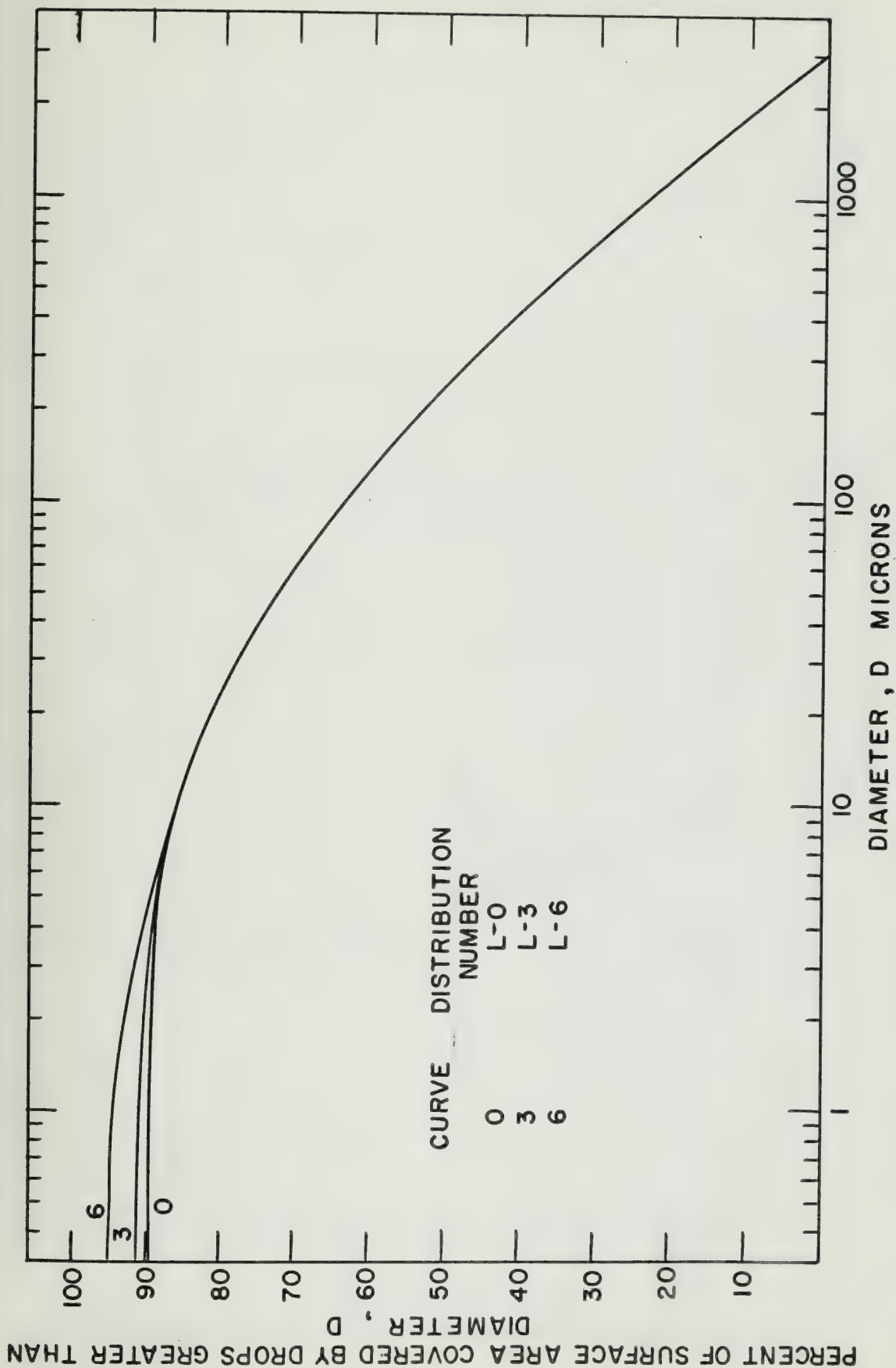


FIG 37 PERCENT OF SURFACE AREA COVERED BY DROPS DURING
LOW PRESSURE CONDENSATION

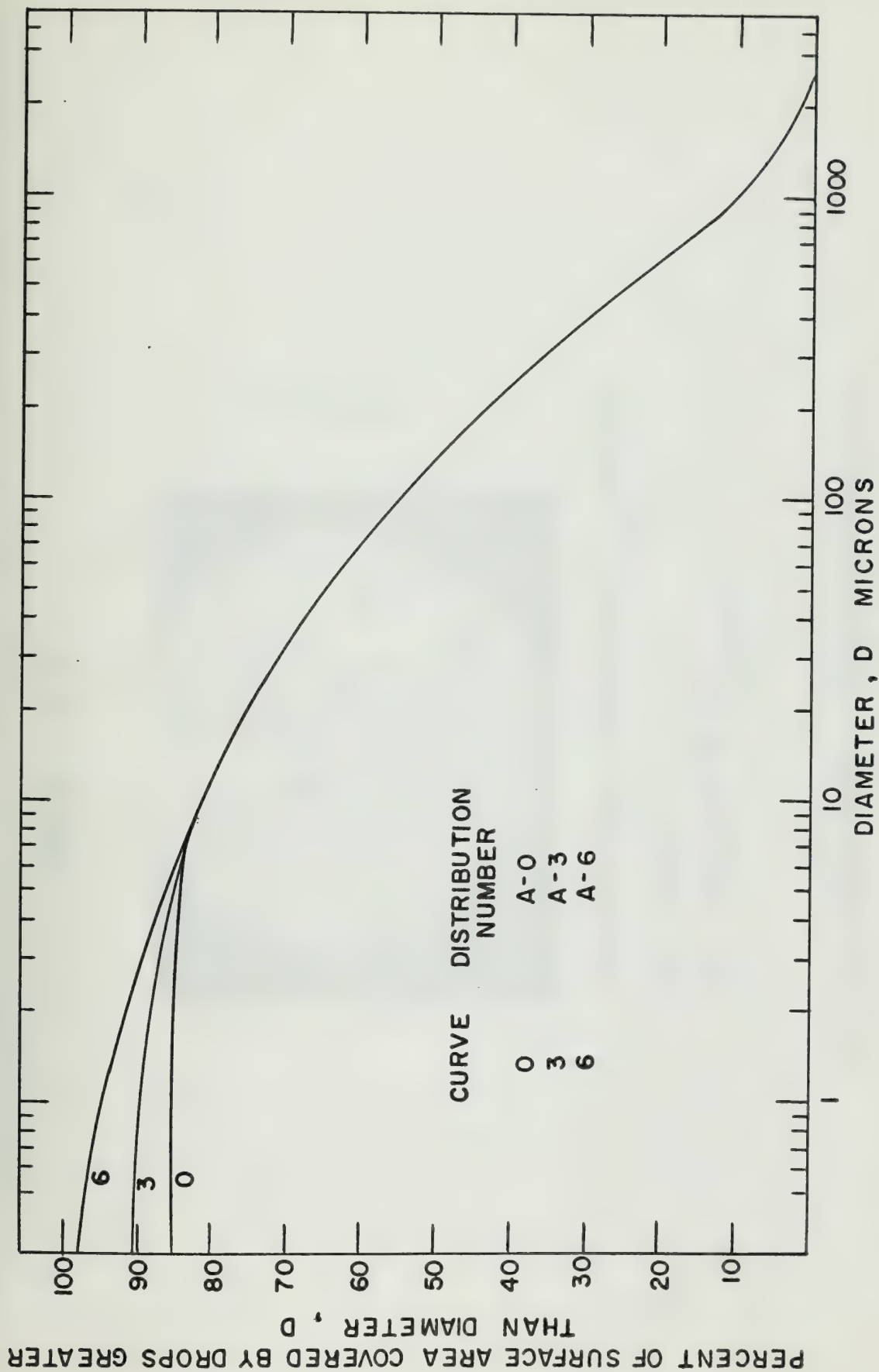
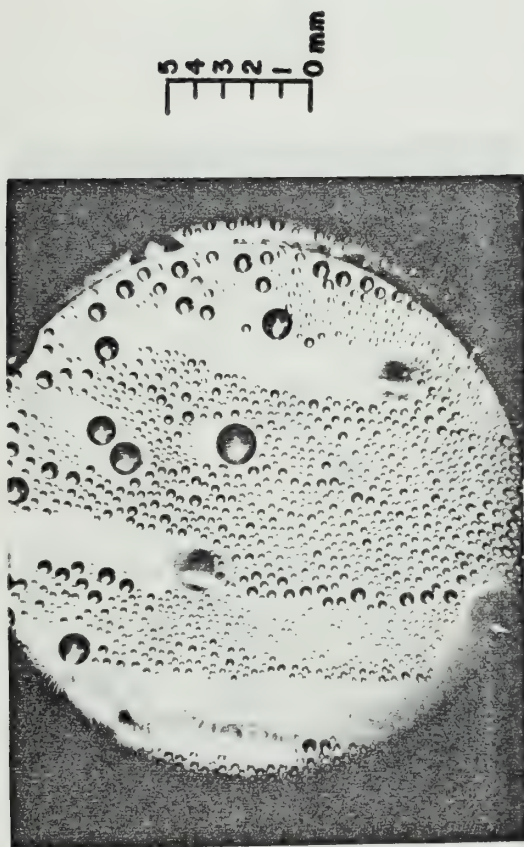


FIG 38 PERCENT OF SURFACE AREA COVERED BY DROPS DURING ATMOSPHERIC PRESSURE CONDENSATION

MAG = 5 x



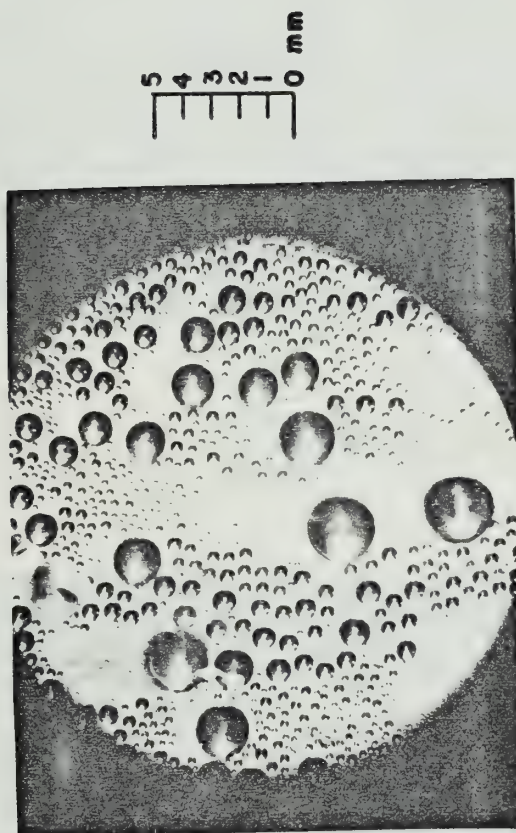
ATMOSPHERIC PRESSURE ($T_{\text{sat}} = 212^{\circ}\text{F}$)

$\Delta T = 2.5^{\circ}\text{F}$

$Q/A = 90,000 \text{ BTU/hr F}^2$

FIG 39 DROPWISE CONDENSATION AT
HIGH HEAT FLUX

MAG = 5 x



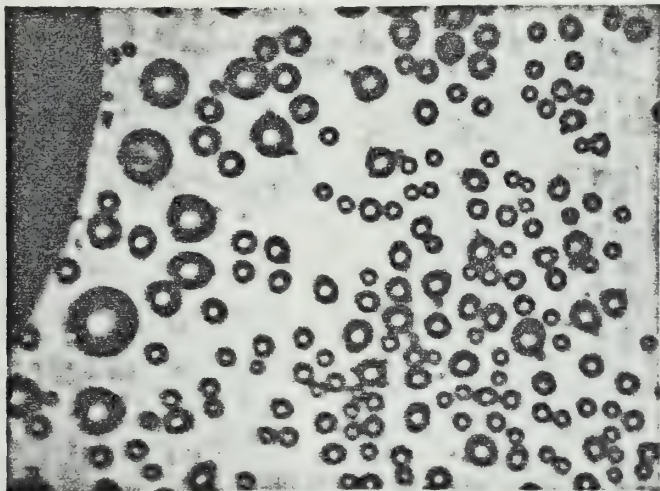
ATMOSPHERIC PRESSURE ($T_{sat} = 212^{\circ}\text{F}$)

$\Delta T = 0.5^{\circ}\text{F}$

$q_A = 16,000 \text{ BTU/hr Ft}^2$

FIG 40 DROPWISE CONDENSATION AT
LOW HEAT FLUX

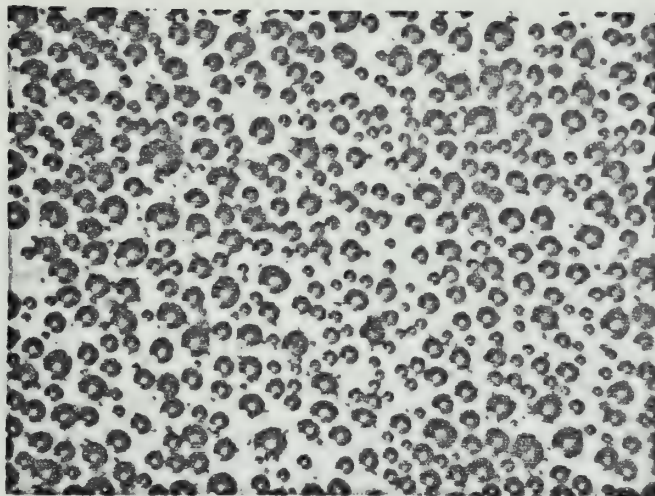
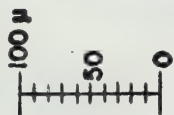
MAG=200 x



LOW PRESSURE ($T_{sat}=88^{\circ}\text{F}$)

$\Delta T = 0.12^{\circ}\text{F}$

$$Q_A = 600 \text{ BTU/hr Ft}^2$$



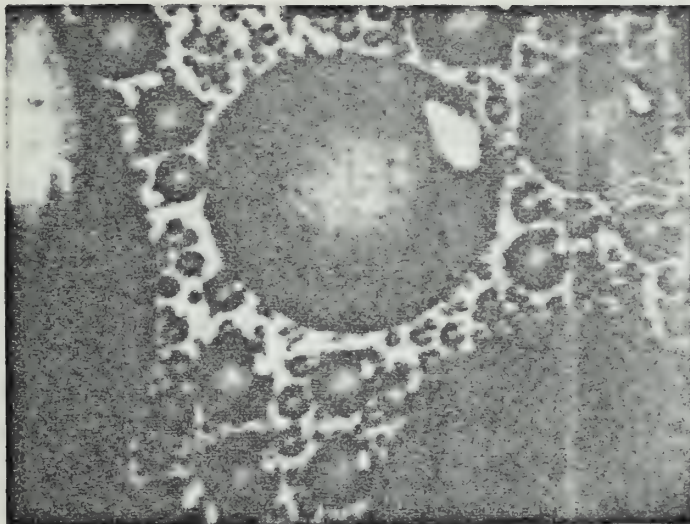
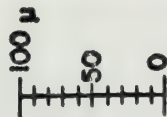
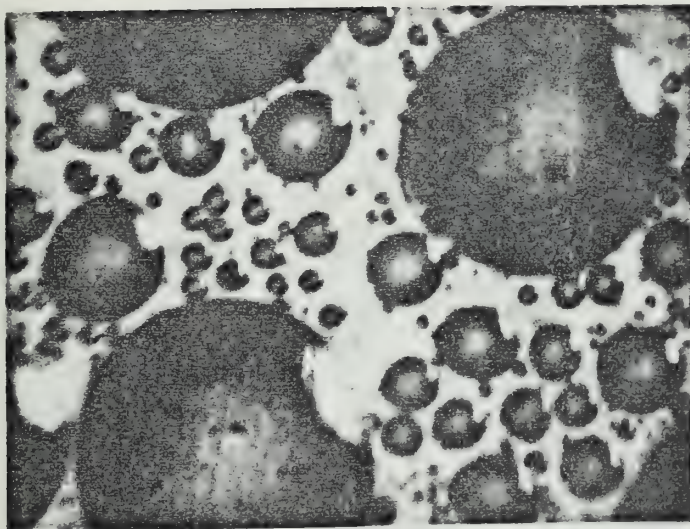
LOW PRESSURE ($T_{sat}=88^{\circ}\text{F}$)

$\Delta T = 0.37^{\circ}\text{F}$

$$Q_A = 4,000 \text{ BTU/hr Ft}^2$$

FIG 4I EFFECT OF ΔT ON NUCLEATION

MAG = 200 x



LOW PRESSURE ($T_{sat} = 88^{\circ}\text{F}$)

$\Delta T = 0.37^{\circ}\text{F}$

$$Q/A = 4,000 \text{ BTU/hr Ft}^2$$

ATMOSPHERIC

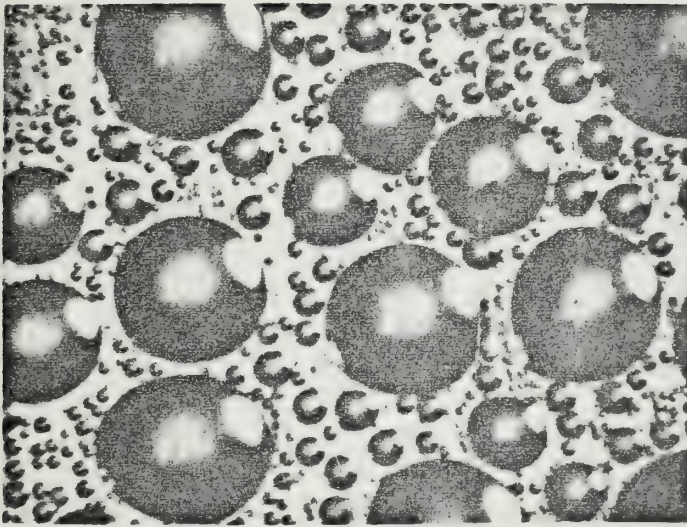
PRESSURE ($T_{sat} = 212^{\circ}\text{F}$)

$\Delta T = 0.37^{\circ}\text{F}$

$$Q/A = 12,000 \text{ BTU/hr Ft}^2$$

FIG 42 EFFECT OF PRESSURE ON NUCLEATION

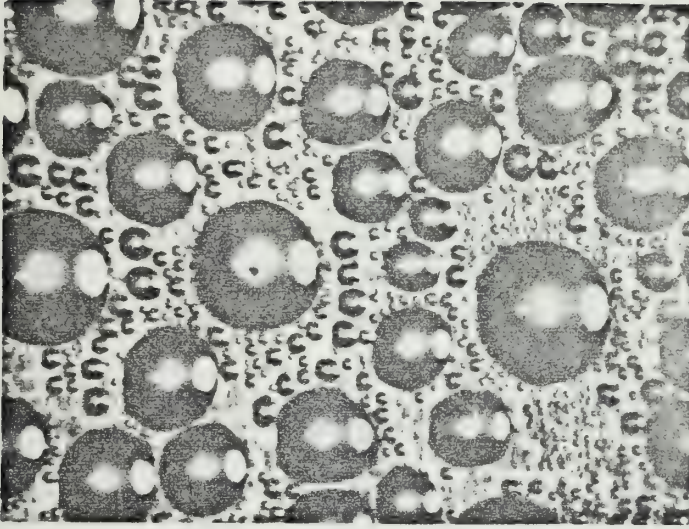
MAG = 120 x



LOW PRESSURE ($T_{sat} = 88^{\circ}\text{F}$)

$\Delta T = 0.37^{\circ}\text{F}$

$$Q/A = 4,000 \text{ BTU/hr Ft}^2$$



ATMOSPHERIC
PRESSURE ($T_{sat} = 212^{\circ}\text{F}$)

$\Delta T = 0.37^{\circ}\text{F}$

$$Q/A = 12,000 \text{ BTU/hr Ft}^2$$

FIG 43 EFFECT OF PRESSURE ON NUCLEATION

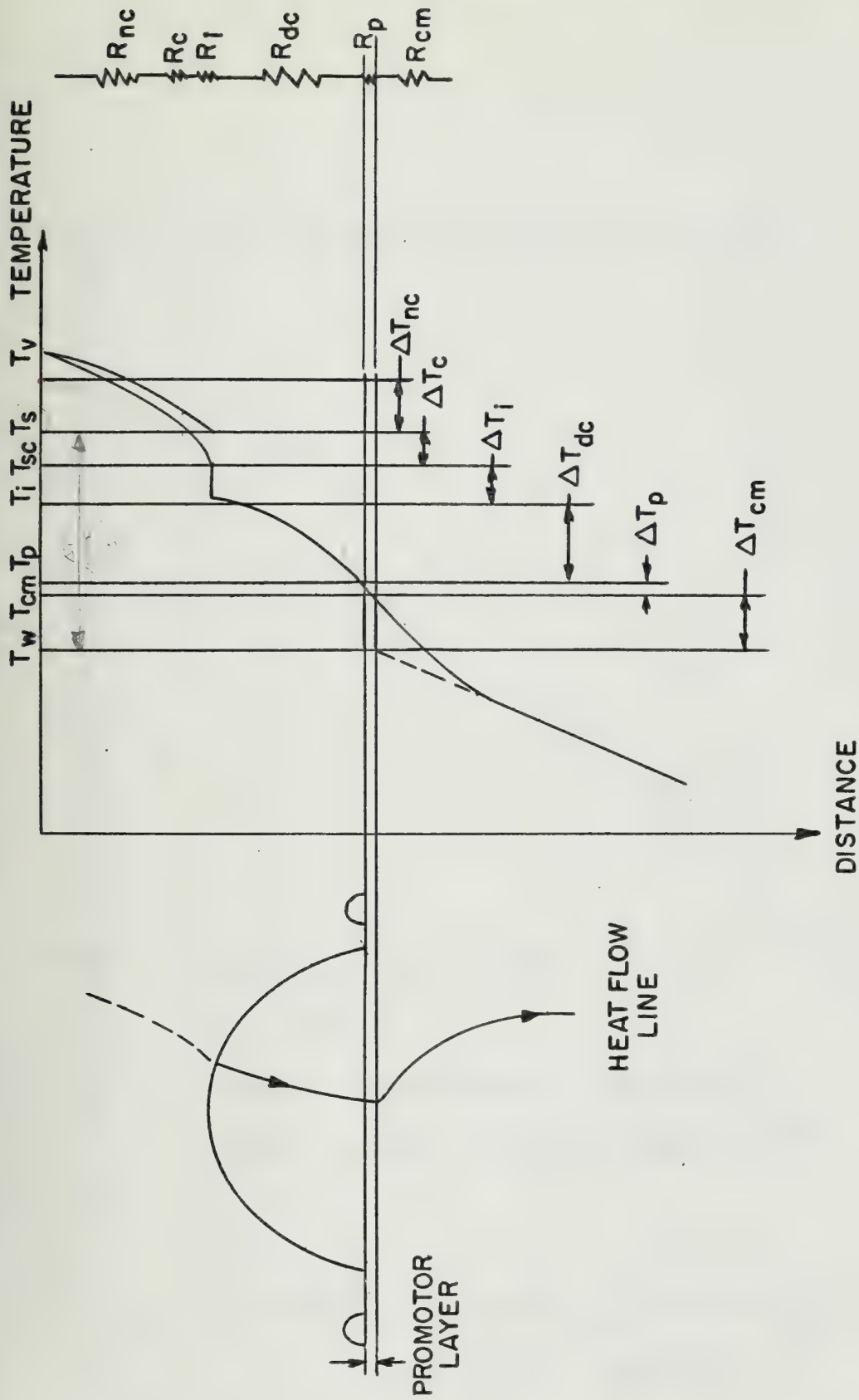


FIG 44 HEAT TRANSFER MODEL FOR DROPWISE CONDENSATION

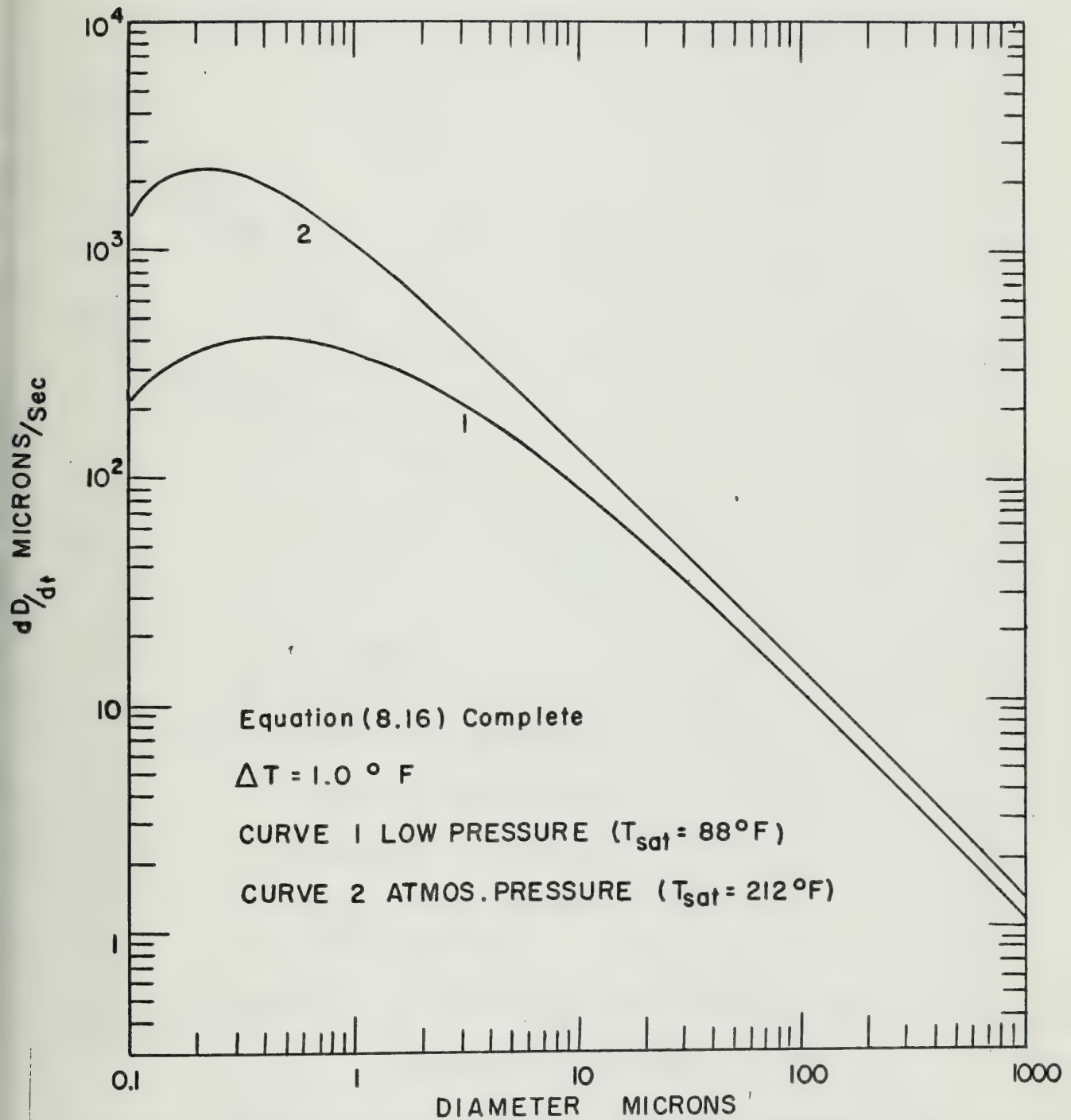


FIG 45 DROP GROWTH RATE DISTRIBUTIONS FOR LOW AND ATMOSPHERIC PRESSURES

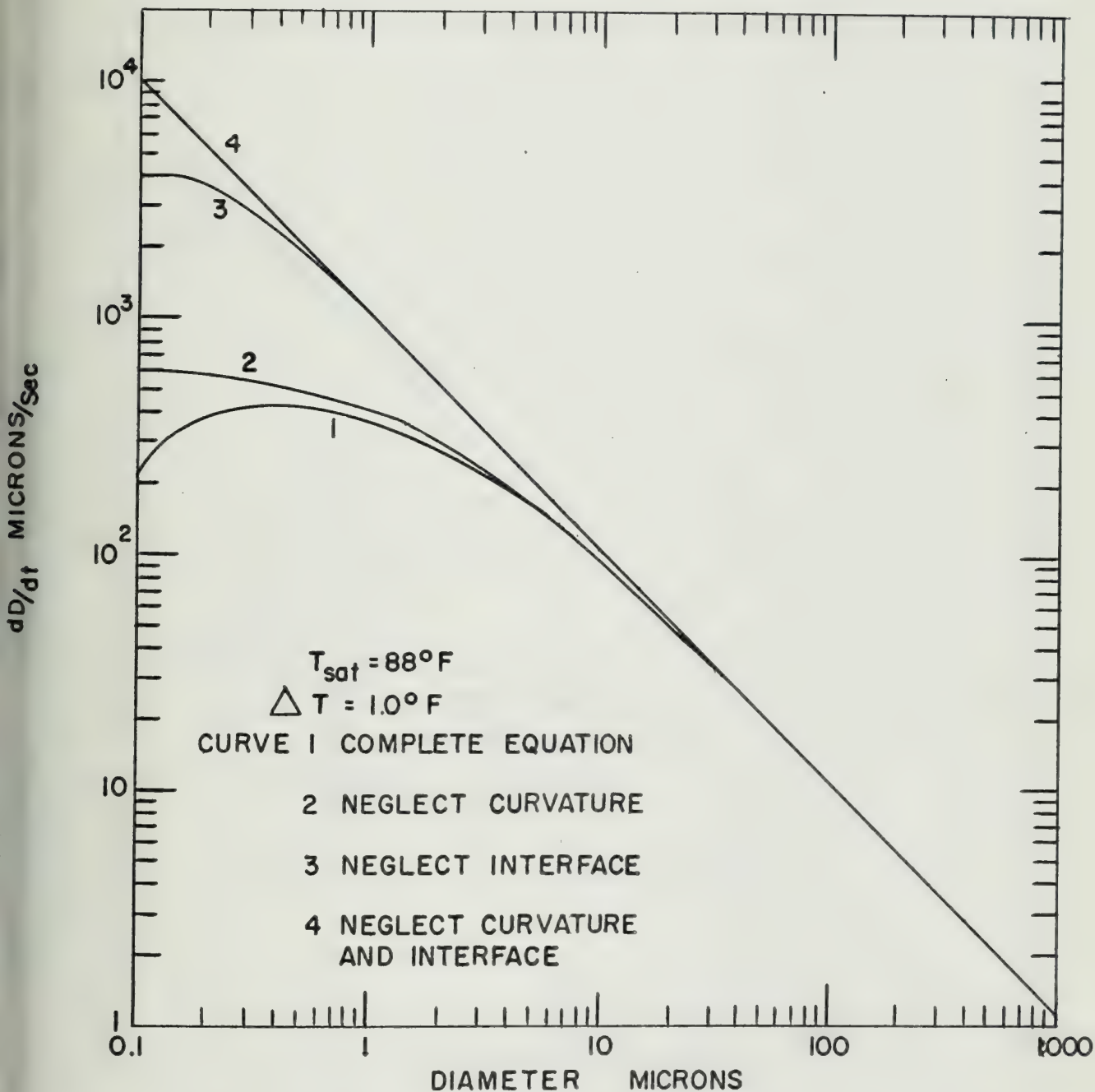


FIG 46 DROP GROWTH RATE DISTRIBUTIONS FOR LOW PRESSURE CONDENSATION (varying equation)

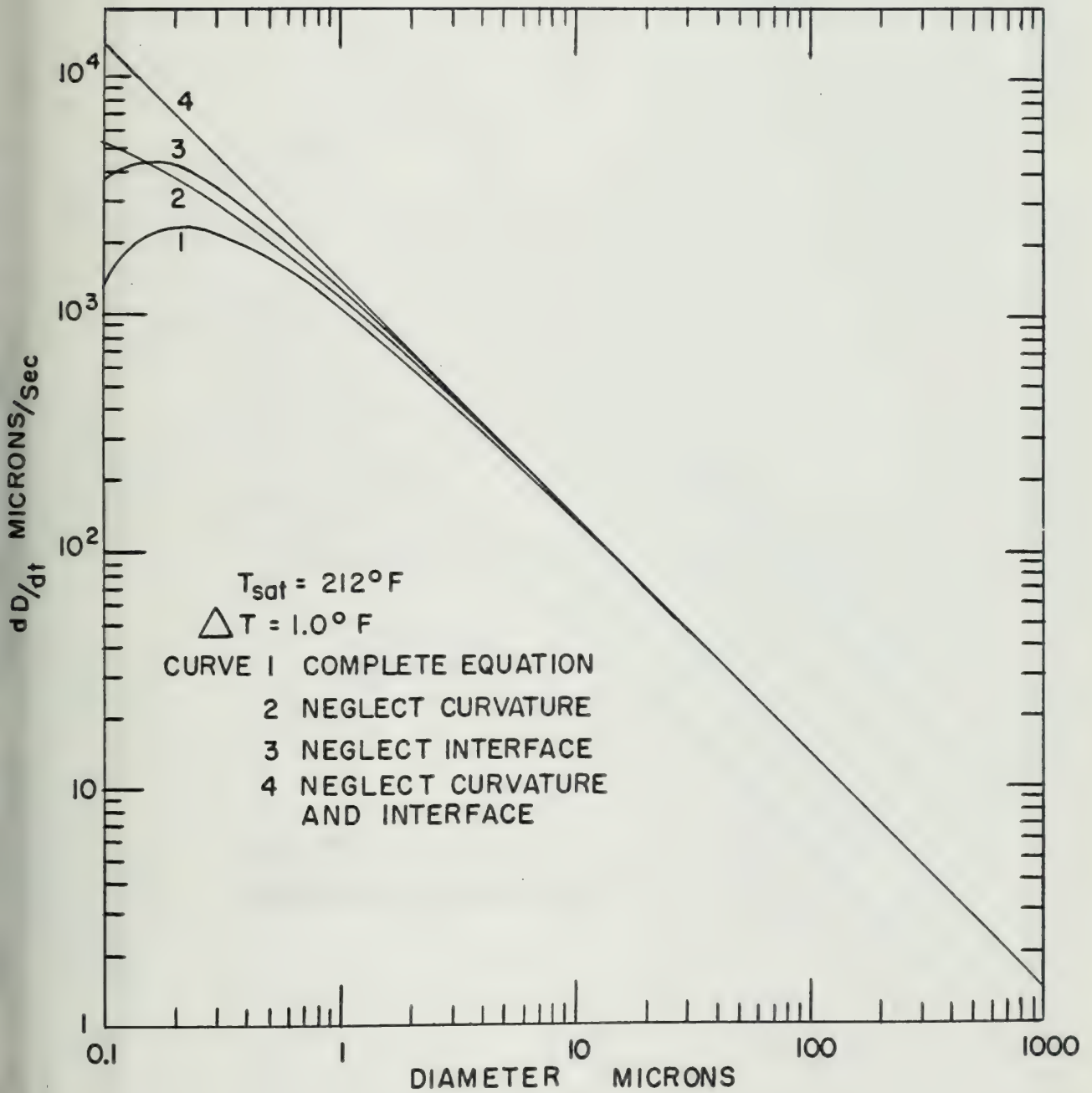


FIG 47 DROP GROWTH RATE DISTRIBUTIONS FOR ATMOSPHERIC PRESSURE CONDENSATION (varying equation)

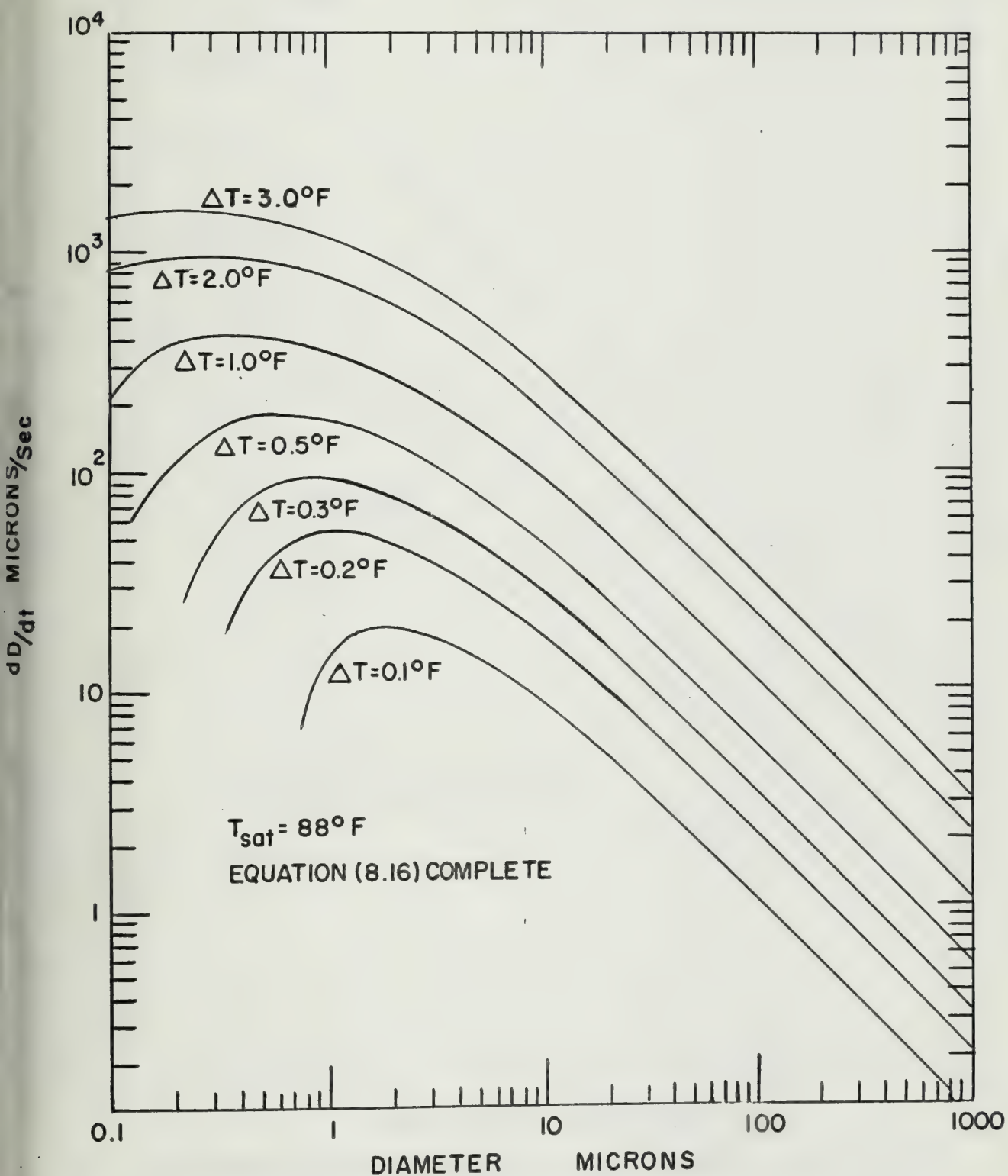


FIG 48 DROP GROWTH RATE DISTRIBUTIONS FOR LOW PRESSURE CONDENSATION (varying ΔT)

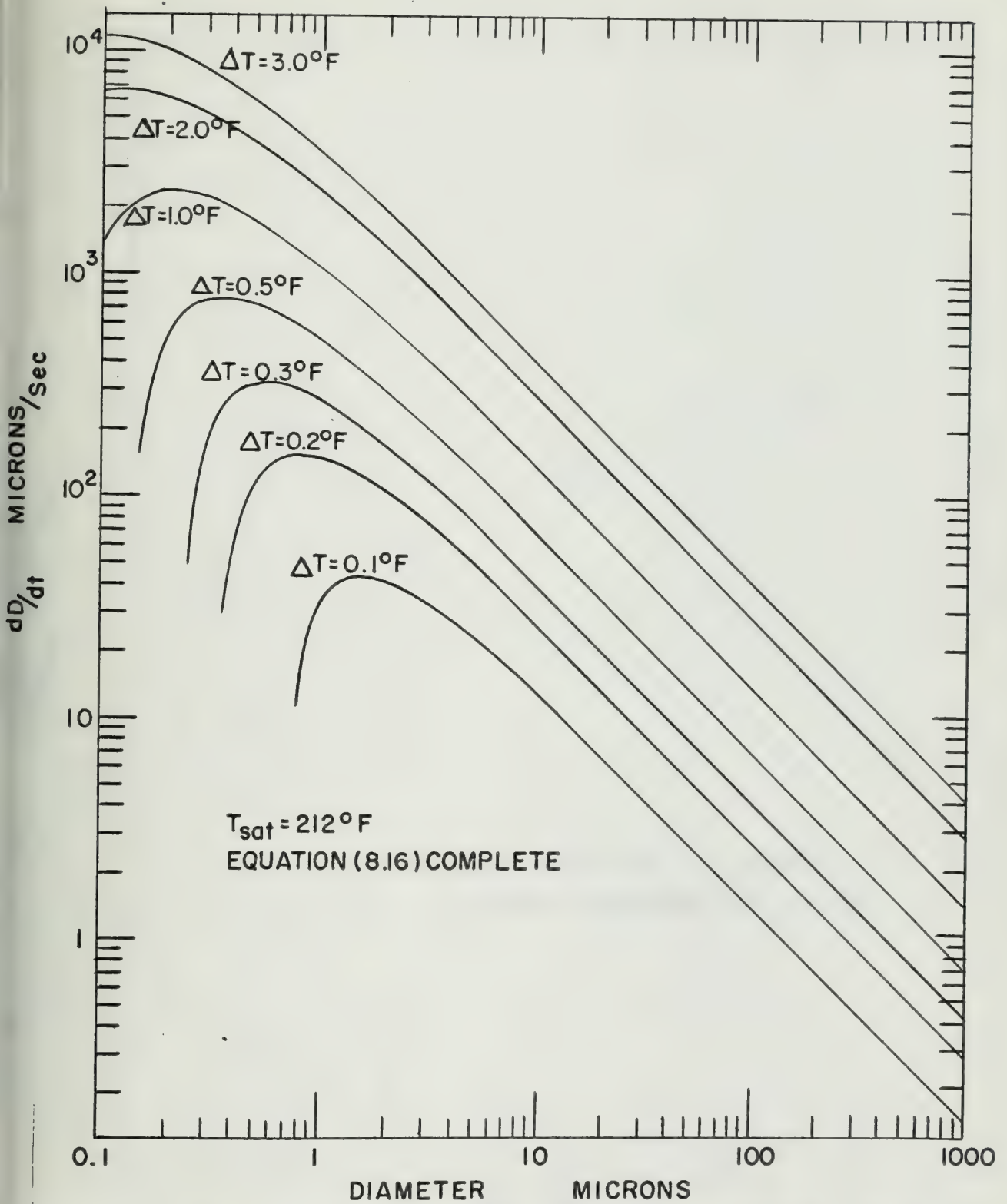


FIG 49 DROP GROWTH RATE DISTRIBUTIONS FOR ATMOSPHERIC PRESSURE CONDENSATION (varying ΔT)

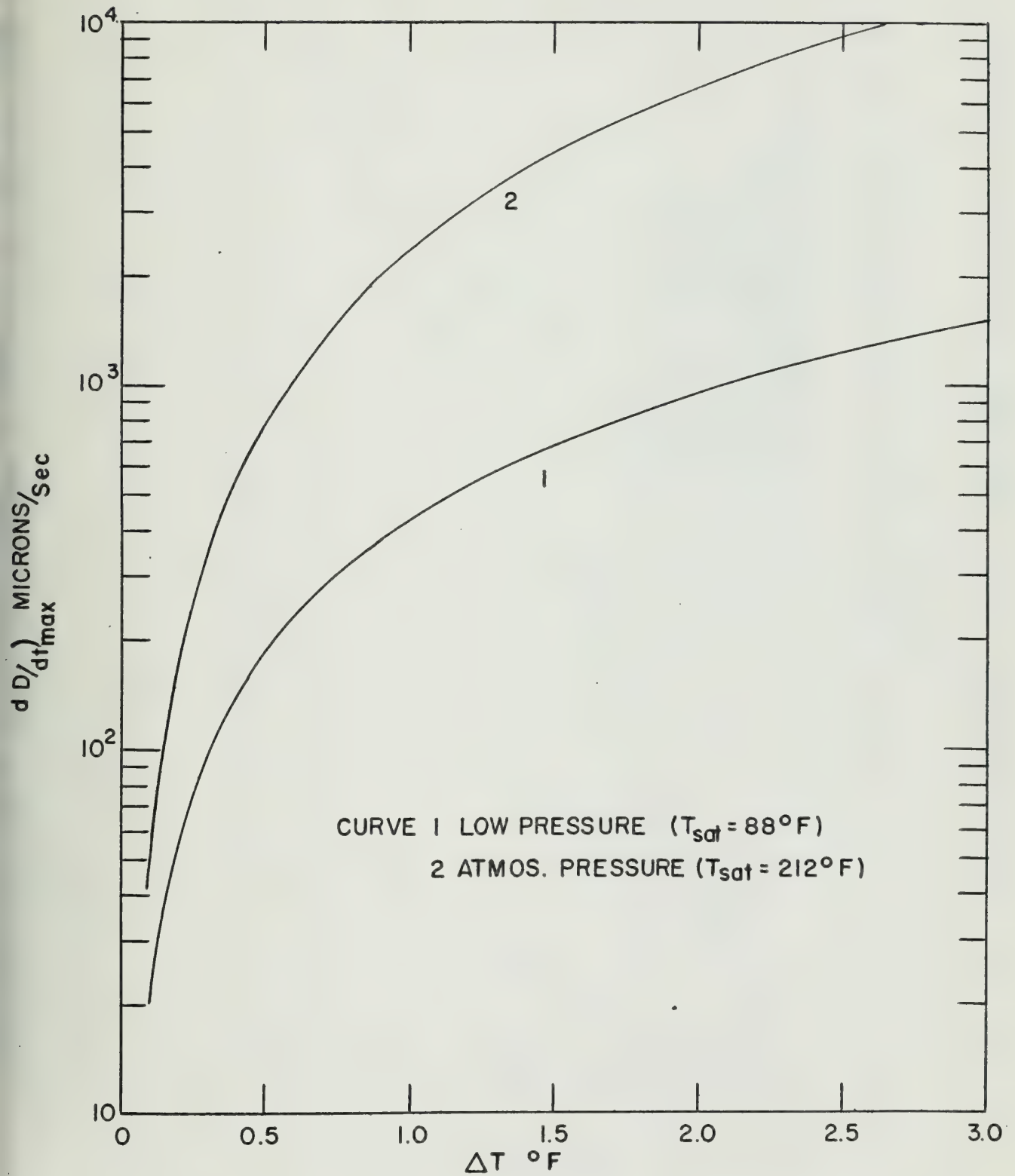


FIG 50 EFFECT OF ΔT ON MAXIMUM DROP GROWTH RATE

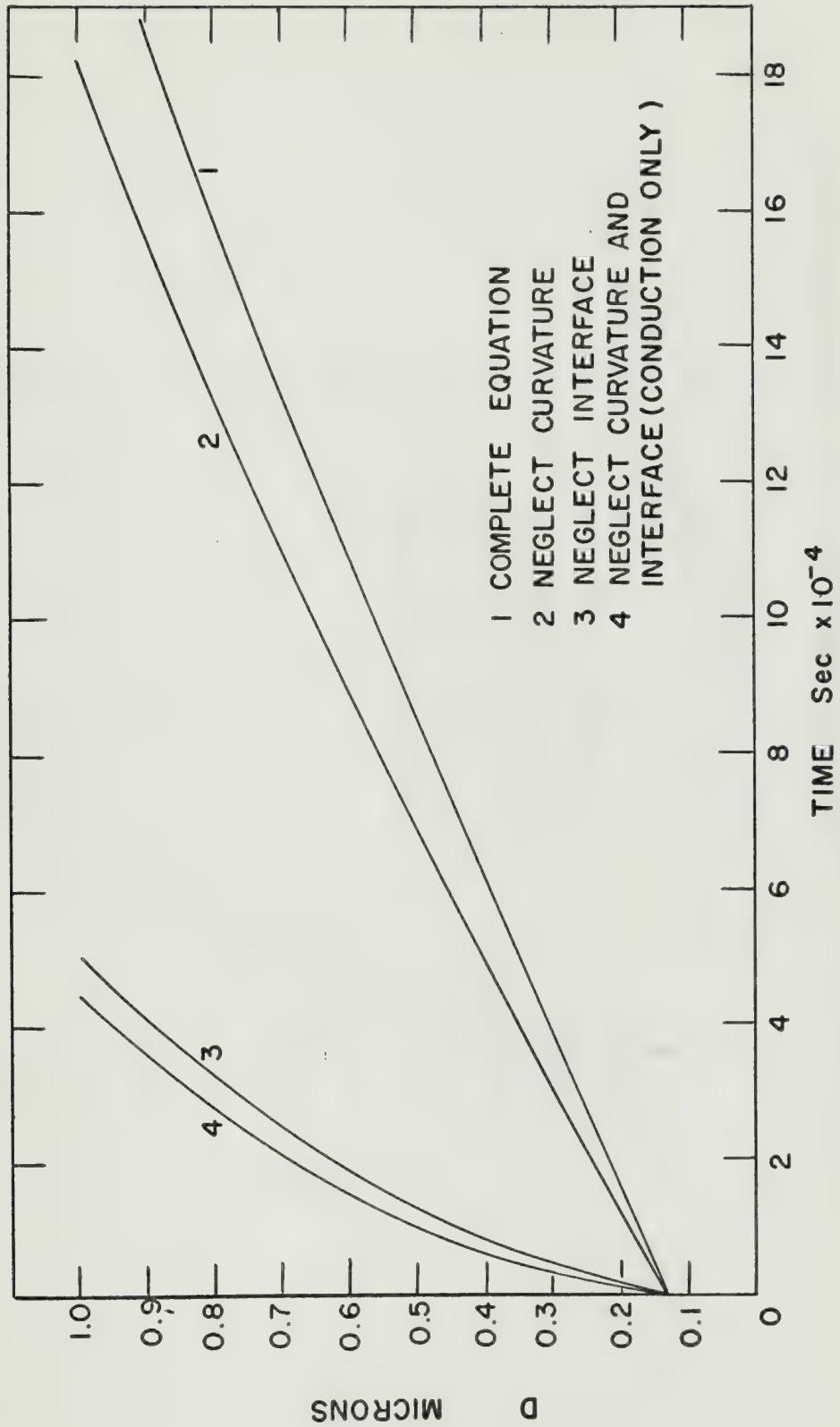


FIG 51 DROP GROWTH RATE FOR LOW PRESSURE CONDENSATION

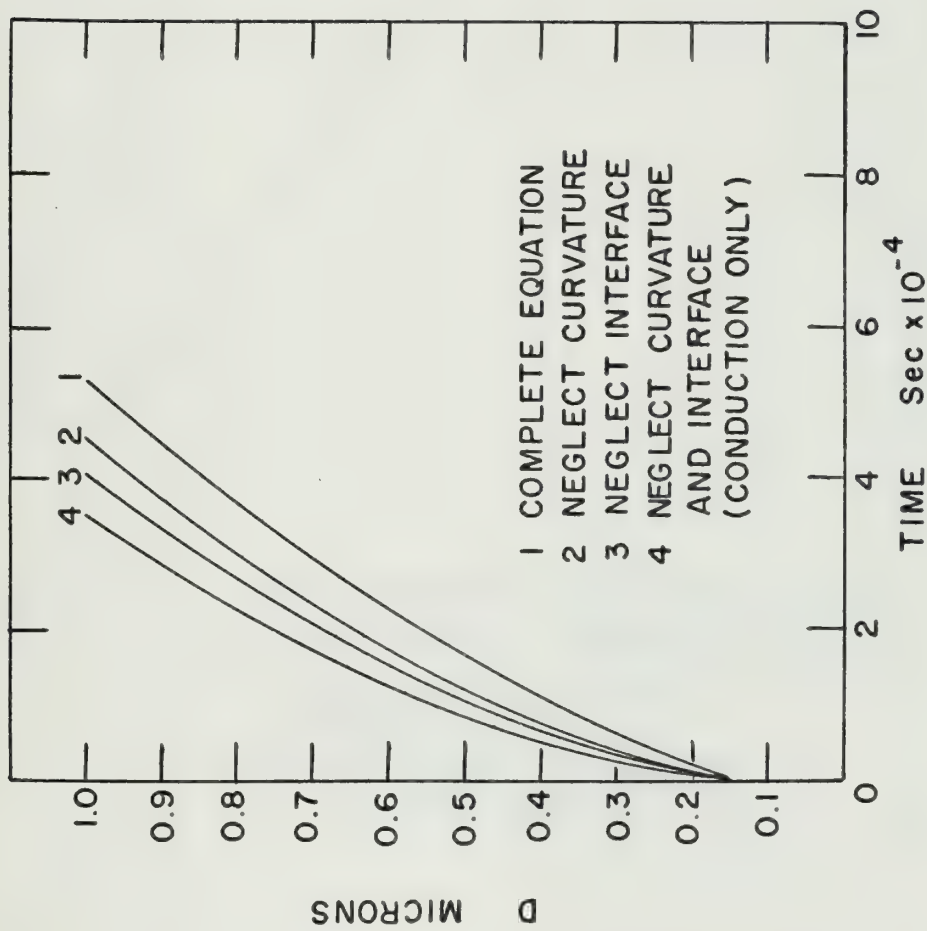


FIG 52 DROP GROWTH RATE FOR ATMOSPHERIC
PRESSURE CONDENSATION

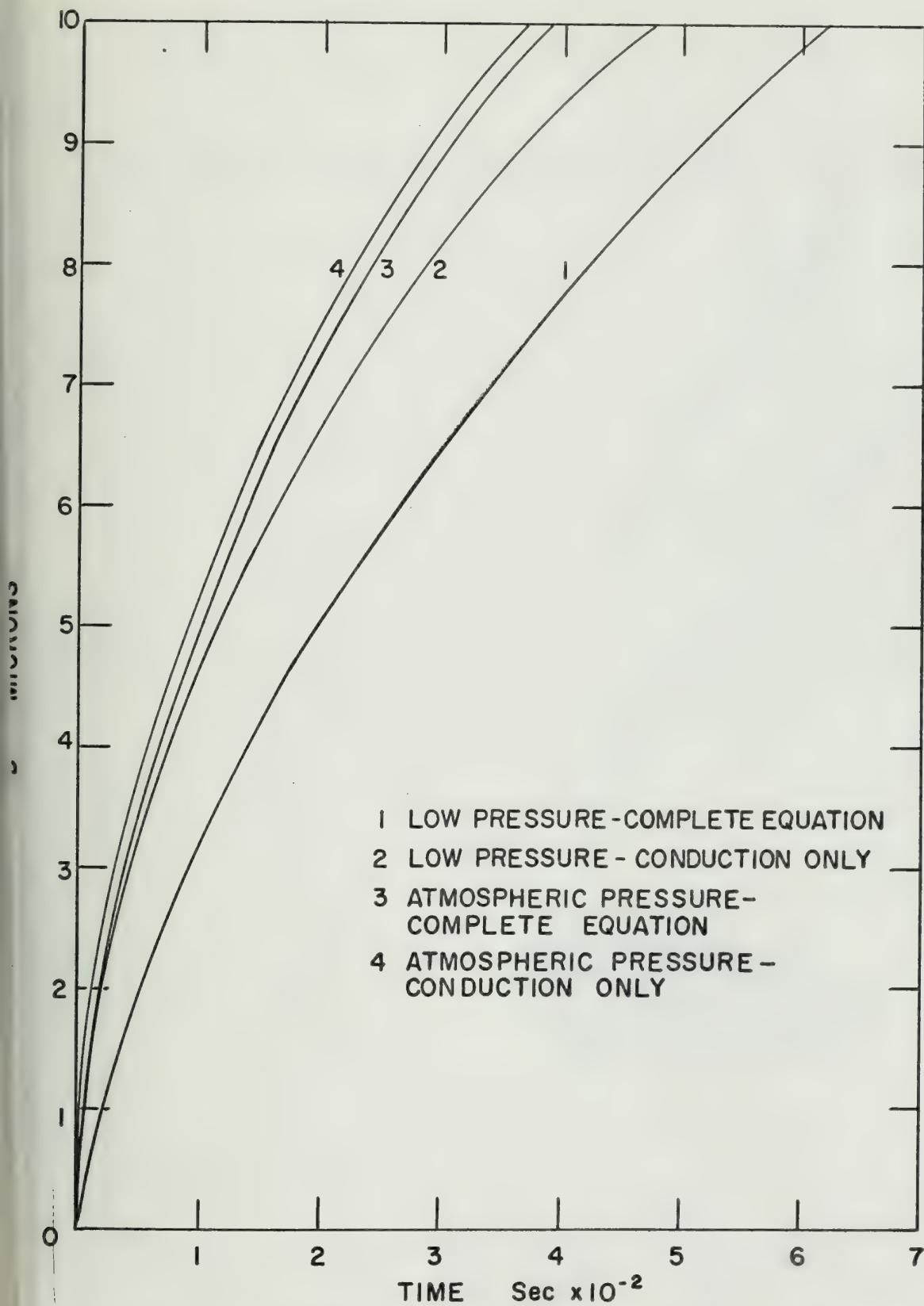


FIG 53 DROP GROWTH RATE FOR LOW AND ATMOSPHERIC PRESSURE CONDENSATION

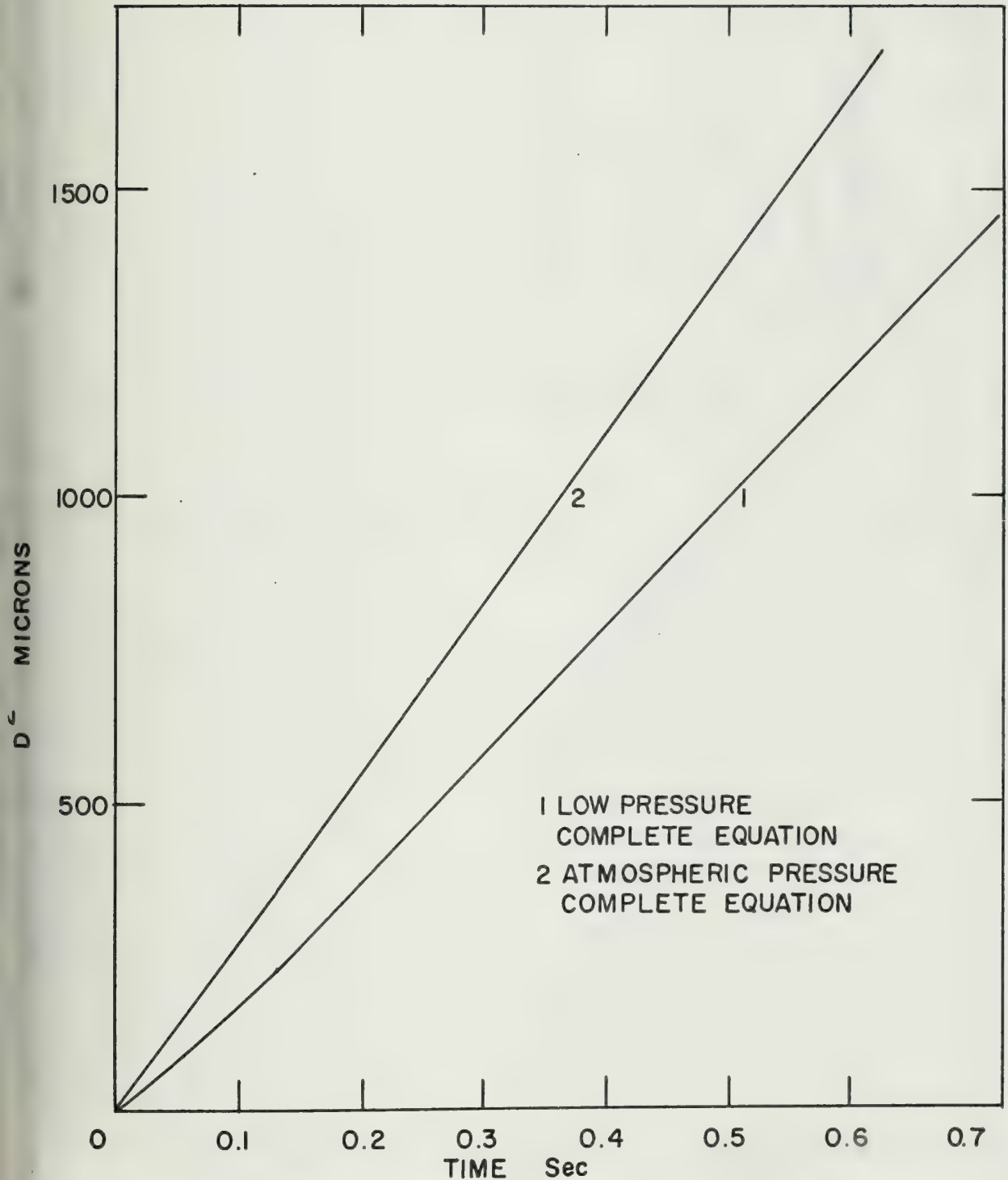


FIG 54 DROP GROWTH RATE FOR LOW AND ATMOSPHERIC CONDENSATION

FRACTION OF MEASURED HEAT FLUX TRANSFERRED THRU
DROPS GREATER THAN DIAMETER, D

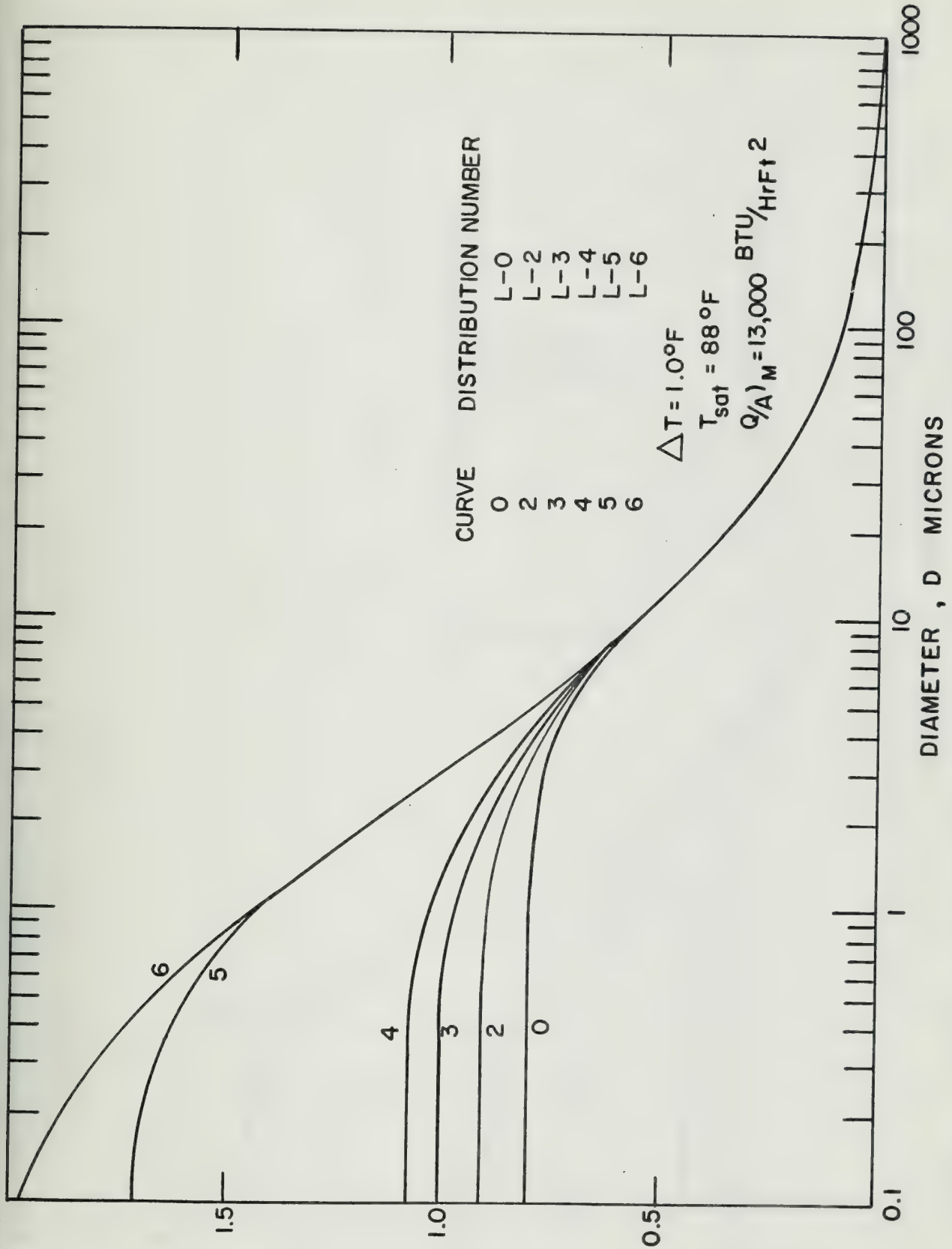


FIG 55 INTEGRATED HEAT FLUX DISTRIBUTION FOR LOW
PRESSURE CONDENSATION

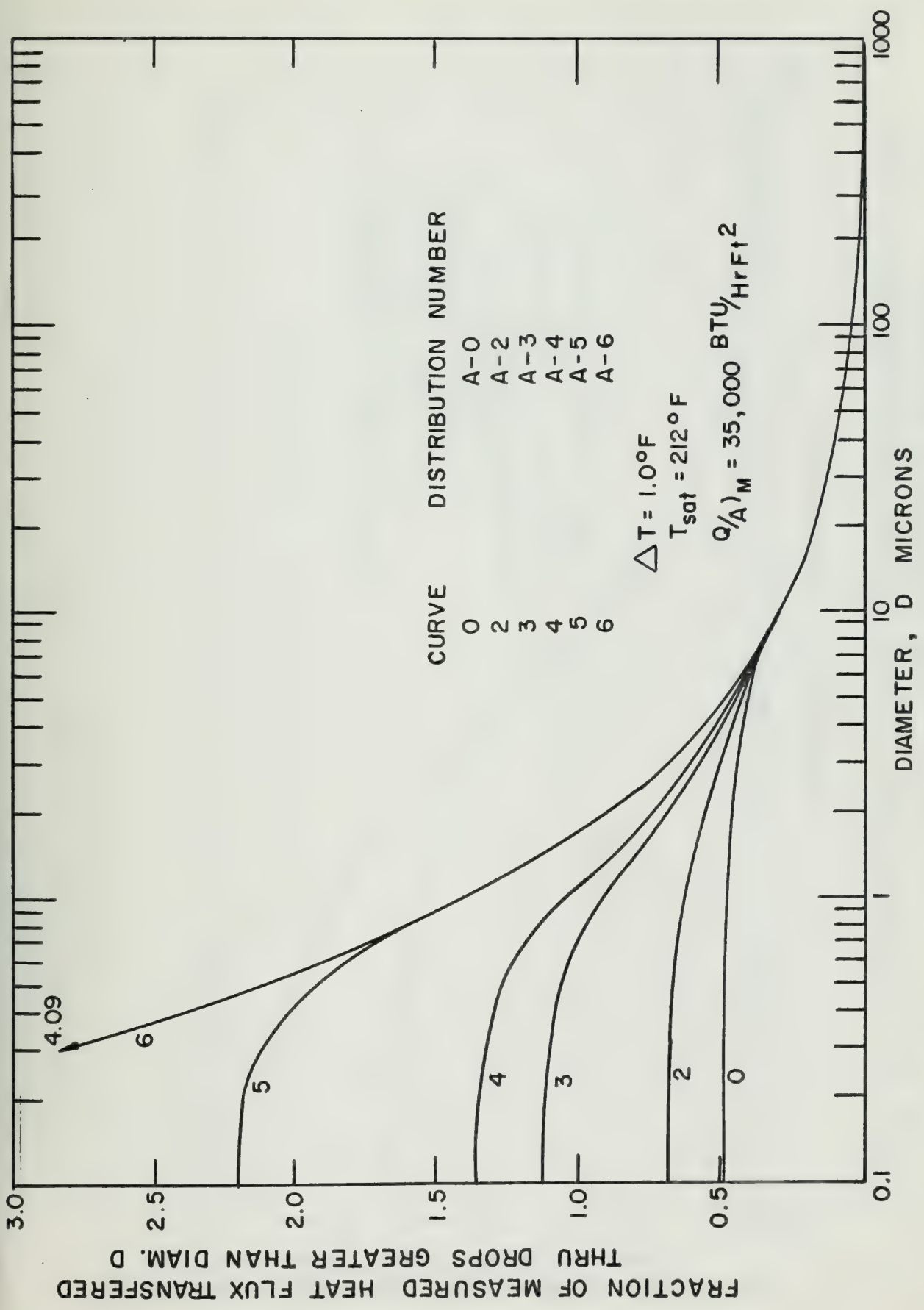


FIG 56 INTEGRATED HEAT FLUX DISTRIBUTION FOR
ATMOSPHERIC PRESSURE CONDENSATION

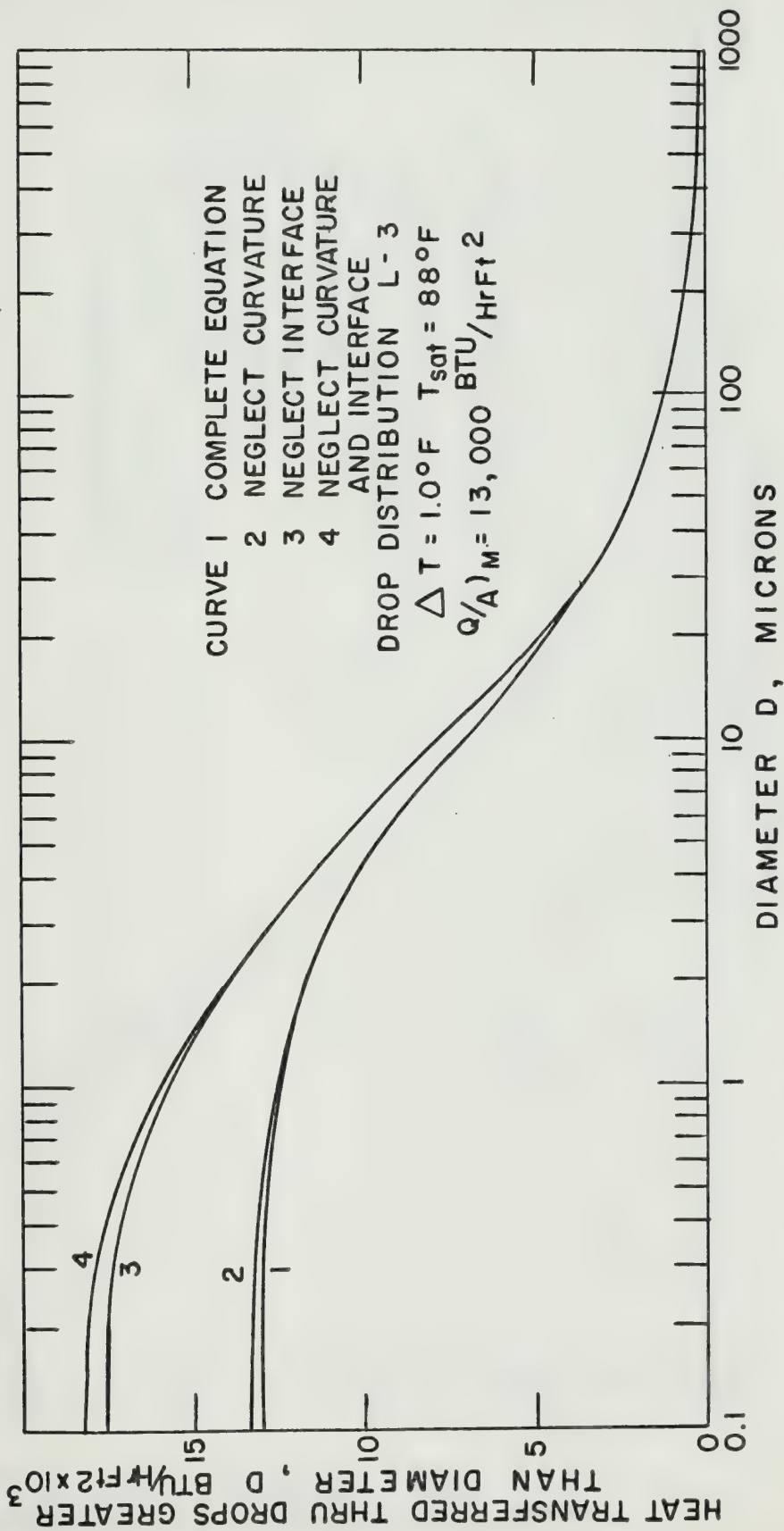


FIG 57 INTEGRATED HEAT FLUX DISTRIBUTION FOR LOW PRESSURE CONDENSATION

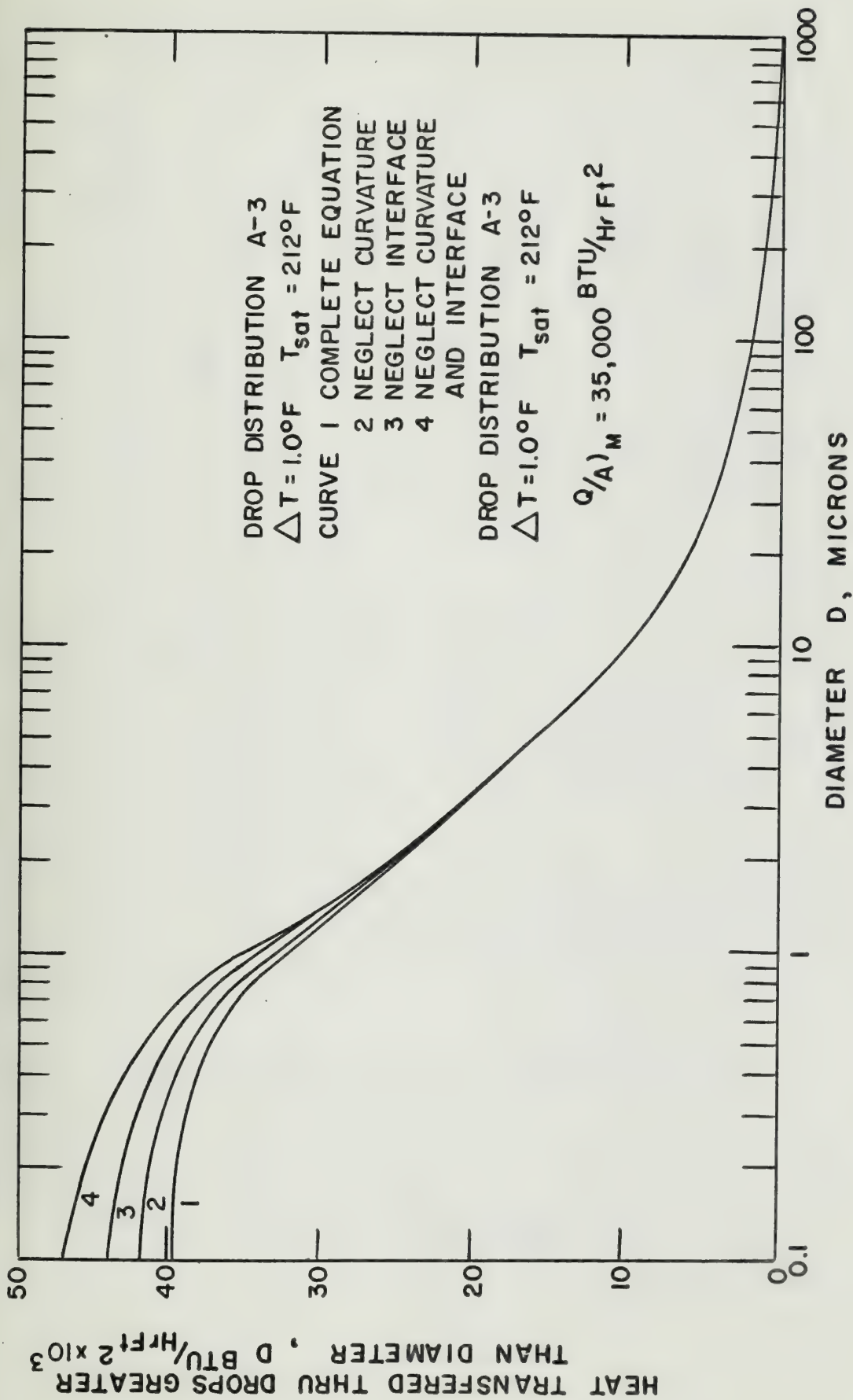


FIG 58 INTEGRATED HEAT FLUX DISTRIBUTIONS FOR
ATMOSPHERIC CONDENSATION

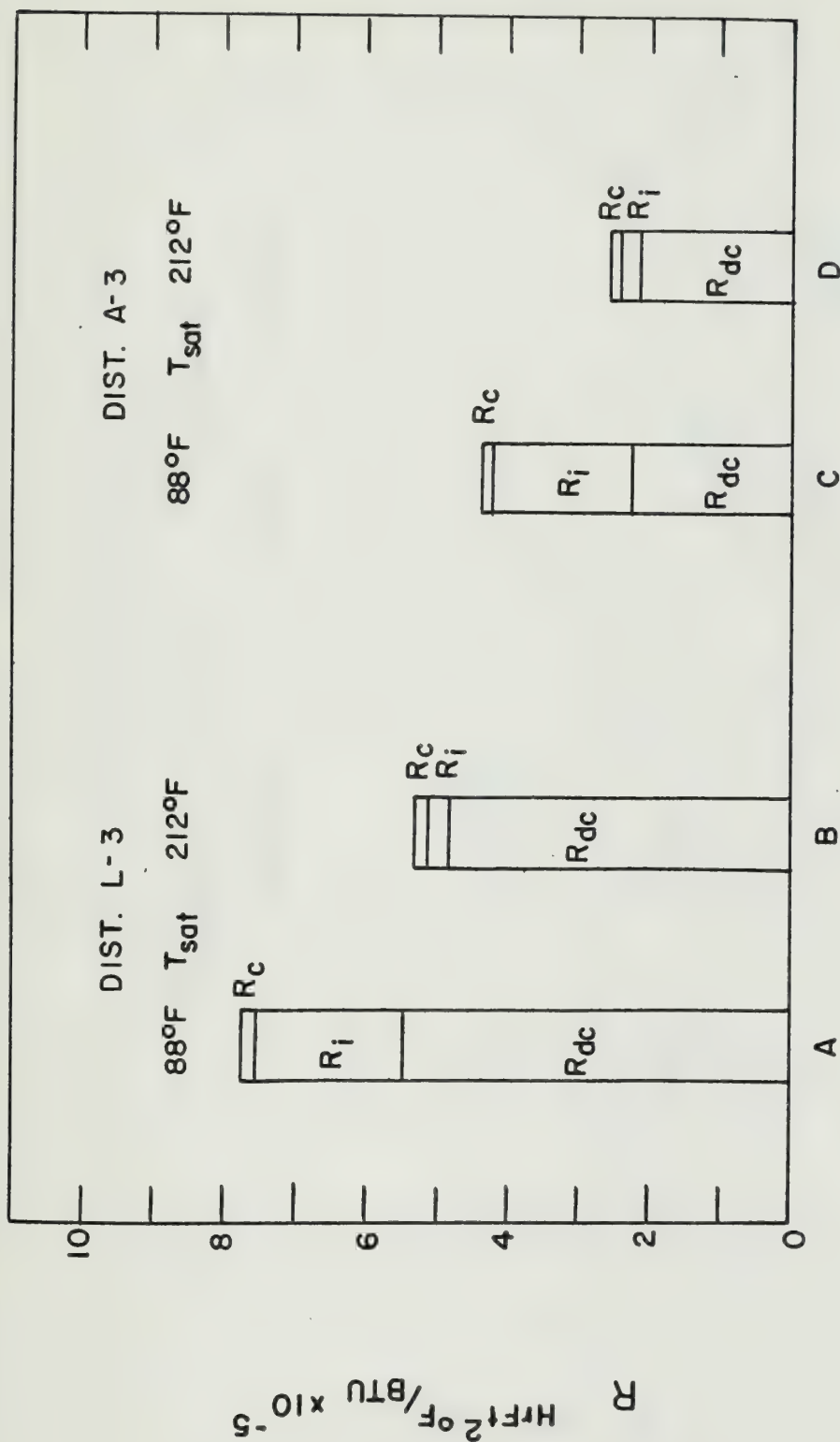


FIG 59 RELATIVE MAGNITUDE OF RESISTANCES

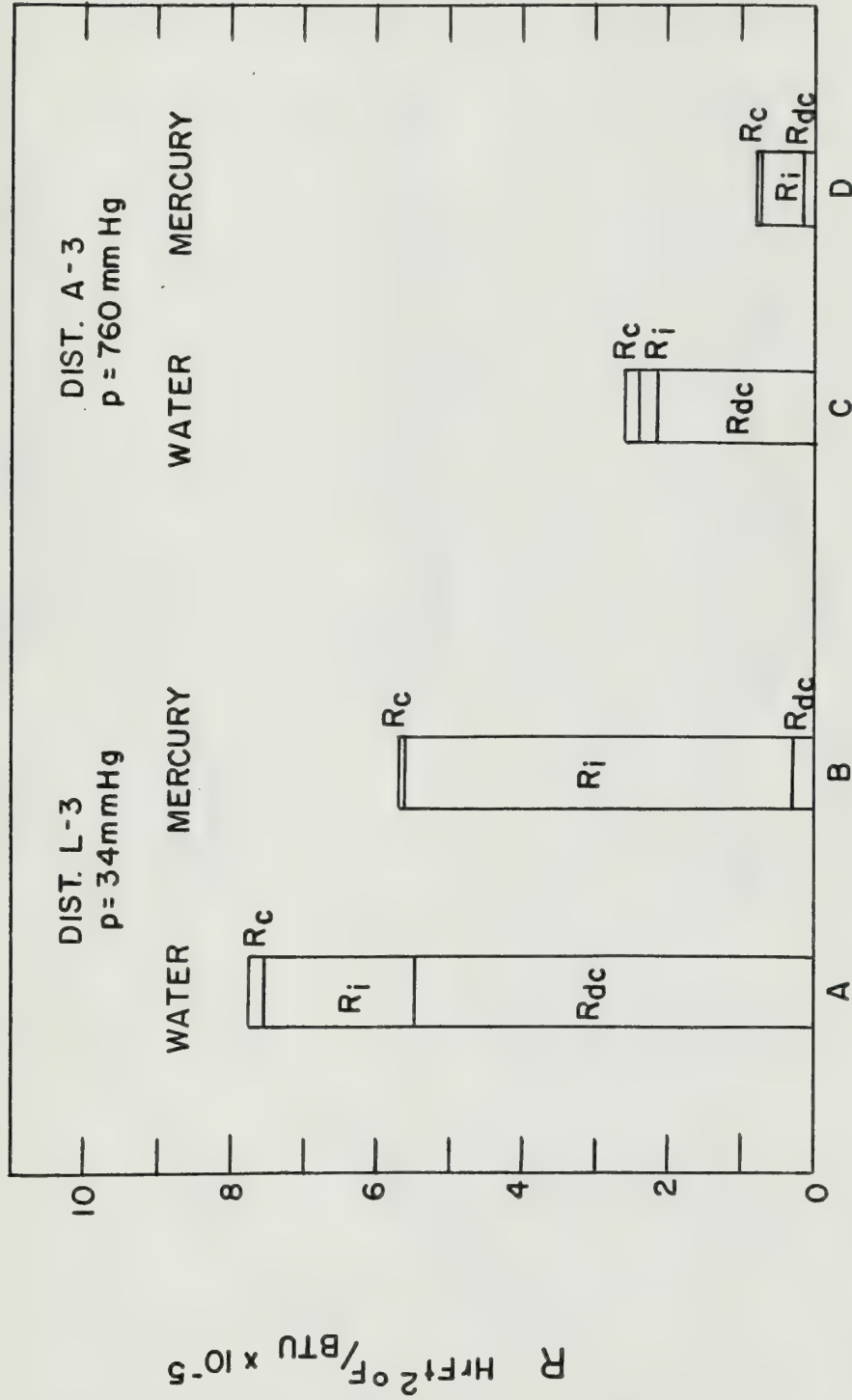


FIG 60 RELATIVE MAGNITUDE OF RESISTANCES FOR WATER AND MERCURY

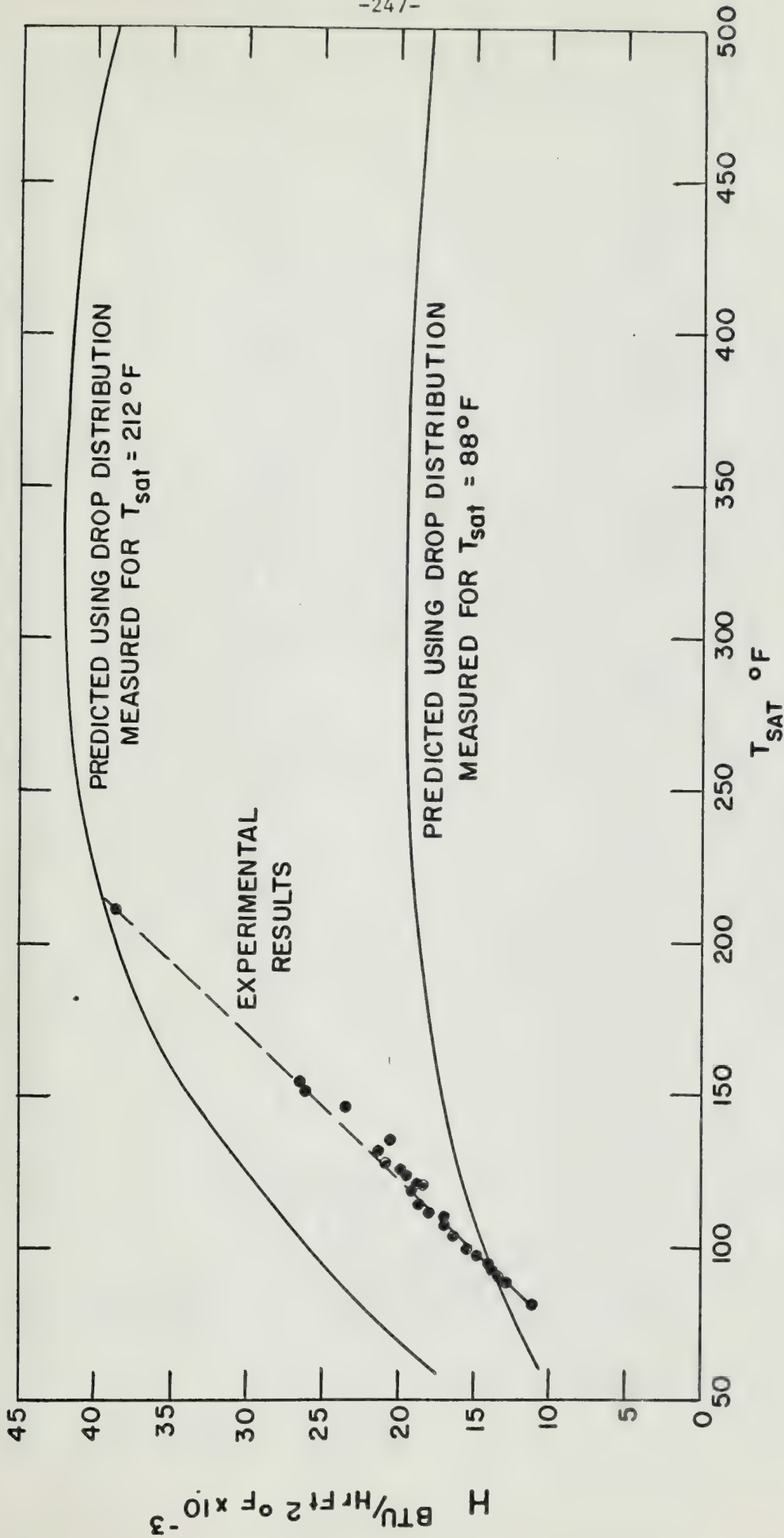


FIG 6I H vs PRESSURE FOR MIRROR SMOOTH SURFACE
PREDICTED vs MEASURED RESULTS

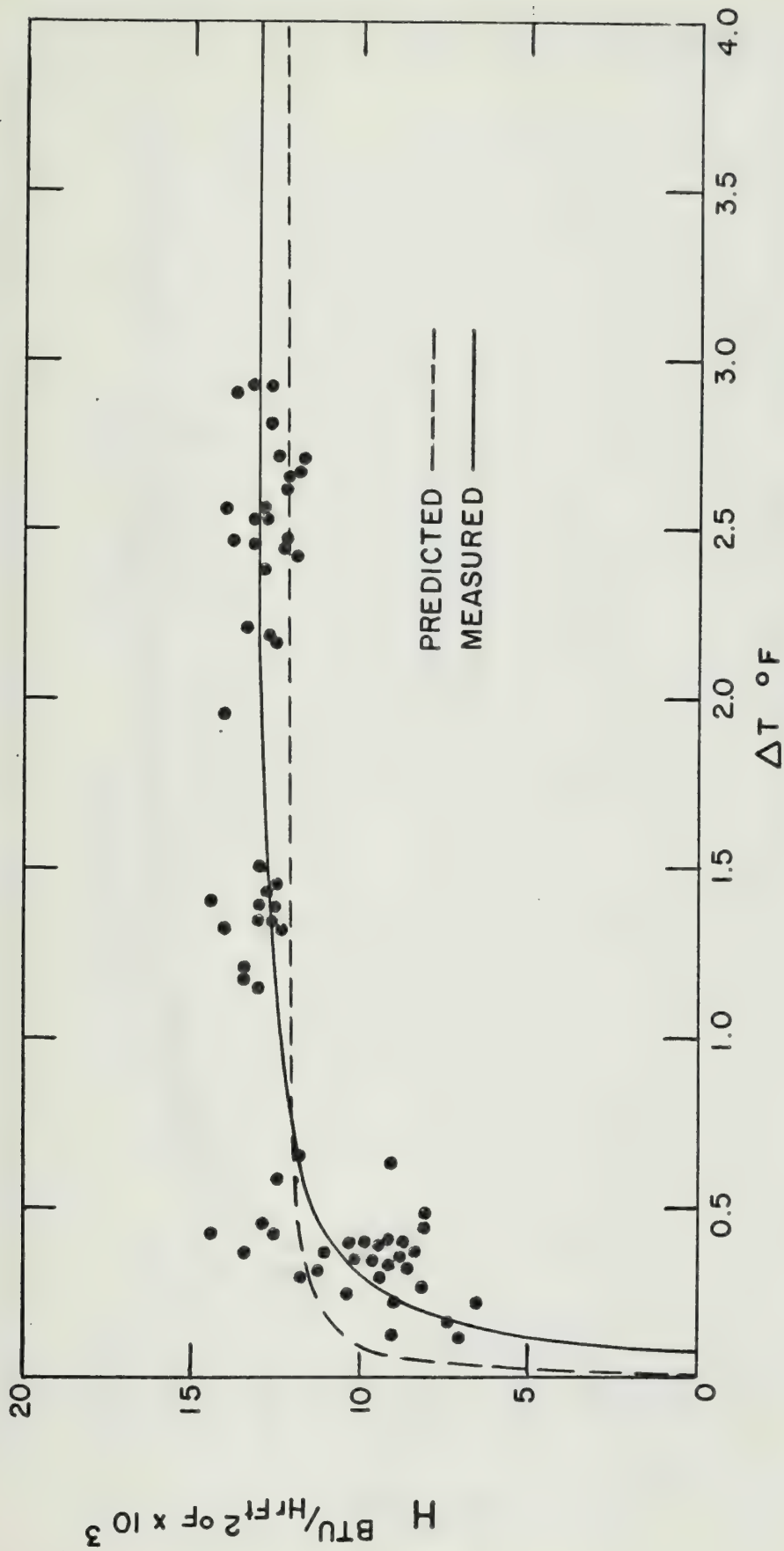


FIG 62 H vs ΔT FOR LOW PRESSURE CONDENSATION, MIRROR SMOOTH SURFACE, PREDICTED vs MEASURED

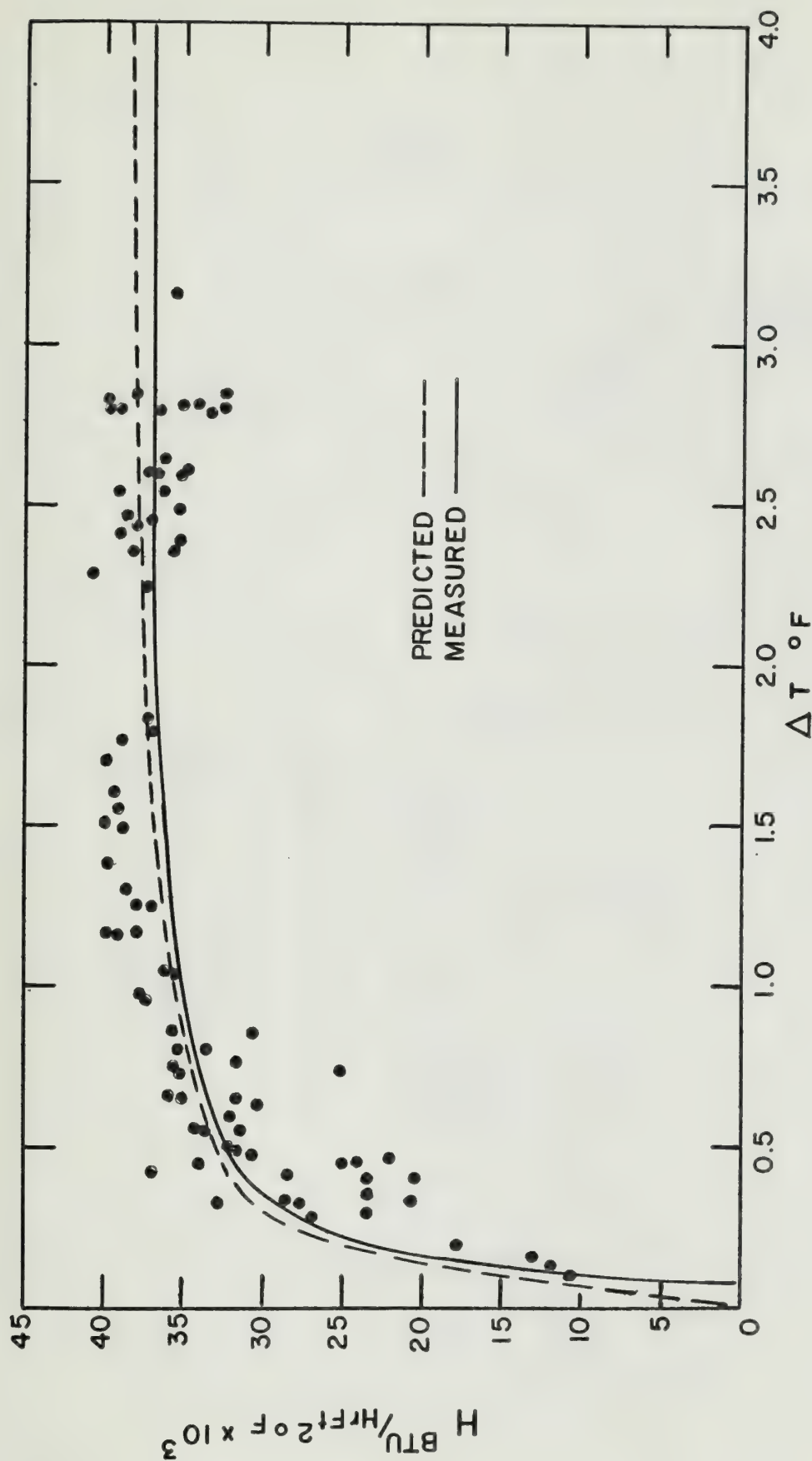
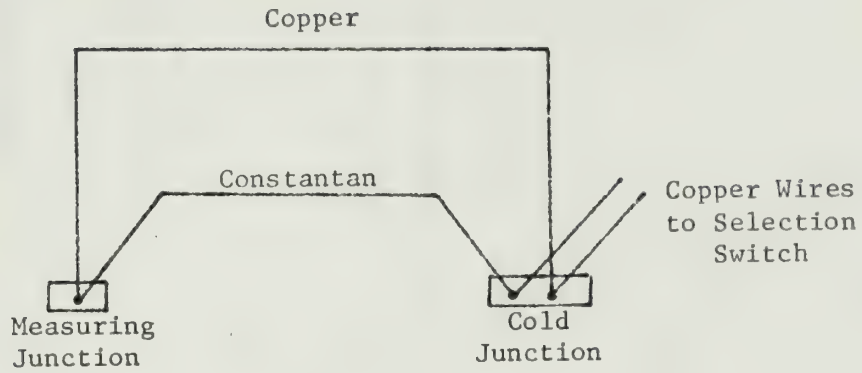
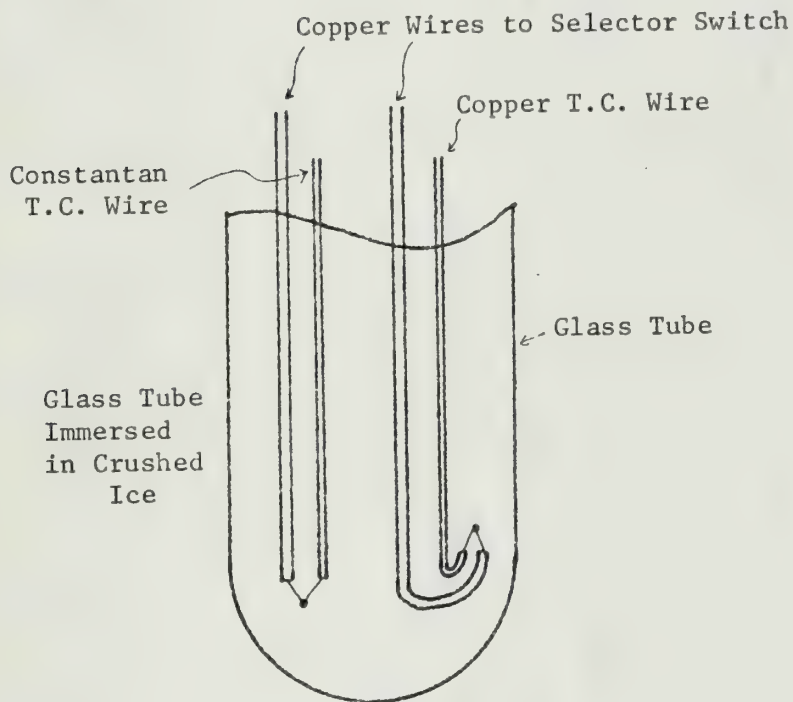


FIG 63 H vs ΔT FOR ATMOSPHERIC PRESSURE CONDENSATION
MIRROR SMOOTH SURFACE, PREDICTED vs MEASURED



a) Thermocouple Circuit



b) Cold Junction Arrangement

Fig. A-1 Thermocouple Set-Up

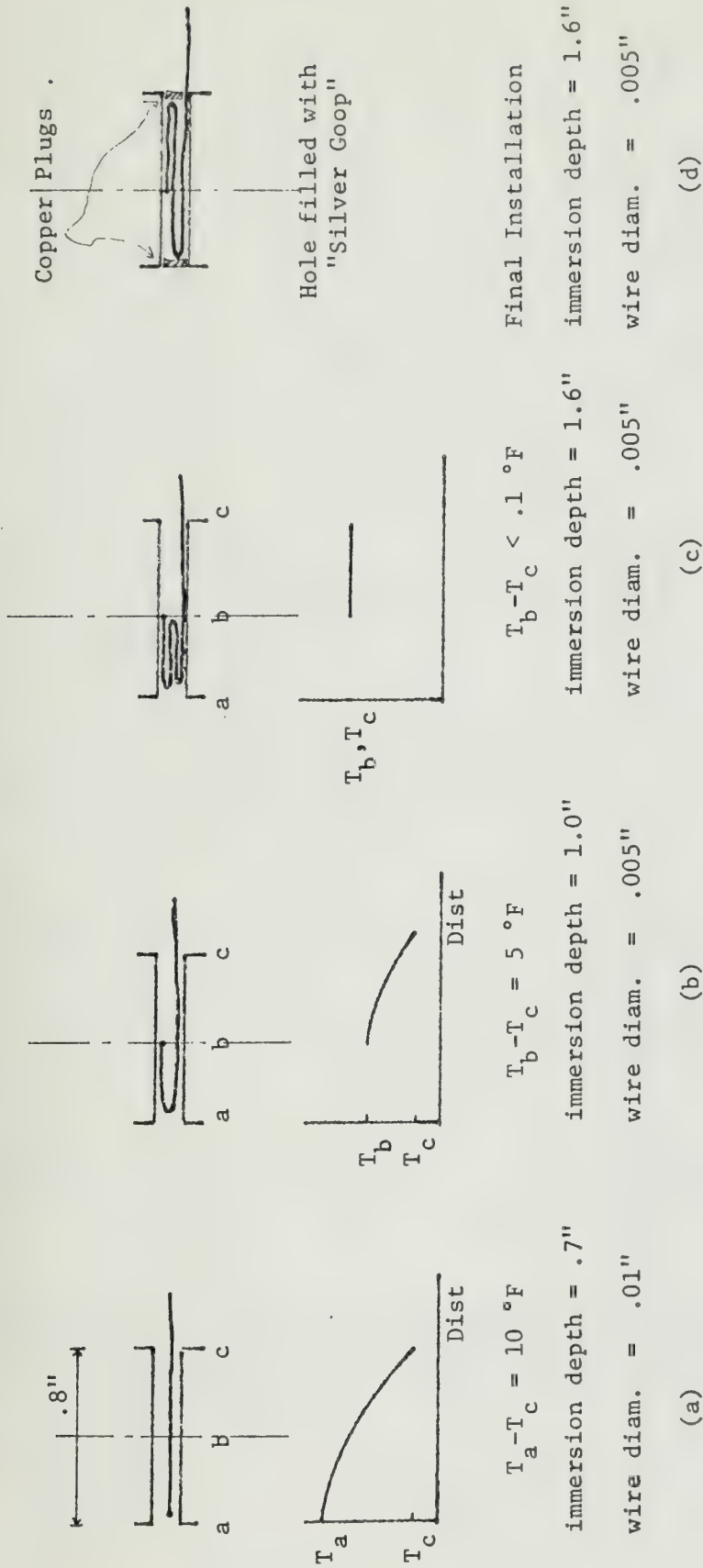


Fig. A-2 Details of Thermocouple Installation.

Hole Diameter is .034"

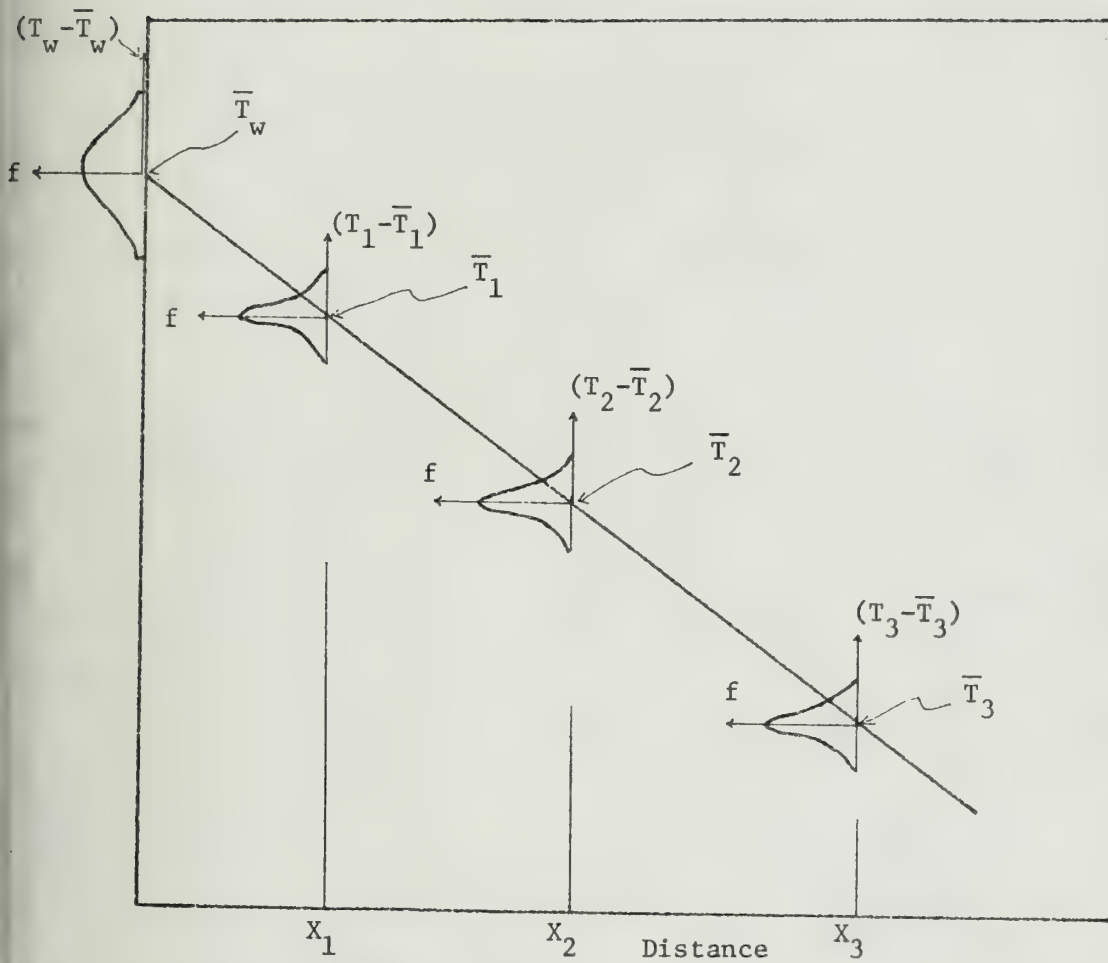


Fig. A-3 Schematic Representation of Temperature Distributions in Holes and at Wall. Reproduced from Wilcox [76].

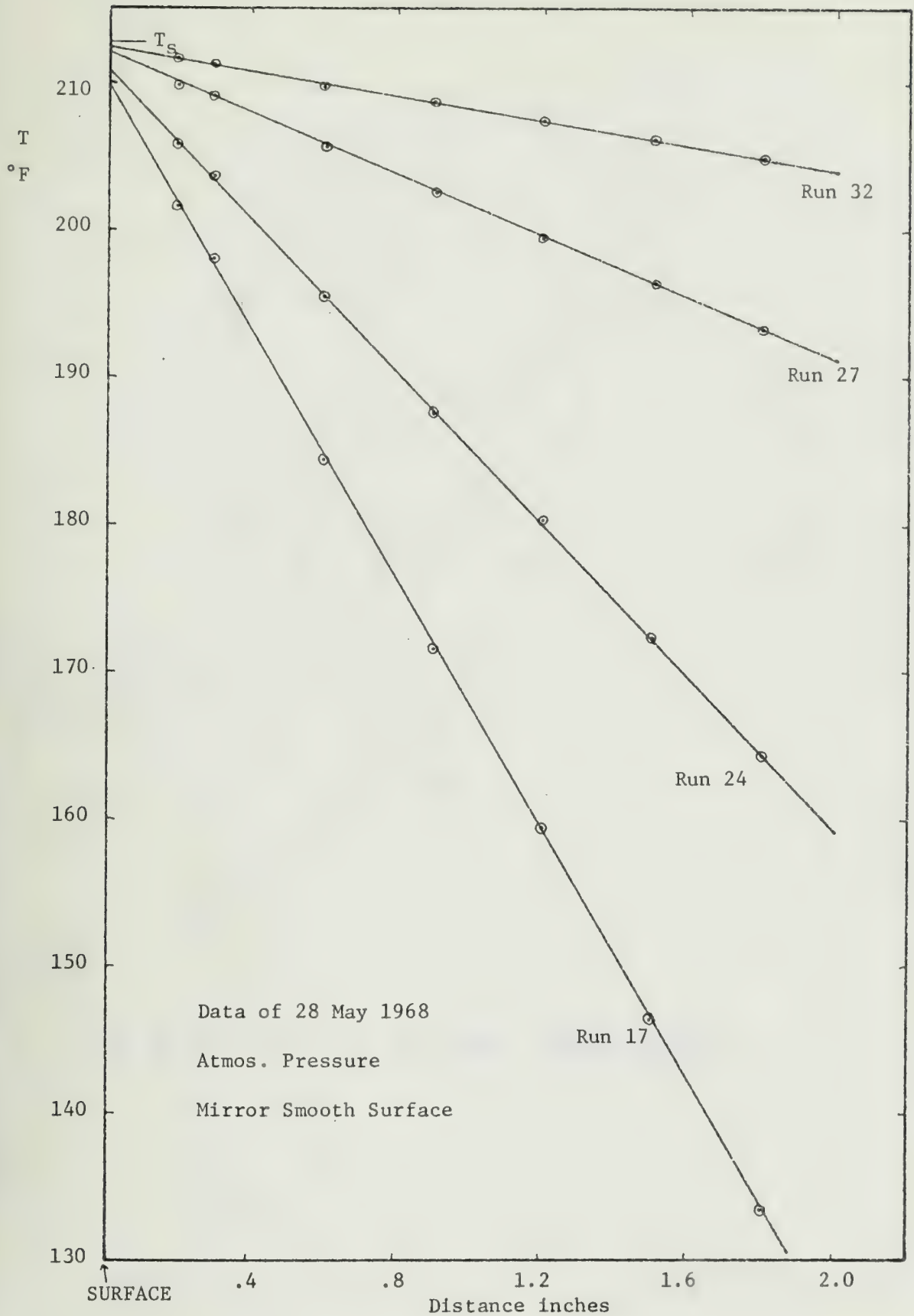


Fig. A-4 Typical Temperature Distributions in Test Section

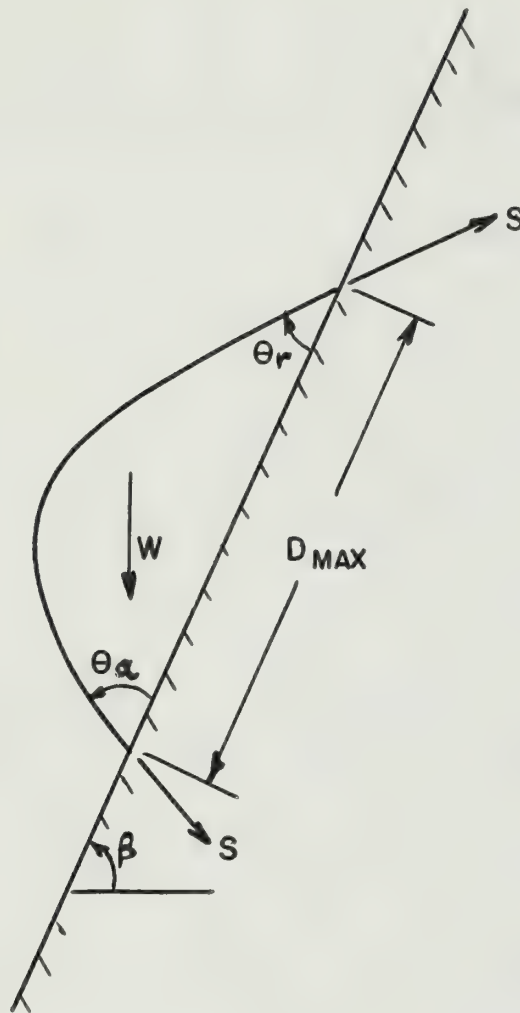


FIG B-I FORCES ACTING ON A DROPLET

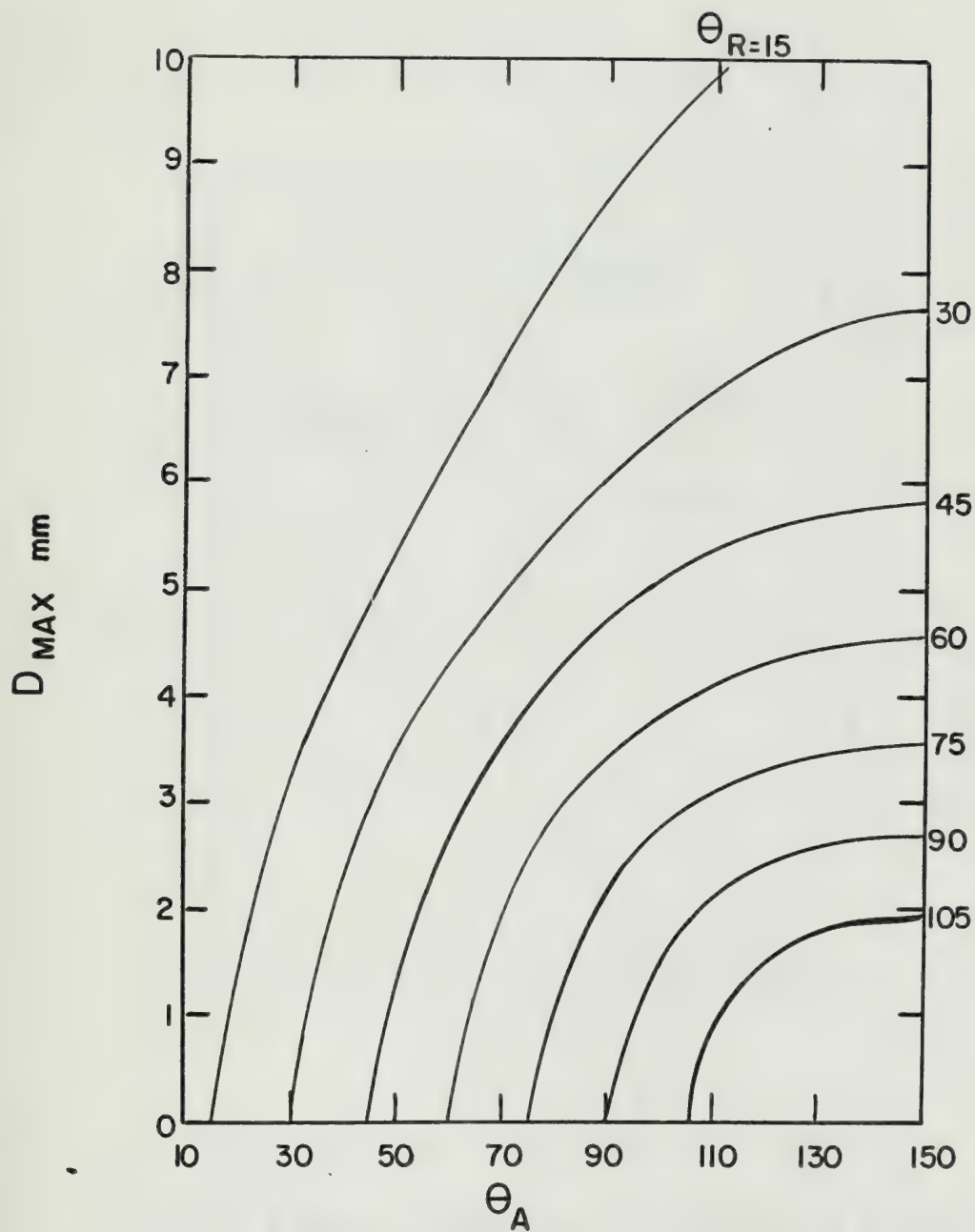


FIG B-2 PREDICTION OF MAXIMUM DROP SIZE
REPRODUCED FROM FATICA AND KATZ [5]

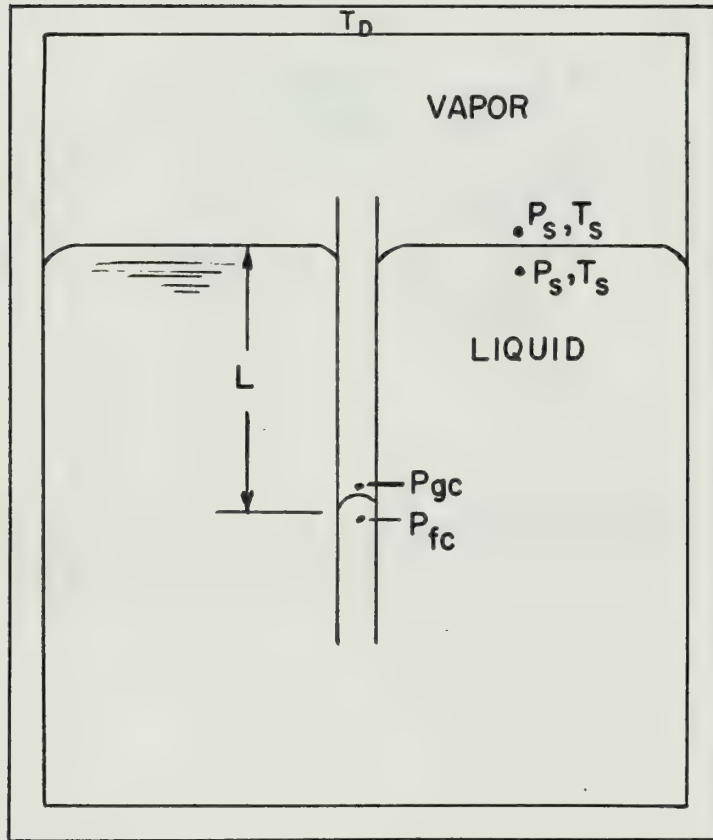


FIG C-1 EQUILIBRIUM OF A VAPOR WITH
A CURVED LIQUID SURFACE

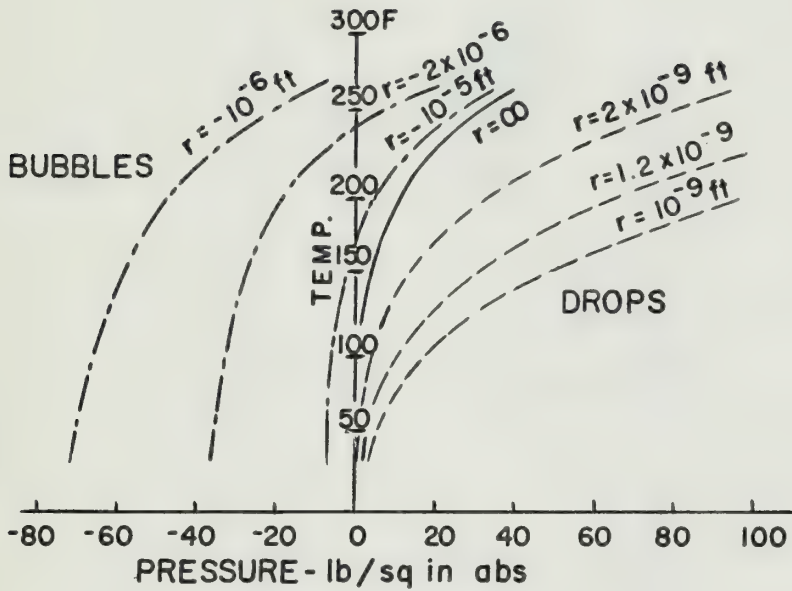


FIG C-2 EQUILIBRIUM BETWEEN LIQUID AND VAPOR AT A CURVED SURFACE
REPRODUCED FROM KEENAN []

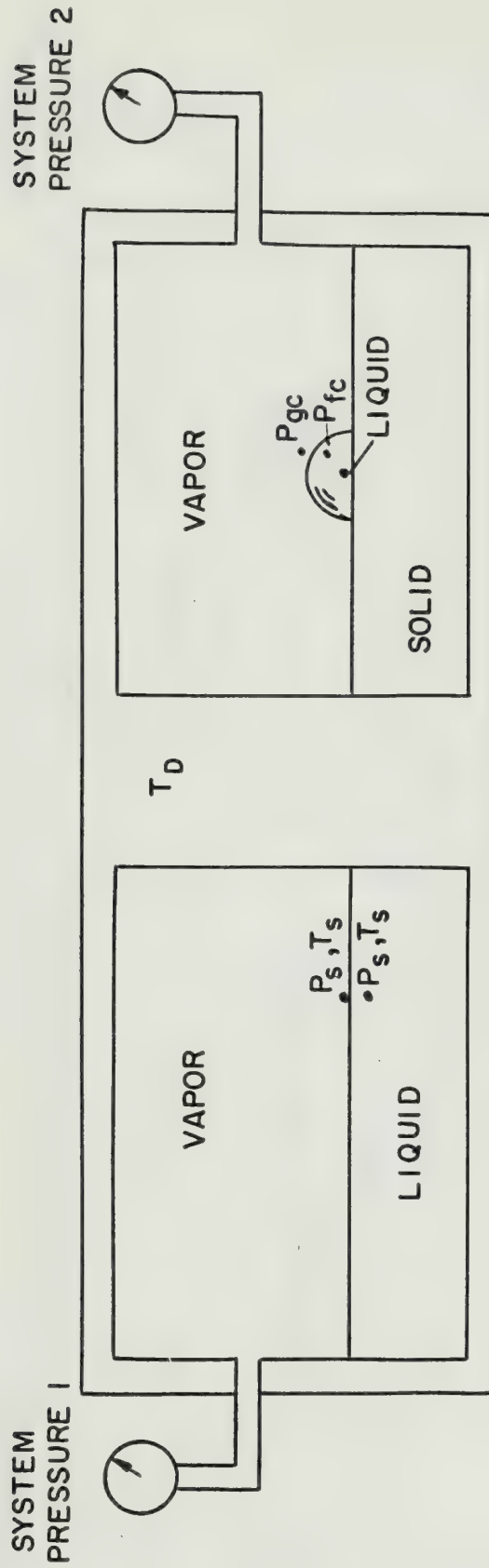


FIG C-3 EQUILIBRIUM OF A LIQUID DROP

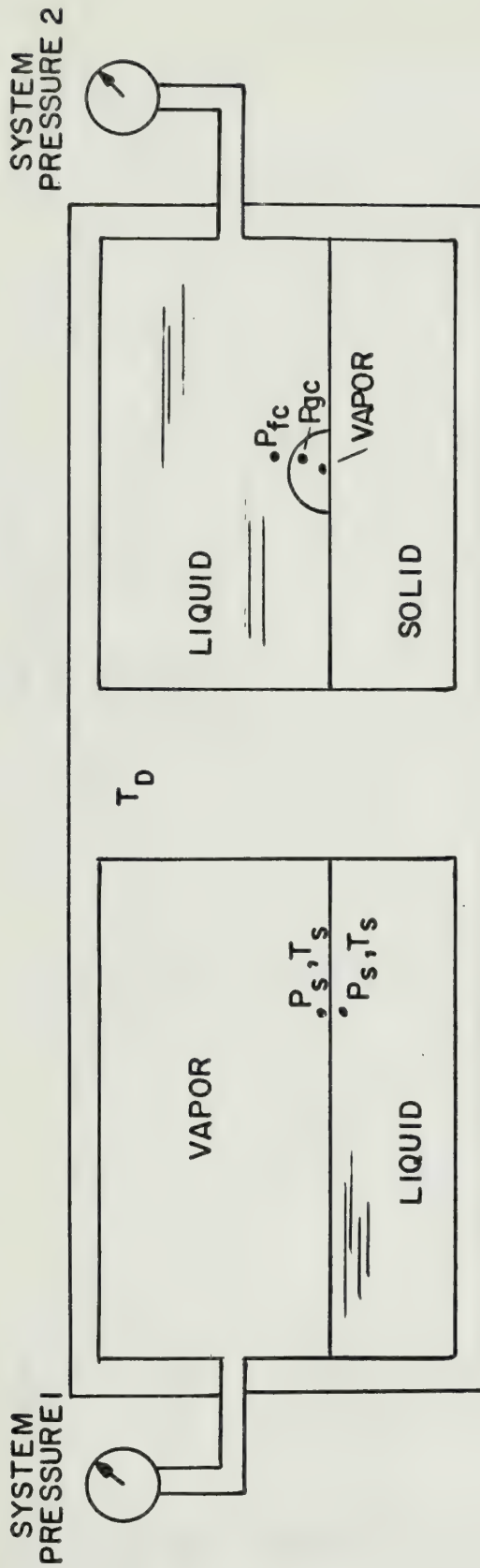


FIG C-4 EQUILIBRIUM OF A VAPOR BUBBLE

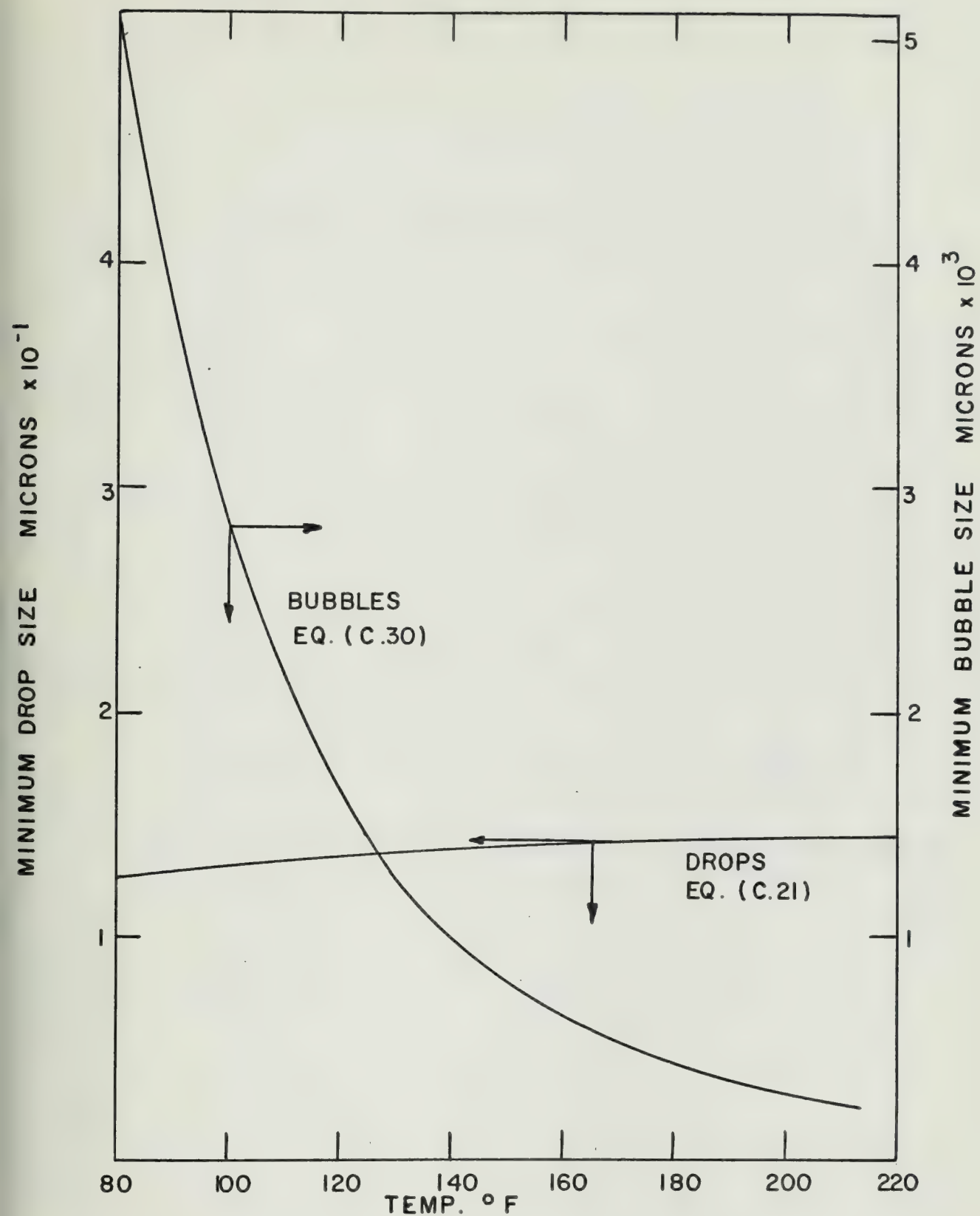


FIG C-5 EFFECT OF TEMPERATURE ON MINIMUM SIZE OF DROPS AND BUBBLES

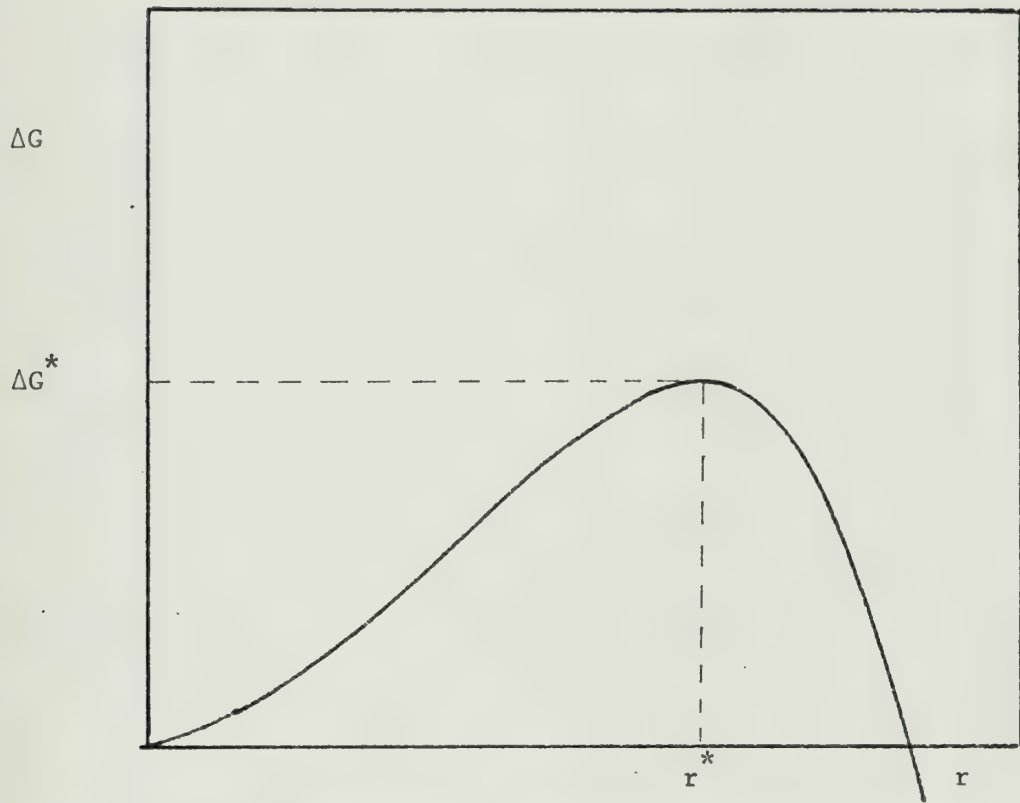


Fig. D-1 The Free Energy of Formation as a Function of Nucleus Size

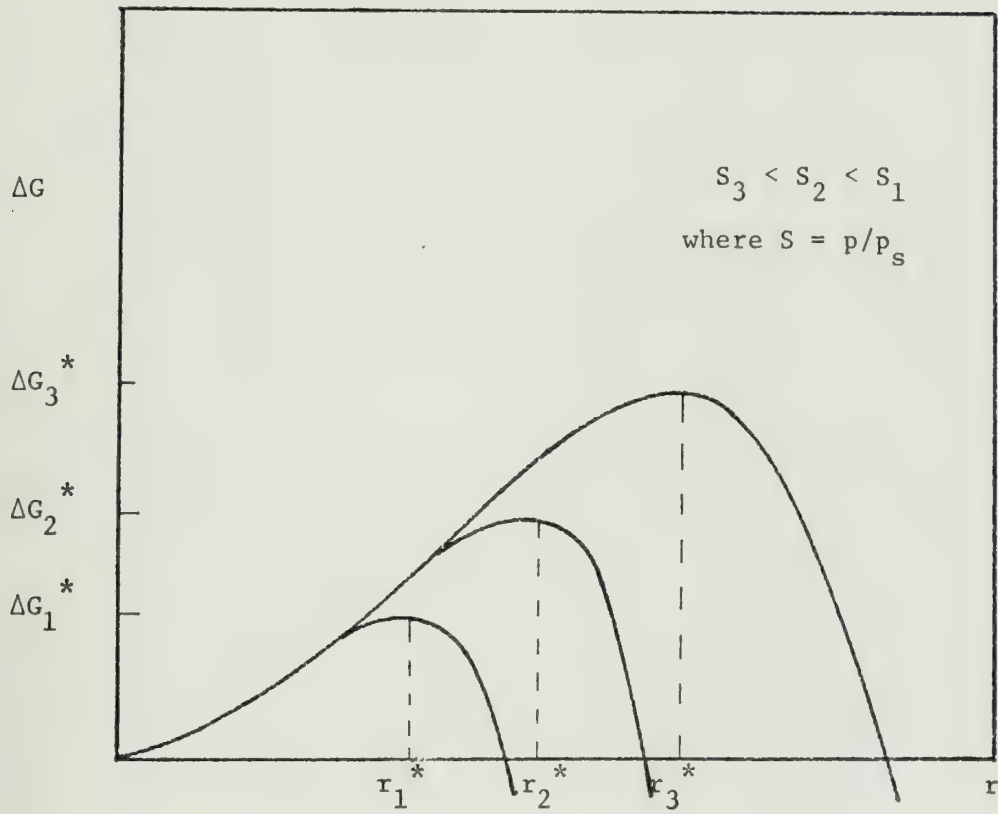


Fig. D-2 Effect of Degree of Supersaturation on the Critical Nucleus Size and Free Energy of Formation

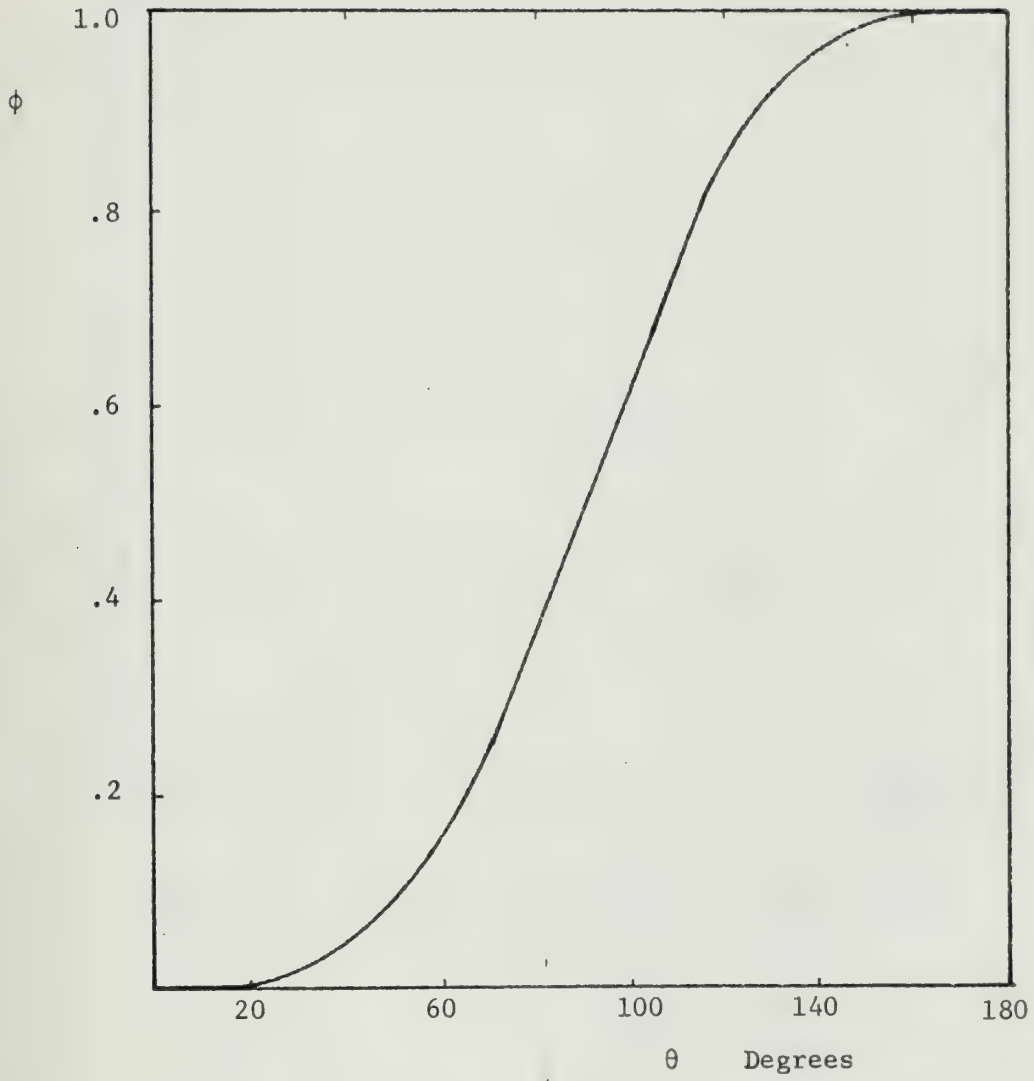


Fig. D-3 Contact Angle Function

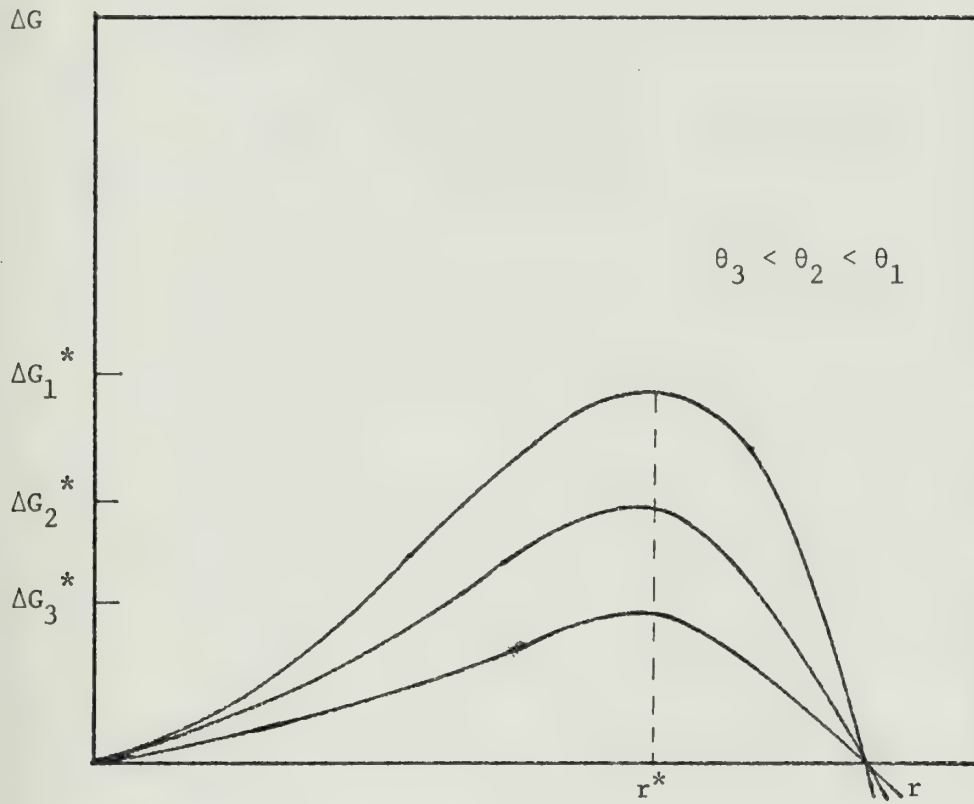


Fig. D-4 Effect of Contact Angle Variation on the Critical Free Energy of Formation

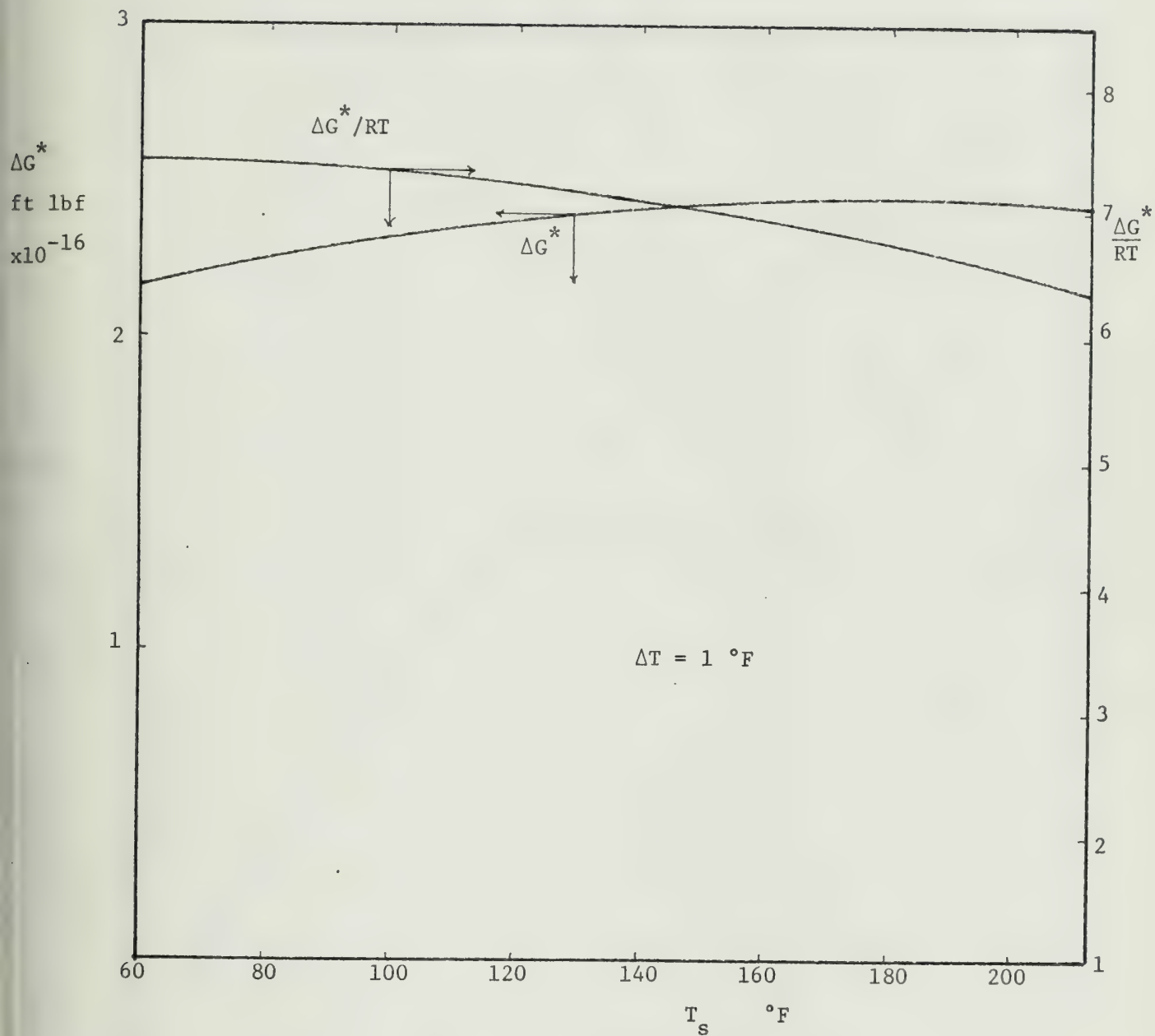


Fig. D-5 Variation in ΔG^* and $\Delta G^*/RT$ with Temperature

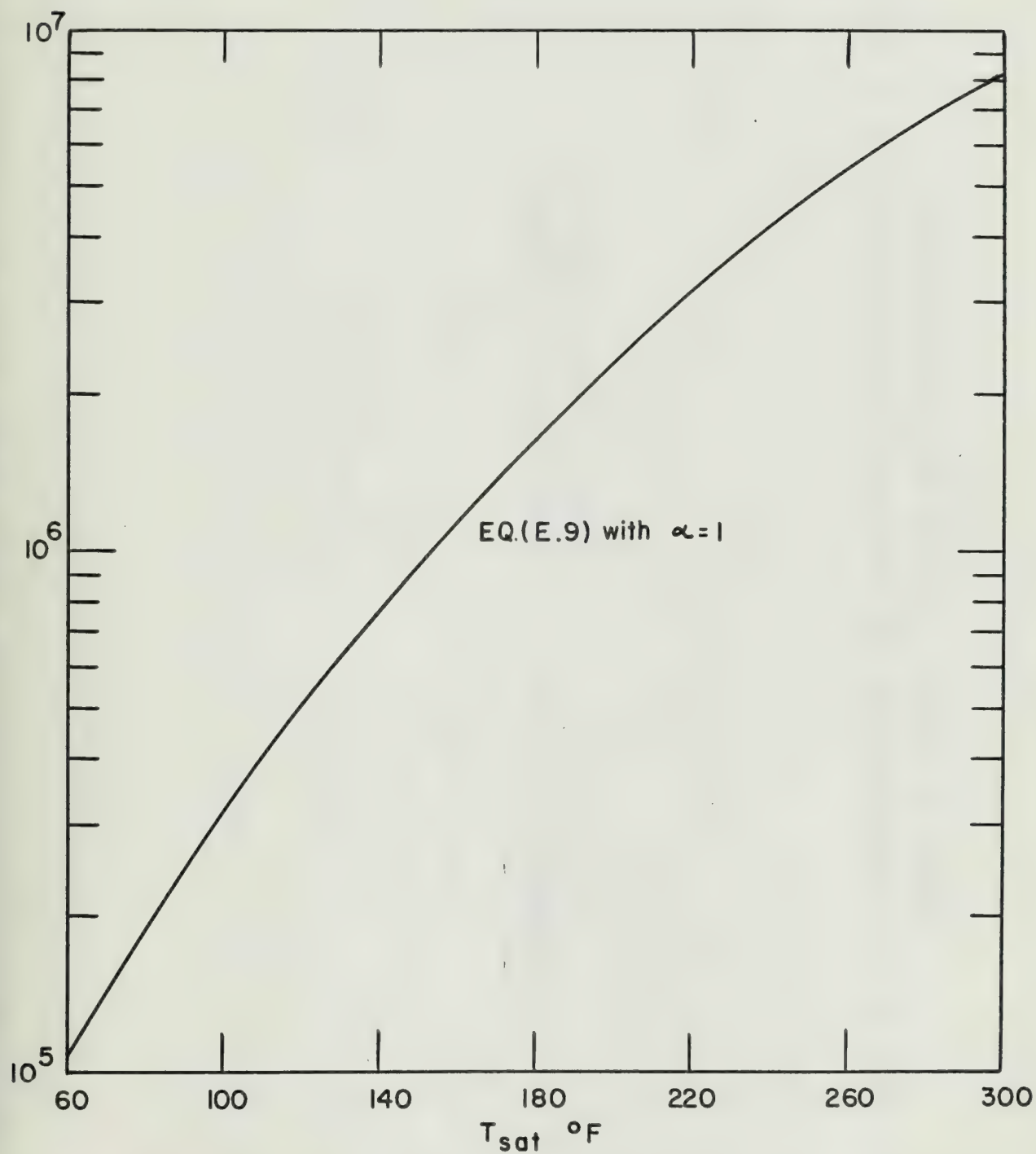


FIG E-1 VARIATION OF INTERFACIAL HEAT TRANSFER COEFFICIENT WITH TEMPERATURE

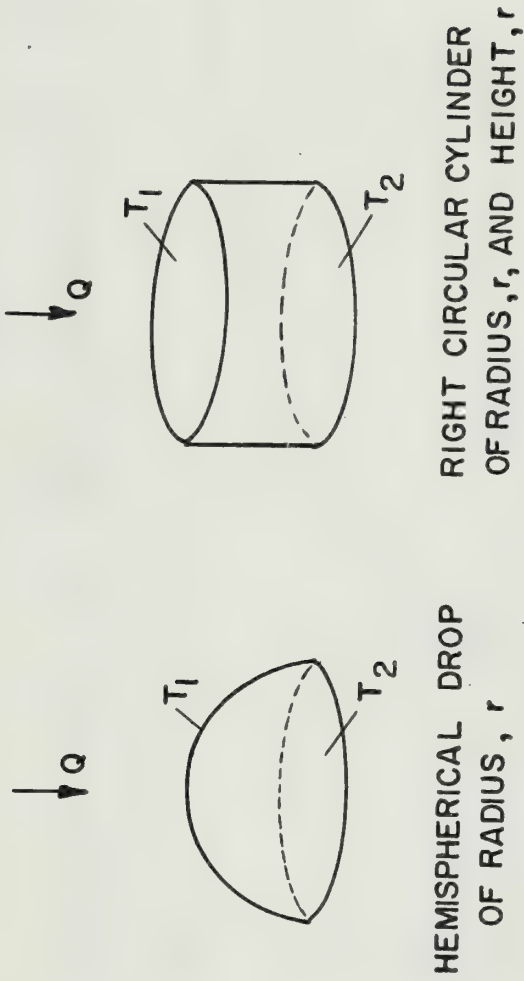


FIG F-1 COMPARISON OF CONDUCTION THROUGH A DROP
AND A RIGHT CIRCULAR CYLINDER

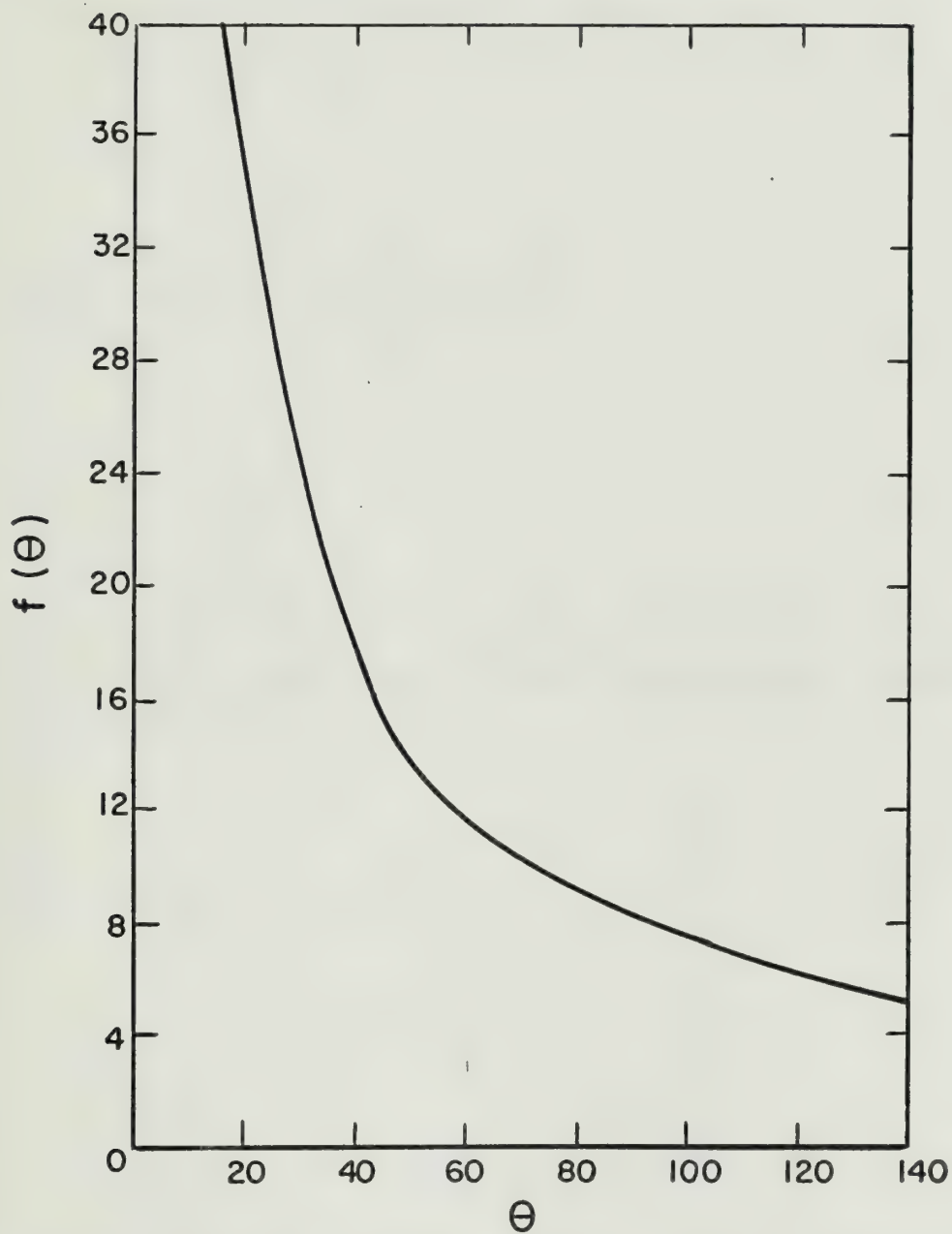


FIG F- 2 DROP CONDUCTION SHAPE
FACTOR, $f(\theta)$
REPRODUCED FROM FATICA AND KATZ [5]

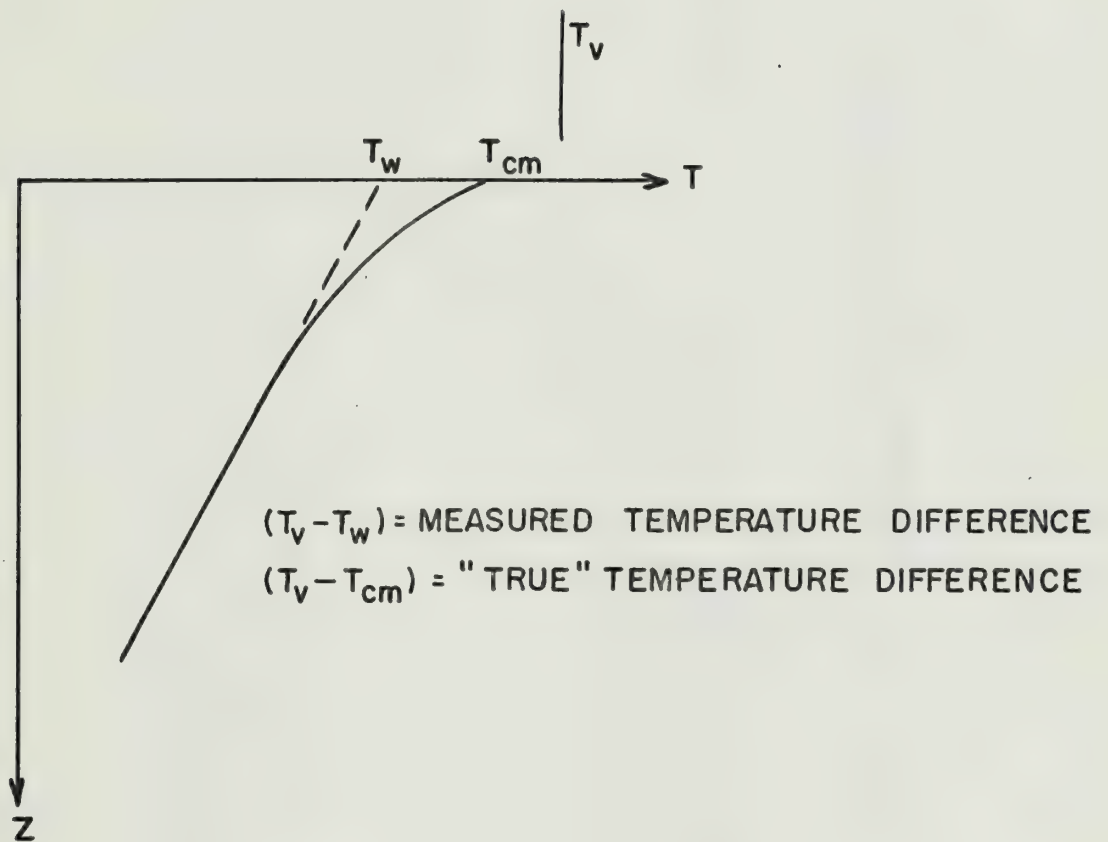


FIG G-1 LOCAL SURFACE TEMPERATURE DUE TO NON-UNIFORM HEAT FLUX OVER SURFACE

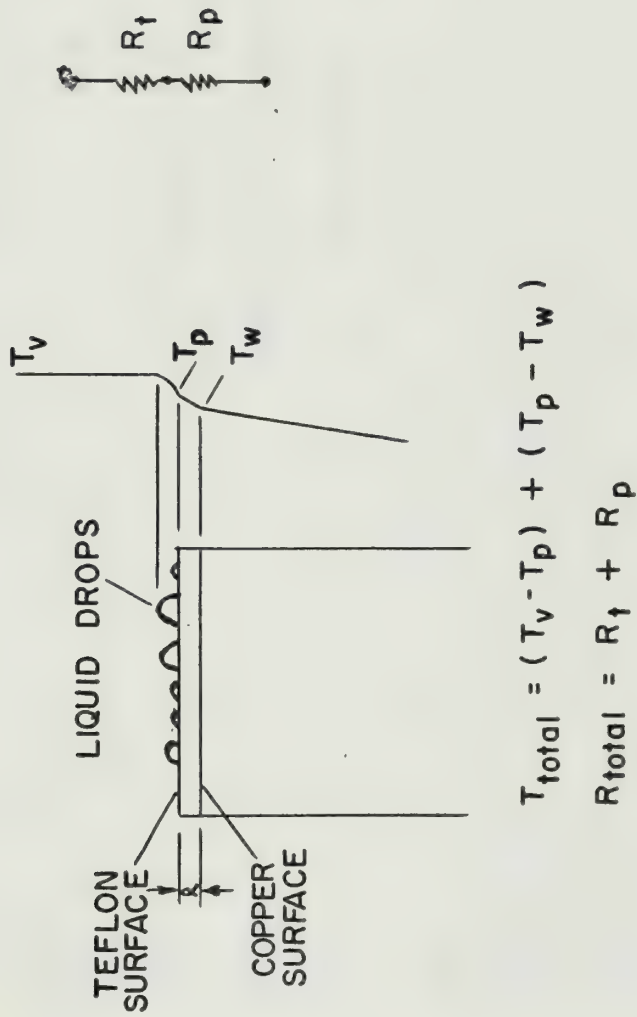


FIG H-1 MODEL OF TEFLON RESISTANCE

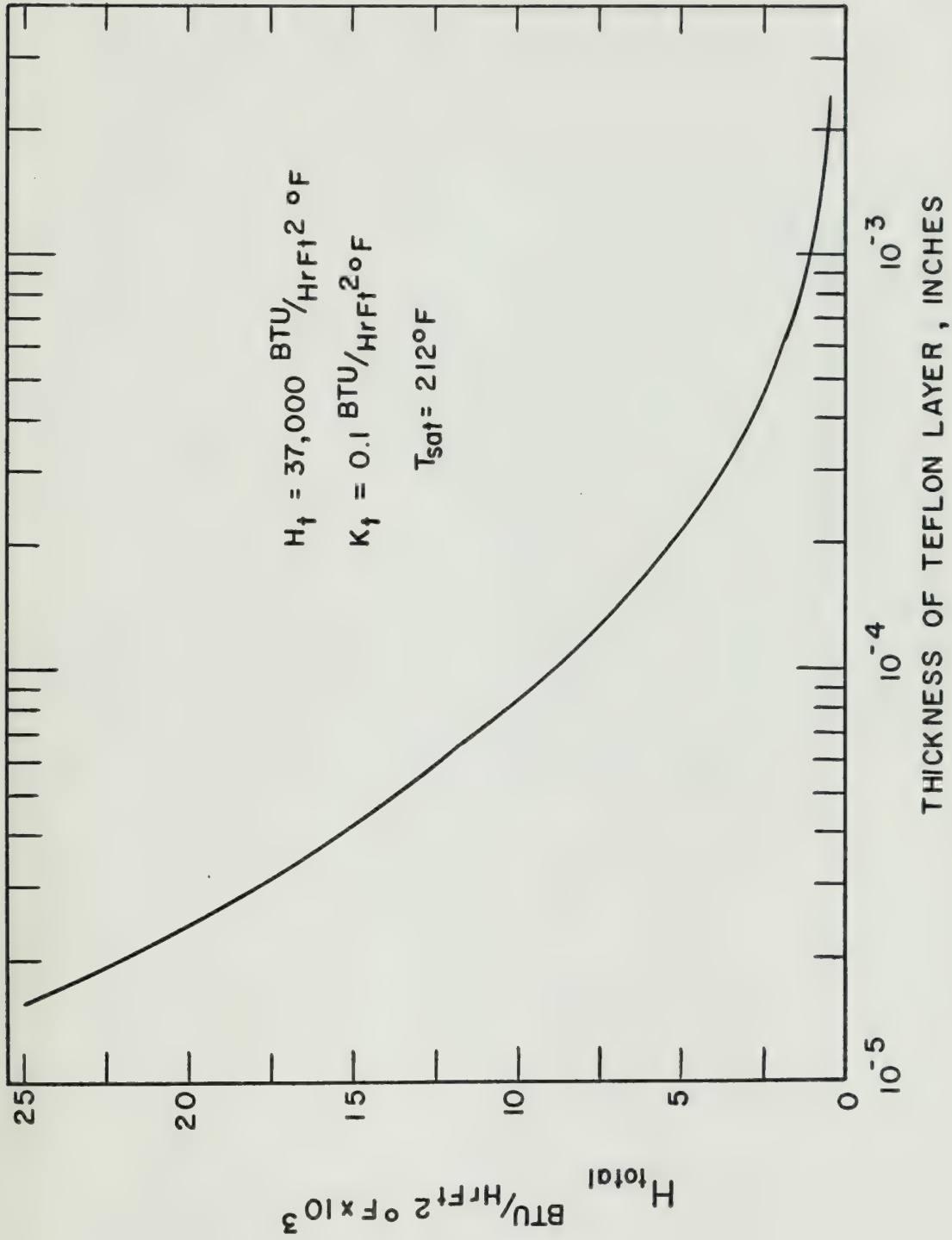


FIG H-2 PREDICTED TOTAL HEAT TRANSFER COEFFICIENT
FOR TEFLON SURFACES

BIOGRAPHICAL NOTE

Clark Graham was born in New York City on June 1, 1942, and attended primary and secondary schools in that city.

He entered the United States Naval Academy in July, 1960. On June 3, 1964, he received the degree of Bachelor of Science, with distinction, and was commissioned an Ensign in the United States Navy.

During his first year of active duty he served on two destroyers, the U.S.S. Ware and the U.S.S. Bird. In June 1965, he entered M.I.T. in the Department of Mechanical Engineering. In February, 1967, he received a degree of Master of Science in Mechanical Engineering and in June, 1967, a Mechanical Engineer Degree. He was elected a member of Sigma Xi in June 1964. Now a Lieutenant, he is scheduled for duty at the Navy Ship Engineering Center at Hyattsville, Maryland.

He married the former Leslie J. Kirkland of Palm Beach, Florida, in April, 1966, and has one son, Geoffrey Clark, age 2.

thesG6522

The limiting heat transfer mechanisms of



3 2768 002 13825 7

DUDLEY KNOX LIBRARY